A novel platform for mechanochemical multicolor lithography and models for solution-phase mechanophore activation

Thesis by

Anna Camille Overholts

In Partial Fulfillment of the Requirements for

the Degree of

Doctor of Philosophy

CALIFORNIA INSTITUTE OF TECHNOLOGY

Pasadena, California

2023

(Defended May 15, 2023)

Anna Camille Overholts
ORCID: 0000-0002-0593-6903

To good friends, good food, and good times

ACKNOWLEDGEMENTS

Caltech has been a unique and special place to work, and I have learned so much during my time here. I first have to thank my advisor Prof. Max Robb, who gave me space and guidance to grow as a scientist and gave me continuous support in my research endeavors. I am especially grateful for everything Max has taught me about science communication – writing, speaking, slide design, the minutiae of figure-making – as that is something I greatly enjoy and will use for the rest of my scientific career. I would also like to thank my committee members Prof. Sarah Reisman, Prof. Scott Cushing, and Prof. Hosea Nelson for their support. I enjoyed every committee meeting and appreciate the real interest that they took in my research and my ideas.

Prior to Caltech, I had many mentors at Cornell who sparked my love for chemistry. I am grateful to Prof. Will Dichtel and Prof. Geoff Coates for letting an enthusiastic young chemistry major who didn't know much about chemistry yet join their labs. In my first research experience in the Dichtel Group, Brian Smith taught me how to plan experiments, handle chemicals, and mostly not break things, and I was continuously inspired by his passion for all things science. My mentor in the Coates Group, Lilli Morris, taught me so much about synthetic organic and polymer chemistry, but just as importantly was an incredibly supportive and kind friend during my time there. Finally, I had the privilege of learning organic chemistry from the incomparable Tom Ruttledge, whose deep love and enthusiasm for teaching chemistry, including silly orgo jokes in every class and long problem-solving sessions in his office, will stay with me forever. I am exceedingly thankful to have had his support and friendship, and I think he'd be proud of what I've accomplished.

The friends I made at Cornell were also influential on my path to where I am now, as a scientist and as a human. Thank you to Allison, Leah, Heather, and Karen for being awesome roommates; Ilana, Wendy, Josh, and Adam for all the fun times working on problem sets and lab reports; and the Alpha Chi Sigma crew, Kelsey, Cynthia, Andrew, John… who are too numerous to name.

Over the years at Caltech, I have met some truly incredible people. My year-mates in the Robb Group have been there with me through everything, whether it was celebration, cry-laughing on the floor, job search stress, failed experiments, or yet another scary email.

Brooke Versaw is one of the strongest people I know and has taught me so much as a scientist, a friend, and a bad-ass woman who knows how to get stuff done. Corey Husic has given me steadfast support over the years and has really been my rock through everything. May Zeng has been a wild ride (Friday dance parties, podcasts, Dungeons and Dragons, impulsive lunch trips) and has been so kind and receptive to my many problems. These guys are more than friends.

The Crellin 360 office has held some other amazing people as well. I am sad to have overlapped with Debbie Tseng for only a few years. Her daily roasts of me have evolved to a place of perfection and I don't know who will keep my ego in check now. I am also grateful for my time with Jolly Patro, who is the kindest person I know and who was always willing to listen to my problems as well as my bad advice for hers. Ross Barber always kept things from getting too serious, but was there for advice and support when I needed it. I learned a great amount from Dr. Peng Liu and Dr. Xiaoran Hu, and I always appreciated their enthusiasm for everything in life, from chemistry to softball. I also had the pleasure of mentoring an undergraduate student, Wendy Granados Razo, whose curiosity was inspiring. The rest of the Robb Group members over the years created a fun and supportive environment that was invaluable to me.

I have many Caltech friends outside the Robb Group to thank as well. Gracie Zhang, for bad TV, dancing, late night Taco Bell, other questionable life decisions, and overall being an amazing roommate and friend. Isabel Klein, who is a constant friend and my most valued confidant, and Bryce Hickam, who taught me the ropes of climbing and is such a positive light in my life. Other climbing buddies, including Danika, Dave, and Nathan. My Formula 1 crew, Sadie, Ham, Jake, and Laura. The Meredith house (Isabel, Bryce, Danika, and Sadie) for brewing, hammocks, and an overall safe haven during quarantine. My recent but much beloved Dungeons & Dragons group with May and Gracie, led by Drew Honson. I have also greatly appreciated time I've spent with the many dogs, cats, and guinea pigs in my friend group – Chula, Shyla, Melvin, Girlie, Green Guy, Harlee, Tarot Card, Hua Hua, and Duo Duo.

I am also so grateful to my family. My parents Lisa and Bob and my brother Ben have given me unending support and invaluable outside perspectives for whatever I was stressed

about at the moment. Growing up, they taught me to be curious and to be proud of being that nerdy weirdo who was constantly reading. Throughout my life, they have always made me feel like I could be whatever I wanted to be and accomplish whatever I set my mind to, so I've gone out and done just that. I am especially grateful for the escapes they've given me from grad school – cute Airbnbs and beaches in Santa Monica with my mom, fast cars at Watkins Glen with my dad, and music and good vibes at the Gorge with Ben and Kristen. The extended Overholts and Venti families have also provided much appreciated support from afar.

The beautiful nature surrounding me in Pasadena has been a balm for my soul. To be able to find absolute silence under the Milky Way in Joshua Tree, camp by the beach in Santa Barbara, hang off a wall in Apple Valley and look out over the desert, or get lost in the mountains has been such a new and treasured experience for me. Even the graffitied sandstone at Stoney Point has a special place in my memory.

Finally, I am so lucky to have had my partner, Kshitij Sadasivan, in my corner for the final few years of graduate school. Thank you to my best friend, climbing partner, hiking buddy, and sous chef. To be able to have such easy joy with you no matter what was going on in the lab was a gift, and I can't wait for all our future adventures.

ABSTRACT

The ability to accurately and quantitatively characterize mechanophore activation is important for informing the fundamental understanding of mechanochemical reactivity, however ultrasound-induced activation rates of scissile mechanophores are routinely deduced from indirect methods of questionable accuracy. Here, the activation rates of two distinct scissile and fluorogenic mechanophores are measured using photoluminescence spectroscopy and compared directly to rates determined using various methods for analyzing chain scission kinetics from GPC measurements. Moreover, analysis of mechanophore activation efficiency reveals an important insight into the consequences of molecular weight dispersity on the characterization of mechanophore reactivity.

We next examine how the identity of a mechanophore, and hence its unique force-coupled reactivity, affects the competition between mechanophore activation and nonspecific polymer backbone scission. Polymers incorporating distinct mechanophores but with putatively similar "chain-centeredness" exhibit widely different mechanochemical activation efficiencies. Furthermore, we employ mechanophores that can be orthogonally cleaved following ultrasonication using heat or light to report on the degree of nonspecific backbone scission that occurs for different mechanophore-containing polymers subjected to ultrasound-induced mechanical force.

Finally, we introduce a mechanophore platform enabling mechanically gated multicolor chromogenic reactivity. The mechanophore is based on an activated furan precursor to donor–acceptor Stenhouse adducts (DASAs) masked as a hetero-Diels–Alder adduct. Mechanochemical activation of the mechanophore unveils the DASA precursor, and subsequent reaction with a secondary amine generates an intensely colored DASA. Critically, the properties of the DASA are controlled by the amine, and thus a single mechanophore can be differentiated post-activation to produce a wide range of functionally diverse DASAs. We highlight this system by establishing the concept of mechanochemical multicolor soft lithography whereby a complex multicolor composite image is printed into a mechanochemically active elastomer through an iterative process of localized compression followed by reaction with different amines.

PUBLISHED CONTENT AND CONTRIBUTIONS

Portions of the work described herein were disclosed in the following publications:

1. Overholts, A. C.; McFadden, M. E.; Robb, M. J. Quantifying activation rates of scissile mechanophores and the influence of dispersity. *Macromolecules* **2022**, *55*, 276-283. https://doi.org/10.1021/acs.macromol.1c02232.

   A.C.O. contributed to the project conception, synthesis, data acquisition and analysis, and manuscript preparation.

2. Overholts, A. C.; Robb, M. J. Examining the impact of relative mechanophore activity on the selectivity of ultrasound-induced mechanochemical chain scission. *ACS Macro Lett.* **2022**, *11*, 733-738. https://doi.org/10.1021/acsmacrolett.2c00217.

   A.C.O. contributed to the project conception, synthesis, data acquisition and analysis, and manuscript preparation.

3. Overholts, A. C.; Granados Razo, W.; Robb, M. J. Mechanically gated formation of donor–acceptor Stenhouse adducts enabling mechanochemical multicolor soft lithography. *Nat. Chem.* **2023**, *15*, 332-338. https://doi.org/10.1038/s41557-022-01126-5.

   A.C.O. contributed to the project conception, synthesis, data acquisition and analysis, and manuscript preparation.

TABLE OF CONTENTS

LIST OF ABBREVIATIONS

±	racemic
Å	angstrom(s)
AM	anthracene–maleimide
aq.	aqueous
ATRP	atom transfer radical polymerization
BHT	butylated hydroxytoluene
Boc	*tert*-butoxycarbonyl
BPA	bisphenol A
br	broad
Bu	butyl
°C	degree(s) Celsius
^{13}C	carbon-13 isotope
calcd	calculated
CD	coumarin dimer
cm	centimeter(s)
cm^{-1}	wavenumber(s)
CoGEF	constrained geometries simulate external force
COSY	correlated spectroscopy
δ	chemical shift in ppm
Δ	heat or difference

$Đ$	dispersity
d	doublet
d	deutero
DASA	donor-acceptor Stenhouse adduct
DCM	dichloromethane
DFT	density functional theory
DIC	*N,N'*-diisopropylcarbodiimde
DMAP	4-dimethylaminopyridine
DMP	Dess–Martin periodinane
DMPA	2,2-dimethoxy-2-phenylacetophenone
DMSO	dimethyl sulfoxide
DP	degree of polymerization
DPTS	4-(dimethylamino)pyridinium 4-toluenesulfonate
EDC	*N*-(3-dimethylaminopropyl)-*N*′-ethylcarbodiimide
EGDMA	ethylene glycol dimethacrylate
EGVE	ethylene glycol vinyl ether
equiv.	equivalent(s)
ESI	electrospray ionization
Et_2O	diethyl ether
EtOAc	ethyl acetate
FM	furan–maleimide
g	gram

GPC	gel permeation chromatography
^{1}H	hydrogen-1 isotope
h	hour(s)
HCl	hydrochloric acid
HEA	hydroxyethyl acrylate
HFIP	1,1,1,3,3,3-hexafluoro-2-propanol
HRMS	high resolution mass spectrometry
I	fluorescence intensity
J	J-coupling
k_x	rate constant derived from (x) method
kDa	kilodalton(s)
kHz	kilohertz
LAH	lithium aluminum hydride
LCMS	liquid chromatography–mass spectrometry
m	multiplet
m_0	molecular weight of a polymer repeat unit
M_{lim}	limiting molecular weight
M_n	number average molecular weight
$M_{n,0}$	initial number average molecular weight
M_{thresh}	threshold molecular weight
MALS	multiangle light scattering
Me	methyl

MeCN	acetonitrile
MeO	methoxy
MeOH	methanol
Me_6TREN	tris[2-(dimethylamino)ethyl]amine
mg	milligram(s)
MHz	megahertz
min	minute(s)
mL	milliliter(s)
mM	millimolar
mmol	millimole(s)
m/z	mass-to-charge ratio
NMR	nuclear magnetic resonance
nN	nanonewton(s)
p	para
PDMS	polydimethylsiloxane
PL	photoluminescence
PMDETA	*N,N,N',N'',N''*-pentamethyldiethylenetriamine
PMA	poly(methyl acrylate)
PMMA	poly(methyl methacrylate)
ppm	parts per million
R	generic group
R_f	retention factor

RI	refractive index
rt	room temperature
s	second(s) or singlet
sat.	saturated
T	temperature
t	triplet
t	tert
T_g	glass transition temperature
t_R	retention time
TBAF	tetra-*n*-butylammonium fluoride
TBDPS	*tert*-butyldiphenylsilyl
TFA	trifluoroacetic acid
THF	tetrahydrofuran
TIPS	triisopropylsilyl
TLC	thin layer chromatography
μL	microliter
μM	micromolar
μs	microsecond
US	ultrasound
UV-vis	ultraviolet-visible
W	watt(s)

Chapter 1

QUANTIFYING ACTIVATION RATES OF SCISSILE MECHANOPHORES AND THE INFLUENCE OF DISPERSITY[1]

The ability to accurately and quantitatively characterize structure–mechanochemical activity relationships is important for informing the fundamental understanding of mechanochemical reactivity and, in turn, the successful advancement of the rapidly growing field of polymer mechanochemistry. Ultrasound-induced mechanical activation of polymers remains one of the most general methods for studying mechanophore reactivity; however, the activation rates of scissile mechanophores are still routinely deduced from changes in polymer size using gel permeation chromatography (GPC) that indirectly report on mechanophore activation with questionable accuracy. Here the rates of ultrasound-induced mechanochemical activation of two distinct scissile and fluorogenic mechanophores are measured using photoluminescence spectroscopy and compared directly to rates determined using various methods for analyzing chain scission kinetics from GPC measurements. This systematic study confirms that the conventional method for analyzing chain scission kinetics is inaccurate and that it provides a misleading picture of mechanophore activity. Instead, time-dependent changes in the GPC refractive index response closely reproduce the rates of mechanophore activation determined spectroscopically. These results expand on prior work by providing a systematic evaluation of the methods used to evaluate mechanophore

[1] Portions of this chapter were adapted from Overholts, A. C.; McFadden, M. E.; Robb, M. J. Quantifying activation rates of scissile mechanophores and the influence of dispersity. *Macromolecules* **2022**, *55*, 276-283. https://doi.org/10.1021/acs.macromol.1c02232.

activation kinetics and emphasize the need for a unified approach to kinetic analysis in the field of polymer mechanochemistry. Moreover, analysis of mechanophore activation efficiency reveals an important insight into the consequences of molecular weight dispersity on the characterization of mechanophore reactivity.

1.1 Introduction

The rapidly developing field of polymer mechanochemistry aims to harness mechanical force to drive specific, productive chemical reactions.[1,2] Force is transmitted by polymer chains to covalently linked molecules called mechanophores with mechanically labile bonds that react chemoselectively.[3,4] A variety of mechanophores have been developed with a wide range of functionality, enabling access to force-responsive polymers for diverse applications.[5–7] Among the many different classes of mechanophores, scissile mechanophores that break apart into two discrete fragments are common and their mechanochemical reaction ultimately results in site-specific cleavage of polymer chains.[8] The changes in polymer molecular weight (chain length) that accompany the reaction of scissile mechanophores are frequently used to indirectly assess mechanochemical activity. A fundamental understanding of the reactivity of mechanophores, and in particular, how reactivity changes as a function of structural variation, is important for advancing structure–mechanochemical activity relationships and empowering the design of new materials.[9–16]

Solution-phase ultrasonication is a ubiquitous technique for applying mechanical force to polymers containing a chain-centered mechanophore that enables straightforward characterization of reactivity.[4,17] During ultrasonication, polymers in the proximity of a

cavitation event experience elongational forces that are maximized near the center of the polymer chain.[8] Although ultrasonication phenomena are relatively complex,[18] the effect is often described by simplified models derived from single molecule extension in well-defined flow fields, in which the force experienced by the polymer scales with chain length.[19] Empirically, the rate of mechanophore activation under ultrasonication is directly proportional to polymer chain length above a critical threshold.[20,21] Ultrasound-induced mechanophore activation can be accurately measured using a variety of spectroscopic techniques including UV-vis absorption,[20,22–25] photoluminescence (PL),[26,27] and NMR spectroscopy,[28–33] whereby the signals corresponding to product formation or mechanophore consumption are monitored over time. However, low mechanophore concentrations typically limit the utility of NMR spectroscopy, and the use of UV-vis or PL spectroscopy requires characteristic absorption or emission properties of the mechanophore or reaction products. Alternatively, reaction progress of scissile mechanophores is conveniently followed using gel permeation chromatography (GPC) to monitor the characteristic evolution in polymer size that putatively reflects the activation and resultant cleavage of the chain-centered mechanophore.

1.2 Methods of Calculating Rate Constants

The rate of ultrasound-induced polymer chain scission, which indirectly reports on the activity of a scissile mechanophore located near the chain midpoint, is routinely characterized using a linearization function applied to time-dependent changes in average molecular weight.[9,12,34–47] The theoretical eq 1.1, which was originally developed to

describe random polymer degradation processes,[48,49] was applied by Sato and Nalepa to the ultrasonic degradation of cellulose derivatives as early as 1978:[50]

$$\frac{1}{M_{n,t}} - \frac{1}{M_{n,0}} = k't \tag{1.1}$$

where $M_{n,t}$ and $M_{n,0}$ are the number average molecular weight at time t and t = 0, respectively, and k' is the apparent rate constant for polymer chain scission. While values of k' with units of mol kg^{-1} min^{-1} are often reported in the literature,[9,12,36–38,45,51] the actual rate constant from this linearization analysis is provided by eq 1.2:

$$k_L = k' \times m_0 \tag{1.2}$$

where k_L has units of min^{-1} after adjusting for the molecular weight of the polymer repeat unit, m_0. Malhotra, to whom this method has sometimes been ascribed, later applied this analysis to characterize the ultrasonic degradation of poly(alkyl methacrylates).[52] The appropriateness of this model, which we refer to here as the linearization method, for describing ultrasound-induced mechanochemical chain scission has been called into question[51] because it does not account for a limiting molecular weight (M_{lim}), below which chains experience insufficient force to cleave further.[53] Rate constants calculated by the linearization method typically correspond to unrealistically long half-lives on the order of days. We note that M_{lim} is distinct from the cutoff or threshold molecular weight (M_{thresh}), which is conventionally defined as the $M_{n,0}$ below which mechanochemical activation does not occur. The value of M_{lim} is dependent upon $M_{n,0}$ and dispersity as chain fragments with molecular weights below M_{thresh} can be produced upon chain scission.[54]

Although the linearization method is commonly used for calculating rates of chain scission from GPC data as described above, other methods have also been employed in the

polymer mechanochemistry literature. In some reports, attenuation of the refractive index (RI) signal at the retention time (t_R) corresponding to the initial polymer peak is fitted to first-order exponential decay to determine a rate constant for chain scission as originally reported by Florea.[21,22,26,55–58] This method is similar to conventional rate analyses performed on small molecule transformations where the consumption of starting material is monitored over time and, unlike methods based on changes to molecular weight averages, is not affected by secondary chain scission events.[26,55,56] Alternatively, others have simply plotted M_n as a function of sonication time and fitted the data to an expression of first-order kinetics to determine a rate constant.[58,59] In contrast to the conventional linearization approach, the rate constants calculated using these other GPC-based methods are generally of the same order of magnitude as spectroscopically determined rate constants for mechanophore activation, suggesting they may be more accurate. In fact, earlier reports from Boydston and Sijbesma indicated that the time-dependent attenuation in GPC-RI signal provides rate constants that are consistent with spectroscopic measurements.[22,26] However, systematic studies that directly compare the results of GPC-based analyses to spectroscopically determined rates of mechanophore activation are limited.

Here we systematically evaluate different methods for analyzing the rate of polymer chain scission from GPC measurements and compare the results to the rate of mechanophore activation measured directly by PL spectroscopy for chain-centered mechanophores that are both scissile and fluorogenic. The rate of mechanophore activation as characterized by PL spectroscopy is most closely reproduced by the time-dependent attenuation in the GPC-RI signal corresponding to the initial polymer peak, while the rate constants calculated using the conventional linearization method are shown to be

particularly inaccurate. Our results also introduce important considerations for the metric of threshold molecular weight, which has been used as a key descriptor of mechanochemical activity, and provide insight into the consequences of molecular weight dispersity on the characterization of mechanophore reactivity.

1.3 Kinetics of AM Mechanical Activation

We initially investigated the rate of ultrasound-induced mechanochemical activation of a chain-centered anthracene–maleimide Diels–Alder adduct mechanophore that is both scissile and fluorogenic (Scheme 1.1). The anthracene–maleimide mechanophore undergoes a retro-[4+2] cycloaddition reaction under mechanical force to generate a fluorescent anthracene moiety.[15,25,60,61] A series of poly(methyl acrylate) (PMA) polymers was prepared via the controlled radical polymerization of methyl acrylate from an anthracene–maleimide bis-initiator (see the ESI for details). The average molecular weight (M_n) of the polymers ranged from 70.7 to 221 kDa with dispersity ($Đ$) ≤ 1.10 as characterized by GPC equipped with RI and multi-angle light scattering (MALS) detectors. Although discussion of the data will emphasize the impact of *molecular weight* on activation kinetics due to the form of eq 1, chain length has been found to be a more accurate descriptor of ultrasound-induced mechanochemical transduction.[20,21] Polymer solutions (2 mg/mL in THF) were subjected to pulsed ultrasound (1 s on/2 s off, 13.6 W/cm^2) in an ice bath and aliquots were periodically removed for analysis by GPC-MALS and PL spectroscopy. It is

Scheme 1.1 Mechanochemical activation of the anthracene–maleimide mechanophore results in polymer chain scission and concomitant generation of a fluorescent anthracene moiety.

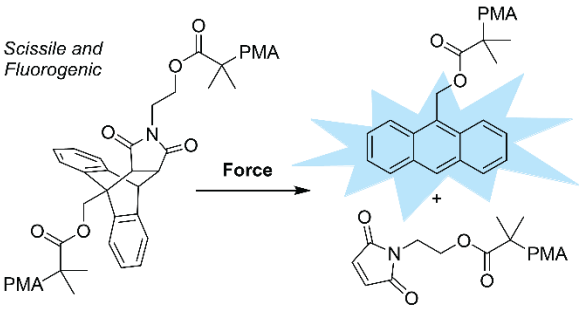

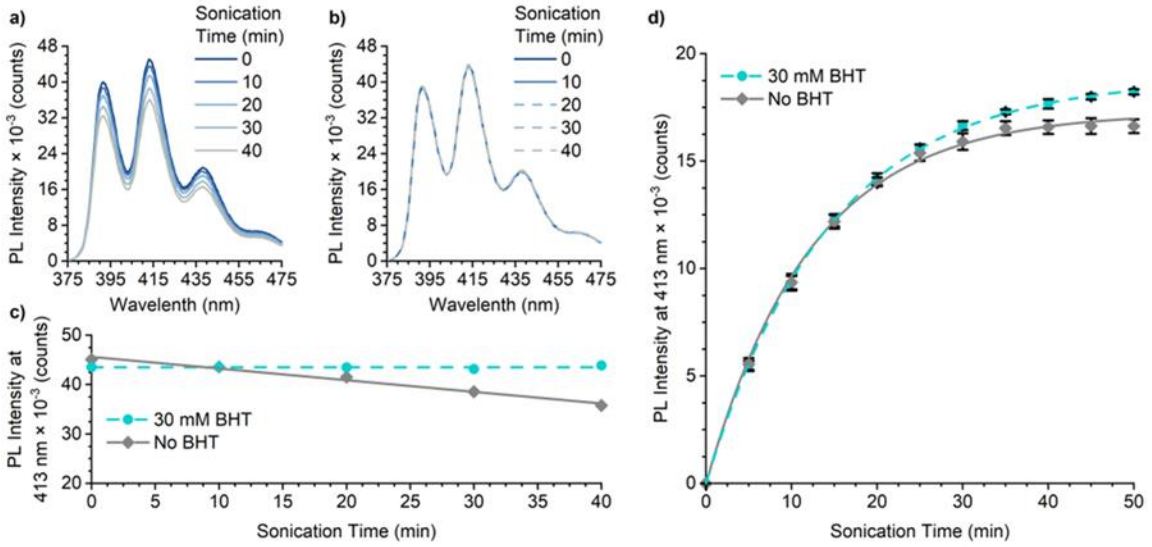

Figure 1.1 Sonication of anthracene-containing polymers results in anthracene degradation, which can be eliminated by addition of 30 mM BHT stabilizer. (a) Photoluminescence spectra acquired during the sonication of **PMMA-1** (2 mg/mL in pure THF, λ_{ex} = 365 nm) monitoring the attenuation of the anthracene peaks. (b) Photoluminescence spectra acquired during the sonication of **PMMA-1** with 30 mM BHT added exhibit no significant change in anthracene fluorescence over time. (c) Time-dependent photoluminescence intensity at 413 nm for the ultrasonication experiments in panels a and b. (d) Time-dependent photoluminescence intensity at 413 nm for ultrasonication of 201 kDa **PMA-1** in THF illustrating attenuation of the product anthracene signal in the absence of BHT, indicative of degradation. Data are averages of three trials and are fitted to eq 1.3.

important to note that 30 mM BHT was added to each polymer solution[32,62] in order to eliminate non-specific degradation of anthracene that was observed during ultrasonication in the absence of a radical inhibitor (Figure 1.1). Ultrasonication experiments were stopped after the PL emission from the mechanochemically generated anthracene moiety reached a nearly constant intensity monitored at 413 nm (λ_{ex} = 365 nm). Each sonication experiment was performed in triplicate and control experiments confirmed that solvent evaporation was negligible, even at long sonication times (Figure 1.2).

For each polymer, the rate of chain scission was evaluated using three distinct analytical methods applied to data obtained from GPC measurements. The results of these analyses were then compared directly to PL measurements performed concurrently for each sonication

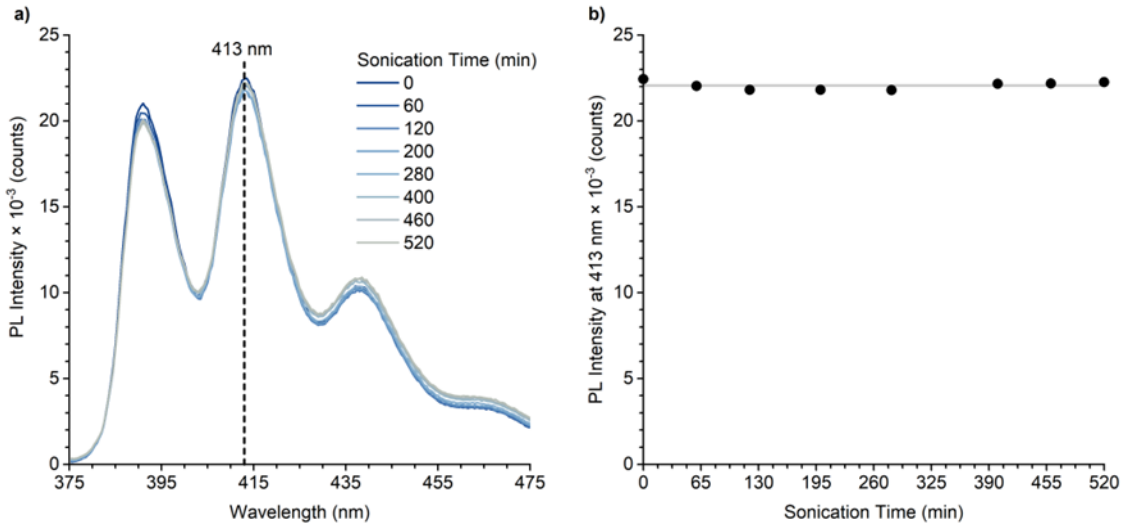

Figure 1.2 Extended ultrasonication of chain-end functional anthracene polymer **PMMA-1** shows negligible evaporation or background fluorescence. (a) Photoluminescence spectra acquired during ultra sonication (2 mg/mL THF, 30 mM BHT, λex = 365 nm). (b) PL intensity at 413 nm plotted as a function of sonication time. The grey line is the average intensity value and is included to guide the eye. Experiments were run in duplicate.

experiment, which report specifically on the mechanochemical retro-[4+2] cycloaddition reaction of the mechanophore. Representative analyses are illustrated in Figure 1.3 for a polymer containing a chain-centered anthracene–maleimide mechanophore with M_n = 108 kDa and $Đ$ = 1.06. Photoluminescence measurements demonstrate the generation of an anthracene product with a characteristic emission spectrum that grows in with increasing sonication time following the expected first-order kinetics (Figure 1.3). The evolution of PL intensity at 413 nm over the time course is fitted to the rate expression given by eq 1.3:

$$I = A(1 - e^{-k_{PL}t}) \tag{1.3}$$

where I is the fluorescence intensity at time t, A is the maximum intensity, and k_{PL} is the rate constant (inset of Figure 1.3a). For the same sonication experiment, the GPC chromatograms (RI response normalized by peak area) demonstrate characteristic features of midchain scission with increasing sonication time, *i.e.*, attenuation of the original polymer peak and

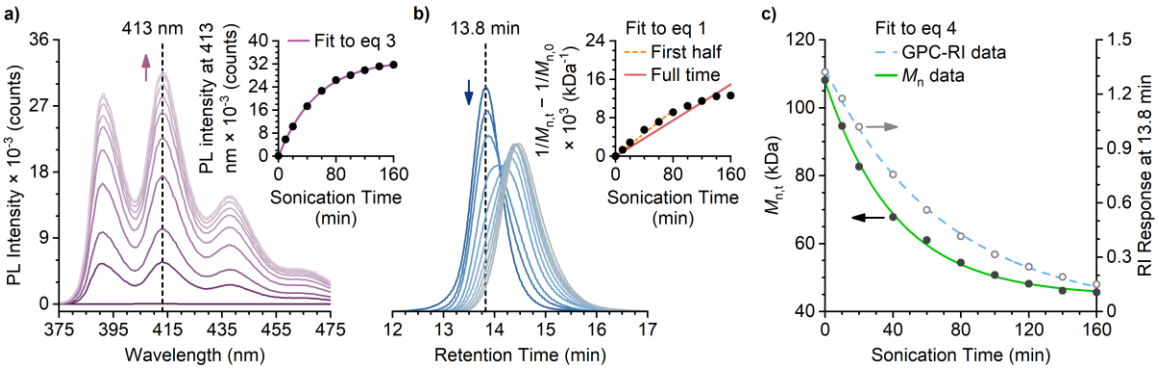

Figure 1.3 Overview of the different methods for analyzing the rate of ultrasound-induced mechanochemical reaction for a representative polymer with a chain-centered anthracene–maleimide mechanophore (M_n = 108 kg/mol; $Đ$ = 1.06). (a) PL spectra acquired during ultrasonication (2 mg/mL in THF with 30 mM BHT, λ_{ex} = 365 nm), monitoring the generation of anthracene. Inset shows the PL intensity at 413 nm as a function of ultrasonication time fitted to eq 1.3. (b) Time-dependent GPC traces (RI response) normalized by integrated area exhibiting features characteristic of midchain scission. Inset shows the results of the conventional linearization analysis using eq 1.1. The fit-determined slope of the linear regression is dependent on the duration of ultrasonication. (c) Alternative analyses performed using the ultrasonication time-dependent GPC data in panel *b*. Values of M_n plotted as a function of ultrasonication time and RI response at t_R = 13.8 min corresponding to the peak maximum of the unsonicated polymer. Both sets of data are fitted to eq 1.4.

growth of a new peak at approximately one-half the original molecular weight (Figure 1.3b). We note that a small amount of secondary chain scission is also evident in the GPC traces for most polymers after extended sonication time. Using eq 1.1, the standard linearization method applied to time-dependent values of M_n gives the plot displayed in the inset of Figure 1.3b. The rate constant, k_L, is obtained from the slope of a linear regression of the data after accounting for m_0, as described by eq 1.2. The data clearly deviate from linearity at extended sonication times, indicating that the calculated value of k_L is dependent upon the duration of the sonication experiment. This deviation occurs as the system approaches $M_{lim,}$ which, as mentioned above, is unaccounted for in eq 1.3 because the model assumes complete degradation to monomer. To further evaluate the impact of this variability, two separate values of k_L were determined for each polymer calculated from linear regressions that include data for the complete sonication time course ("full time") as well as a truncated data set for the first half of the sonication experiment only ("first half"), as illustrated in the inset of

Figure 1.3b. The two alternative methods employed for calculating rate constants of polymer chain scission from the same GPC measurements are illustrated in Figure 1.3c. The time-dependent values of M_n and the RI response at 13.8 min corresponding to the unsonicated polymer are fitted to a standard first-order rate expression given by eq 1.4:

$$y = C + Be^{-kt} \tag{1.4}$$

to obtain rate constants k_M and k_{RI}, respectively. For the time-dependent GPC-RI analysis, the constant C is constrained to 0. For the time-dependent changes in M_n, the variables are fit-determined parameters, although we note that they correspond to meaningful quantities where $C = M_{lim}$ and $B = M_{n,0} - M_{lim}$.[53]

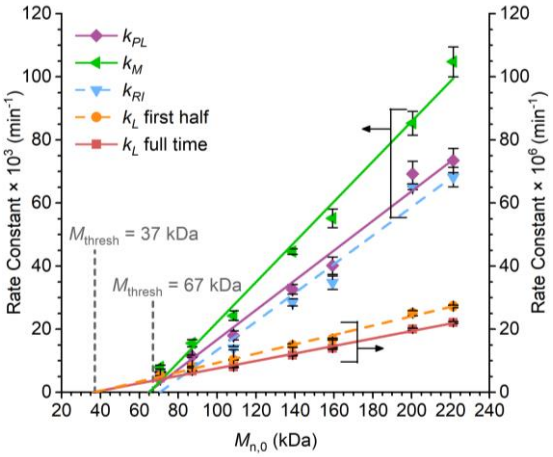

Figure 1.4 Rate constants determined in THF using different analytical methods for the ultrasound-induced mechanical activation of polymers containing a chain-centered anthracene–maleimide mechanophore as a function of initial M_n. Only the rates of polymer chain scission (k_{RI}) calculated from time-dependent changes in GPC-RI response accurately reproduce the rates of mechanophore activation determined spectroscopically from PL measurements (k_{PL}). Data points and error bars represent average values and standard deviation from three replicate experiments. The average values of M_{thresh} calculated from rate constants k_L ("first half" and "full time") and (k_{PL}, k_M, and k_{RI}) are indicated.

The average rate constants determined for polymer chain scission and mechanochemical activation of the anthracene–maleimide mechanophore using each analytical method are plotted as a function of the initial M_n of the polymer and fitted using a linear regression (Figure 1.4). The rate constants calculated using the standard linearization method (k_L) underestimate the rate of mechanophore activation measured by PL spectroscopy by several orders of magnitude (note the distinct y-axis scales in Figure 1.4). Additionally, values of k_L calculated using only the data

from the first half of the sonication time course are consistently greater than values of k_L that account for the full sonication time, confirming that the results of this analysis across the series of polymer molecular weights are influenced by the duration of the sonication experiments, which is often arbitrarily chosen. The rate constants calculated from time-dependent changes in M_n (k_M) overestimate the rate of mechanophore activation by approximately 35% compared to the spectroscopically determined rate constants. The dispersity of synthetic polymers as well as the occurrence of secondary, non-specific chain fragmentation leads to poor modeling of time-dependent changes in molecular weight using a singular rate of chain cleavage. Indeed, this model has previously been demonstrated to underestimate M_n at early sonication times and overestimate the measured values at later sonication times.[53] On the other hand, the rate constants derived from time-dependent changes in GPC-RI values (k_{RI}) closely match the spectroscopically determined rates of mechanophore activation across the entire polymer series, consistent with the prior findings of Boydston and Sijbesma from isolated studies.[22,26] Unlike the time-dependent M_n analysis, the calculated values of k_{RI} are not influenced by secondary chain fragmentation since only the concentration of the starting polymer is measured. However, it is important to note that the GPC peak corresponding to the original polymer and the RI signal corresponding to the fragmentation products must be fully resolved.[26,56] The slight underestimation of k_{RI} values relative to the spectroscopically determined rate constants is consistent with partial overlap in these signals, as illustrated in Figure 1.3b.

The cutoff or threshold molecular weight (M_{thresh}) putatively represents a critical chain length below which ultrasound-induced mechanochemical activation does not occur and

serves as a descriptor of mechanochemical activity.[9,12] Mechanophores with a lower value of M_{thresh} are more reactive as less force is required to achieve mechanochemical activation. Values of M_{thresh} reported previously for various cyclobutane[9] and furan–maleimide[12] mechanophores are in a relatively narrow range of approximately 12–30 kDa, which were determined from the linear regression of chain scission rates obtained using the linearization method for polymers of varying $M_{n,0}$. Similarly, we determine an M_{thresh} value of 37 kDa for the chain-centered anthracene–maleimide mechanophore by extrapolating the values of k_L, as illustrated in Figure 1.4. It is worth noting that, although the slope of the curves differs, the value of M_{thresh} is approximately the same whether or not the full time course for the sonication experiment is included in the determination of each rate constant. Significantly, however, the rate constants determined from PL measurements predict a much higher M_{thresh} value of 65 kDa. Extrapolating molecular weight-dependent rate constants k_{RI} and k_M returns similarly large M_{thresh} values of 71 kDa and 65 kDa, respectively (Figure 1.5). Because the values of k_{PL} report specifically on the

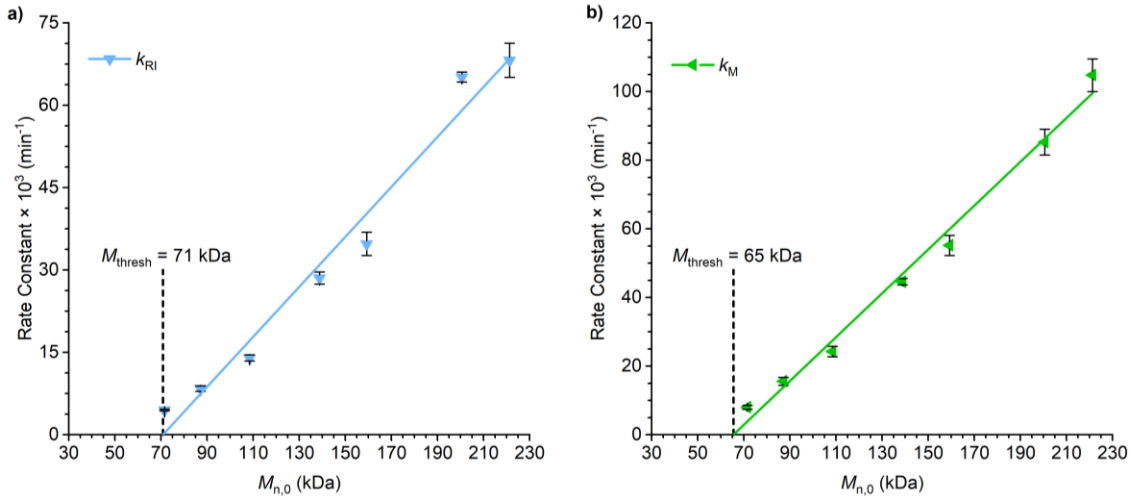

Figure 1.5 (a) Linear regression of rate constants (k_{RI}) determined from GPC-RI measurements for the ultrasound-induced mechanical activation of **PMA-1** with a chain-centered anthracene–maleimide mechanophore in THF provides a M_{thresh} value of 71 kDa. (b) Linear regression of rate constants (k_M) determined from time-dependent M_n data provides an M_{thresh} value of 65 kDa. Data points and error bars represent average values and standard deviation from three replicate experiments.

mechanochemical retro-Diels–Alder reaction of the anthracene–maleimide mechanophore, the corresponding value of M_{thresh} is expected to provide a more accurate descriptor of force-sensitivity compared to the results of the linearization analysis. We return to this discussion and the interpretation of the differences in predicted M_{thresh} values below.

Scheme 1.2 Mechanochemical activation of a coumarin dimer mechanophore results in the generation of a fluorescent coumarin molecule.

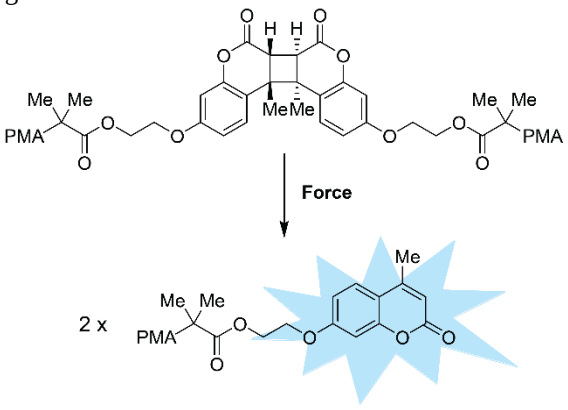

1.4 Kinetics of CD Mechanical Activation

To test the generality of our results, the same analytical methods were applied to the ultrasound-induced mechanochemical activation of a second mechanophore that exhibits both scissile and fluorogenic properties similar to the anthracene–maleimide mechanophore. We selected the coumarin dimer mechanophore reported by Craig and coworkers that undergoes a retro-[2+2] cycloaddition reaction under force, resulting in the generation of two fluorescent coumarin derivatives (Scheme 1.2).[31] A series of PMA polymers containing a chain-centered coumarin dimer mechanophore with M_n in the range 78.7–206 kDa and $Đ \leq$ 1.09 was prepared and subjected to ultrasonication (see section 1.7.2 for details). Sonication experiments were performed under similar conditions as those described above except that a solvent mixture of MeCN/MeOH (3:1) was used, which was found to provide more predictable and reproducible photoluminescence behavior of the coumarin fluorophore. Unlike anthracene, control experiments demonstrated that BHT inhibitor was unnecessary for the coumarin system, although a small increase in background fluorescence was observed

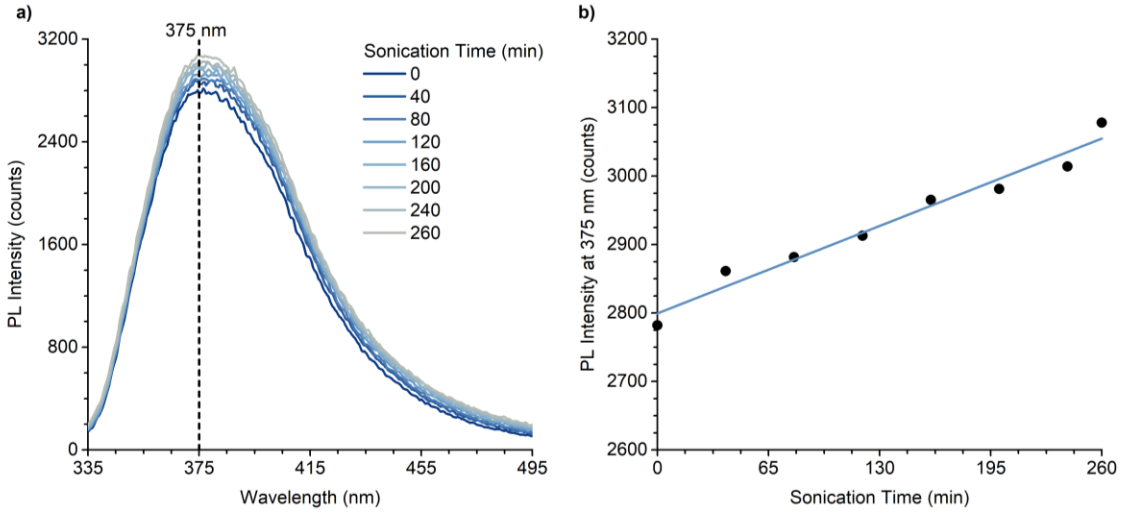

Figure 1.6 Representative sonication experiment of chain-end functional coumarin polymer **PMA-3** for determining a background correction. (a) PL spectra of aliquots removed during sonication, and (b) time-dependent PL intensity at 375 nm fit to a line. Experiments were run in triplicate and the slopes of the linear regressions averaged to obtain a background fluorescence correction factor of 0.796 min^{-1}.

upon sonication that was accounted for in each experiment (Figure 1.6). The rate constants for chain scission and mechanophore activation calculated using each analytical method produce qualitatively similar results as those for the anthracene–maleimide mechanophore (Figure 1.7 and Figure 1.8). Rate constants determined from the time-dependent attenuation of the GPC-RI signal corresponding to the initial polymer peak (k_{RI}) are again in close agreement with the spectroscopically measured rate constants (k_{PL}) for the series of polymers with varying $M_{n,0}$, while poorer fidelity is observed using the other kinetic models. A similar trend in M_{thresh} as that determined for the anthracene–maleimide mechanophore was also observed for the coumarin dimer mechanophore. An M_{thresh} value of 55 kDa was determined for the coumarin dimer in MeCN/MeOH (3:1) by extrapolating values of k_L, while higher M_{thresh} values of 67 kDa and 71 kDa are obtained from PL and GPC-RI measurements, respectively (Figure 1.9).

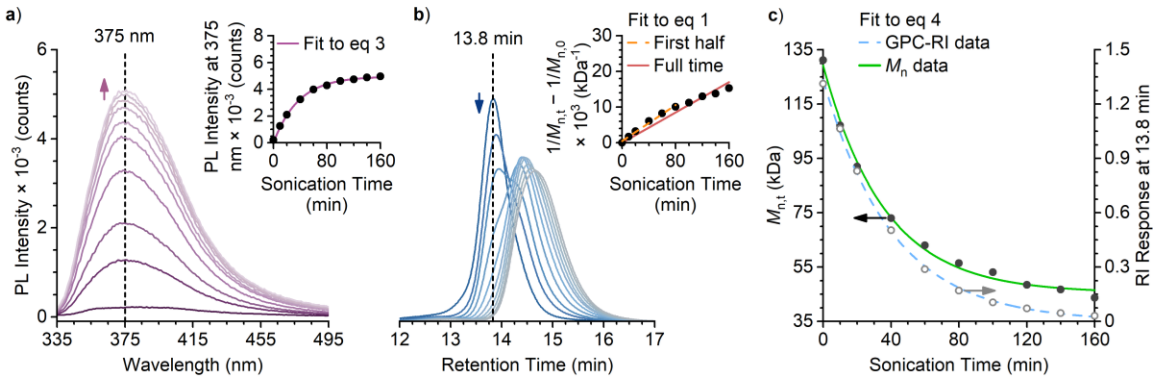

Figure 1.7 Overview of the different methods for analyzing the rate of ultrasound-induced mechanochemical reaction for a representative **PMA-2** containing a chain-centered coumarin dimer mechanophore (M_n = 132 kg/mol; $Đ$ = 1.06). (a) Photoluminescence spectra acquired during ultrasonication (2 mg/mL in 3:1 MeCN/MeOH, λ_{ex} = 320 nm), monitoring the generation of coumarin. Inset shows the photoluminescence intensity at 375 nm as a function of ultrasonication time and fitted to eq 1.3. (b) Time-dependent GPC traces (RI response) normalized by integrated area exhibiting features characteristic of midchain scission. Inset shows the results of the conventional linearization rate analysis using eq 1.1. The fit-determined slope of the linear regression is dependent on the duration of ultrasonication. (c) Alternative analyses performed using the ultrasonication time-dependent GPC data in panel *b*. Values of M_n plotted as a function of ultrasonication time and RI response at t_R = 13.8 min corresponding to the peak maximum of the unsonicated polymer. Both sets of data are fitted to eq 1.4.

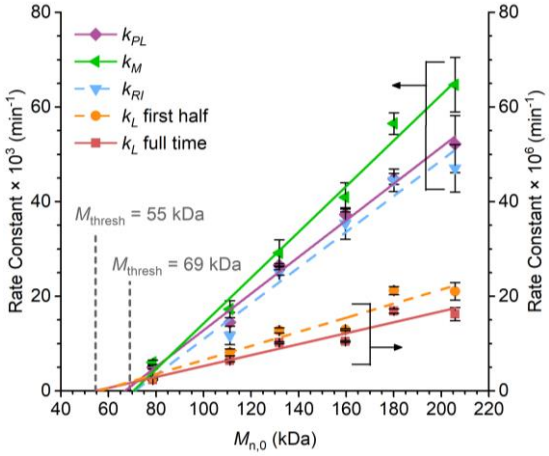

Figure 1.8 Rate constants determined in MeCN/MeOH (3:1) using different analytical methods for the ultrasound-induced mechanical activation of polymers containing a chain-centered coumarin dimer mechanophore as a function of initial M_n. Only the rates of polymer chain scission (k_{RI}) calculated from time-dependent changes in GPC-RI response accurately reproduce the rates of mechanophore activation determined spectroscopically from PL measurements (k_{PL}). Data points and error bars represent average values and standard deviation from three replicate experiments. The average values of M_{thresh} calculated from rate constants k_L ("first half" and "full time") and (k_{PL}, k_M, and k_{RI}) are indicated.

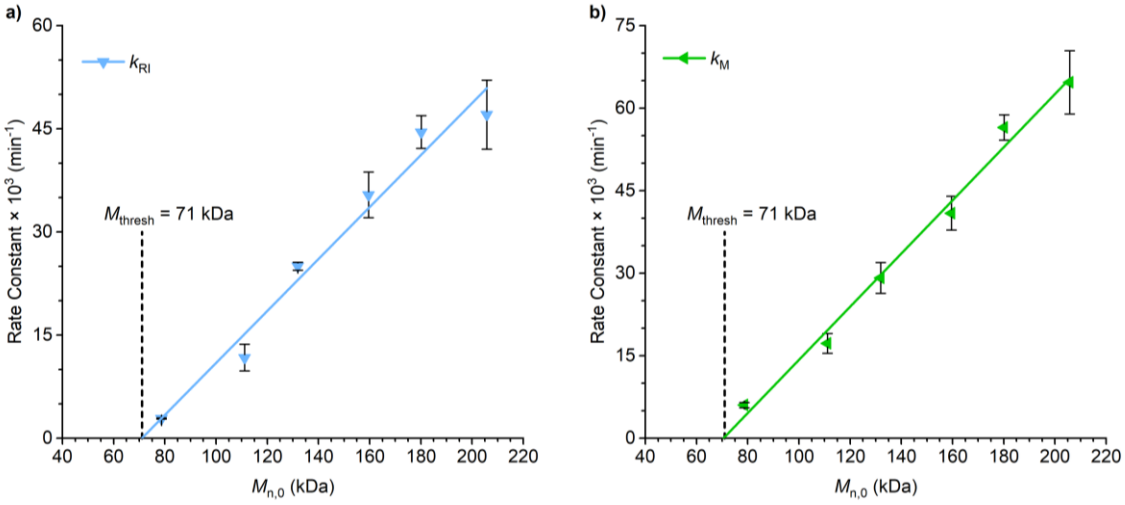

Figure 1.9 (a) Linear regression of rate constants (k_{RI}) determined from GPC-RI measurements for the ultrasound-induced mechanical activation of **PMA-2** with a chain-centered coumarin dimer mechanophore in MeCN/MeOH (3:1) provides a M_{thresh} value of 71 kDa. (b) Linear regression of rate constants (k_M) determined from time-dependent M_n data provide an M_{thresh} value of 71 kDa. Data points and error bars represent average values and standard deviation from three replicate experiments.

1.5 Evaluation of the Impact of Dispersity

Returning to the considerable discrepancy in M_{thresh} values predicted by the conventional linearization method and the other kinetic models above, we synthesized a chain-centered anthracene–maleimide polymer with an M_n of 43.3 kDa ($Đ$ = 1.05), which is well below the M_{thresh} value of 65 kDa predicted by PL measurements for that mechanophore. Interestingly, ultrasound-induced mechanophore activation was still observed, albeit at an exceedingly slow rate (k_{PL} = 2.3 × 10^{-3} min^{-1}). For polymers with molecular weight dispersity and for which $M_{n,0} < M_{thresh}$, we reasoned that some fraction of chains in the distribution may still be long enough to experience sufficient force to achieve mechanophore activation (Figure 1.10a). To test this hypothesis, the maximum fractional mechanophore activation achieved upon ultrasonication was quantified using PL spectroscopy for chain-centered anthracene–

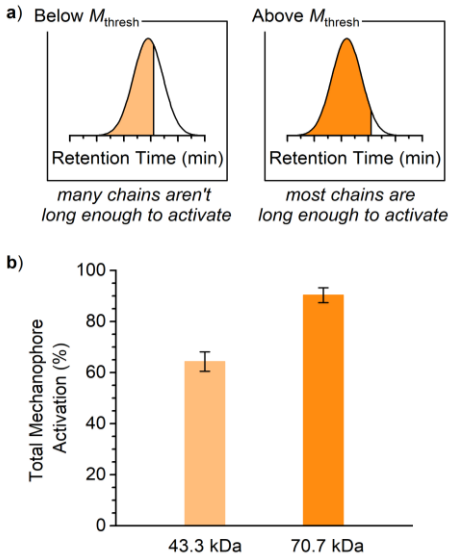

Figure 1.10 (a) Schematic illustrating the proposed interpretation of M_{thresh} that accounts for significantly lower mechanophore activation for polydisperse polymers with $M_{n,0} < M_{thresh}$. (b) Activation efficiency for 43.3 and 70.7 kDa polymers with a chain-centered anthracene–maleimide mechanophore. Error bars represent standard deviation from three replicate experiments.

maleimide polymers with $M_{n,0}$ below (43.3 kDa) and slightly above (70.7 kDa) the M_{thresh} value of 65 kDa predicted from PL measurements (see section 1.7.4 for details). For the 70.7 kDa polymer with $M_{n,0} > M_{thresh}$, the total mechanophore activation reaches 90 ± 3% with extended sonication (Figure 1.10b). In contrast, a substantially lower maximum mechanophore activation of 64 ± 4% is achieved for the 43.3 kDa polymer with $M_{n,0} < M_{thresh}$, suggesting that a smaller fraction of chains in the distribution is activated with ultrasonication. As stated above, the threshold molecular weight predicted by the linearization method is typically recognized as the $M_{n,0}$ (i.e., *average* molecular weight) below which no mechanophore activation occurs.[1,4] The results here suggest a more nuanced interpretation of M_{thresh} that points to an explicit chain length below which force is insufficient for mechanophore activation. Consistent with this model, when the molecular weight distributions for both polymers are bifurcated at 43 kDa, the area of the GPC chromatograms

above this discrete molecular weight value is 61% for the 43.3 kDa polymer and 94% for the 70.7 kDa polymer, in good agreement with the measured mechanophore activation efficiencies (Figure 1.11). This calculation assumes 100% theoretical mechanophore activation, which in this case appears to be reasonable. However, competition between nonspecific backbone scission and mechanophore activation depends on factors other than molecular weight, including the identity (i.e., reactivity) of the mechanophore. We contrast the theory presented above with prior arguments about the impact of dispersity on mechanophore activation efficiency that relate specifically to the position of the mechanophore in the polymer chain, rather than the distribution of chain lengths in a polydisperse sample.[31] Additionally, we note that for smaller polymers and/or those with higher dispersity that exhibit lower mechanophore activation efficiency, the measured rate constants consequently only reflect the fraction of chains in the distribution that is sufficiently

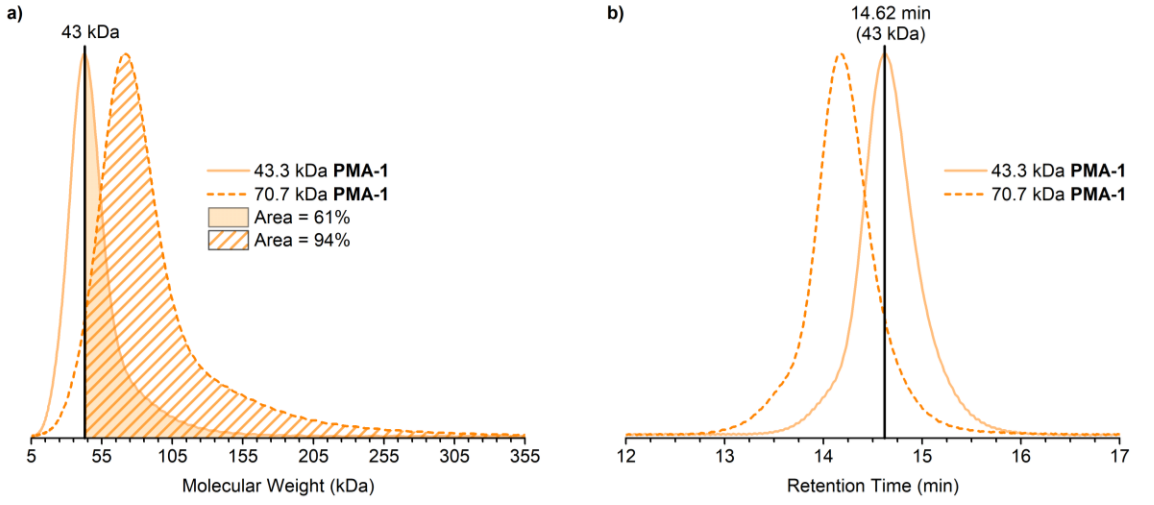

Figure 1.11 Analysis of the effect of molecular weight distribution on the mechanochemical activation of **PMA-1** containing a chain-centered anthracene–maleimide mechanophore with M_n below (43.3. kDa) and slightly above (70.7 kDa) the spectroscopically determined value of M_{thresh} (65 kDa). (a) The area of each GPC chromatogram (RI response) above 43 kDa (denoted by a vertical black line) is 61% for the 43.3 kDa polymer and 94% for the 70.7 kDa polymer, consistent with the measured mechanophore activation efficiencies of 64 ± 4% and 90 ± 3%, respectively. These data further support the model describing an explicit chain length below which mechanophore activation does not occur. (b) The same GPC data are plotted in the more conventional format with respect to retention time.

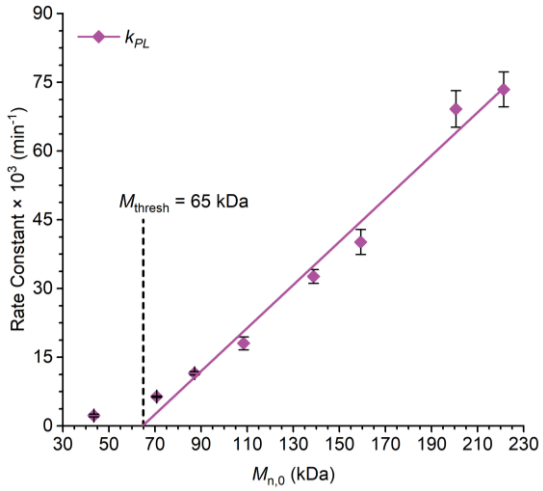

Figure 1.12 Rate constants determined from PL measurements for the ultrasound-induced mechanical activation of **PMA-1** containing a chain-centered anthracene–maleimide mechanophore. The linear regression excludes the data point for the polymer with $M_{n,0}$ = 43.3 kDa, which clearly deviates from the linear trend. Data points and error bars represent average values and standard deviation from three replicate experiments.

long to activate, leading to a value that is larger than would be expected based on the linear regression of molecular weight-dependent activation kinetics (Figure 1.12).

1.6 Conclusions

The ability to accurately and quantitatively characterize structure–mechanochemical activity relationships is important for the advancement of fundamental understanding in the rapidly evolving field of polymer mechanochemistry. While specialized techniques such as single molecule force spectroscopy facilitate precise measurements of force–rate behavior,[63,14,64] ultrasound-induced mechanical activation of polymers remains one of the most general methods for studying mechanophore reactivity. However, despite isolated comparative studies of alternative kinetic analyses, activation rates are routinely deduced from changes in polymer molecular weight that indirectly report on mechanophore activation using inaccurate analytical methods. Here, the rates of ultrasound-induced mechanochemical activation for two different scissile and fluorogenic mechanophores were systematically

measured using photoluminescence spectroscopy and compared directly to rate constants determined using three different methods for analyzing chain scission kinetics from GPC measurements. For each series of polymers, the spectroscopically determined rate constants for mechanophore activation are closely reproduced by fitting the time-dependent attenuation of the GPC refractive index (RI) response for the initial polymer peak to a first-order rate expression. In contrast, other methods of evaluating chain scission rates, including the prevailing linearization approach commonly referred to as the Malhotra or Nalepa method, significantly mischaracterize the rate of mechanophore activation.

This study expands on prior observations by providing a systematic assessment of the methods used to evaluate mechanophore activation kinetics, validating the use of the simple GPC-RI method for characterizing the reactivity of scissile mechanophores. The results emphasize the need for a unified approach to kinetic analysis in the field of polymer mechanochemistry. In addition, analysis of the molecular weight-dependent activation efficiency for an anthracene–maleimide mechanophore suggests that a more nuanced interpretation of the cutoff or threshold molecular weight (M_{thresh}) is needed to properly account for the inherent molecular weight dispersity of polymers. Contrary to convention, we find that the fraction of chains that achieves mechanophore activation is diminished for polymers with M_n below the value of M_{thresh} determined spectroscopically; however, the rate of mechanophore activation is non-zero. These results indicate that molecular weight distribution, and not simply M_n or average DP, needs to be considered in the interpretation of ultrasound-induced mechanochemical reactivity.

1.7 Experimental Section

1.7.1 General Experimental Details

Reagents from commercial sources were used without further purification unless otherwise noted. Methyl acrylate was passed through a short plug of basic alumina to remove inhibitor immediately prior to use. Dry THF and MeCN were obtained from a Pure Process Technology solvent purification system. All reactions were performed under a N_2 atmosphere unless specified otherwise.

NMR spectra were recorded using a 400 MHz Bruker Avance III HD with Prodigy Cryoprobe or a 400 MHz Bruker Avance Neo. All ^{1}H NMR spectra are reported in δ units, parts per million (ppm), and were measured relative to the signals for residual chloroform (7.26 ppm) in deuterated solvent. All ^{13}C NMR spectra were measured in deuterated solvents and are reported in ppm relative to the signals for chloroform (77.16 ppm). Multiplicity and qualifier abbreviations are as follows: s = singlet, d = doublet, t = triplet, q = quartet, m = multiplet.

High resolution mass spectra (HRMS) were obtained from a JEOL JMS-600H magnetic sector spectrometer equipped with a fast atom bombardment (FAB) ionization source.

Analytical gel permeation chromatography (GPC) was performed using an Agilent 1260 series pump equipped with two Agilent PLgel MIXED-B columns (7.5 x 300 mm), an Agilent 1200 series diode array detector, a Wyatt 18-angle DAWN HELEOS light scattering detector, and an Optilab rEX differential refractive index detector. The mobile phase was THF at a flow rate of 1 mL/min. Molecular weights and molecular weight distributions were calculated by light scattering using a dn/dc value of 0.062 mL/g (25 °C) for poly(methyl acrylate) and 0.082 mL/g (25 °C) for poly(methyl methacrylate).

Photoluminescence spectra were recorded on a Shimadzu RF-6000 spectrofluorophotometer in a quartz microcuvette (Starna 18F-Q-10-GL14-S).

Photochemical reactions were performed using a 36 W UV100A Honeywell Air Treatment System with a Philips PL-L Hg lamp, or a 4 Watt UVLS-24 EL Series UV Lamp.

Ultrasound experiments were performed inside a sound abating enclosure using a Vibra Cell 505 liquid processor equipped with a 0.5-inch diameter solid probe (part #630-0217), sonochemical adapter (part #830-00014), and a Suslick reaction vessel made by the Caltech glass shop (analogous to vessel #830-00014 from Sonics and Materials).

Compounds **S1**,[65] **S3**,[65] **S4**,[66] and **S6**[67] were synthesized following the procedures reported in the literature. Compound **S2**[31] was synthesized using a modified procedure as described in detail below.

Chart 1.1 Structures of initiators (**S1**, **S2**, **S3**) and small molecule reference compounds (**S4** and **S5**) used in this study.

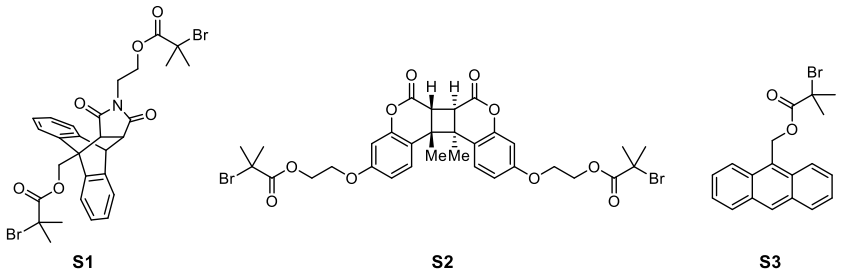

Chart 1.2 Structures of polymers **PMA-1**, **PMA-2**, **PMA-3**, and **PMMA-1**.

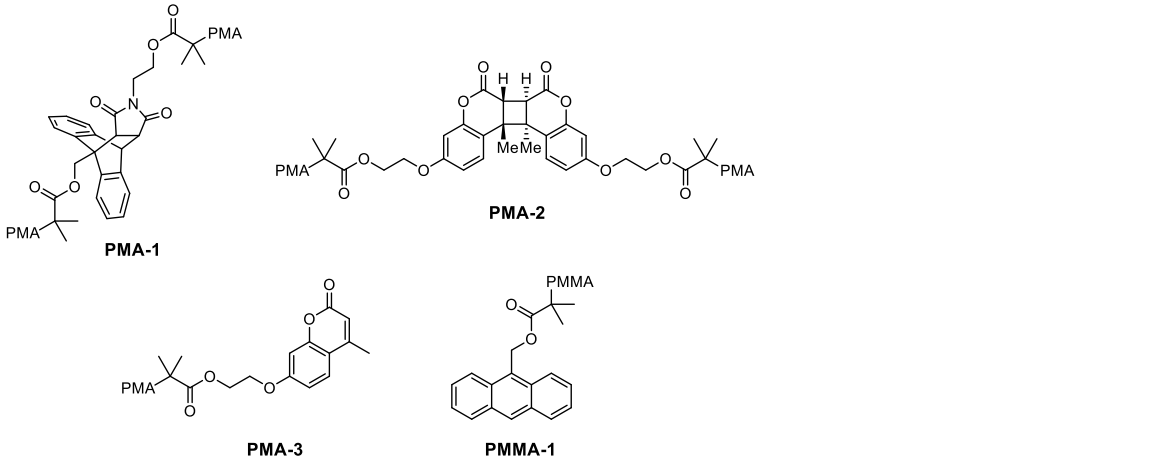

1.7.2 Synthesis and Characterization of Initiators and Polymers

Scheme 1.3 Synthesis of Coumarin Dimer Initiator S2.

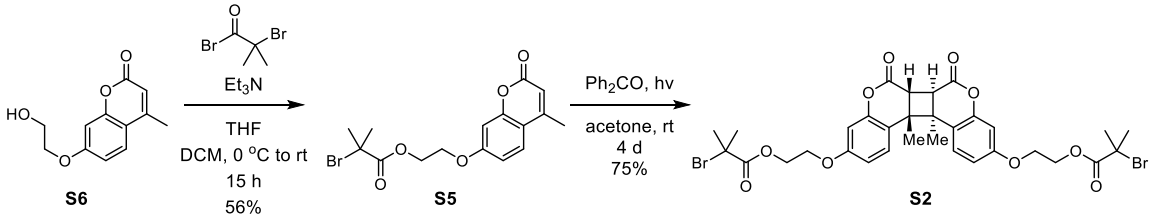

2-((4-methyl-2-oxo-2H-chromen-7-yl)oxy)ethyl 2-bromo-2-methylpropanoate (S5). A flame-dried two-neck flask equipped with a stir bar was charged with **S6**[67] (1.07 g, 4.86 mmol), dry THF (20 mL), and dry DCM (45 mL). The mixture was stirred until all solids dissolved followed by the addition of triethylamine (1 mL, 7.18 mmol). The reaction was cooled to 0 °C, after which α-bromoisobutyryl bromide (0.9 mL, 7.28 mmol) was added slowly. After addition was complete, the reaction was removed from the ice bath and warmed to room temperature. After stirring for 15 h, an aqueous solution of saturated NH_4Cl (50 mL) was added and the organic layer was separated. The aqueous layer was extracted with DCM

(3 x 50 mL) and the combined organic layers were washed with brine (50 mL). The organic phase was dried over $MgSO_4$, filtered, and concentrated under reduced pressure. The crude mixture was redissolved in EtOAc (50 mL) and washed with 1 M NaOH (3 x 15 mL) and then brine (15 mL). The organic phase was dried over $MgSO_4$, filtered, and concentrated under reduced pressure. The crude material was recrystallized from DCM/hexanes to yield the title compound as a white crystalline solid (1.00 g, 56%).

TLC (20% EtOAC/hexanes): R_f = 0.24

^{1}H NMR (400 MHz, CDCl3) δ: 7.51 (d, *J* = 8.8 Hz, 1H), 6.88 (dd, *J* = 8.8, 2.5 Hz, 1H), 6.83 (d, *J* = 2.5 Hz, 1H), 6.15 (broad q, *J* = 1.3 Hz, 1H), 4.61–4.50 (m, 2H), 4.34–4.23 (m, 2H), 2.40 (d, *J* = 1.2 Hz, 3H), 1.94 (s, 6H).

^{13}C{^{1}H} NMR (101 MHz, $CDCl_3$) δ: 171.7, 161.5, 161.3, 155.3, 152.6, 125.8, 114.2, 112.7, 112.4, 101.9, 66.2, 63.8, 55.46, 30.8, 18.8.

HRMS (ESI, *m/z*): calcd for $[C_{16}H_{18}BrO_5]^+$ $(M+H)^+$ 369.0338, found 369.0358.

(((6aR,6bR,12bR,12cR)-12b,12c-dimethyl-6,7-dioxo-6,6a,6b,7,12b,12c-hexahydrocyclobuta[1,2-c:4,3-c']dichromene-3,10-diyl)bis(oxy))bis(ethane-2,1-diyl) bis(2-bromo-2-methylpropanoate) (S2). Compound **S5** (1.00 g, 2.71 mmol) and benzophenone (244 mg, 1.34 mmol) were added to a 20 mL scintillation vial equipped with a stir bar and a septum cap. Acetone (8 mL) was added and the solution was sparged with N_2 for 30 min. The vial was partially submerged in a water bath and irradiated with a high pressure mercury lamp (36 W) while stirring for 4 days. The solution was then concentrated under reduced pressure and the crude material eluted through a plug of silica gel, first with 20% EtOAC/hexanes then with EtOAc. The former eluent was discarded and the latter

portion was collected and concentrated under reduced pressure. The crude material was recrystallized from EtOAc/hexanes to yield the title compound as a white crystalline solid (749 mg, 75%). ^{1}H and ^{13}C NMR spectra match the characterization data reported previously.[31]

TLC (20% EtOAc/hexanes): R_f = 0.15

^{1}H NMR (400 MHz, CDCl3) δ: 7.05 (d, *J* = 8.6 Hz, 2H), 6.80 (dd, *J* = 8.6, 2.6 Hz, 2H), 6.65 (d, *J* = 2.6 Hz, 2H), 4.58–4.51 (m, 4H), 4.28–4.20 (m, 4H), 3.38 (s, 2H), 1.95 (s, 12H), 1.24 (s, 6H).

^{13}C{^{1}H} NMR (101 MHz, $CDCl_3$) δ: 171.8, 166.0, 159.3, 151.8, 128.3, 115.8, 112.6, 103.5, 66.1, 64.0, 55.5, 46.8, 45.1, 30.9, 26.5.

Representative Procedure for the Synthesis of Poly(Methyl Acrylate) (PMA) Polymer Containing a Chain-Centered Mechanophore. PMA polymers were synthesized by controlled radical polymerization following the procedure by Nguyen *et al*.[68] A 25 mL Schlenk flask equipped with a stir bar was charged with initiator **S2** (16.7 mg, 0.226 mmol), DMSO (2 mL), methyl acrylate (2 mL), and freshly cut copper wire (2.0 cm length, 20 gauge). The flask was sealed, the solution was deoxygenated with three freeze-pump-thaw cycles, and then allowed to warm to rt and backfilled with nitrogen. Me_6TREN (17 μL, 0.0636 mmol) was added via microsyringe. After stirring at rt for 2 h, the flask was opened to air and the solution was diluted with DCM. The polymer solution was precipitated into cold methanol (3x) and the isolated material was dried under vacuum to yield 1.46 g of **PMA-2** (70%). M_n = 78.7 kDa, $Đ$ = 1.05.

Synthesis of Chain-End Functional Control Polymer PMMA-1 Containing an Anthracene End Group. A 25 mL Schlenk flask equipped with a stir bar was charged with initiator **3** (7.7 mg, 0.0216 mmol), DMSO (5 mL), methyl methacrylate (5 mL), and freshly cut copper wire (2.0 cm length, 20 gauge). The flask was sealed, the solution was deoxygenated with three freeze-pump-thaw cycles, and then allowed to warm to rt and backfilled with nitrogen. PMDETA (11 μL, 0.0527 mmol) was added via microsyringe. After stirring at rt for 47 h, the flask was opened to air and the solution was diluted with DCM. The polymer solution was precipitated into cold methanol (3x) and the isolated material was dried under vacuum to yield 1.49 g of **PMMA-1** (28%). M_n = 140 kDa, $Đ$ = 1.89.

Synthesis of Chain-End Functional Polymer PMA-3 Containing a Coumarin End Group. PMA-2 (20.0 mg, 160 kDa, $Đ$ = 1.05) was dissolved in a 3:1 mixture of MeCN/MeOH (50 mL) in a quartz tube equipped with a stir bar and sealed with a rubber septum. The solution was irradiated with UV light (254 nm) for 60 min, then stored in the dark. Analysis by GPC provided a measured M_n of 78.7 kDa ($Đ$ = 1.07), approximately one-half the initial M_n (see **Table 1.1**). Analysis by ^{1}H NMR spectroscopy confirmed complete conversion of **PMA-2** to **PMA-3** (**Figure 1.13**).

Table 1.1 Summary of M_n and $Đ$ data for **PMA-1, PMA-2, PMA-3,** and **PMMA-1**.

	M_n (kDa)	$Đ$		M_n (kDa)	$Đ$
PMA-1	43.3	1.05	**PMA-2**	78.7	1.05
	70.7	1.07		111	1.07
	87.1	1.05		132	1.06
	108	1.06		160	1.05
	139	1.05		180	1.05
	159	1.06		206	1.09
	201	1.07	**PMA-3**	78.7	1.07
	221	1.10	**PMMA-1**	140	1.89

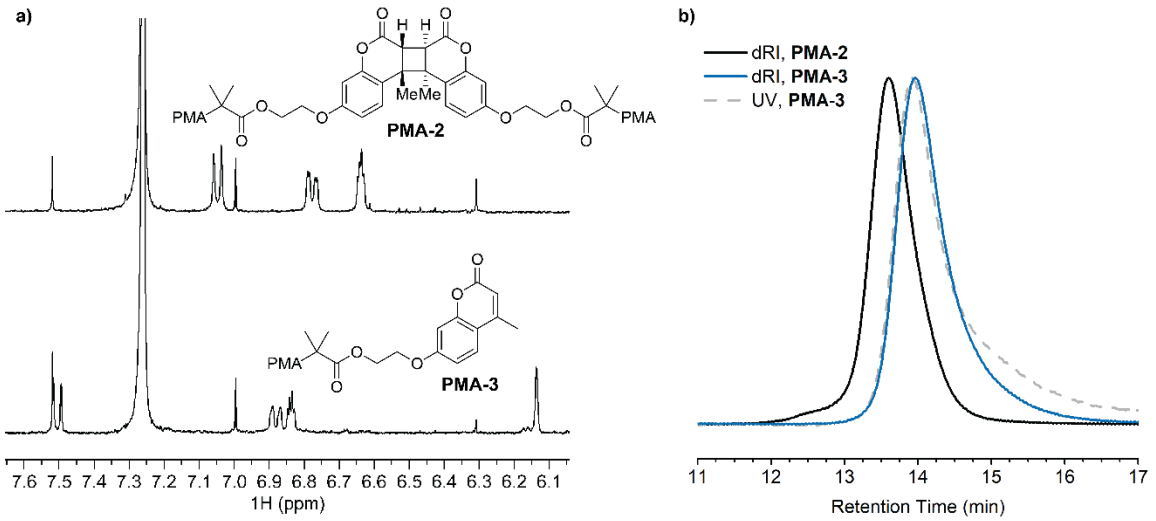

Figure 1.13 Characterization of the photochemical cleavage of **PMA-2** to produce coumarin chain-end functional polymer **PMA-3**. (a) Partial ^{1}H NMR spectra demonstrating complete conversion of the coumarin dimer after irradiation with 254 nm UV light. (b) GPC traces (RI response) demonstrating a clean shift in retention time from starting material **PMA-2** (black line) to cleaved product **PMA-3** after photoirradiation (blue line). Monitoring the GPC elution with a UV detector at 320 nm (dashed gray line) corresponding to the absorption of coumarin confirms chain-end functionality.

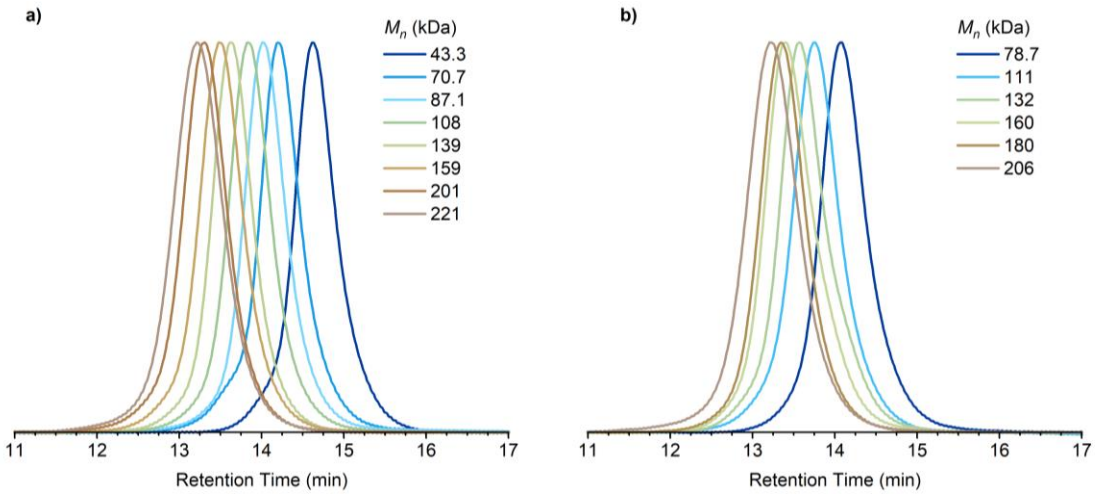

Figure 1.14 GPC traces (RI response) of polymers used in this study containing a chain-centered mechanophore. (a) **PMA-1** series (anthracene–maleimide), and (b) **PMA-2** series (coumarin dimer).

1.7.3 Description of Sonication Experiments and Fluorescence Spectroscopy

General Procedure for Ultrasonication Experiments. An oven-dried sonication vessel was fitted with rubber septa, placed onto the sonication probe, and allowed to cool under a stream of dry argon. The vessel was charged with a solution of the polymer in anhydrous solvent (THF or 3:1 MeCN/MeOH, 2.0 mg/mL, 20 mL) and submerged in an ice bath. The solution was sparged continuously with argon beginning 10 min prior to sonication and for the duration of the sonication experiment. Pulsed ultrasound (1 s on/2 s off, 30% amplitude, 20 kHz, 13.6 W/cm^2) was then applied to the system. Aliquots (1.0 mL) were removed at specified time points (sonication "on" time) and filtered through a 0.45 μm PTFE syringe filter prior to analysis by GPC and fluorescence spectroscopy. Ultrasonic intensity was calibrated using the method described by Berkowski et al.[6]

Analysis of Sonicated Polymer Samples by Fluorescence Spectroscopy. Aliquots from the sonication experiment were added to a microcuvette. Emission spectra for **PMA-1** and **PMMA-1** were recorded at 375–480 nm using an excitation wavelength of λ_{ex} = 365 nm. Emission spectra for polymers **PMA-2** and **PMA-3** were recorded at 330–500 nm using an excitation wavelength of λ_{ex} = 320 nm.

1.7.4 Determination of Total Mechanophore Activation (%)

Characterization of Activation Efficiency for the Anthracene–Maleimide Mechanophore. Samples of **S4** in THF at various concentrations were prepared and PL spectra were acquired to construct the calibration curve shown in Figure 1.15. The theoretical PL intensity for each sonication experiment based on the concentration of mechanophore was determined from this calibration curve and used as the value for 100% activation.

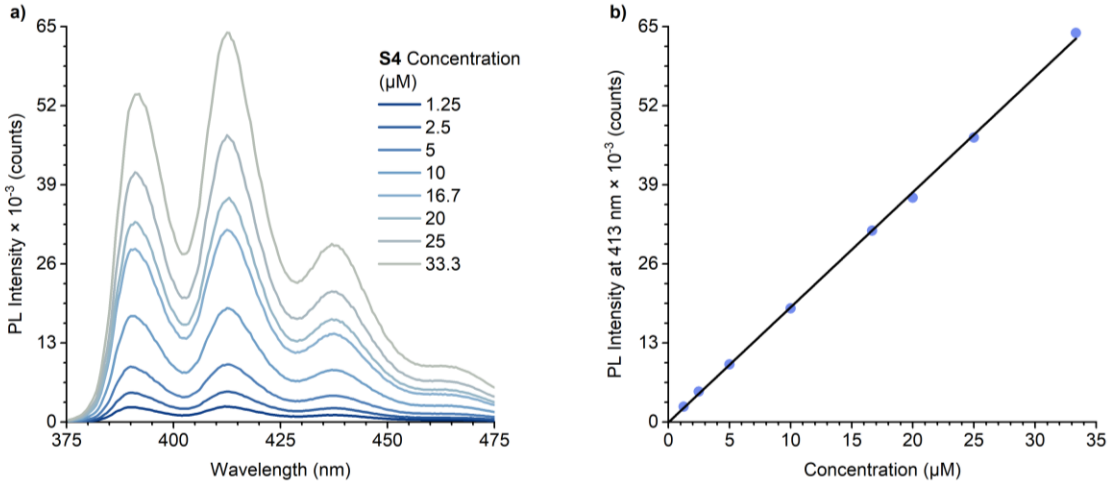

Figure 1.15 Construction of a calibration curve for experimental determination of the concentration of anthracene-containing polymer. (a) Photoluminescence emission spectra (λ_{ex} = 365 nm), and (b) PL intensity at 413 nm for solutions of compound **S4** in THF as a function of concentration. A linear regression of the data in (b) gives the calibration function y=1893*x.

Calculation of Percent Activation for the Anthracene–Maleimide Mechanophore. Time-dependent PL values at the relevant emission wavelength (413 nm for **PMA-1**) were fit to eq 3. The fit-determined plateau value (*A*) was used as the maximum activation for that sonication experiment (see Figure 1.16 and Figure 1.17 for representative examples). The predicted plateau value (*A*) determined from each experiment was then divided by the PL value calculated for full conversion (i.e., 100% mechanophore activation) as described above.

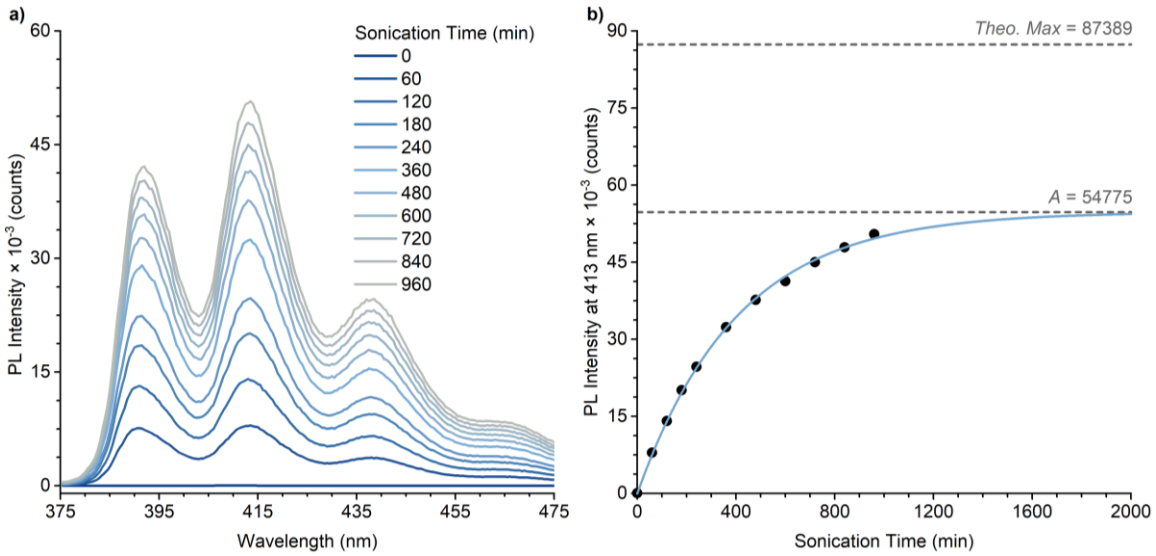

Figure 1.16 (a) Representative PL measurements for polymer **PMA-1** (M_n = 43.3 kg/mol; $Đ$ = 1.05) containing a chain-centered anthracene–maleimide mechanophore. (b) Photoluminescence intensity at 413 nm as a function of ultrasonication time, which is fitted to eq 1.3 to determine the plateau PL intensity, *A*. The predicted plateau value *A* is compared to the maximum theoretical PL intensity determined from the calibration curve and based on the concentration of mechanophore in order to derive percent activation.

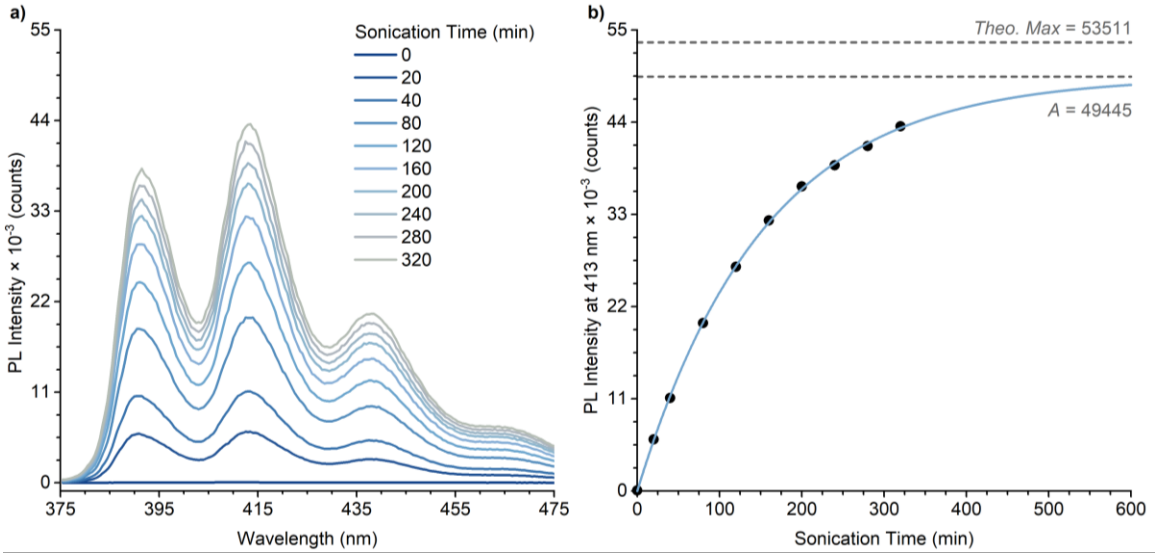

Figure 1.17 (a) Representative PL measurements for polymer **PMA-1** (M_n = 70.7 kg/mol; $Đ$ = 1.07) containing a chain-centered anthracene–maleimide mechanophore. (b) Photoluminescence intensity at 413 nm as a function of ultrasonication time, which is fitted to eq 1.3 to determine the plateau PL intensity, *A*. The predicted plateau value *A* is compared to the maximum theoretical PL intensity determined from the calibration curve and based on the concentration of mechanophore in order to derive percent activation.

1.7.5 Tabulated Data for Determined Rate Constants and M_{thresh} Values

Table 1.2 Rate constants and standard deviation for all ultrasonication experiments.

	$M_{n,0}$ (kDa)	k_{PL} x10^{-3} (min^{-1})	k_M x10^{-3} (min^{-1})	k_{RI} x10^{-3} (min^{-1})	k_L (first half) x10^{-6} (min^{-1})	k_L (full time) x10^{-6} (min^{-1})
PMA-1	43.3	2.3 ± 0.3	--	--	--	--
	70.7	6.4 ± 0.1	8.0 ± 0.6	4.5 ± 0.1	5.2 ± 0.1	4.5 ± 0.3
	87.1	11.5 ± 0.4	15.6 ± 1.2	8.4 ± 0.5	8.0 ± 0.3	6.7 ± 0.2
	108	18.0 ± 1.4	24.3 ± 1.5	14.0 ± 0.5	10.3 ± 0.05	8.0 ± 0.2
	139	32.6 ± 1.5	44.6 ± 0.9	28.5 ± 1.1	14.8 ± 0.5	11.8 ± 0.2
	159	40.2 ± 2.7	55.2 ± 3.0	34.8 ± 2.1	16.8 ± 0.3	13.9 ± 0.3
	201	69.2 ± 4.0	85.3 ± 3.8	65.2 ± 0.9	25.1 ± 0.8	20.0 ± 0.3
	221	73.5 ± 3.8	104.8 ± 4.7	68.2 ± 3.1	27.3 ± 0.4	22.1 ± 0.3
PMA-2 in 3:1 MeCN/ MeOH	78.7	5.0 ± 0.3	6.0 ± 0.5	2.9 ± 0.1	2.9 ± 0.2	2.3 ± 0.1
	111	14.5 ± 2.1	17.3 ± 1.8	11.7 ± 1.9	8.1 ± 0.7	6.4 ± 0.2
	132	26.6 ± 0.3	29.2 ± 2.8	25.0 ± 0.6	12.8 ± 0.6	10.2 ± 0.2
	160	37.2 ± 1.2	40.9 ± 3.1	35.4 ± 3.3	12.9 ± 0.2	10.4 ± 0.2
	180	44.8 ± 1.2	56.5 ± 2.3	44.5 ± 2.4	21.2 ± 0.9	16.9 ± 0.5
	206	52.2 ± 6.0	64.7 ± 5.8	47.1 ± 5.0	21.1 ± 1.9	16.2 ± 1.4

Table 1.3 Values of M_{thresh} (kDa) calculated from linear regressions of specified rate constants.

	k_{PL}	k_{RI}	k_M	k_L (first half)	k_L (full time)
PMA-1 in THF	65	71	65	37	36
PMA-2 in MeCN/MeOH	67	71	71	56	55

1.7.6 Tabulated Characterization Data for All Sonication Experiments

Table 1.4 PL intensity (λ_{em} = 413 nm) for **PMA-1** (M_n = 43.3 kDa) upon ultrasonication in THF.

Sonication time (min)	**Trial 1**	**Trial 2**	**Trial 3**
0	103	52	54
60	7103	7910	6782
120	12722	14111	12549
180	18091	20067	17689
240	23432	24648	22464
360	31164	32365	30680
480	38003	37654	35952
600	43768	41284	40780
720	43668	45002	44404
840	45570	47916	48538
960	48437	50477	51020

Table 1.5 Determined M_n (kDa), PL intensity (λ_{em} = 413 nm), and RI response for **PMA-1** (M_n = 70.7 kDa) upon ultrasonication in THF.

	Trial 1			**Trial 2**			**Trial 3**		
Sonication time (min)	M_n	**PL**	**RI**	M_n	**PL**	**RI**	M_n	**PL**	**RI**
0	71.3	60	1.39	71.7	55	1.33	69.2	61	1.32
20	63.6	6161	1.29	64.0	5770	1.23	65.0	6729	1.24
40	59.7	11106	1.21	60.9	10317	1.17	59.2	11422	1.15
80	51.9	20030	1.00	51.1	19020	0.94	51.1	19544	0.95
120	47.8	26745	0.83	48.5	26028	0.79	46.3	26497	0.78
160	42.1	32288	0.68	43.3	31410	0.65	42.2	31269	0.65
200	37.5	36354	0.56	40.0	35599	0.54	40.5	34620	0.55
240	37.3	38846	0.46	38.5	38574	0.47	37.0	37645	0.48
280	34.7	41164	0.40	37.6	40839	0.42	37.7	39791	0.40
320	33.6	43506	0.34	35.0	41614	0.34	36.0	41857	0.34

Table 1.6 Determined M_n (kDa), PL intensity (λ_{em} = 413 nm), and RI response for **PMA-1** (M_n = 87.1 kDa) upon ultrasonication in THF.

Sonication time (min)	Trial 1			Trial 2			Trial 3		
	M_n	PL	RI	M_n	PL	RI	M_n	PL	RI
0	87.1	--	1.47	86.6	--	1.47	87.8	79	1.43
10	80.5	4204	1.36	81.8	4097	1.38	79.7	4522	1.32
20	75.0	8005	1.27	75.1	7492	1.27	74.2	8442	1.24
40	64.7	14719	1.05	64.2	14271	1.06	65.1	15018	1.05
60	59.3	20288	0.86	59.9	19756	0.88	57.5	20518	0.88
80	51.7	24548	0.72	52.5	23639	0.73	51.8	24775	0.75
100	50.1	27654	0.61	48.3	26815	0.62	48.2	28062	0.64
120	46.6	30010	0.51	48.0	29032	0.51	45.5	30684	0.54
140	43.7	32185	0.45	44.8	30815	0.45	45.1	33072	0.49
160	43.4	33646	0.38	43.3	32938	0.38	43.8	34640	0.43
180	40.6	34889	0.32	42.4	34930	0.31	41.8	35479	0.38

Table 1.7 Determined M_n (kDa), PL intensity (λ_{em} = 413 nm), and RI response for **PMA-1** (M_n = 108 kDa) upon ultrasonication in THF.

Sonication time (min)	Trial 1			Trial 2			Trial 3		
	M_n	PL	RI	M_n	PL	RI	M_n	PL	RI
0	108	55	1.32	109	58	1.34	108	49	1.35
10	94.6	5767	1.18	96.8	5183	1.21	92.7	5687	1.19
20	82.7	10262	1.02	83.0	9365	1.04	80.9	10114	1.03
40	67.8	17370	0.76	69.2	16230	0.78	67.2	17129	0.77
60	61.1	22663	0.56	61.0	21249	0.60	61.6	22418	0.56
80	54.4	26345	0.42	54.9	24866	0.46	54.5	25304	0.43
100	50.8	28052	0.31	51.8	27469	0.34	52.2	27685	0.31
120	48.2	29803	0.25	48.8	29091	0.27	48.9	28785	0.26
140	46.1	31104	0.19	46.6	30411	0.21	47.3	30305	0.19
160	45.7	31697	0.15	43.9	31490	0.18	46.4	30828	0.15

Table 1.8 Determined M_n (kDa), PL intensity (λ_{em} = 413 nm), and RI response for **PMA-1** (M_n = 139 kDa) upon ultrasonication in THF.

Sonication time (min)	Trial 1			Trial 2			Trial 3		
	M_n	PL	RI	M_n	PL	RI	M_n	PL	RI
0	137	--	1.49	140	--	1.48	139	59	1.39
5	117	4149	1.30	119	4300	1.31	122	4208	1.24
10	107	7464	1.14	105	7780	1.13	107	7436	1.10
20	90.7	12780	0.86	90.2	13173	0.84	88.4	12924	0.83
30	77.2	16803	0.64	78.0	17434	0.61	77.6	17269	0.62
40	68.6	19760	0.44	70.2	20083	0.45	71.7	20260	0.46
50	64.6	21967	0.38	65.5	21987	0.33	69.1	22815	0.34
60	64.0	23489	0.26	65.1	22923	0.23	62.2	23980	0.27
70	59.2	24586	0.21	59.8	24127	0.19	59.2	25200	0.21
80	57.7	24834	0.17	57.0	25110	0.15	59.8	25961	0.15
90	56.1	25518	0.13	54.8	25963	0.12	56.3	26552	0.12

Table 1.9 Determined M_n (kDa), PL intensity (λ_{em} = 413 nm), and RI response for **PMA-1** (M_n = 159 kDa) upon ultrasonication in THF.

Sonication time (min)	Trial 1			Trial 2			Trial 3		
	M_n	PL	RI	M_n	PL	RI	M_n	PL	RI
0	160	61	1.29	160	63	1.31	158	45	1.34
5	133	4274	1.13	134	4217	1.14	133	4593	1.12
10	115	7625	0.99	118	7523	0.98	113	8030	0.94
15	103	10448	0.83	106	10306	0.81	102	10889	0.78
20	90.6	12943	0.69	95.1	12725	0.66	92.5	13232	0.65
30	83.0	16375	0.48	82.3	16445	0.45	81.4	16588	0.44
40	74.5	18771	0.34	74.5	18316	0.30	73.4	18850	0.31
50	67.9	20190	0.25	71.0	19804	0.20	66.0	20036	0.22
60	65.0	21182	0.19	65.0	21750	0.15	62.0	21248	0.16
70	62.1	22268	0.14	61.2	22213	0.11	61.9	21842	0.12

Table 1.10 Determined M_n (kDa), PL intensity (λ_{em} = 413 nm), and RI response for **PMA-1** (M_n = 201 kDa) upon ultrasonication in THF.

	Trial 1			**Trial 2**			**Trial 3**		
Sonication time (min)	M_n	**PL**	**RI**	M_n	**PL**	**RI**	M_n	**PL**	**RI**
0	197	54	1.36	202	57	1.37	202	49	1.36
5	147	5286	1.02	147	5730	1.04	155	5387	1.06
10	121	9249	0.74	119	9697	0.74	124	9103	0.79
15	103	12153	0.51	106	12578	0.53	107	12023	0.55
20	90.2	14251	0.36	89.8	14375	0.38	92.6	13855	0.38
25	82.8	15530	0.25	83.3	15805	0.27	87.0	15458	0.25
30	78.8	16811	--	78.2	16732	0.20	77.3	16420	0.17
35	74.0	17312	0.13	74.3	17405	0.14	75.7	17167	0.12
40	68.7	17891	0.09	70.5	17666	0.10	75.1	17446	0.08
45	66.6	--	0.06	69.3	18092	0.07	69.3	17909	0.06
50	65.6	18360	0.05	65.5	18117	0.05	65.4	18213	0.04

Table 1.11 Determined M_n (kDa), PL intensity (λ_{em} = 413 nm), and RI response for **PMA-1** (M_n = 221 kDa) upon ultrasonication in THF.

	Trial 1			**Trial 2**			**Trial 3**		
Sonication time (min)	M_n	**PL**	**RI**	M_n	**PL**	**RI**	M_n	**PL**	**RI**
0	221	57	1.20	220	41	1.22	223	53	1.19
3.33	167	3782	0.99	173	3674	1.00	174	3717	1.01
6.66	141	6716	0.81	143	6438	0.81	145	6673	0.82
10	124	8907	0.63	128	8680	0.65	126	8952	0.65
15	107	11393	0.40	109	11202	0.43	108	11367	0.46
20	95.7	13341	0.27	94.6	13170	0.31	93.9	13179	0.32
25	88.3	14441	0.19	87.5	14234	0.21	85.8	14363	0.23
30	80.8	15237	0.13	81.5	15321	0.15	84.0	15028	0.15
35	74.5	15778	0.11	77.5	15929	0.11	78.3	15544	0.11
40	72.6	16046	0.08	71.2	16332	0.09	74.6	16041	0.09

Table 1.12 Determined M_n (kDa), PL intensity (λ_{em} = 375 nm), and RI response for **PMA-2** (M_n = 78.7 kDa) upon ultrasonication in 3:1 MeCN/MeOH.

Sonication time (min)	Trial 1			Trial 2			Trial 3		
	M_n	PL	RI	M_n	PL	RI	M_n	PL	RI
0	78.8	324.8	1.32	78.5	303.1	1.31	78.7	330.5	1.35
40	68.9	1753.1	1.18	71.8	1716.5	1.21	70.8	1651.4	1.23
80	60.7	2898.8	1.03	63.4	2906.8	1.06	64.5	2727.8	1.09
120	57.1	3908.9	0.91	56.8	3870.0	0.94	58.2	3762.5	0.96
160	54.6	4649.0	0.81	53.5	4746.0	0.82	54.4	4458.3	0.85
200	52.7	5365.1	0.72	49.7	5374.2	0.73	53.2	5116.6	0.77
280	46.5	6332.0	0.58	45.4	6438.3	0.57	48.1	6071.6	0.63
400	44.1	7286.1	0.42	41.9	7456.1	0.40	43.8	7130.5	0.45
440	41.8	7654.6	0.38	41.1	7560.6	0.38	42.3	7537.2	0.40
480	41.0	7783.4	0.32	40.2	7644.0	0.34	40.9	7853.6	0.36

Table 1.13 Determined M_n (kDa), PL intensity (λ_{em} = 375 nm), and RI response for **PMA-2** (M_n = 111 kDa) upon ultrasonication in 3:1 MeCN/MeOH.

Sonication time (min)	Trial 1			Trial 2			Trial 3		
	M_n	PL	RI	M_n	PL	RI	M_n	PL	RI
0	110	229.9	1.41	111	234.2	1.39	113	248.5	1.31
20	82.4	1815.2	1.08	88.1	1710.4	1.13	91.1	1492.4	1.11
40	72.3	2913.2	0.81	74.8	2851.4	0.88	79.4	2532.6	0.91
80	57.9	4266.1	0.48	60.1	4308.0	0.51	63.5	3958.7	0.60
120	51.6	5027.4	0.27	51.4	5220.1	0.31	56.4	4792.0	0.40
160	45.3	5469.0	0.16	46.8	5725.0	0.19	50.7	5398.8	0.28
200	43.9	5744.3	0.12	43.8	6077.4	0.13	46.2	5604.8	0.19
240	41.4	5765.3	0.08	42.5	6245.9	0.10	44.9	5939.7	0.15
260	40.7	5919.6	0.06	41.3	6247.6	0.06	43.8	6222.2	0.13

Table 1.14 Determined M_n (kDa), PL intensity (λ_{em} = 375 nm), and RI response for **PMA-2** (M_n = 132 kDa) upon ultrasonication in 3:1 MeCN/MeOH.

	Trial 1			**Trial 2**			**Trial 3**		
Sonication time (min)	M_n	**PL**	**RI**	M_n	**PL**	**RI**	M_n	**PL**	**RI**
0	131	209.0	1.31	132	222.2	1.30	133	238.3	1.30
10	107	1257.0	1.06	102	1418.0	1.03	99.9	1418.9	1.01
20	92.0	2083.1	0.83	86.1	2269.9	0.79	87.7	2220.4	0.80
40	72.9	3245.2	0.50	69.3	3350.3	0.46	72.0	3213.2	0.47
60	63.0	3982.5	0.29	61.5	4044.6	0.27	64.3	3847.6	0.29
80	56.4	4281.2	0.17	55.1	4433.6	0.16	57.5	4201.8	0.18
100	53.1	4621.7	0.10	50.7	4642.4	0.11	52.9	4500.7	0.11
120	48.5	4742.8	0.07	48.9	4753.9	0.07	48.9	4728.9	0.07
140	46.7	4875.0	0.05	44.9	5132.0	0.05	46.3	4875.3	0.05
160	43.7	4955.9	0.03	44.7	5202.6	0.03	44.9	4921.6	0.04
180	41.5	5079.6	0.03	41.4	5249.5	0.03	43.5	5098.2	0.02

Table 1.15 Determined M_n (kDa), PL intensity (λ_{em} = 375 nm), and RI response for **PMA-2** (M_n = 160 kDa) upon ultrasonication in 3:1 MeCN/MeOH.

	Trial 1			**Trial 2**			**Trial 3**		
Sonication time (min)	M_n	**PL**	**RI**	M_n	**PL**	**RI**	M_n	**PL**	**RI**
0	156	152.0	1.27	160	179.12	1.27	163	218.3	1.27
10	118	1412.5	0.91	117	1411.6	0.91	116	1435.7	0.92
20	96.2	2260.0	0.61	93.5	2339.8	0.61	96.7	2258.5	0.66
40	75.7	3293.4	0.26	73.2	3276.4	0.27	75.8	3220.4	0.35
60	65.0	3753.7	0.12	63.3	3663.7	0.13	66.0	3569.3	0.19
80	57.6	4010.9	0.07	58.2	3918.8	0.07	58.0	3854.4	0.12
100	52.5	4266.2	0.04	53.1	4115.5	0.04	54.3	3984.8	0.08
120	50.0	4309.1	0.03	49.6	4299.7	0.03	51.2	4161.0	0.05
140	46.8	4354.4	0.02	46.4	4419.4	0.02	48.4	4227.5	0.03
160	45.3	4302.0	0.01	44.2	4266.4	0.02	44.4	4237.5	0.02

Table 1.16 Determined M_n (kDa), PL intensity (λ_{em} = 375 nm), and RI response for **PMA-2** (M_n = 180 kDa) upon ultrasonication in 3:1 MeCN/MeOH.

	Trial 1			**Trial 2**			**Trial 3**		
Sonication time (min)	M_n	**PL**	**RI**	M_n	**PL**	**RI**	M_n	**PL**	**RI**
0	179	145.4	1.38	181	145.4	1.37	180	146.3	1.38
5	146	906.1	1.15	154	861.0	1.12	148	816.2	1.15
10	123	1549.2	0.94	124	1466.5	0.96	123	1413.7	0.92
20	97.9	2465.6	0.59	92.4	2468.7	0.61	97.9	2240.4	0.56
30	81.5	3071.9	0.36	81.6	3032.5	0.38	83.0	2807.2	0.33
40	74.5	3454.1	0.22	72.6	3370.3	0.24	76.8	3055.3	0.20
50	68.5	3763.1	0.15	66.6	3694.9	0.15	69.2	3346.6	0.11
60	63.3	3963.5	0.10	63.4	3847.1	0.09	64.4	3488.7	0.07
70	59.3	4046.6	0.06	59.2	3950.5	0.06	61.8	3624.6	0.04
80	56.8	4159.4	0.04	56.0	3982.3	0.04	57.4	3672.7	0.03

Table 1.17 Determined M_n (kDa), PL intensity (λ_{em} = 375 nm), and RI response for **PMA-2** (M_n = 206 kDa) upon ultrasonication in 3:1 MeCN/MeOH.

	Trial 1			**Trial 2**			**Trial 3**		
Sonication time (min)	M_n	**PL**	**RI**	M_n	**PL**	**RI**	M_n	**PL**	**RI**
0	203	154.4	1.23	208	136.7	1.20	206	130.3	1.22
5	155	901.3	0.99	164	877.7	1.00	159	768.6	1.03
10	126	1450.3	0.76	140	1436.0	0.82	137	1292.6	0.83
20	96.3	2169.9	0.42	110	2262.1	0.51	107	2050.4	0.53
30	82.4	2566.8	0.24	92.8	2755.3	0.30	89.8	2489.6	0.33
40	76.0	2882.3	0.15	80.9	3123.7	0.19	80.8	2794.2	0.19
50	68.5	2934.9	0.09	76.2	3269.8	0.11	75.8	3004.9	0.13
60	64.6	3028.1	0.06	71.6	3412.6	0.08	71.3	3098.9	0.09
70	60.6	3186.6	0.03	68.0	3540.6	0.05	65.1	3207.1	0.07
80	57.4	3190.6	0.03	64.0	3623.9	0.03	63.5	3264.2	0.05

1.8 References

(1) Caruso, M. M.; Davis, D. A.; Shen, Q.; Odom, S. A.; Sottos, N. R.; White, S. R.; Moore, J. S. Mechanically-Induced Chemical Changes in Polymeric Materials. *Chem. Rev.* **2009**, *109*, 5755–5798.

(2) Beyer, M. K.; Clausen-Schaumann, H. Mechanochemistry: The Mechanical Activation of Covalent Bonds. *Chem. Rev.* **2005**, *105*, 2921–2948.

(3) Li, J.; Nagamani, C.; Moore, J. S. Polymer Mechanochemistry: From Destructive to Productive. *Acc. Chem. Res.* **2015**, *48*, 2181–2190.

(4) May, P. A.; Moore, J. S. Polymer mechanochemistry: techniques to generate molecular force via elongational flows. *Chem. Soc. Rev.* **2013**, *42*, 7497–7506.

(5) Ghanem, M. A.; Basu, A.; Behrou, R.; Boechler, N.; Boydston, A. J.; Craig, S. L.; Lin, Y.; Lynde, B. E.; Nelson, A.; Shen, H.; Storti, D. W. The role of polymer mechanochemistry in responsive materials and additive manufacturing. *Nat. Rev. Mater.* **2021**, *6*, 84–98.

(6) Chen, Y.; Mellot, G.; Luijk, D. van; Creton, C.; Sijbesma, R. P. Mechanochemical tools for polymer materials. *Chem. Soc. Rev.* **2021**, *50*, 4100–4140.

(7) Izak-Nau, E.; Campagna, D.; Baumann, C.; Göstl, R. Polymer mechanochemistry-enabled pericyclic reactions. *Polym. Chem.* **2020**, *11*, 2274–2299.

(8) Berkowski, K. L.; Potisek, S. L.; Hickenboth, C. R.; Moore, J. S. Ultrasound-Induced Site-Specific Cleavage of Azo-Functionalized Poly(ethylene glycol). *Macromolecules* **2005**, *38*, 8975–8978.

(9) Kryger, M. J.; Munaretto, A. M.; Moore, J. S. Structure–Mechanochemical Activity Relationships for Cyclobutane Mechanophores. *J. Am. Chem. Soc.* **2011**, *133*, 18992–18998.

(10) Black, A. L.; Orlicki, J. A.; Craig, S. L. Mechanochemically triggered bond formation in solid-state polymers. *J. Mater. Chem.* **2011**, *21*, 8460–8465.

(11) Robb, M. J.; Kim, T. A.; Halmes, A. J.; White, S. R.; Sottos, N. R.; Moore, J. S. Regioisomer-Specific Mechanochromism of Naphthopyran in Polymeric Materials. *J. Am. Chem. Soc.* **2016**, *138*, 12328–12331.

(12) Stevenson, R.; De Bo, G. Controlling Reactivity by Geometry in Retro-Diels–Alder Reactions under Tension. *J. Am. Chem. Soc.* **2017**, *139*, 16768–16771.

(13) Lin, Y.; Barbee, M. H.; Chang, C.-C.; Craig, S. L. Regiochemical Effects on Mechanophore Activation in Bulk Materials. *J. Am. Chem. Soc.* **2018**, *140*, 15969–15975.

(14) Barbee, M. H.; Kouznetsova, T.; Barrett, S. L.; Gossweiler, G. R.; Lin, Y.; Rastogi, S. K.; Brittain, W. J.; Craig, S. L. Substituent Effects and Mechanism in a Mechanochemical Reaction. *J. Am. Chem. Soc.* **2018**, *140*, 12746–12750.

(15) Konda, S. S. M.; Brantley, J. N.; Varghese, B. T.; Wiggins, K. M.; Bielawski, C. W.; Makarov, D. E. Molecular Catch Bonds and the Anti-Hammond Effect in Polymer Mechanochemistry. *J. Am. Chem. Soc.* **2013**, *135*, 12722–12729.

(16) Versaw, B. A.; McFadden, M. E.; Husic, C. C.; Robb, M. J. Designing naphthopyran mechanophores with tunable mechanochromic behavior. *Chem. Sci.* **2020**, *11*, 4525–4530.

(17) Lenhardt, J. M.; Black Ramirez, A. L.; Lee, B.; Kouznetsova, T. B.; Craig, S. L. Mechanistic Insights into the Sonochemical Activation of Multimechanophore Cyclopropanated Polybutadiene Polymers. *Macromolecules* **2015**, *48*, 6396–6403.

(18) Basedow, A. M.; Ebert, K. H. Ultrasonic degradation of polymers in solution. *Adv. Polym. Sci.* **1977**, *22*, 83–148.

(19) Odell, J. A.; Keller, A. Flow-induced chain fracture of isolated linear macromolecules in solution. *J. Polym. Sci. Polym. Phys.* **1986**, *24*, 1889–1916.

(20) May, P. A.; Munaretto, N. F.; Hamoy, M. B.; Robb, M. J.; Moore, J. S. Is Molecular Weight or Degree of Polymerization a Better Descriptor of Ultrasound-Induced Mechanochemical Transduction? *ACS Macro Lett.* **2016**, *5*, 177–180.

(21) Schaefer, M.; Icli, B.; Weder, C.; Lattuada, M.; Kilbinger, A. F. M.; Simon, Y. C. The Role of Mass and Length in the Sonochemistry of Polymers. *Macromolecules* **2016**, *49*, 1630–1636.

(22) Göstl, R.; Sijbesma, R. P. π-extended anthracenes as sensitive probes for mechanical stress. *Chem. Sci.* **2015**, *7*, 370–375.

(23) Pan, Y.; Zhang, H.; Xu, P.; Tian, Y.; Wang, C.; Xiang, S.; Boulatov, R.; Weng, W. A Mechanochemical Reaction Cascade for Controlling Load-Strengthening of a Mechanochromic Polymer. *Angew. Chem. Int. Ed.* **2020**, *59*, 21980–21985.

(24) McFadden, M. E.; Robb, M. J. Generation of an Elusive Permanent Merocyanine via a Unique Mechanochemical Reaction Pathway. *J. Am. Chem. Soc.* **2021**, *143*, 7925–7929.

(25) Li, J.; Shiraki, T.; Hu, B.; Wright, R. A. E.; Zhao, B.; Moore, J. S. Mechanophore Activation at Heterointerfaces. *J. Am. Chem. Soc.* **2014**, *136*, 15925–15928.

(26) Church, D. C.; Peterson, G. I.; Boydston, A. J. Comparison of Mechanochemical Chain Scission Rates for Linear versus Three-Arm Star Polymers in Strong Acoustic Fields. *ACS Macro Lett.* **2014**, *3*, 648–651.

(27) Hu, X.; Zeng, T.; Husic, C. C.; Robb, M. J. Mechanically Triggered Small Molecule Release from a Masked Furfuryl Carbonate. *J. Am. Chem. Soc.* **2019**, *141*, 15018–15023.

(28) Zhang, H.; Li, X.; Lin, Y.; Gao, F.; Tang, Z.; Su, P.; Zhang, W.; Xu, Y.; Weng, W.; Boulatov, R. Multi-modal mechanophores based on cinnamate dimers. *Nat. Commun.* **2017**, *8*, 1147.

(29) Lenhardt, J. M.; Black, A. L.; Craig, S. L. gem-Dichlorocyclopropanes as Abundant and Efficient Mechanophores in Polybutadiene Copolymers under Mechanical Stress. *J. Am. Chem. Soc.* **2009**, *131*, 10818–10819.

(30) Lenhardt, J. M.; Ogle, J. W.; Ong, M. T.; Choe, R.; Martinez, T. J.; Craig, S. L. Reactive Cross-Talk between Adjacent Tension-Trapped Transition States. *J. Am. Chem. Soc.* **2011**, *133*, 3222–3225.

(31) Kean, Z. S.; Gossweiler, G. R.; Kouznetsova, T. B.; Hewage, G. B.; Craig, S. L. A Coumarin Dimer Probe of Mechanochemical Scission Efficiency in the Sonochemical Activation of Chain-Centered Mechanophore Polymers. *Chem. Commun.* **2015**, *51*, 9157–9160.

(32) Chen, Z.; Zhu, X.; Yang, J.; Mercer, J. A. M.; Burns, N. Z.; Martinez, T. J.; Xia, Y. The cascade unzipping of ladderane reveals dynamic effects in mechanochemistry. *Nat. Chem.* **2020**, *12*, 302–309.

(33) Sha, Y.; Zhang, Y.; Xu, E.; Wang, Z.; Zhu, T.; Craig, S. L.; Tang, C. Quantitative and Mechanistic Mechanochemistry in Ferrocene Dissociation. *ACS Macro Lett.* **2018**, *7*, 1174–1179.

(34) Hu, X.; McFadden, M. E.; Barber, R. W.; Robb, M. J. Mechanochemical Regulation of a Photochemical Reaction. *J. Am. Chem. Soc.* **2018**, *140*, 14073–14077.

(35) Kryger, M. J.; Ong, M. T.; Odom, S. A.; Sottos, N. R.; White, S. R.; Martinez, T. J.; Moore, J. S. Masked Cyanoacrylates Unveiled by Mechanical Force. *J. Am. Chem. Soc.* **2010**, *132*, 4558–4559.

(36) Kida, J.; Imato, K.; Goseki, R.; Aoki, D.; Morimoto, M.; Otsuka, H. The photoregulation of a mechanochemical polymer scission. *Nat. Commun.* **2018**, *9*, 1–6.

(37) Robb, M. J.; Moore, J. S. A Retro-Staudinger Cycloaddition: Mechanochemical Cycloelimination of a β-Lactam Mechanophore. *J. Am. Chem. Soc.* **2015**, *137*, 10946–10949.

(38) Zhang, M.; De Bo, G. Mechanical Susceptibility of a Rotaxane. *J. Am. Chem. Soc.* **2019**, *141*, 15879–15883.

(39) Lee, B.; Niu, Z.; Wang, J.; Slebodnick, C.; Craig, S. L. Relative Mechanical Strengths of Weak Bonds in Sonochemical Polymer Mechanochemistry. *J. Am. Chem. Soc.* **2015**, *137*, 10826–10832.

(40) Duan, H.-Y.; Wang, Y.-X.; Wang, L.-J.; Min, Y.-Q.; Zhang, X.-H.; Du, B.-Y. An Investigation of the Selective Chain Scission at Centered Diels–Alder Mechanophore under Ultrasonication. *Macromolecules* **2017**, *50*, 1353–1361.

(41) Levy, A.; Wang, F.; Lang, A.; Galant, O.; Diesendruck, C. E. Intramolecular Cross-Linking: Addressing Mechanochemistry with a Bioinspired Approach. *Angew. Chem. Int. Ed.* **2017**, *56*, 6431–6434.

(42) Wang, F.; Burck, M.; Diesendruck, C. E. Following Homolytic Mechanochemical Kinetics with a Pyrenyl Nitrone Spin Trap. *ACS Macro Lett.* **2017**, *6*, 42–45.

(43) Levy, A.; Gaver, E.; Wang, F.; Galant, O.; Diesendruck, C. E. The effect of intramolecular cross links on the mechanochemical fragmentation of polymers in solution. *Chem. Commun.* **2017**, *53*, 10132–10135.

(44) Baumann, C.; Göstl, R. Triazole-Extended Anthracenes as Optical Force Probes. *Synlett* **2021**, *32*, DOI: 10.1055/s-0040-1720924.

(45) Nagamani, C.; Liu, H.; Moore, J. S. Mechanogeneration of Acid from Oxime Sulfonates. *J. Am. Chem. Soc.* **2016**, *138*, 2540–2543.

(46) Tan, M.; Hu, Z.; Dai, Y.; Peng, Y.; Zhou, Y.; Shi, Y.; Li, Y.; Chen, Y. A Simple Mechanochromic Mechanophore Based on Aminothiomaleimide. *ACS Macro Lett.* **2021**, 1423–1428.

(47) Karman, M.; Verde-Sesto, E.; Weder, C.; Simon, Y. C. Mechanochemical Fluorescence Switching in Polymers Containing Dithiomaleimide Moieties. *ACS Macro Lett.* **2018**, *7*, 1099–1104.

(48) Jellinek, H. H. G. Degradation of high polymers. *J. Polym. Sci.* **1950**, *5*, 264–265.

(49) Haward, R. N. Degradation of ethyl cellulose in solution. *J. Polym. Sci.* **1950**, *5*, 635–636.

(50) Sato, T.; Nalepa, D. E. Shear degradation of cellulose derivatives. *J. Appl. Polym. Sci.* **1978**, *22*, 865–867.

(51) Akbulatov, S.; Boulatov, R. Experimental Polymer Mechanochemistry and its Interpretational Frameworks. *ChemPhysChem* **2017**, *18*, 1422–1450.

(52) Malhotra, S. L. Ultrasonic Solution Degradations of Poly(Alkyl Methacrylates). *J. Macromol. Sci., Chem. A.* **1986**, *23*, 729–748.

(53) Akyüz, A.; Catalgil-Giz, H.; Giz, A. T. Kinetics of Ultrasonic Polymer Degradation: Comparison of Theoretical Models with On-Line Data. *Macromol. Chem. Phys.* **2008**, *209*, 801–809.

(54) Ayer, M. A.; Verde-Sesto, E.; Liu, C. H.; Weder, C.; Lattuada, M.; Simon, Y. C. Modeling ultrasound-induced molecular weight decrease of polymers with multiple scissile azo-mechanophores. *Polym. Chem.* **2021**, *12*, 4093–4103.

(55) Florea, M. New use of size exclusion chromatography in kinetics of mechanical degradation of polymers in solution. *J. Appl. Polym. Sci.* **1993**, *50*, 2039–2045.

(56) Peterson, G. I.; Bang, K.-T.; Choi, T.-L. Mechanochemical Degradation of Denpols: Synthesis and Ultrasound-Induced Chain Scission of Polyphenylene-Based Dendronized Polymers. *J. Am. Chem. Soc.* **2018**, *140*, 8599–8608.

(57) Peterson, G. I.; Noh, J.; Bang, K.-T.; Ma, H.; Kim, K. T.; Choi, T.-L. Mechanochemical Degradation of Brush Polymers: Kinetics of Ultrasound-Induced Backbone and Arm Scission. *Macromolecules* **2020**, *53*, 1623–1628.

(58) Peterson, G. I.; Lee, J.; Choi, T.-L. Multimechanophore Graft Polymers: Mechanochemical Reactions at Backbone–Arm Junctions. *Macromolecules* **2019**, *52*, 9561–9568.

(59) Wang, Z.; Craig, S. L. Stereochemical effects on the mechanochemical scission of furan–maleimide Diels–Alder adducts. *Chem. Commun.* **2019**, *55*, 12263–12266.

(60) Sung, J.; Robb, M. J.; White, S. R.; Moore, J. S.; Sottos, N. R. Interfacial Mechanophore Activation Using Laser-Induced Stress Waves. *J. Am. Chem. Soc.* **2018**, *140*, 5000–5003.

(61) Kabb, C. P.; O'Bryan, C. S.; Morley, C. D.; Angelini, T. E.; Sumerlin, B. S. Anthracene-based mechanophores for compression-activated fluorescence in polymeric networks. *Chem. Sci.* **2019**, *10*, 7702–7708.

(62) Yang, J.; Horst, M.; Werby, S. H.; Cegelski, L.; Burns, N. Z.; Xia, Y. Bicyclohexene-peri-naphthalenes: Scalable Synthesis, Diverse Functionalization, Efficient Polymerization, and Facile Mechanoactivation of Their Polymers. *J. Am. Chem. Soc.* **2020**, *142*, 14619–14626.

(63) Gossweiler, G. R.; Kouznetsova, T. B.; Craig, S. L. Force-Rate Characterization of Two Spiropyran-Based Molecular Force Probes. *J. Am. Chem. Soc.* **2015**, *137*, 6148–6151.

(64) Wang, L.; Yu, Y.; Razgoniaev, A. O.; Johnson, P. N.; Wang, C.; Tian, Y.; Boulatov, R.; Craig, S. L.; Widenhoefer, R. A. Mechanochemical Regulation of Oxidative Addition to a Palladium(0) Bisphosphine Complex. *J. Am. Chem. Soc.* **2020**, *142*, 17714–17720.

(65) Li, J.; Shiraki, T.; Hu, B.; Wright, R. A. E.; Zhao, B.; Moore, J. S. Mechanophore Activation at Heterointerfaces. *J. Am. Chem. Soc.* **2014**, *136*, 15925–15928.

(66) Holden, D. A.; Guillet, J. E. Singlet Electronic Energy Transfer in Polymers Containing Naphthalene and Anthracene Chromophores. *Macromolecules* **1980**, *13*, 289–295.

(67) Shaughnessy, K. H.; Kim, P.; Hartwig, J. F. A Fluorescence-Based Assay for High-Throughput Screening of Coupling Reactions. Application to Heck Chemistry. *J. Am. Chem. Soc.* **1999**, *121*, 2123–2132.

(68) Nguyen, N. H.; Rosen, B. M.; Lligadas, G.; Percec, V. Surface-Dependent Kinetics of Cu(0)-Wire-Catalyzed Single-Electron Transfer Living Radical Polymerization of Methyl Acrylate in DMSO at 25 °C. *Macromolecules* **2009**, *42*, 2379–2386.

Appendix A

Spectra Relevant to Chapter 1: Quantifying Activation Rates of Scissile Mechanophore and the Influence of Dispersity

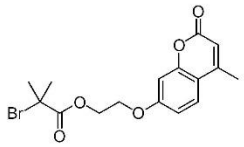

S5

^{1}H (400 MHz, $CDCl_3$)

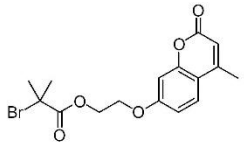

S5

^{13}C (101 MHz, $CDCl_3$)

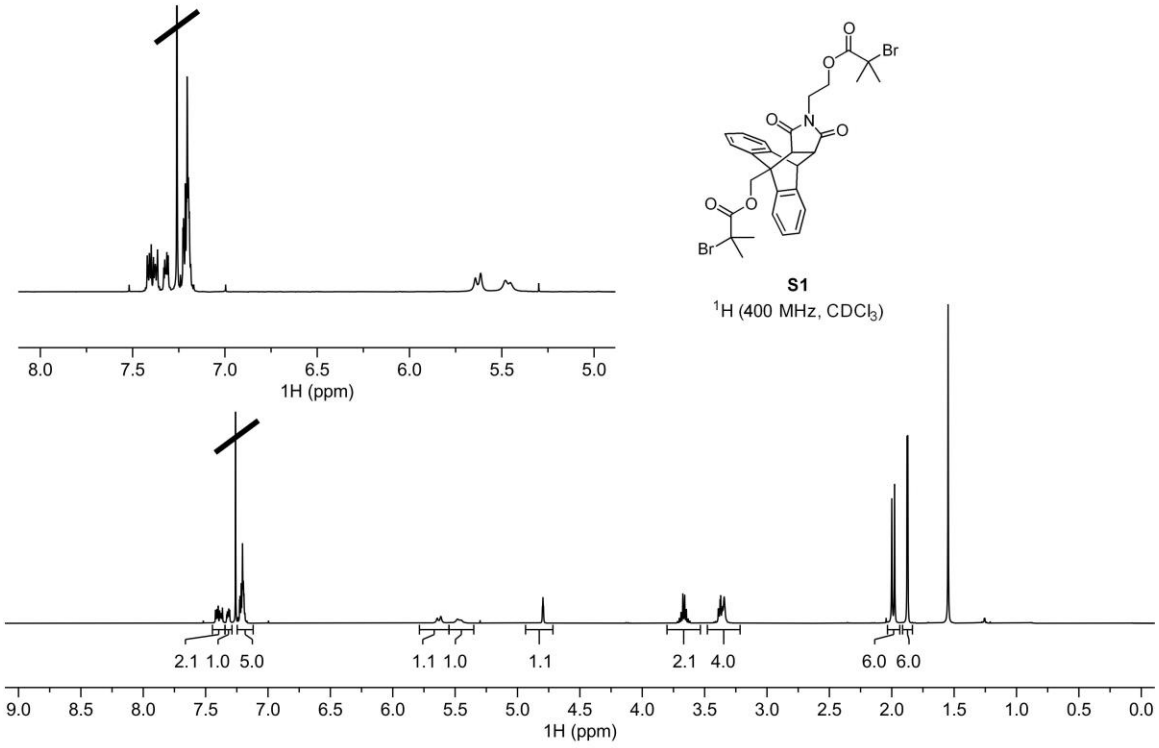
Br
O
N
Br
S1
1H (400 MHz, CDCl3)
8.0 7.5 7.0 6.5 6.0 5.5 5.0
1H (ppm)
2.1 1.0 5.0
1.1 1.0
1.1
2.1 4.0
6.0 6.0
9.0 8.5 8.0 7.5 7.0 6.5 6.0 5.5 5.0 4.5 4.0 3.5 3.0 2.5 2.0 1.5 1.0 0.5 0.0
1H (ppm)

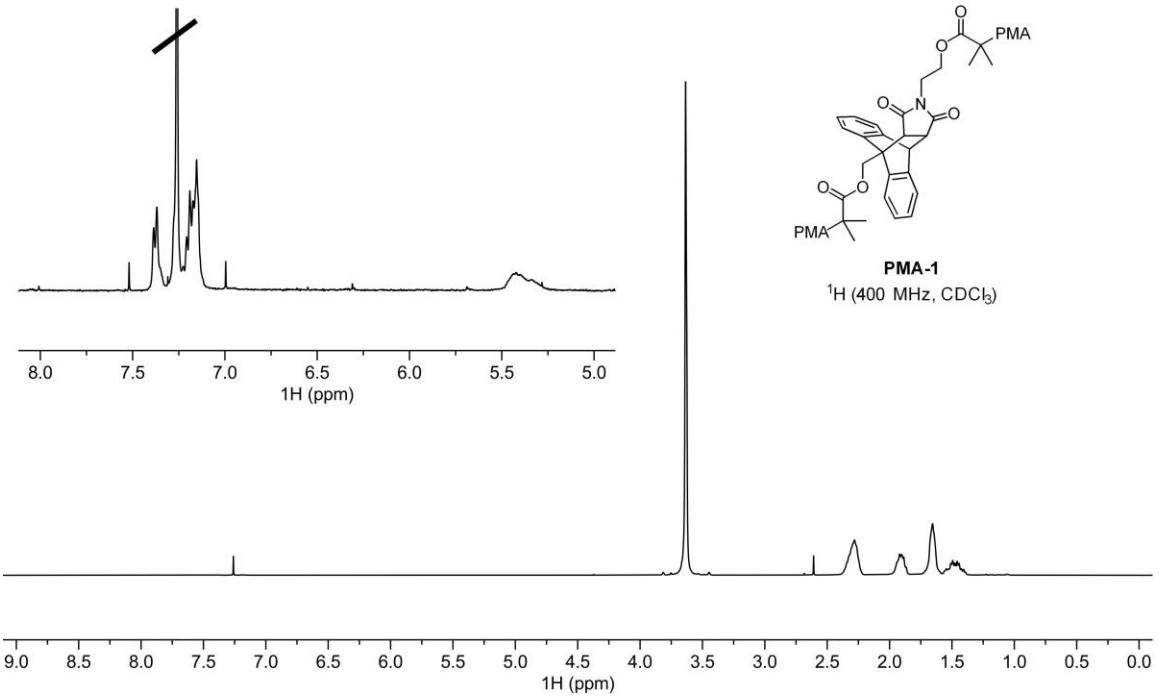
PMA
PMA-1
1H (400 MHz, CDCl3)
8.0 7.5 7.0 6.5 6.0 5.5 5.0
1H (ppm)
9.0 8.5 8.0 7.5 7.0 6.5 6.0 5.5 5.0 4.5 4.0 3.5 3.0 2.5 2.0 1.5 1.0 0.5 0.0
1H (ppm)

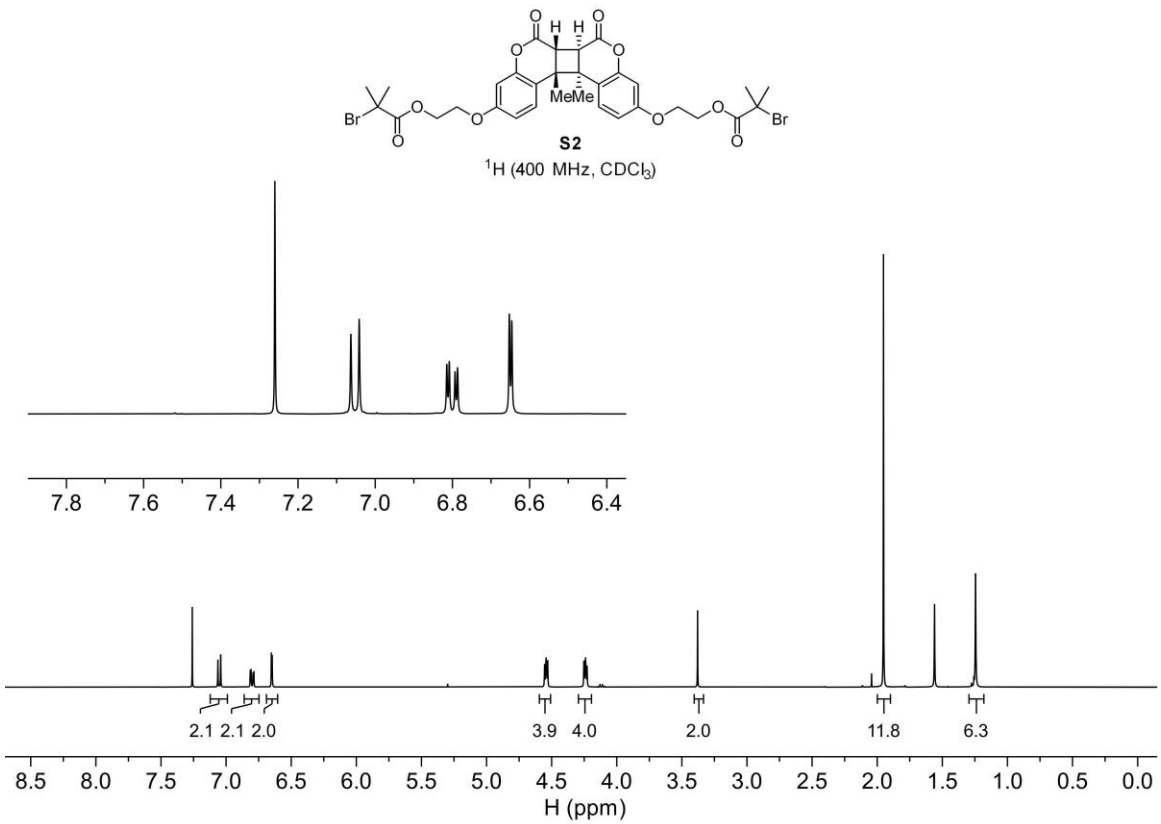
S2
1H (400 MHz, CDCl3)
2.1 2.1 2.0
3.9 4.0
2.0
11.8
6.3
H (ppm)

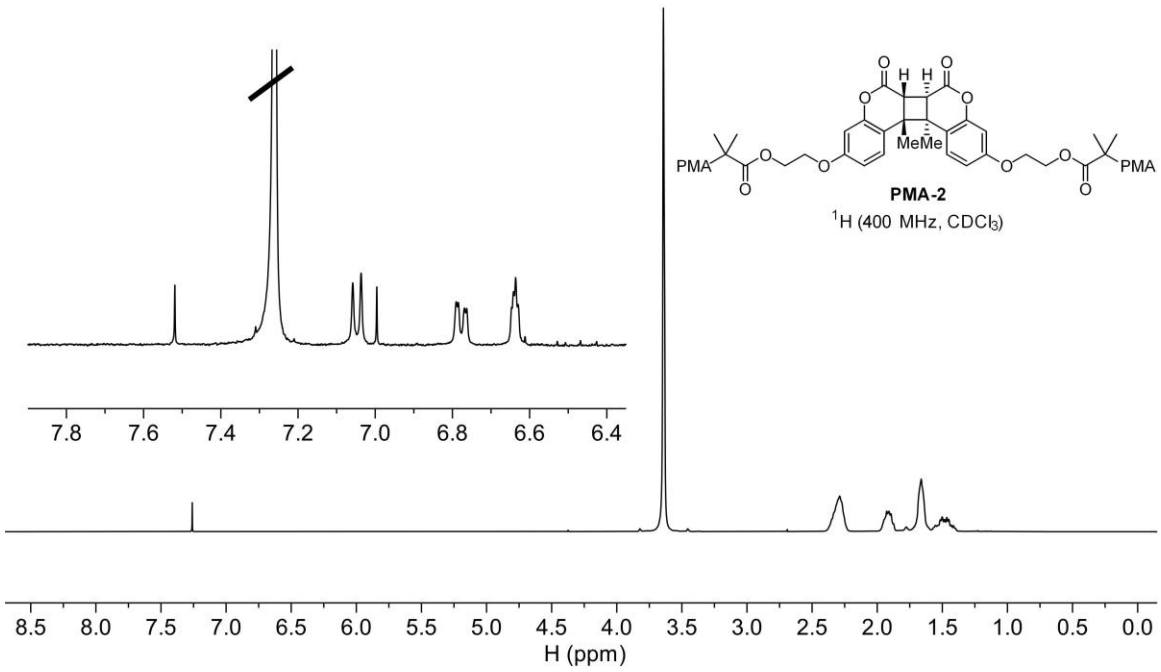
PMA-2
1H (400 MHz, CDCl3)
H (ppm)

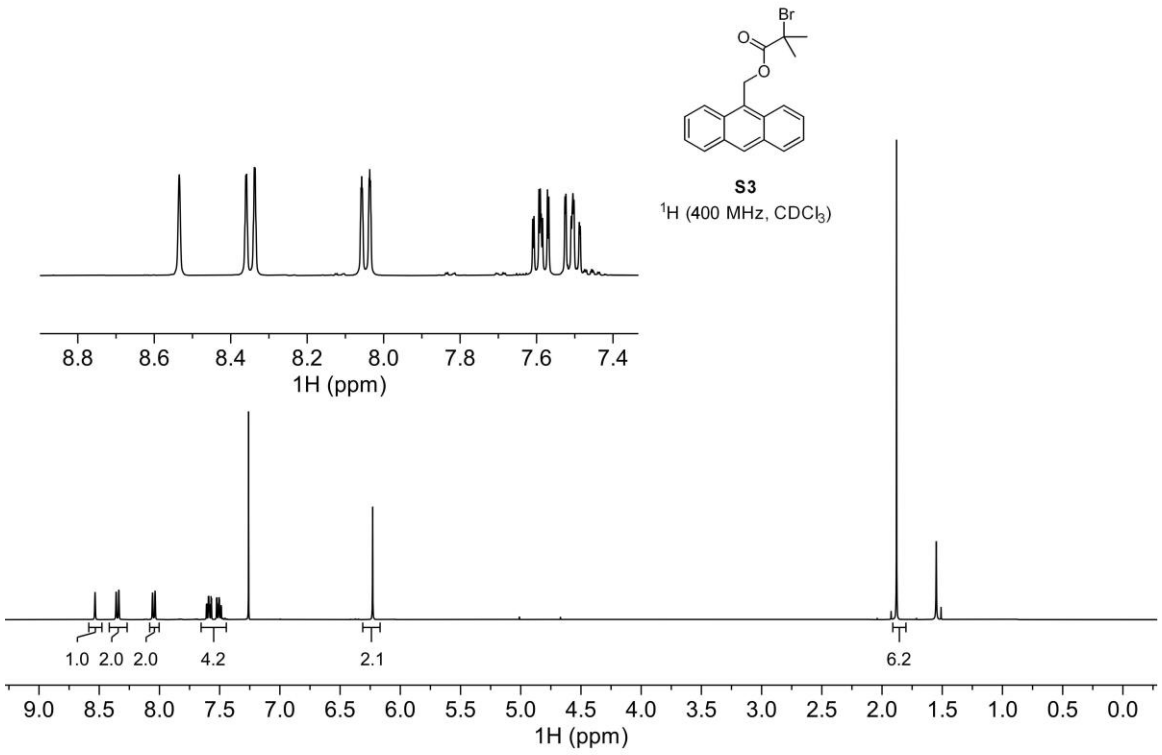
Br
O
O
S3
1H (400 MHz, CDCl3)
8.8 8.6 8.4 8.2 8.0 7.8 7.6 7.4
1H (ppm)
1.0 2.0 2.0 4.2 2.1 6.2
9.0 8.5 8.0 7.5 7.0 6.5 6.0 5.5 5.0 4.5 4.0 3.5 3.0 2.5 2.0 1.5 1.0 0.5 0.0
1H (ppm)

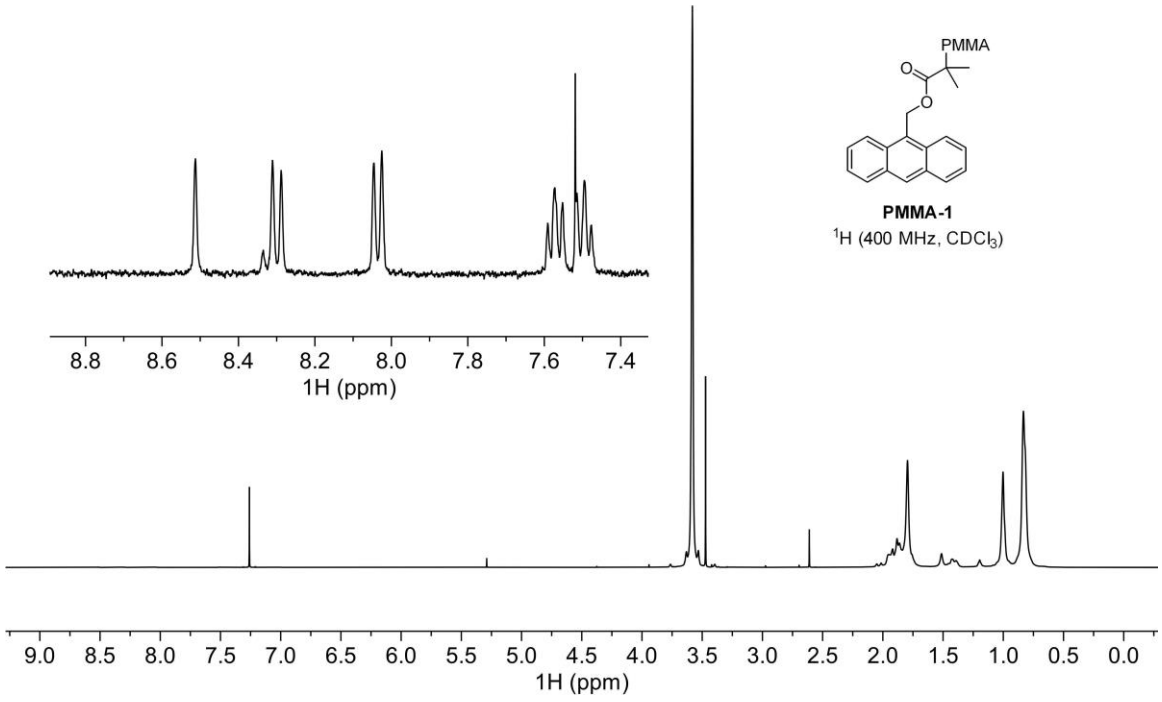
PMMA
O
O
PMMA-1
1H (400 MHz, CDCl3)
8.8 8.6 8.4 8.2 8.0 7.8 7.6 7.4
1H (ppm)
9.0 8.5 8.0 7.5 7.0 6.5 6.0 5.5 5.0 4.5 4.0 3.5 3.0 2.5 2.0 1.5 1.0 0.5 0.0
1H (ppm)

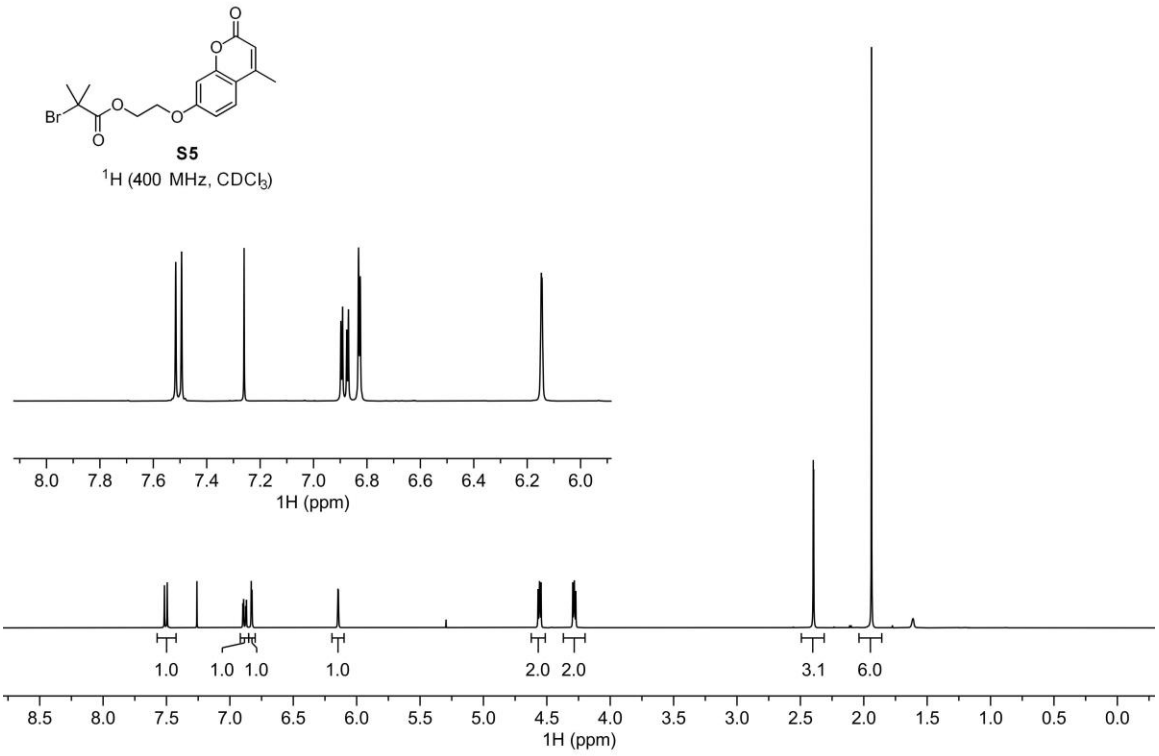
Br
O
O
O
O
O
S5
1H (400 MHz, CDCl3)
8.0 7.8 7.6 7.4 7.2 7.0 6.8 6.6 6.4 6.2 6.0
1H (ppm)
1.0 1.0 1.0 1.0 2.0 2.0 3.1 6.0
8.5 8.0 7.5 7.0 6.5 6.0 5.5 5.0 4.5 4.0 3.5 3.0 2.5 2.0 1.5 1.0 0.5 0.0
1H (ppm)

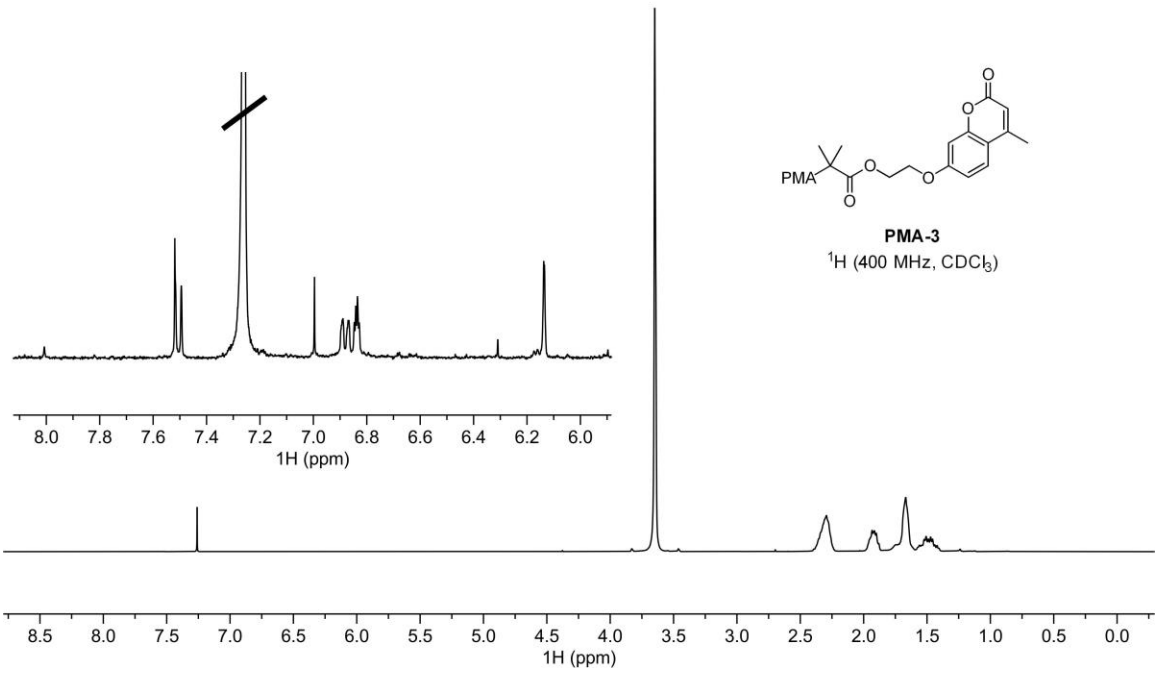
PMA
O
O
O
O
PMA-3
1H (400 MHz, CDCl3)
8.0 7.8 7.6 7.4 7.2 7.0 6.8 6.6 6.4 6.2 6.0
1H (ppm)
8.5 8.0 7.5 7.0 6.5 6.0 5.5 5.0 4.5 4.0 3.5 3.0 2.5 2.0 1.5 1.0 0.5 0.0
1H (ppm)

Chapter 2

EXAMINING THE IMPACT OF RELATIVE MECHANOPHORE ACTIVATION ON THE SELECTIVITY OF ULTRASOUND-INDUCED MECHANOCHEMICAL CHAIN SCISSION[1]

Despite recent advances in polymer mechanochemistry, a more complete understanding of the factors that dictate the ultrasound-induced mechanochemical activation efficiency of mechanophores is necessary. Here, we examine how the identity of a mechanophore, and hence its unique force-coupled reactivity, affects the competition between mechanophore activation and nonspecific polymer backbone scission. Polymers incorporating distinct mechanophores but with putatively similar "chain-centeredness" exhibit widely different mechanochemical activation efficiencies. Furthermore, we employ mechanophores that can be orthogonally cleaved following ultrasonication using heat or light to report on the degree of nonspecific backbone scission that occurs for different mechanophore-containing polymers subjected to ultrasound-induced mechanical force. Our results illustrate that the identity of the mechanophore as well as its position in the polymer chain are inextricably important parameters that together control the selectivity of mechanophore activation during ultrasonication.

---

[1] Portions of this chapter were adapted from Overholts, A. C. and Robb, M. J. Examining the impact of relative mechanophore activation on the selectivity of ultrasound-induced mechanochemical chain scission. *ACS Macro Letters* **2022**, *11*, 733-738. https://doi.org/10.1021/acsmacrolett.2c00217.

2.1 Introduction

Mechanical force is typically considered destructive, causing the degradation of polymeric materials by rupturing covalent bonds in polymer chains. The incorporation of stress-sensitive molecules called mechanophores into the backbones of polymers, however, facilitates the transduction of mechanical force into a productive chemical response.[1,2] Central to the mechanophore hypothesis is the realization of mechanically selective scission of weak bonds within the mechanophore scaffold over the cleavage of covalent bonds elsewhere in the polymer backbone.[3] An early report by Encina characterized the effect of weak peroxide linkages in a polyvinylpyrrolidone backbone that were installed to increase the rate of polymer chain scission under mechanical force.[4] In 2005, Moore and coworkers advanced this concept by demonstrating the site-specific chain scission of a polymer incorporating a relatively weak azo group upon ultrasound-induced mechanical activation.[5] The mechanophore concept was cemented in 2007 with the introduction of benzocyclobutene mechanochemistry, in which the mechanical scission of a weak bond in the benzocyclobutene unit promotes a formal electrocyclic ring-opening reaction to generate a reactive *ortho*-quinodimethide intermediate.[6] This burgeoning field of research has since produced more than one hundred different mechanophores with a broad range of force-coupled reactivity and functionality.[7,8]

Ultrasound-induced mechanical activation of polymers in dilute solution is a useful and common technique for characterizing the reactivity of mechanophores. Solvodynamic shear resulting from cavitation exerts elongational forces on linear polymers that are maximized near the chain midpoint.[9] Polymers are commonly prepared by controlled radical polymerization from a mechanophore bis-initiator, which is expected to incorporate

a single mechanophore unit near the chain midpoint to facilitate efficient mechanical activation during ultrasonication.[3,10] This common notion originates from research on the ultrasonic degradation of polystyrene, in which models indicated that chain cleavage occurred with the greatest probability within 15% of the center of the polymer.[11] Nevertheless, forces large enough to achieve covalent bond activation are distributed over a substantial portion of the polymer chain.[12] Multimechanophore polymers that incorporate many non-scissile mechanophore units along the length of the polymer backbone have been demonstrated to achieve over 80% activation upon ultrasonication.[13] This observation is also consistent with the original report from Moore and coworkers demonstrating selective cleavage at the azo group even when it was located 10 kDa from the center of a 40 kDa poly(ethylene glycol) chain.[5]

The position of the mechanophore unit in a polymer backbone has previously been implicated as a principal factor that affects the efficiency of ultrasound-induced mechanophore activation relative to nonspecific backbone scission. In 2015, Craig and coworkers studied how the spatial distribution of a coumarin dimer mechanophore in polymers synthesized by controlled radical polymerization affects mechanochemical activation efficiency.[14] Despite the polymers having a relatively narrow dispersity of 1.12 that may otherwise indicate a high degree of "chain-centeredness," a low mechanophore activation efficiency of ~35% was observed. The authors speculated that undesired termination processes during polymerization could account for a significant fraction of chains containing an off-center mechanophore. Indeed, fractionating the polymer improved the activation efficiency to ~50%. Modeling further indicated that the proportion of coumarin dimer units located in the middle 15% of the chains increased from 46% to 63%

upon fractionation, consistent with the observed increase in mechanophore activation efficiency. While these results confirmed that the position of the mechanophore plays an important role, the force-coupled reactivity of the mechanophore is also anticipated to be a critical factor in determining activation efficiency due to the distribution of force along a polymer chain.[12,14,15] To the best of our knowledge, this latter point has not been satisfactorily addressed for polymers incorporating a single mechanophore.

Here, we study the competition between mechanophore activation and nonspecific backbone scission for a series of scissile mechanophores with putatively different reactivity but similar chain-centeredness. Polymers synthesized using a consistent controlled radical polymerization method starting from the mechanophore bis-initiators exhibit significantly different activation efficiency with ultrasonication. These results suggest that the selectivity for mechanophore activation is strongly influenced by the reactivity of the mechanophore, which must be considered in conjunction with its position in the polymer chain. Using two different mechanophores that can be cleaved by an orthogonal stimulus after sonication, we further demonstrate that mechanophore reactivity is a key factor that determines activation efficiency by controlling the degree of competition between mechanophore activation and nonspecific chain scission.

2.2 Theoretical Outcomes of Mechanophore Reactivity and Position

We first considered how the force-sensitivity of a mechanophore in concert with its location in the polymer chain would affect the selectivity for mechanophore activation versus nonspecific backbone scission with ultrasonication. The anthracene–maleimide (AM)[16] and coumarin dimer (CD)[14] mechanophores were initially identified due to their

scissile nature and fluorogenic properties, which enable the straightforward determination of activation efficiency as demonstrated previously.[14,17] Density functional calculations using the constrained geometries simulate external force (CoGEF) method[18] predict that the AM and CD mechanophores exhibit significantly different mechanochemical reactivity, with values of F_{max} predicted to be 4.1 and 5.9 nN, respectively (Figure 2.1a).[7] Values of F_{max} from CoGEF calculations have been demonstrated to be good indicators of the relative mechanochemical reactivity of mechanophores.[7] According to the bead–rod model,[19] the force experienced by a polymer chain in an extensional flow field is distributed parabolically about the chain center with peak forces in the range necessary for C–C bond cleavage on the μs timescale (Figure 2.1b).[12] Given this force distribution and in accordance with previously recognized ideas,[14] both the reactivity and the location of a mechanophore unit in the polymer chain are inextricably important parameters that control mechanophore activation efficiency, which is exemplified by comparing the CD and AM mechanophores. In order for the relatively unreactive CD mechanophore to undergo

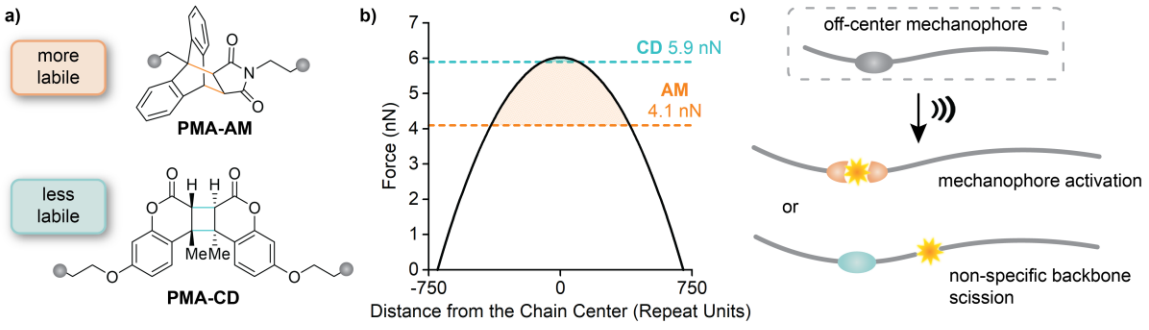

Figure 2.1 Putative model for mechanophore activation by ultrasound-induced mechanical force, demonstrating the connection between mechanophore reactivity and chain-centeredness. (a) Structures of the anthracene–maleimide mechanophore and the coumarin dimer mechanophore predicted by CoGEF to react at disparate forces of 4.1 nN and 5.9 nN, respectively. (b) Theoretical force distribution along a 120 kDa poly(methyl acrylate) chain (DP = 1,400) during ultrasound-induced extension illustrating that a more reactive mechanophore will experience forces high enough to achieve activation over a larger proportion of the chain. (c) Hypothetical illustration comparing the effect of mechanophore reactivity on the nature of mechanochemical chain scission for polymers with an off-center mechanophore.

selective mechanical activation, it must be located in close proximity to the center of the polymer chain. In contrast, the force exerted on the more reactive AM mechanophore will still exceed its critical activation force even when it is located a significant distance from the chain midpoint. Therefore, two identical polymer chains with an off-center CD or AM mechanophore would be expected to have divergent reaction outcomes, that is, mechanochemical activation of the AM mechanophore and nonspecific backbone scission in the polymer incorporating the CD mechanophore (Figure 2.1c). This is undoubtedly a simplistic representation of the reactivity in this system, but it nonetheless illustrates the important relationship between the activity of a mechanophore and its position in a polymer chain.

2.3 Differential Activation Efficiency of AM and CD Mechanophore

To investigate this theory, two series of poly(methyl acrylate) polymers containing either an anthracene–maleimide (**PMA-AM**) or a coumarin dimer (**PMA-CD**) mechanophore were prepared via controlled radical polymerization and the ultrasound-induced mechanophore activation efficiency was determined using photoluminescence (PL) spectroscopy (see the SI for details). Upon mechanical activation, the AM mechanophore undergoes a formal retro-[4+2] cycloaddition reaction to produce a fluorescent anthracene species,[20] while the CD mechanophore undergoes a formal retro-[2+2] cycloaddition reaction to generate two fluorescent coumarin moieties.[14] Each polymer was synthesized following a consistent method using an AM or CD mechanophore functionalized with terminal α-bromoisobutyryl ester groups as the bis-initiator in the controlled radical polymerization of methyl acrylate with Cu wire/Me_6TREN in DMSO at room

temperature.[21] Polymerizations were well-controlled with polymer molecular weights (M_n) in the range 60.2–221 kDa for the **PMA-AM** series and 78.7–206 kDa for the **PMA-CD** series with all polymers having a $Đ \leq 1.10$. These molecular weights are all well above the threshold molecular weight for each mechanophore.[17] It is reasonable to expect that each polymer has a similar degree of chain-centeredness of the mechanophore unit; however, characterizing the trend in mechanophore activation efficiency over the entire range of polymers in each series further minimizes error associated with random termination or other processes. Dilute solutions of each polymer were subjected to pulsed ultrasonication (2 mg/mL, 1 s on/2 s off, 13.6 W/cm^2) in an ice bath and aliquots were removed periodically for analysis by PL spectroscopy following previously reported procedures (see section 2.6.4 for details).[17] Ultrasonication was stopped in each case once the PL signal from the mechanically generated product reached a nearly constant value and the data were fit to an expression of first order kinetics to determine the maximum mechanophore activation in each experiment (Figure 2.2 and Figure 2.3).

The mechanophore activation efficiencies determined for **PMA-AM** and **PMA-CD** are illustrated in Figure 2.4. Activation efficiency is defined as the percentage of mechanophores that react at completion (i.e., extended sonication). Strikingly, a mechanophore activation efficiency of 96% is observed for the AM mechanophore while only 32% mechanophore activation is achieved for the CD mechanophore, on average, across the entire range of polymer molecular weights. We demonstrated previously that the activation efficiency for an AM mechanophore decreases to 64% for a 43 kDa **PMA-AM** polymer, consistent with having a significant fraction of chains in the molecular weight distribution that experiences insufficient mechanical force to achieve activation.[17] Above

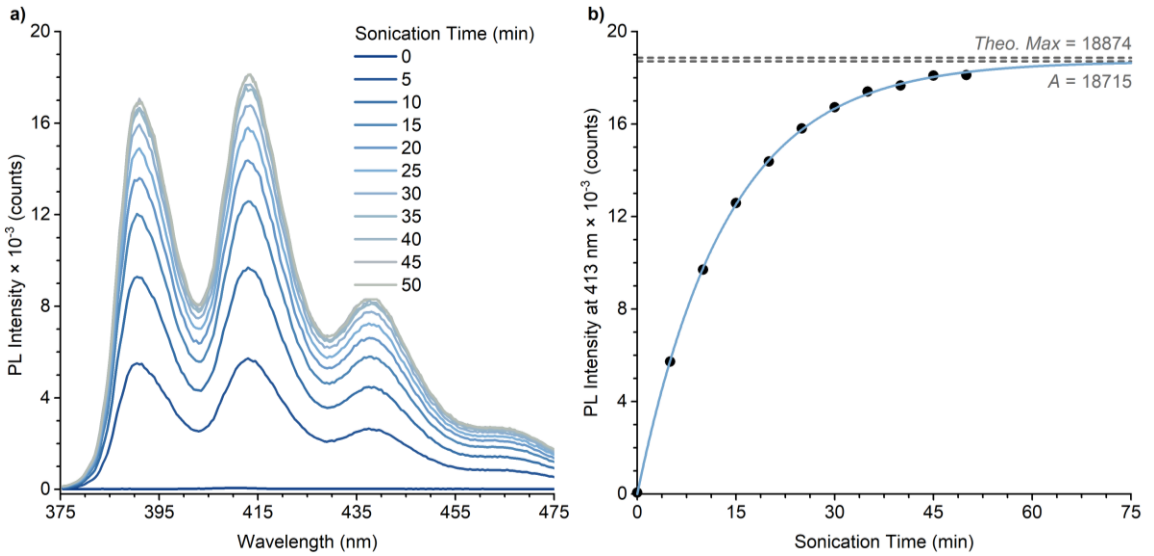

Figure 2.2 (a) Representative PL measurements for polymer **PMA-AM** (M_n = 201 kg/mol; $Đ$ = 1.07). (b) Photoluminescence intensity at 413 nm as a function of ultrasonication time, which is fitted to eq 2.2 to determine the plateau PL intensity, *A*. The predicted plateau value *A* is compared to the maximum theoretical PL intensity determined from the calibration curve and based on the concentration of mechanophore to derive percent activation.

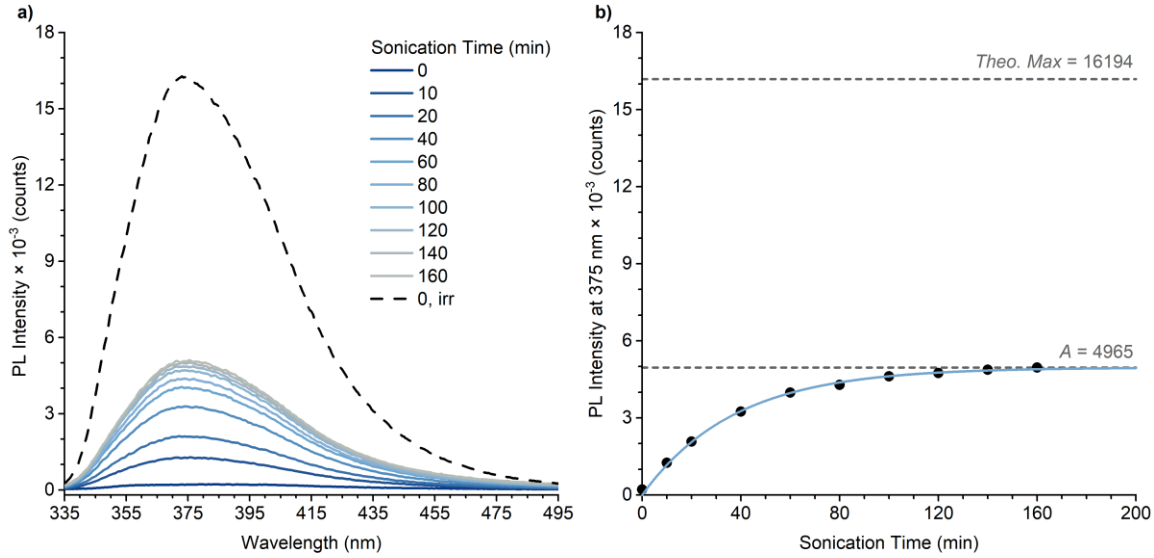

Figure 2.3 (a) Representative PL measurements for polymer **PMA-CD** (M_n = 132 kg/mol; $Đ$ = 1.06). The unsonicated sample is irradiated with 254 nm light for 60 s to fully cleave the coumarin dimer (black dashed trace), providing the maximum theoretical PL intensity and facilitating the calculation of percent activation. (b) PL intensity at 375 nm as a function of ultrasonication time, which is fitted to eq 2.2 to determine the plateau PL intensity, *A*. The predicted plateau value *A* is compared to the maximum theoretical PL intensity from photoirradiation to derive percent activation.

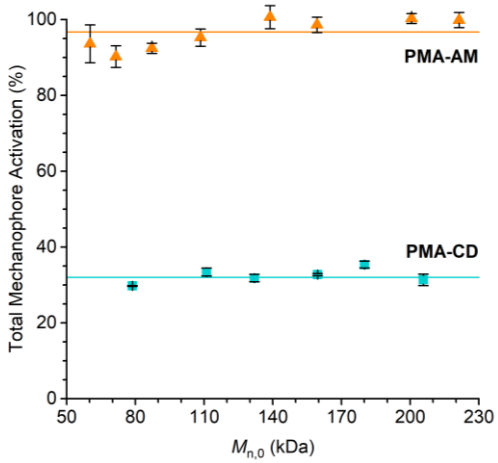

Figure 2.4 Activation efficiency for anthracene–maleimide and coumarin dimer mechanophores over the range of initial polymer molecular weights. The solid lines indicate the average total activation determined for each mechanophore. Data points and error bars represent average values and standard deviation from three replicate experiments.

this threshold molecular weight, the nearly constant activation efficiency measured is notable considering it is in opposition to the molecular weight dependent trend in mechanophore activation previously observed for multimechanophore polymers.[12] In that system, a greater extent of mechanophore activation occurs per chain scission event for polymers with lower initial molecular weight. It is clear that across the molecular weight range surveyed here, all of the AM mechanophores experience the requisite force for activation and mechanophore activation outcompetes nonspecific backbone scission. In the case of **PMA-CD**, the force on the polymer is ultimately leveled by the strength of the C–C bonds in the backbone, resulting in a relatively narrow window of activation as illustrated by the model in Figure 2.1b. Assuming the two series of polymers here have a similar positional distribution of the mechanophore in the polymer chains, the significant discrepancy in activation efficiency reflects the inherent difference in reactivity between the AM and CD mechanophores that leads to different relative amounts of mechanophore activation versus nonspecific backbone scission. The total mechanophore activation

observed here for the CD mechanophore agrees well with the prior measurements by Craig and coworkers referenced above, despite differences in ultrasonication conditions.[14] Furthermore, the nearly quantitative activation efficiency for the AM mechanophore is noteworthy given that there is some anticipated deviation in the position of the mechanophore units relative to the chain midpoint that results from the imperfect controlled radical polymerization process.[14] It is nonetheless consistent with the model exemplified in Figure 2.1. These results emphasize the significant variability in the reactivity of different mechanophores and its importance on ultrasound-induced mechanochemical activation efficiency.

2.4 Quantification of Nonspecific Backbone Scission

To more directly investigate the competition between mechanophore activation and nonspecific chain scission, we turned our attention to mechanophores that exhibit orthogonal reactivity with light or heat, enabling the scission of any intact mechanophores that remain after ultrasonication. A similar strategy was recently employed to estimate mechanochemical activation efficiency in multimechanophore azo-linked polymers.[22] As characterized extensively by Craig and coworkers, the CD mechanophore also cleaves rapidly and completely upon irradiation with 254 nm light and is well-suited for this analysis (Figure 2.5a).[14] Given the high thermal stability of the AM mechanophore, we targeted a furan–maleimide (FM) mechanophore that has a relatively low predicted F_{max} of 3.9 nN[7] and is predisposed to undergo a retro-[4+2] cycloaddition reaction upon mechanical activation as well as heating to complement the investigation of **PMA-CD**.[23–25] Analogous to the **PMA-CD** series, polymers containing the FM mechanophore (**PMA-FM**) were synthesized using

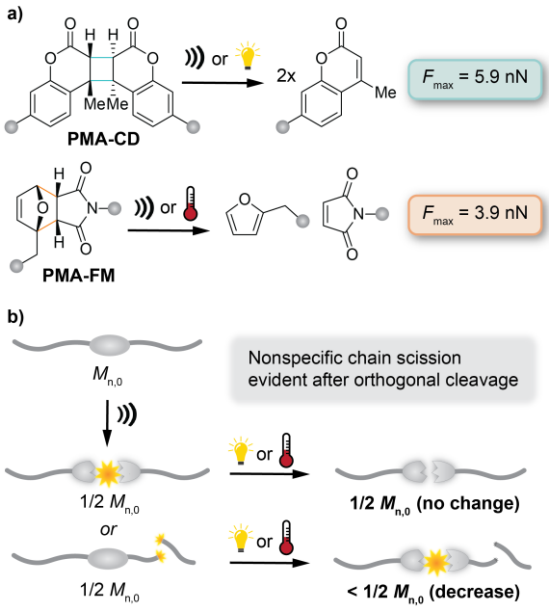

Figure 2.5 (a) Reactivity of furan–maleimide and coumarin dimer mechanophores. Values of F_{max} are predictions from CoGEF. (b) Simplified schematic illustrating the potential outcomes of ultrasound-induced mechanochemical activation and subsequent orthogonal cleavage of intact mechanophores using heat or light. Only polymers that undergo nonspecific backbone scission exhibit a decrease in M_n after the orthogonal cleavage step.

the same controlled radical polymerization method from a FM bis-initiator to provide a series of polymers with M_n in the range 83.3–182 kDa and $Đ \leq 1.13$ (see section 2.6.3 for details). Ultrasound-induced mechanochemical activation of the polymers followed by the cleavage of any unreacted mechanophores using light (CD) or heat (FM) allows the amount of nonspecific backbone scission that occurs for each polymer upon ultrasonication to be determined indirectly, as illustrated in Figure 2.5b. After one complete polymer scission cycle, the molecular weight will be reduced to ½ $M_{n,0}$, regardless of whether the scission event happened as a result of mechanophore activation or nonspecific backbone cleavage. However, subsequent reduction in M_n upon the orthogonal activation of any remaining intact mechanophore units using light or heat would necessarily reflect nonspecific backbone cleavage that occurred during ultrasonication.

Solutions of **PMA-CD** and **PMA-FM** (2 mg/mL in 3:1 MeCN/MeOH) were subjected to pulsed ultrasonication (1 s on/1 s off, 13.6 W/cm^2) in an ice bath and aliquots were removed at various intervals for molecular weight analysis by gel permeation chromatography equipped with refractive index and multiangle light scattering detectors. We first verified that the FM mechanophore is more reactive than the CD mechanophore. The rate of mechanochemical activation was determined to be significantly faster for **PMA-FM** compared to **PMA-CD** based on the trends for three different molecular weight samples (Figure 2.6).[17] Similarly, we also confirmed that the mechanically-induced scission of **PMA-CD** is faster than backbone cleavage in a PMA homopolymer that does not contain any mechanophore. Analysis by ^{1}H NMR spectroscopy revealed a mechanophore activation efficiency of 69–74% for **PMA-FM** after extended sonication, which is significantly higher than that observed for **PMA-CD** (Figure 2.7).

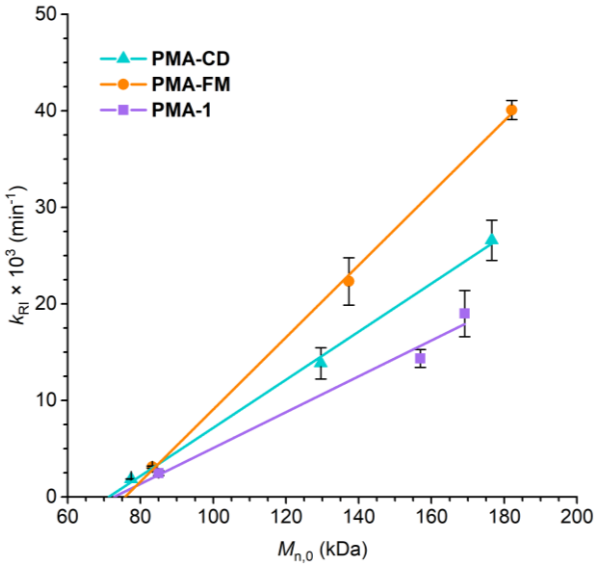

Figure 2.6 Rate constants determined in 3:1 MeCN/MeOH based on time-dependent refractive index response for ultrasound-induced mechanochemical activation (pulsed 1 s on/ 1 s off) as a function of initial M_n. Data are for polymers containing a furan–maleimide (**PMA-FM**) and coumarin dimer mechanophore (**PMA-CD**), as well as a PMA homopolymer that does not contain a mechanophore (**PMA-1**). Data points represent the average from two or three experiments with error bars denoting the range of the measurements. We note that the predicted values of M_{thresh} are not expected to be accurate given the limited data set.

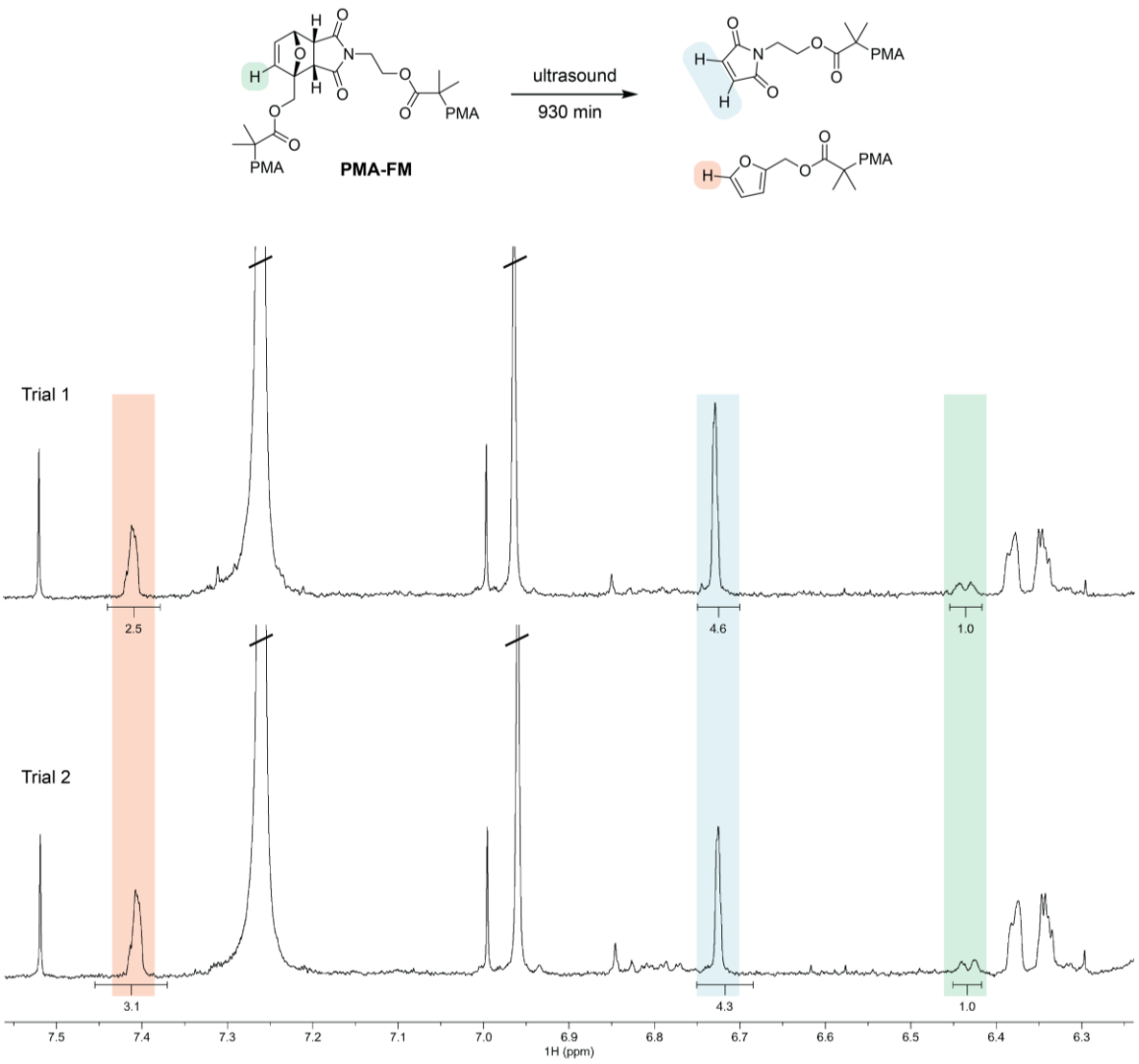

Figure 2.7 ^{1}H NMR spectra (400 MHz, $CDCl_3$) of **PMA-FM** (M_n = 83.3 kg/mol; $Đ$ = 1.13) after 930 minutes of ultrasonication in 3:1 MeCN/MeOH. Percent activation is determined from integration of the highlighted protons. Integration of the maleimide proton signals (blue) relative to the signal for residual starting material (green) gives an average conversion of 69%, while integration of the signal corresponding to the proton on the furan product (orange) gives an average conversion of 74% for the retro-Diels–Alder reaction.

With this background knowledge, we then set out to evaluate the degree of mechanophore activation versus nonspecific chain scission for **PMA-CD** and **PMA-FM** (Figure 2.8). The same aliquots removed from the ultrasonication experiments for molecular weight analysis were subjected to the appropriate orthogonal activation method using heat or light and the molecular weight was measured again. Control experiments demonstrated that 60 s of irradiation with 254 nm light was sufficient to quantitatively cleave **PMA-CD** (Figure 2.9). Heating **PMA-FM** at 70 °C for 24 h resulted in nearly complete cleavage as evidenced by ^{1}H NMR spectroscopy, although we note that a small shoulder remained in the GPC trace of the heated sample corresponding to ~8% of residual intact polymer (Figure 2.9 and Figure 2.10). We confirmed that the PMA backbone was unaffected by both orthogonal cleavage conditions (Figure 2.11). Polymers with molecular weights of ~80 kDa were selected for initial analysis to favor a single chain scission event on the timescale of the ultrasonication experiments as the small size of the cleavage products will preclude further

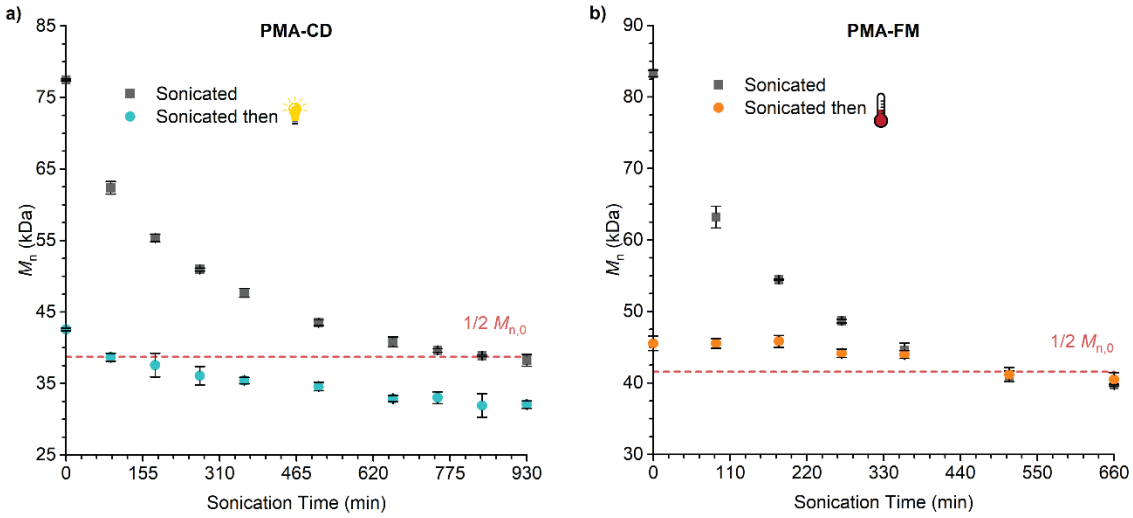

Figure 2.8 Values of M_n plotted as a function of sonication time for aliquots taken immediately after ultrasonication (2 mg/mL in 3:1 MeCN/MeOH) and then after subsequent cleavage using heat or light. (a) Data for **PMA-CD**, $M_{n,0}$ = 77.5 kDa. (b) Data for **PMA-FM**, $M_{n,0}$ = 83.3 kDa. Dashed lines at ½$M_{n,0}$ are included as a guide. Data points are the average from two experiments with error bars denoting the range of the two measurements.

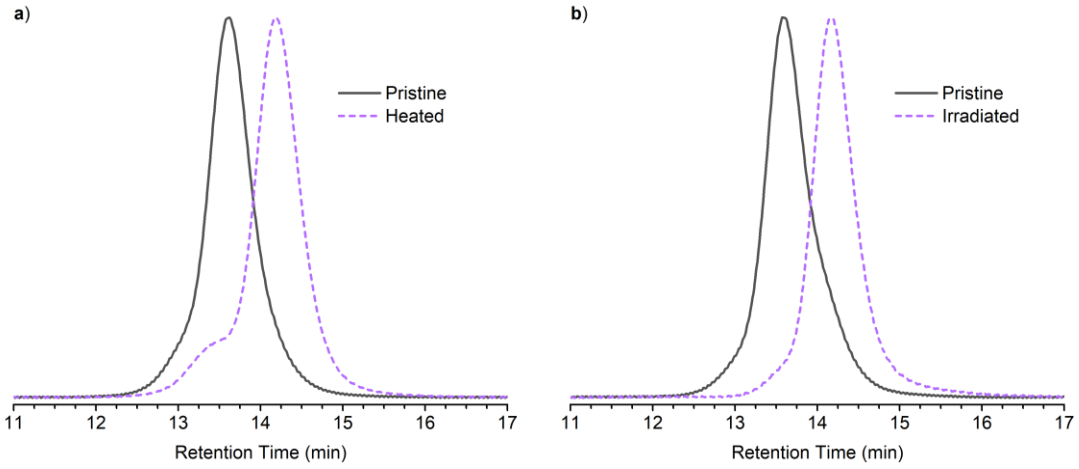

Figure 2.9 Control experiments demonstrating orthogonal cleavage of mechanophore-containing polymers in 3:1 MeCN/MeOH. (a) **PMA-FM** (M_n = 137 kg/mol; $Đ$ = 1.10) after heating at 70 °C for 24 h, and (b) **PMA-CD** (M_n = 132 kg/mol; $Đ$ = 1.06) after irradiation with 254 nm light for 60 s.

mechanochemical reaction.[1] The M_n of **PMA-CD** approaches ½$M_{n,0}$ after ~15 h of ultrasonication; yet, even at relatively early timepoints, the M_n of the UV-irradiated samples begins to fall significantly below ½$M_{n,0}$ (Figure 2.8a). On the other hand, the M_n of **PMA-FM** approaches ½$M_{n,0}$ more quickly, consistent with it being more reactive than **PMA-CD**.

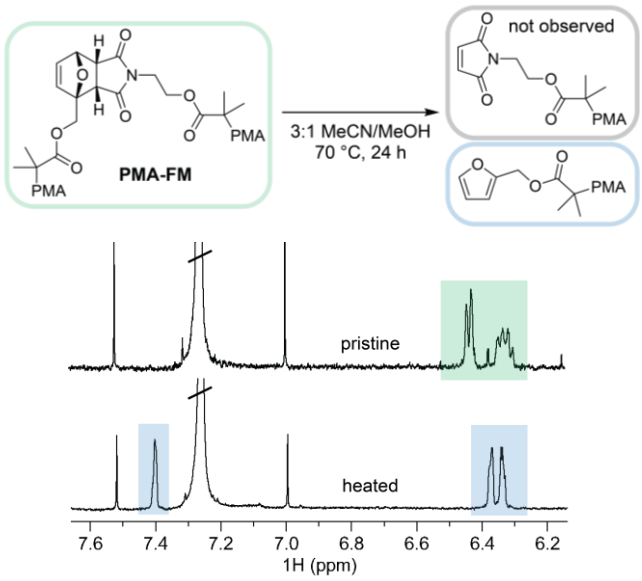

Figure 2.10 ^{1}H NMR spectra (400 MHz, $CDCl_3$) demonstrating complete conversion of **PMA-FM** via retro-Diels–Alder reaction upon heating at 70 °C for 24 h. The maleimide protons are not observed after the reaction, presumably due to instability under the reaction conditions.

More importantly, the time-dependent M_n of the sonicated polymer samples and the M_n of those heated post-sonication converge toward the end of the experiment in stark contrast to the data for **PMA-CD** (Figure 2.8b and Figure 2.12). These results align with the model presented in Figure 2.5 and suggest that **PMA-CD** experiences a greater degree of nonspecific backbone scission compared to the more reactive **PMA-FM** upon ultrasound-induced mechanochemical activation, which contributes to a lower mechanophore activation efficiency. The same overall trend is observed for larger polymers although it is important to note that secondary chain cleavage results in molecular weights below $½M_{n,0}$, as expected (Figure 2.13, Figure 2.14, and Figure 2.15).

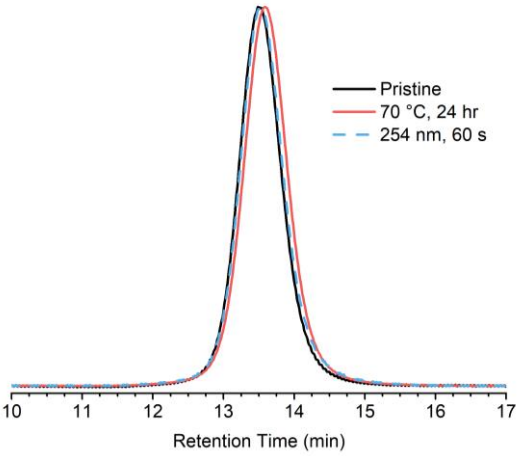

Figure 2.11 GPC traces (RI response) of unfunctionalized control polymer **PMA-1** (M_n = 169 kDa, $Đ$ = 1.11) after heating (red line) and UV irradiation (blue dashed line) illustrating minimal change, demonstrating the stability of the polymer under these conditions.

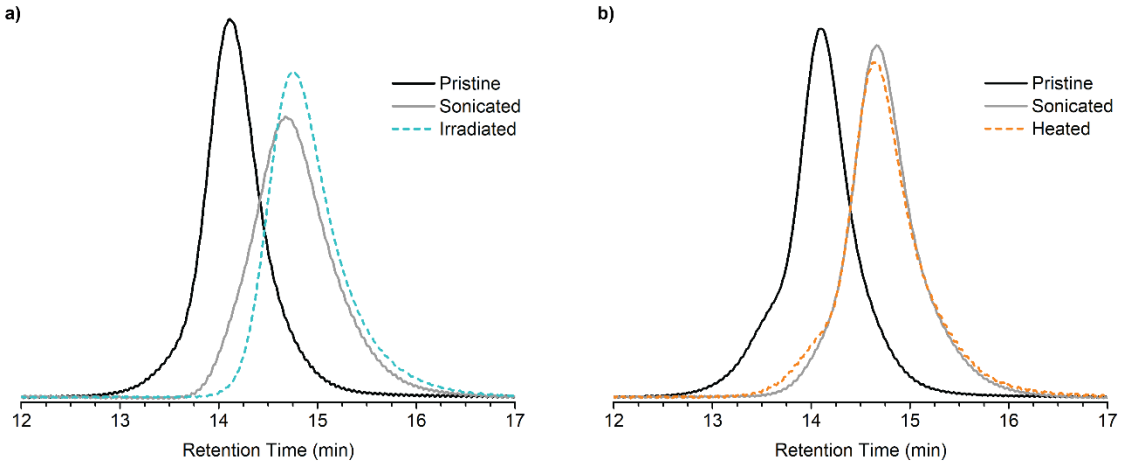

Figure 2.12 Representative examples of GPC traces (RI response) normalized by peak area corresponding to pristine polymer, after sonication to ~$½M_{n,0}$, and the sonicated polymer after orthogonal cleavage using heat or light. (a) **PMA-CD** (M_n = 78.7, $Đ$ = 1.05) after 930 minutes of sonication time, and (b) **PMA-FM** (M_n = 83.3 kDa, $Đ$ = 1.13) after 660 minutes of sonication time. A shift in the sonicated **PMA-CD** trace is observed after UV irradiation, while the sonicated **PMA-FM** trace exhibits minimal change after heating.

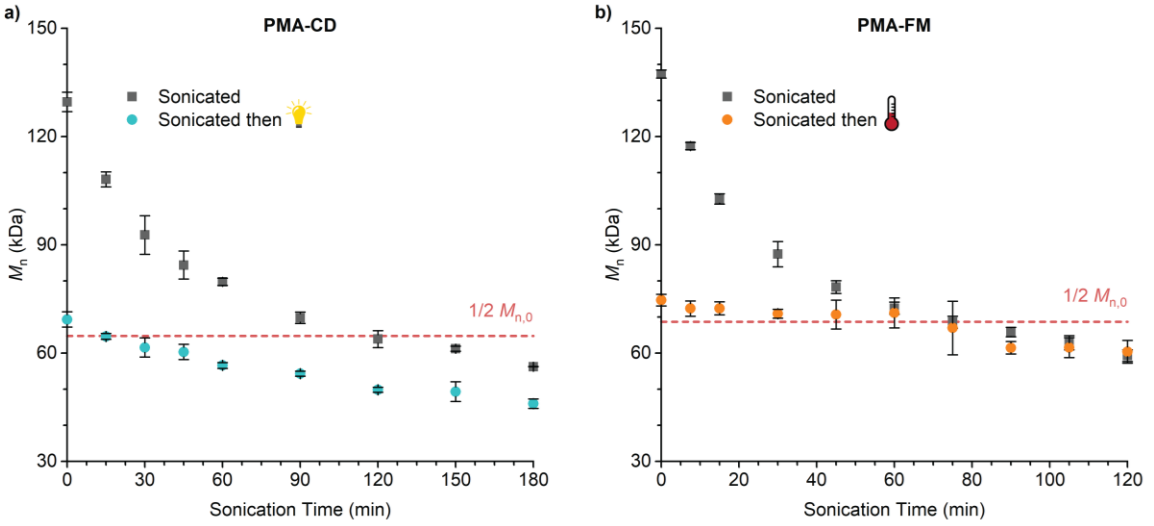

Figure 2.13 Values of M_n plotted as a function of ultrasonication time for aliquots taken immediately after ultrasonication (2 mg/mL in 3:1 MeCN/MeOH) and then after orthogonal cleavage using heat or UV light. (a) Data for **PMA-CD** (M_n = 132 kg/mol; $Đ$ = 1.06) containing a coumarin dimer mechanophore. (b) Data for **PMA-FM** (M_n = 137 kg/mol; $Đ$ = 1.10) containing a furan–maleimide mechanophore. Lines at ½ $M_{n,0}$ are included as a guide. Data points represent the average from two experiments with error bars denoting the range of the two measurements.

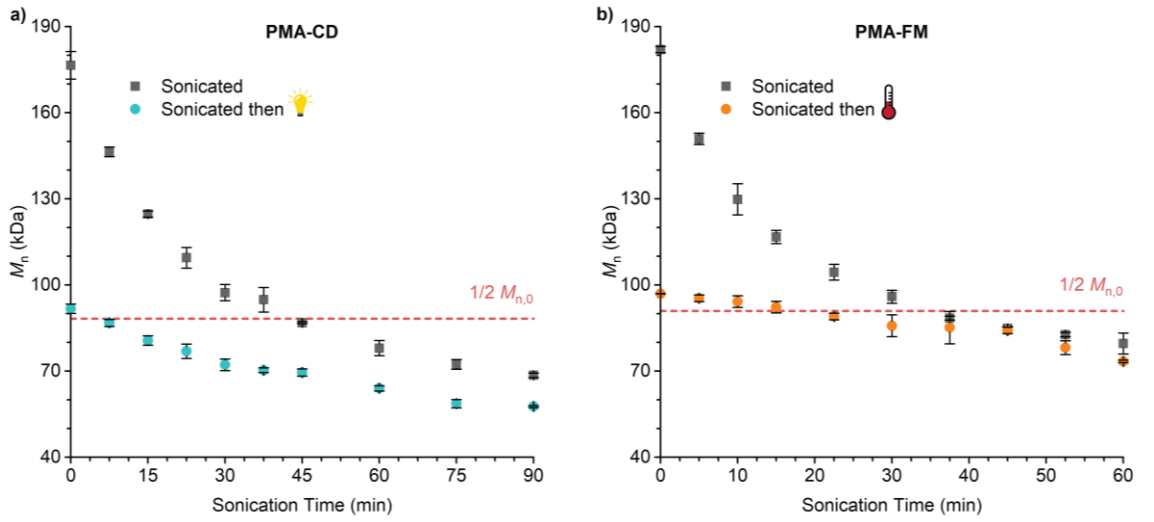

Figure 2.14 Values of M_n plotted as a function of ultrasonication time for aliquots taken immediately after ultrasonication (2 mg/mL in 3:1 MeCN/MeOH) and then after orthogonal cleavage using heat or UV light. (a) Data for **PMA-CD** (M_n = 180 kg/mol; $Đ$ = 1.05) containing a coumarin dimer mechanophore. (b) Data for **PMA-FM** (M_n = 182 kg/mol; $Đ$ = 1.10) containing a furan–maleimide mechanophore. Lines at ½ $M_{n,0}$ are included as a guide. Data points represent the average from two experiments with error bars denoting the range of the two measurements.

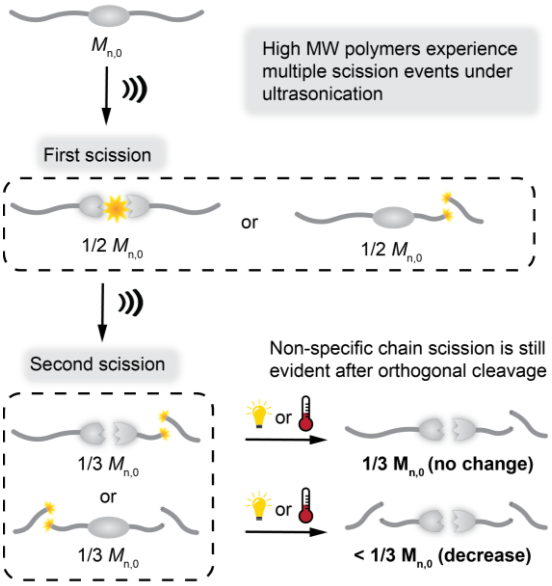

Figure 2.15 Simplified schematic illustrating the potential outcomes of ultrasound-induced mechanochemical activation of high molecular weight polymers that undergo multiple scission reactions, and subsequent orthogonal cleavage of intact mechanophores using heat or light. After extended ultrasonication, only polymers that undergo nonspecific backbone scission exhibit a decrease in M_n after the orthogonal cleavage step.

2.5 Conclusions

In summary, we demonstrate that the identity of a mechanophore and thus its unique force-coupled reactivity, in concert with its position in the polymer chain,[14] dictates the efficiency of ultrasound-induced mechanochemical activation. For polymers with a putatively similar positional distribution of the mechanophore relative to the chain midpoint, differences in mechanophore reactivity result in pronounced changes in the selectivity for mechanophore activation. Significantly, 96% activation of the anthracene–maleimide mechanophore is achieved upon ultrasonication compared to only 32% activation of the coumarin dimer mechanophore across two series of polymers synthesized using identical controlled radical polymerization methods. Using the coumarin dimer mechanophore and a furan–maleimide mechanophore that can be orthogonally cleaved with light and heat, respectively, we further

demonstrate that greater competition between mechanophore activation and nonspecific backbone scission contributes to the lower mechanochemical activation efficiency for less reactive mechanophores like the coumarin dimer. Although these results are intuitive, they emphasize that the conventional dogma of "chain-centeredness" provides an incomplete picture and that the requisite proximity of a mechanophore to the chain midpoint where mechanical force is maximized during ultrasonication is relative to the reactivity of the individual mechanophore.

2.6 Experimental Section

2.6.1 General Experimental Details

Reagents from commercial sources were used without further purification unless otherwise noted. Methyl acrylate was passed through a short plug of basic alumina to remove inhibitor immediately prior to use. Dry THF and acetonitrile were obtained from a Pure Process Technology solvent purification system. All reactions were performed under a N_2 atmosphere unless specified otherwise.

NMR spectra were recorded using a 400 MHz Bruker Avance III HD with Prodigy Cryoprobe or a 400 MHz Bruker Avance Neo. All ^{1}H NMR spectra are reported in δ units, parts per million (ppm), and were measured relative to the signals for residual chloroform (7.26 ppm) in deuterated solvent.

Analytical gel permeation chromatography (GPC) was performed using an Agilent 1260 series pump equipped with two Agilent PLgel MIXED-B columns (7.5 x 300 mm), an Agilent 1200 series diode array detector, a Wyatt 18-angle DAWN HELEOS light scattering detector, and an Optilab rEX differential refractive index detector. The mobile phase was THF at a flow rate of 1 mL/min. Molecular weights and molecular weight distributions were calculated by light scattering using a dn/dc value of 0.062 mL/g (25 °C) for poly(methyl acrylate).

Photoluminescence spectra were recorded on a Shimadzu RF-6000 spectrofluorophotometer using a quartz microcuvette (Starna 18F-Q-10-GL14-S).

Photochemical reactions were performed using a 4 Watt UVLS-24 EL Series UV Lamp.

Ultrasound experiments were performed inside a sound abating enclosure using a Vibra Cell 505 liquid processor equipped with a 0.5-inch diameter solid probe (part #630-0217),

sonochemical adapter (part #830-00014), and a Suslick reaction vessel made by the Caltech glass shop (analogous to vessel #830-00014 from Sonics and Materials).

Compounds **S1**,[26] **S2**,[17] **S3**,[27] and **S4**[28] were synthesized following the procedures reported in the literature.

Chart 2.1 Structures of initiators and small molecules used in this study.

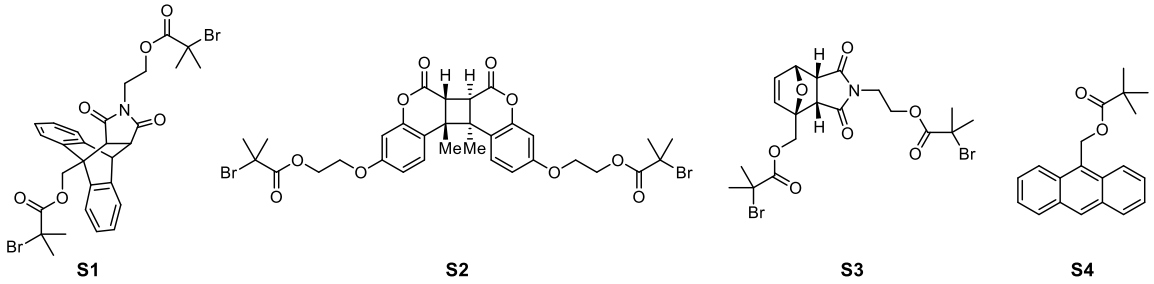

Chart 2.2 Structures of polymers **PMA-AM**, **PMA-CD**, **PMA-FM**, and **PMA-1**.

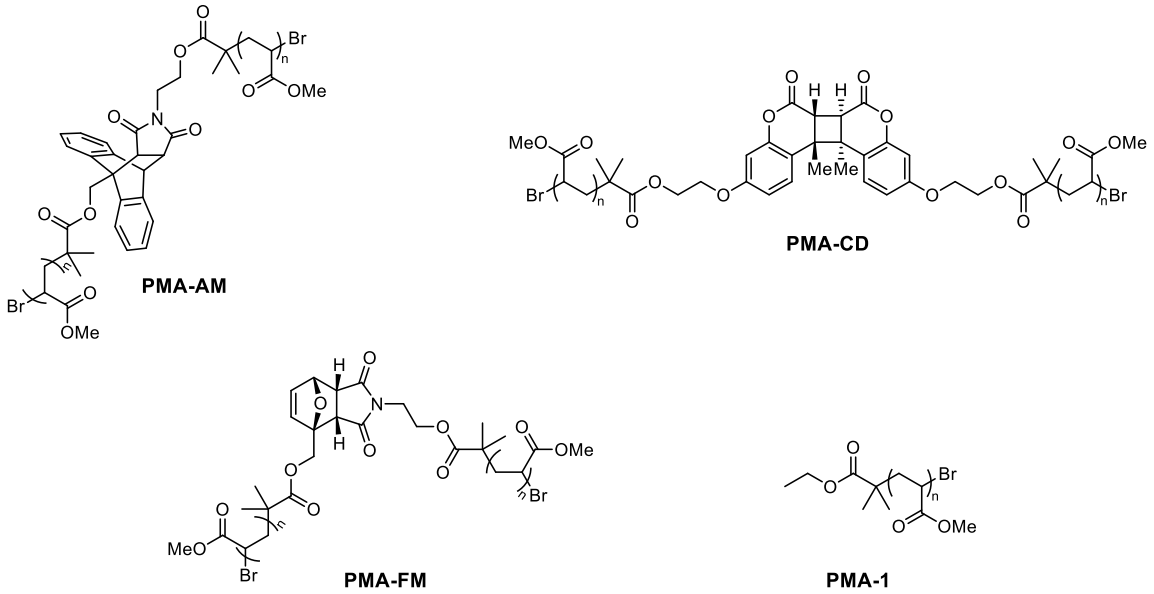

2.6.2 Modeling of Ultrasound-Induced Force Distribution

Calculation of the distribution of force along a polymer chain in an ultrasonication-induced flow field. The following equation and procedure were adapted from Lenhardt et al.[29] The distribution of force along a polymer chain using the bead–rod model[30] is described by eq 2.1:

$$F(i) = 6\pi abS\dot{\varepsilon}\left(\frac{n^2}{8} - \frac{i^2}{2}\right) \tag{2.1}$$

where a is the bead radius, b is the rod length, η is the solvent viscosity, S is the shielding factor, $\dot{\varepsilon}$ is the strain rate, and n is the number of repeat units. Values of a = 1.65 and b = 2.6 Å were estimated for poly(methyl acrylate) (PMA). The plot in Figure 2.1b was constructed for a PMA polymer with n = 1400 in THF at 0 °C using values η = 6.08 x 10^{-4} N*s*m^{-2},[31] S = 1, and ε = 5 x 10^7 s^{-1}.

2.6.3 Synthetic Details

Representative procedure for the synthesis of Poly(Methyl Acrylate) (PMA) polymers containing a mechanophore near the chain midpoint. PMA polymers were synthesized by controlled radical polymerization following the procedure by Nguyen *et al*.[21] A 25 mL Schlenk flask equipped with a stir bar was charged with initiator **S2** (16.7 mg, 0.226 mmol), DMSO (2 mL), methyl acrylate (2 mL), and freshly cut copper wire (2.0 cm length, 20 gauge). The flask was sealed, the solution was deoxygenated with three freeze-pump-thaw cycles, and then allowed to warm to rt and backfilled with nitrogen. Me_6TREN (17 µL, 0.0636 mmol) was added via microsyringe to initiate the polymerization. After stirring at rt for 2 h, the flask was opened to air and the solution was diluted with dichloromethane. The

polymer solution was precipitated into cold methanol (3x) and the isolated material was dried under vacuum to yield 1.46 g of **PMA-CD** (70%). M_n = 78.7 kDa, $Đ$ = 1.05.

Representative procedure for the synthesis of Poly(Methyl Acrylate) (PMA) polymers not containing a mechanophore. A 25 mL Schlenk flask equipped with a stir bar was charged with ethyl α-bromoisobutyrate (2 μL, 0.010 mmol), DMSO (4.8 mL), methyl acrylate (4.8 mL), and freshly cut copper wire (2.0 cm length, 20 gauge). The flask was sealed, the solution was deoxygenated with three freeze-pump-thaw cycles, and then allowed to warm to rt and backfilled with nitrogen. Me_6TREN (5 μL, 0.019 mmol) was added via microsyringe to initiate the polymerization. After stirring at rt for 2 h, the flask was opened to air and the solution was diluted with dichloromethane. The polymer solution was precipitated into cold methanol (3x) and the isolated material was dried under vacuum to yield 1.96 g of **PMA-1** (39%). M_n = 169 kDa, $Đ$ = 1.11.

Table 2.1 Summary of M_n and $Đ$ data for **PMA-AM, PMA-CD, PMA-FM,** and **PMA-1**.

	M_n (kDa)	$Đ$		M_n (kDa)	$Đ$
PMA-AM	60.2	1.07	**PMA-CD**	78.7	1.05
	70.7	1.07		111	1.07
	87.1	1.05		132	1.06
	108	1.06		160	1.05
	139	1.05		180	1.05
	159	1.06		206	1.09
	201	1.07	**PMA-FM**	83.3	1.13
	221	1.10		137	1.10
				182	1.10
			PMA-1	85.0	1.06
				157	1.08
				169	1.11

2.6.4 Description of Sonication Experiments and Fluorescence Spectroscopy

General Procedure for Ultrasonication Experiments. An oven-dried sonication vessel was fitted with rubber septa, placed onto the sonication probe, and allowed to cool under a stream of dry argon. The vessel was charged with a dilute solution of the polymer (2.0 mg/mL, 20 mL) and submerged in an ice bath. Sonications of **PMA-AM** were run in THF with 30 mM butylated hydroxytoluene (BHT). All other sonications were run in 3:1 MeCN/MeOH, which has been shown to provide reproducible photoluminescence spectra for the CD mechanophore.[17] The solution was sparged continuously with argon beginning 10 min prior to sonication and for the duration of the sonication experiment. Pulsed ultrasound (30% amplitude, 20 kHz, 13.6 W/cm^2) was then applied to the system. Aliquots (1.0 mL) were removed at specified time points (sonication "on" time) and filtered through a 0.45 μm PTFE syringe filter prior to analysis by GPC and fluorescence spectroscopy. For **PMA-AM** and **PMA-CD**, sonications were run until the PL signal from the mechanically generated product reached a nearly constant value (Figure 2.2 and Figure 2.3). For **PMA-FM**, sonications were run until the reaction reached approximately full conversion as indicated by the complete attenuation of the original polymer peak in the GPC chromatogram (RI response). A representative example is shown in Figure 2.16a. A representative example of GPC-RI data from a **PMA-CD** sonication experiment is shown below in Figure 2.16b. Ultrasonic intensity was calibrated using the method described by Berkowski et al.[32]

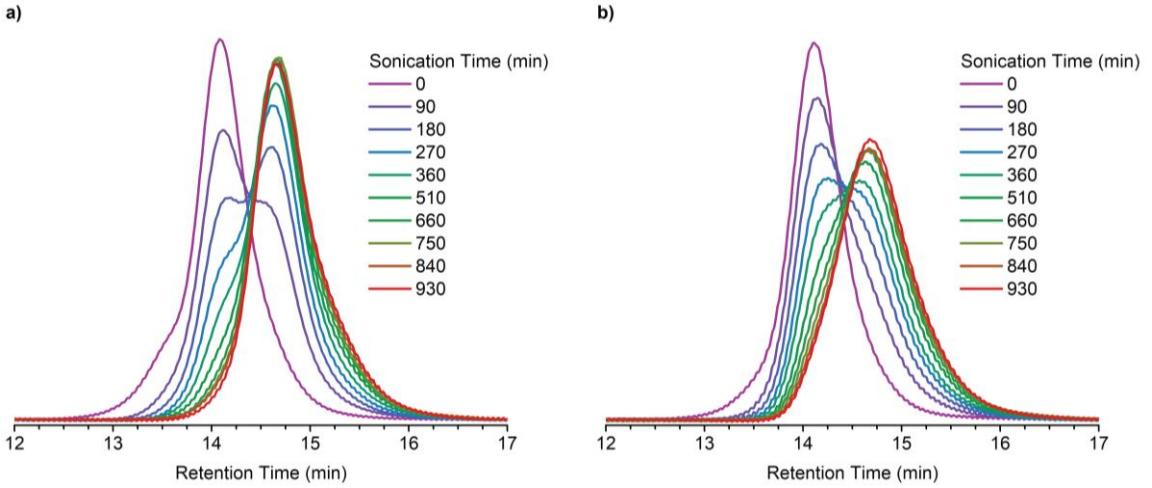

Figure 2.16 Time-dependent GPC traces (RI response) normalized by peak area for the sonication of (a) **PMA-FM** (M_n = 83.3 kDa, $Đ$ = 1.13) and (b) **PMA-CD** (M_n = 78.7, $Đ$ = 1.05), illustrating complete attenuation of the initial polymer peak after 930 min.

Analysis of Sonicated Polymer Samples by Fluorescence Spectroscopy. Aliquots from the sonication experiment were added to a quartz microcuvette. Emission spectra for **PMA-AM** were recorded at 375–480 nm using an excitation wavelength of λ_{ex} = 365 nm. Emission spectra for **PMA-CD** were recorded at 330–500 nm using an excitation wavelength of λ_{ex} = 320 nm.

2.6.5 Determination of Mechanophore Activation Efficiency

Characterization of Activation Efficiency for the Anthracene–Maleimide Mechanophore. Samples of small molecule anthracene model compound **S4** in THF at various concentrations were prepared and PL spectra were acquired to construct the calibration curve shown below in Figure 2.17. The theoretical PL intensity for each sonication experiment based on the concentration of mechanophore was determined from this calibration curve and used as the value for 100% activation. A representative example is

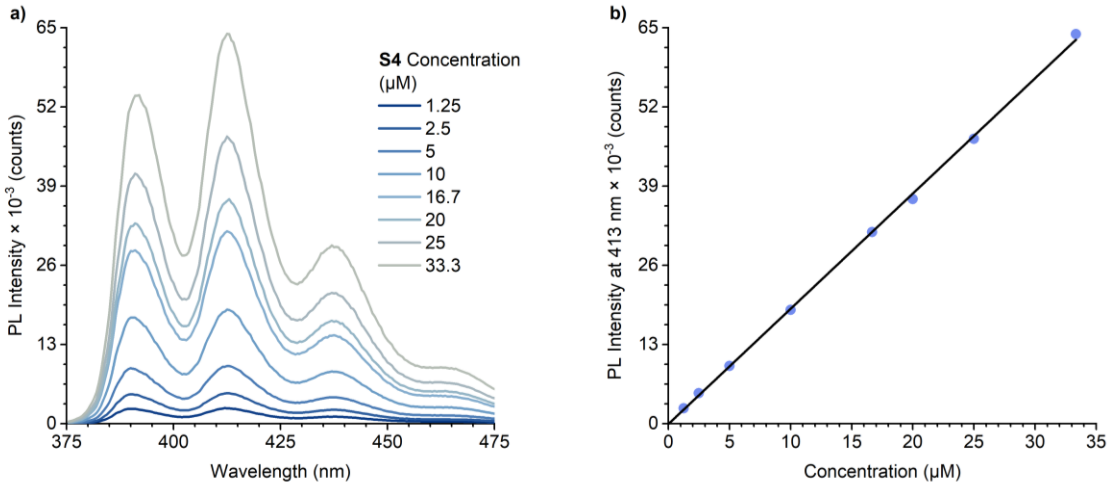

Figure 2.17 Construction of a calibration curve for experimental determination of the concentration of anthracene-containing polymer. (a) Photoluminescence emission spectra (λ_{ex} = 365 nm), and (b) PL intensity at 413 nm for solutions of compound **S4** in THF as a function of concentration. A linear regression of the data in (b) gives the calibration function Y = 1893X.

shown above in Figure 2.2. Data is provided below in Table 2.3, Table 2.4, Table 2.5, Table 2.6, Table 2.7, Table 2.8, Table 2.9, and Table 2.10 for each sonication experiment.

Characterization of Activation Efficiency for the Coumarin Dimer Mechanophore. For each sonication, an aliquot of polymer solution prior to sonication was added to a quartz cuvette and irradiated with 254 nm light for 60 s and a PL spectrum was acquired. Further irradiation did not lead to any increase in PL intensity, indicating that the coumarin dimer was fully cleaved after 60 s of UV irradiation. The PL intensity at the peak maximum for the photoirradiated sample was then used as the value for 100% activation. A representative example is shown above in Figure 2.3. Data is provided below in Table 2.11, Table 2.12, Table 2.13, Table 2.14, Table 2.15, and Table 2.16 for each sonication experiment. For one sonication experiment performed on **PMA-CD** with M_n = 180 kDa, aliquots taken at specified timepoints were irradiated for 60 s and the PL spectra were subsequently acquired (Figure 2.18). All of the spectra acquired after photoirradiation exhibit the same PL intensity,

indicating minimal side reactivity for the CD mechanophore or the mechanochemical reaction products during the sonication experiment.

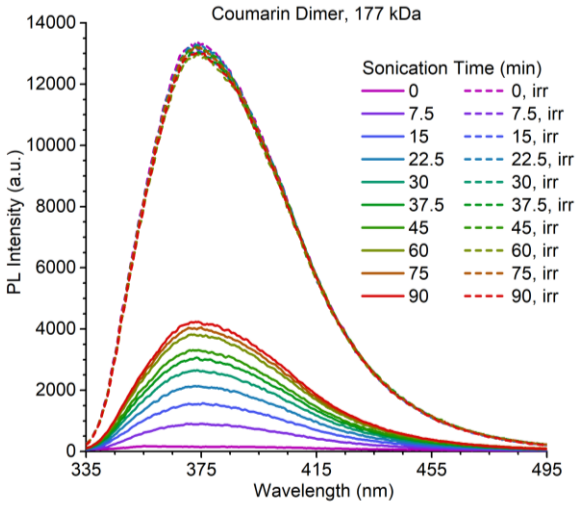

Figure 2.18 Ultrasonication of **PMA-CD** (M_n = 180 kg/mol, $Đ$ = 1.05) results in increasing photoluminescence emission (2 mg/mL in 3:1 MeCN/MeOH, λ_{ex} = 320 nm) corresponding to the generation of fluorescent coumarin moieties (solid lines). After irradiation of each aliquot with 254 nm UV light for 60 s, all remaining coumarin dimer units are cleaved and the photoluminescence emission corresponds to full conversion to the coumarin monomer (dashed lines).

Characterization of Activation Efficiency for the Furan–Maleimide Mechanophore. After each sonication, the polymer solution was filtered through a 0.45 μm PTFE syringe filter, concentrated under reduced pressure, and the residue was redissolved in $CDCl_3$ for ^1H NMR analysis. Integration of signals corresponding to the remaining intact mechanophore (6.43 ppm, 1H) and the maleimide (6.73 ppm, 2H) or furan (7.4 ppm, 1H) mechanochemical reaction products were used to calculate mechanophore conversion.[27] The average mechanophore conversion calculated using the signals for the maleimide product and the furan product was 69% and 74%, respectively. Representative examples are illustrated above in Figure 2.7.

Calculation of Percent Activation for PMA-AM and PMA-CD. Time-dependent PL values at the relevant emission wavelength (413 nm for **PMA-AM** and 375 nm for **PMA-CD**) were fit to eq 2.2 following a previously described procedure.[17] The fit-determined plateau value (A) was used as the maximum activation for that sonication experiment (see Figure 2.2b and Figure 2.3b above for representative examples). The predicted plateau value (A) determined from each experiment was then divided by the PL value calculated for full conversion (i.e., 100% mechanophore activation) as described above for **PMA-AM** and **PMA-CD**.

$$I = A(1 - e^{-kt}) \tag{2.2}$$

2.6.6 Tabulated Data for Determined Rate Constants

Rate constants were determined from the time-dependent attenuation of GPC-RI response following the method described in the literature.[17]

Table 2.2 Rate constants determined for ultrasonication experiments in 3:1 MeCN/MeOH (pulsed 1 s on/ 1 s off). Reported k_{RI} values are an average of at least two replicate trials.

	$M_{n,0}$ (kDa)	Avg. k_{RI} x10^3 (min^{-1})
PMA-CD	78.7	1.9
	132	13.9
	180	26.6
PMA-FM	83.3	3.1
	137	22.3
	182	40.1
PMA-1	85.0	2.5
	157	14.4
	169	19.0

2.6.7 Tabulated Characterization Data for All Ultrasonication Experiments

Table 2.3 Determined PL response (λ_{em} = 413 nm) for **PMA-AM** (M_n = 60.2 kDa) upon ultrasonication (1 s on, 2 s off) in THF. The concentration of the mechanophore was 33.2 μM.

	Trial 1	Trial 2	Trial 3
Sonication time (min)	**PL**	**PL**	**PL**
0	52	56	63
40	8782	8240	8395
80	15938	15378	15314
120	22174	21619	21880
200	32933	32110	32849
280	39863	38759	39851
400	46642	45537	48074
440	47538	47174	49641
480	48916	49142	50786
520	50087	50924	53483

Table 2.4 Determined PL response (λ_{em} = 413 nm) for **PMA-AM** (M_n = 70.7 kDa) upon ultrasonication (1 s on, 2 s off) in THF. The concentration of the mechanophore was 28.3 μM.

	Trial 1	**Trial 2**	**Trial 3**
Sonication time (min)	**PL**	**PL**	**PL**
0	60	55	61
20	6161	5770	6729
40	11106	10317	11422
80	20030	19020	19544
120	26745	26028	26497
160	32288	31410	31269
200	36354	35599	34620
240	38846	38574	37645
280	41164	40839	39791
320	43506	41614	41857

Table 2.5 Determined PL response (λ_{em} = 413 nm) for **PMA-AM** (M_n = 87.1 kDa) upon ultrasonication (1 s on, 2 s off) in THF. The concentration of the mechanophore was 23.0 μM.

	Trial 1	**Trial 2**	**Trial 3**
Sonication time (min)	**PL**	**PL**	**PL**
0	--	--	79
10	4204	4097	4522
20	8005	7492	8442
40	14719	14271	15018
60	20288	19756	20518
80	24548	23639	24775
100	27654	26815	28062
120	30010	29032	30684
140	32185	30815	33072
160	33646	32938	34640
180	34889	34930	35479

Table 2.6 Determined PL response (λ_{em} = 413 nm) for **PMA-AM** (M_n = 108 kDa) upon ultrasonication (1 s on, 2 s off) in THF. The concentration of the mechanophore was 18.4 μM.

	Trial 1	**Trial 2**	**Trial 3**
Sonication time (min)	**PL**	**PL**	**PL**
0	55	58	49
10	5767	5183	5687
20	10262	9365	10114
40	17370	16230	17129
60	22663	21249	22418
80	26345	24866	25304
100	28052	27469	27685
120	29803	29091	28785
140	31104	30411	30305
160	31697	31490	30828

Table 2.7 Determined PL response (λ_{em} = 413 nm) for **PMA-AM** (M_n = 139 kDa) upon ultrasonication (1 s on, 2 s off) in THF. The concentration of the mechanophore was 14.4 μM.

	Trial 1	**Trial 2**	**Trial 3**
Sonication time (min)	**PL**	**PL**	**PL**
0	--	--	59
5	4149	4300	4208
10	7464	7780	7436
20	12780	13173	12924
30	16803	17434	17269
40	19760	20083	20260
50	21967	21987	22815
60	23489	22923	23980
70	24586	24127	25200
80	24834	25110	25961
90	25518	25963	26552

Table 2.8 Determined PL response (λ_{em} = 413 nm) for **PMA-AM** (M_n = 159 kDa) upon ultrasonication (1 s on, 2 s off) in THF. The concentration of the mechanophore was 12.6 μM.

	Trial 1	**Trial 2**	**Trial 3**
Sonication time (min)	**PL**	**PL**	**PL**
0	61	63	45
5	4274	4217	4593
10	7625	7523	8030
15	10448	10306	10889
20	12943	12725	13232
30	16375	16445	16588
40	18771	18316	18850
50	20190	19804	20036
60	21182	21750	21248
70	22268	22213	21842

Table 2.9 Determined PL response (λ_{em} = 413 nm) for **PMA-AM** (M_n = 201 kDa) upon ultrasonication (1 s on, 2 s off) in THF. The concentration of the mechanophore was 9.97 μM.

	Trial 1	**Trial 2**	**Trial 3**
Sonication time (min)	**PL**	**PL**	**PL**
0	54	57	49
5	5286	5730	5387
10	9249	9697	9103
15	12153	12578	12023
20	14251	14375	13855
25	15530	15805	15458
30	16811	16732	16420
35	17312	17405	17167
40	17891	17666	17446
45	--	18092	17909
50	18360	18117	18213

Table 2.10 Determined PL response (λ_{em} = 413 nm) for **PMA-AM** (M_n = 221 kDa) upon ultrasonication (1 s on, 2 s off) in THF. The concentration of the mechanophore was 9.04 μM.

	Trial 1	**Trial 2**	**Trial 3**
Sonication time (min)	**PL**	**PL**	**PL**
0	57	41	53
3.33	3782	3674	3717
6.66	6716	6438	6673
10	8907	8680	8952
15	11393	11202	11367
20	13341	13170	13179
25	14441	14234	14363
30	15237	15321	15028
35	15778	15929	15544
40	16046	16332	16041

Table 2.11 Determined PL response (λ_{em} = 375 nm) for **PMA-CD** (M_n = 78.7 kDa) upon ultrasonication (1 s on, 2 s off) in 3:1 MeCN/MeOH.

	Trial 1	**Trial 2**	**Trial 3**
Sonication time (min)	**PL**	**PL**	**PL**
0	325	303	331
40	1753	1717	1651
80	2899	2907	2728
120	3909	3870	3763
160	4649	4746	4458
200	5365	5374	5117
280	6332	6438	6072
400	7286	7456	7131
440	7655	7561	7537
480	7783	7644	7854
0, irr	**28420**	**28272**	**28955**

Table 2.12 Determined PL response (λ_{em} = 375 nm) for **PMA-CD** (M_n = 111 kDa) upon ultrasonication (1 s on, 2 s off) in 3:1 MeCN/MeOH.

	Trial 1	**Trial 2**	**Trial 3**
Sonication time (min)	**PL**	**PL**	**PL**
0	230	234	249
20	1815	1710	1492
40	2913	2851	2533
80	4266	4308	3959
120	5027	5220	4792
160	5469	5725	5399
200	5744	6077	5605
240	5765	6246	5940
260	5920	6248	6222
0, irr	**17983**	**18472**	**19150**

Table 2.13 Determined PL response (λ_{em} = 375 nm) for **PMA-CD** (M_n = 132 kDa) upon ultrasonication (1 s on, 2 s off) in 3:1 MeCN/MeOH.

	Trial 1	**Trial 2**	**Trial 3**
Sonication time (min)	**PL**	**PL**	**PL**
0	209	222	238
10	1257	1418	1419
20	2083	2270	2220
40	3245	3350	3213
60	3983	4045	3848
80	4281	4434	4202
100	4622	4642	4501
120	4743	4754	4729
140	4875	5132	4875
160	4956	5203	4922
180	5080	5250	5098
0, irr	**16189**	**15651**	**15634**

Table 2.14 Determined PL response (λ_{em} = 375 nm) for **PMA-CD** (M_n = 160 kDa) upon ultrasonication (1 s on, 2 s off) in 3:1 MeCN/MeOH.

	Trial 1	**Trial 2**	**Trial 3**
Sonication time (min)	**PL**	**PL**	**PL**
0	152	179	218
10	1413	1412	1436
20	2260	2340	2259
40	3293	3276	3220
60	3754	3664	3569
80	4011	3919	3854
100	4266	4116	3985
120	4309	4300	4161
140	4354	4419	4228
160	4302	4266	4238
0, irr	**13087**	**13101**	**12645**

Table 2.15 Determined PL response (λ_{em} = 375 nm) for **PMA-CD** (M_n = 180 kDa) upon ultrasonication (1 s on, 2 s off) in 3:1 MeCN/MeOH.

	Trial 1	**Trial 2**	**Trial 3**
Sonication time (min)	**PL**	**PL**	**PL**
0	145	145	146
5	906	861	816
10	1549	1467	1414
20	2466	2469	2240
30	3072	3033	2807
40	3454	3370	3055
50	3763	3695	3347
60	3964	3847	3489
70	4047	3951	3625
80	4159	3982	3673
0, irr	**12046**	**11312**	**10821**

Table 2.16 Determined PL response (λ_{em} = 375 nm) for **PMA-CD** (M_n = 206 kDa) upon ultrasonication (1 s on, 2 s off) in 3:1 MeCN/MeOH.

	Trial 1	**Trial 2**	**Trial 3**
Sonication time (min)	**PL**	**PL**	**PL**
0	154	137	130
5	901	878	769
10	1450	1436	1293
20	2170	2262	2050
30	2567	2755	2490
40	2882	3124	2794
50	2935	3270	3005
60	3028	3413	3099
70	3187	3541	3207
80	3191	3624	3264
0, irr	**9638**	**11562**	**11048**

Table 2.17 Determined GPC-RI response for **PMA-CD** (M_n = 78.7 kDa) upon ultrasonication (1 s on, 1 s off) in 3:1 MeCN/MeOH.

	Trial 1	**Trial 2**
Sonication time (min)	**RI**	**RI**
0	1.41	1.43
90	1.20	1.17
180	0.99	0.99
270	0.83	0.83
360	0.68	0.71
510	0.53	0.53
660	0.41	0.40
750	0.36	0.35
840	0.31	0.31
930	0.29	0.26

Table 2.18 Determined GPC-RI response for **PMA-CD** (M_n = 132 kDa) upon ultrasonication (1 s on, 1 s off) in 3:1 MeCN/MeOH.

	Trial 1	**Trial 2**
Sonication time (min)	**RI**	**RI**
0	1.36	1.38
15	1.11	1.18
30	0.89	0.98
45	0.69	0.80
60	0.58	0.63
90	0.34	0.44
120	0.22	0.30
150	0.15	0.21
180	0.09	0.14

Table 2.19 Determined GPC-RI response for **PMA-CD** (M_n = 180 kDa) upon ultrasonication (1 s on, 1 s off) in 3:1 MeCN/MeOH.

	Trial 1	**Trial 2**	**Trial 3**
Sonication time (min)	**RI**	**RI**	**RI**
0	1.42	1.45	1.44
7.5	1.24	1.24	1.20
15	1.05	1.04	0.98
22.5	0.87	0.86	0.77
30	0.69	0.70	0.61
37.5	0.56	0.57	-
45	0.46	0.45	0.40
60	0.29	0.30	0.24
75	0.20	0.20	0.15
90	0.15	0.14	0.10

Table 2.20 Determined GPC-RI response for **PMA-FM** (M_n = 83.3 kDa) upon ultrasonication (1 s on, 1 s off) in 3:1 MeCN/MeOH.

	Trial 1	**Trial 2**
Sonication time (min)	**RI**	**RI**
0	1.34	1.34
90	1.05	1.01
180	0.77	0.75
270	0.56	0.53
360	0.42	0.38
510	0.27	0.25
660	0.20	0.18
750	0.16	0.16
840	0.13	0.14
930	0.12	0.11

Table 2.21 Determined GPC-RI response for **PMA-FM** (M_n = 137 kDa) upon ultrasonication (1 s on, 1 s off) in 3:1 MeCN/MeOH.

	Trial 1	**Trial 2**	**Trial 3**
Sonication time (min)	**RI**	**RI**	**RI**
0	1.38	1.38	1.39
7.5	1.21	1.19	1.18
15	1.04	1.02	1.01
30	0.80	0.72	0.71
45	0.59	0.52	0.51
60	0.45	0.37	0.38
75	0.34	0.29	0.28
90	0.27	0.23	0.22
105	0.21	0.18	0.18
120	0.17	0.14	0.14

Table 2.22 Determined GPC-RI response for **PMA-FM** (M_n = 182 kDa) upon ultrasonication (1 s on, 1 s off) in 3:1 MeCN/MeOH.

	Trial 1	**Trial 2**
Sonication time (min)	**RI**	**RI**
0	1.36	1.38
5	1.15	1.16
10	0.93	0.97
15	0.74	0.78
22.5	0.53	0.58
30	0.40	0.42
37.5	0.28	0.30
45	0.23	0.23
52.5	0.18	0.17
60	0.14	0.13

Table 2.23 Determined GPC-RI response for **PMA-1** (M_n = 85.0 kDa) upon ultrasonication (1 s on, 1 s off) in 3:1 MeCN/MeOH.

	Trial 1	**Trial 2**
Sonication time (min)	**RI**	**RI**
0	1.56	1.54
90	1.19	1.18
180	0.94	0.86
270	0.76	0.65
360	0.61	0.53
510	0.47	0.40
660	0.36	0.30
750	0.31	0.26
840	0.27	0.22
930	0.22	0.19

Table 2.24 Determined GPC-RI response for **PMA-1** (M_n = 157 kDa) upon ultrasonication (1 s on, 1 s off) in 3:1 MeCN/MeOH.

	Trial 1	**Trial 2**
Sonication time (min)	**RI**	**RI**
0	1.31	1.29
15	1.04	1.05
30	0.88	0.81
45	0.70	0.63
60	0.56	0.52
90	0.38	0.33
120	0.25	0.22
150	0.17	0.16
180	0.11	0.12

Table 2.25 Determined GPC-RI response for **PMA-1** (M_n = 169 kDa) upon ultrasonication (1 s on, 1 s off) in 3:1 MeCN/MeOH.

	Trial 1	**Trial 2**
Sonication time (min)	**RI**	**RI**
0	1.28	1.29
7.5	1.12	1.16
15	0.99	0.98
30	0.76	0.71
45	0.56	0.51
60	0.43	0.30
75	0.37	0.28
90	0.28	0.23
105	0.20	0.18
120	0.17	0.13
135	0.14	0.10

Table 2.26 Determined M_n (kDa) before and after photocleavage for **PMA-CD** (M_n = 78.7 kDa) upon ultrasonication (1 s on, 1 s off) in 3:1 MeCN/MeOH.

	Trial 1		**Trial 2**	
Sonication time (min)	M_n	**M_n after cleavage**	M_n	**M_n after cleavage**
0	77.6	42.7	77.4	42.4
90	63.0	39.1	61.8	38.3
180	55.7	38.7	55.0	36.4
270	51.1	37.0	50.8	35.2
360	48.1	35.1	47.3	35.8
510	43.8	34.2	43.2	35.0
660	41.3	33.2	40.3	32.6
750	39.5	33.6	39.8	32.4
840	38.8	33.1	39.0	30.7
930	38.8	31.7	37.7	32.4

Table 2.27 Determined M_n (kDa) before and after photocleavage for **PMA-CD** (M_n = 132 kDa) upon ultrasonication (1 s on, 1 s off) in 3:1 MeCN/MeOH.

	Trial 1		**Trial 2**	
Sonication time (min)	M_n	**M_n after cleavage**	M_n	**M_n after cleavage**
0	128	67.8	132	70.8
15	107	64.1	110	65.2
30	89.0	59.7	96.5	63.4
45	81.7	58.8	87.2	61.9
60	79.0	56.0	80.5	57.2
90	68.7	53.8	70.9	54.8
120	62.2	50.3	65.6	49.4
150	60.7	47.4	61.7	51.3
180	56.3	45.1	56.2	47.0

Table 2.28 Determined M_n (kDa) before and after photocleavage for **PMA-CD** (M_n = 180 kDa) upon ultrasonication (1 s on, 1 s off) in 3:1 MeCN/MeOH.

	Trial 1		**Trial 2**	
Sonication time (min)	M_n	M_n **after cleavage**	M_n	M_n **after cleavage**
0	181	92.7	171	92.7
7.5	148	88.2	145	86.0
15	126	78.9	124	82.2
22.5	113	74.6	110	79.6
30	95.0	73.2	101	73.6
37.5	93.7	69.5	99.6	70.3
45	86.7	70.9	87.2	69.3
60	78.5	64.5	80.4	64.5
75	70.6	58.1	74.0	60.3
90	69.0	57.3	69.1	58.0

Table 2.29 Determined M_n (kDa) before and after thermal cleavage for **PMA-FM** (M_n = 83.3 kDa) upon ultrasonication (1 s on, 1 s off) in 3:1 MeCN/MeOH.

	Trial 1		**Trial 2**	
Sonication time (min)	M_n	M_n **after cleavage**	M_n	M_n **after cleavage**
0	83.6	44.8	83.0	46.5
90	64.3	45.1	62.1	46.0
180	54.5	45.3	54.4	46.4
270	48.9	43.7	48.5	44.6
360	45.3	44.4	43.8	43.6
510	41.5	40.5	40.4	41.9
660	39.8	41.2	39.6	39.9
750	38.8	40.0	38.2	41.9
840	36.2	39.6	37.4	39.6
930	36.8	37.9	37.4	37.3

Table 2.30 Determined M_n (kDa) before and after thermal cleavage for **PMA-FM** (M_n = 137 kDa) upon ultrasonication (1 s on, 1 s off) in 3:1 MeCN/MeOH.

	Trial 1		Trial 2	
Sonication time (min)	M_n	**M_n after cleavage**	M_n	**M_n after cleavage**
0	137	74.5	137	73.2
7.5	116	74.0	117	70.0
15	103	70.3	104	73.5
30	86.5	70.6	91.3	69.9
45	77.1	72.1	80.3	73.8
60	72.1	71.3	74.3	75.2
75	67.4	60.0	70.5	66.3
90	65.4	59.7	67.3	61.5
105	64.1	60.0	64.0	59.9
120	59.8	58.2	60.6	59.0

Table 2.31 Determined M_n (kDa) before and after thermal cleavage for **PMA-FM** (M_n = 182 kDa) upon ultrasonication (1 s on, 1 s off) in 3:1 MeCN/MeOH.

	Trial 1		Trial 2	
Sonication time (min)	M_n	**M_n after cleavage**	M_n	**M_n after cleavage**
0	181	96.9	183	97.0
5	152	94.6	150	96.2
10	126	92.8	134	95.7
15	115	93.7	118	90.9
22.5	103	88.2	106	89.8
30	94.4	83.1	97.5	88.5
37.5	88.9	81.2	88.0	89.1
45	84.5	85.0	85.4	83.4
52.5	82.2	76.5	83.2	79.9
60	77.1	73.1	82.2	73.7

2.7 References

(1) Caruso, M. M.; Davis, D. A.; Shen, Q.; Odom, S. A.; Sottos, N. R.; White, S. R.; Moore, J. S. Mechanically-Induced Chemical Changes in Polymeric Materials. *Chem. Rev.* **2009**, *109*, 5755–5798.

(2) Beyer, M. K.; Clausen-Schaumann, H. Mechanochemistry: The Mechanical Activation of Covalent Bonds. *Chem. Rev.* **2005**, *105*, 2921–2948.

(3) Li, J.; Nagamani, C.; Moore, J. S. Polymer Mechanochemistry: From Destructive to Productive. *Acc. Chem. Res.* **2015**, *48*, 2181–2190.

(4) Encina, M. V.; Lissi, E.; Sarasúa, M.; Gargallo, L.; Radic, D. Ultrasonic degradation of polyvinylpyrrolidone: Effect of peroxide linkages. *J. Polym. Sci. B Polym. Lett. Ed.* **1980**, *18*, 757–760.

(5) Berkowski, K. L.; Potisek, S. L.; Hickenboth, C. R.; Moore, J. S. Ultrasound-Induced Site-Specific Cleavage of Azo-Functionalized Poly(ethylene glycol). *Macromolecules* **2005**, *38*, 8975–8978.

(6) Hickenboth, C. R.; Moore, J. S.; White, S. R.; Sottos, N. R.; Baudry, J.; Wilson, S. R. Biasing reaction pathways with mechanical force. *Nature* **2007**, *446*, 423–427.

(7) Klein, I. M.; Husic, C. C.; Kovács, D. P.; Choquette, N. J.; Robb, M. J. Validation of the CoGEF Method as a Predictive Tool for Polymer Mechanochemistry. *J. Am. Chem. Soc.* **2020**, *142*, 16364–16381.

(8) Chen, Y.; Mellot, G.; Luijk, D. van; Creton, C.; P. Sijbesma, R. Mechanochemical tools for polymer materials. *Chem. Soc. Rev.* **2021**, *50*, 4100–4140.

(9) May, P. A.; Moore, J. S. Polymer mechanochemistry: techniques to generate molecular force via elongational flows. *Chem. Soc. Rev.* **2013**, *42*, 7497–7506.

(10) Potisek, S. L.; Davis, D. A.; Sottos, N. R.; White, S. R.; Moore, J. S. Mechanophore-Linked Addition Polymers. *J. Am. Chem. Soc.* **2007**, *129*, 13808–13809.

(11) Van Der Hoff, B. M. E.; Glynn, P. A. R. The Rate of Degradation by Ultrasonation of Polystyrene in Solution. *Journal of Macromolecular Science: Part A - Chemistry* **1974**, *8*, 429–449.

(12) Lenhardt, J. M.; Black Ramirez, A. L.; Lee, B.; Kouznetsova, T. B.; Craig, S. L. Mechanistic Insights into the Sonochemical Activation of Multimechanophore Cyclopropanated Polybutadiene Polymers. *Macromolecules* **2015**, *48*, 6396–6403.

(13) Lenhardt, J. M.; Black, A. L.; Craig, S. L. gem-Dichlorocyclopropanes as Abundant and Efficient Mechanophores in Polybutadiene Copolymers under Mechanical Stress. *J. Am. Chem. Soc.* **2009**, *131*, 10818–10819.

(14) Kean, Z. S.; Gossweiler, G. R.; Kouznetsova, T. B.; Hewage, G. B.; Craig, S. L. A Coumarin Dimer Probe of Mechanochemical Scission Efficiency in the Sonochemical Activation of Chain-Centered Mechanophore Polymers. *Chem. Commun.* **2015**, *51*, 9157–9160.

(15) Lee, B.; Niu, Z.; Wang, J.; Slebodnick, C.; Craig, S. L. Relative Mechanical Strengths of Weak Bonds in Sonochemical Polymer Mechanochemistry. *J. Am. Chem. Soc.* **2015**, *137*, 10826–10832.

(16) Konda, S. S. M.; Brantley, J. N.; Varghese, B. T.; Wiggins, K. M.; Bielawski, C. W.; Makarov, D. E. Molecular Catch Bonds and the Anti-Hammond Effect in Polymer Mechanochemistry. *J. Am. Chem. Soc.* **2013**, *135*, 12722–12729.

(17) Overholts, A. C.; McFadden, M. E.; Robb, M. J. Quantifying Activation Rates of Scissile Mechanophores and the Influence of Dispersity. *Macromolecules* **2022**, *55*, 276–283.

(18) Beyer, M. K. The mechanical strength of a covalent bond calculated by density functional theory. *J. Chem. Phys.* **2000**, *112*, 7307–7312.

(19) Odell, J. A.; Keller, A. Flow-induced chain fracture of isolated linear macromolecules in solution. *J. Polym. Sci. B Polym. Phys.* **1986**, *24*, 1889–1916.

(20) Church, D. C.; Peterson, G. I.; Boydston, A. J. Comparison of Mechanochemical Chain Scission Rates for Linear versus Three-Arm Star Polymers in Strong Acoustic Fields. *ACS Macro Lett.* **2014**, *3*, 648–651.

(21) Nguyen, N. H.; Rosen, B. M.; Lligadas, G.; Percec, V. Surface-Dependent Kinetics of Cu(0)-Wire-Catalyzed Single-Electron Transfer Living Radical Polymerization of Methyl Acrylate in DMSO at 25 °C. *Macromolecules* **2009**, *42*, 2379–2386.

(22) Ayer, M. A.; Verde-Sesto, E.; Liu, C. H.; Weder, C.; Lattuada, M.; Simon, Y. C. Modeling ultrasound-induced molecular weight decrease of polymers with multiple scissile azo-mechanophores. *Polym. Chem.* **2021**, *12*, 4093–4103.

(23) Min, Y.; Huang, S.; Wang, Y.; Zhang, Z.; Du, B.; Zhang, X.; Fan, Z. Sonochemical Transformation of Epoxy–Amine Thermoset into Soluble and Reusable Polymers. *Macromolecules* **2015**, *48*, 316–322.

(24) Stevenson, R.; De Bo, G. Controlling Reactivity by Geometry in Retro-Diels–Alder Reactions under Tension. *J. Am. Chem. Soc.* **2017**, *139*, 16768–16771.

(25) Duan, H.-Y.; Wang, Y.-X.; Wang, L.-J.; Min, Y.-Q.; Zhang, X.-H.; Du, B.-Y. An Investigation of the Selective Chain Scission at Centered Diels–Alder Mechanophore under Ultrasonication. *Macromolecules* **2017**, *50*, 1353–1361.

(26) Li, J.; Shiraki, T.; Hu, B.; Wright, R. A. E.; Zhao, B.; Moore, J. S. Mechanophore Activation at Heterointerfaces. *J. Am. Chem. Soc.* **2014**, *136*, 15925–15928.

(27) Stevenson, R.; De Bo, G. Controlling Reactivity by Geometry in Retro-Diels–Alder Reactions under Tension. *J. Am. Chem. Soc.* **2017**, *139*, 16768–16771.

(28) Holden, D. A.; Guillet, J. E. Singlet Electronic Energy Transfer in Polymers Containing Naphthalene and Anthracene Chromophores. *Macromolecules* **1980**, *13*, 289–295.

(29) Lenhardt, J. M.; Black Ramirez, A. L.; Lee, B.; Kouznetsova, T. B.; Craig, S. L. Mechanistic Insights into the Sonochemical Activation of Multimechanophore Cyclopropanated Polybutadiene Polymers. *Macromolecules* **2015**, *48*, 6396–6403.

(30) Odell, J. A.; Keller, A. Flow-induced chain fracture of isolated linear macromolecules in solution. *J. Polym. Sci. Polym. Phys.* **1986**, *24*, 1889–1916.

(31) Carvajal, C.; Tölle, K. J.; Smid, J.; Szwarc, M. Studies of Solvation Phenomena of Ions and Ion Pairs in Dimethoxyethane and Tetrahydrofuran. *J. Am. Chem. Soc.* **1965**, *87*, 5548–5553.

(32) Berkowski, K. L.; Potisek, S. L.; Hickenboth, C. R.; Moore, J. S. Ultrasound-Induced Site-Specific Cleavage of Azo-Functionalized Poly(ethylene glycol). *Macromolecules* **2005**, *38*, 8975–8978.

Chapter 3

MECHANICALLY GATED FORMATION OF DONOR–ACCEPTOR STENHOUSE ADDUCTS ENABLING MECHANOCHEMICAL MULTICOLOR SOFT LITHOGRAPHY[1]

Stress-sensitive molecules called mechanophores undergo productive chemical transformations in response to mechanical force. A variety of mechanochromic mechanophores, which change color in response to stress, have been developed, but modulating the properties of the dyes generally requires the independent preparation of discrete derivatives. Here we introduce a mechanophore platform enabling mechanically gated multicolor chromogenic reactivity. The mechanophore is based on an activated furan precursor to donor–acceptor Stenhouse adducts (DASAs) masked as a hetero-Diels–Alder adduct. Mechanochemical activation of the mechanophore unveils the DASA precursor and subsequent reaction with a secondary amine generates an intensely colored DASA. Critically, the properties of the DASA are controlled by the amine and thus a single mechanophore can be differentiated post-activation to produce a wide range of functionally diverse DASAs. We highlight this system by establishing the concept of mechanochemical multicolor soft lithography whereby a complex multicolor composite image is printed into a

[1] Portions of this chapter were adapted from Overholts, A. C.; Granados Razo, W.; Robb, M. J. Mechanically gated formation of donor–acceptor Stenhouse adducts enabling mechanochemical multicolor soft lithography. *Nat. Chem.* **2023**, *15*, 332-338. https://doi.org/10.1038/s41557-022-01126-5.

mechanochemically active elastomer through an iterative process of localized compression followed by reaction with different amines.

3.1 Introduction

Covalent polymer mechanochemistry has enabled many exciting opportunities for the design of force-responsive polymeric materials.[1,2] Mechanical force typically leads to the degradation of materials by rupturing covalent bonds in the backbones of polymers. By covalently incorporating stress-sensitive molecules called mechanophores into polymer chains, however, force is transduced selectively to weak bonds in the mechanophore to elicit a productive chemical transformation.[3] Mechanical force is a ubiquitous and versatile stimulus that can be applied using a variety of methods including solution-phase ultrasonication;[4] focused ultrasound;[5] and tension, compression, or shear in solid polymeric materials.[6–8] The spatiotemporal control afforded by many mechanochemical activation techniques makes mechanical force an attractive stimulus for a wide range of materials applications including the release of small molecules,[9] structural transformations such as changes in conductivity[10] or crosslinking,[11] and changes in color or luminescence,[6] among many others.[12]

Mechanochromic mechanophores, in particular, have been widely developed as molecular force probes, empowering the visualization of critical stress and/or strain in materials.[13] These same attributes also make force-induced color changes in polymeric materials appealing for patterning and encryption. Pioneering research by Davis *et al.* demonstrated the force-induced ring-opening reaction of spiropyran in polymeric materials activated under tension and compression to generate a highly colored merocyanine dye (Figure 3.1a).[6] While many different mechanochromic mechanophores have now been developed with a range of structures and reactivity, modulating the photophysical properties of the dyes typically requires distinct derivatives to be synthesized

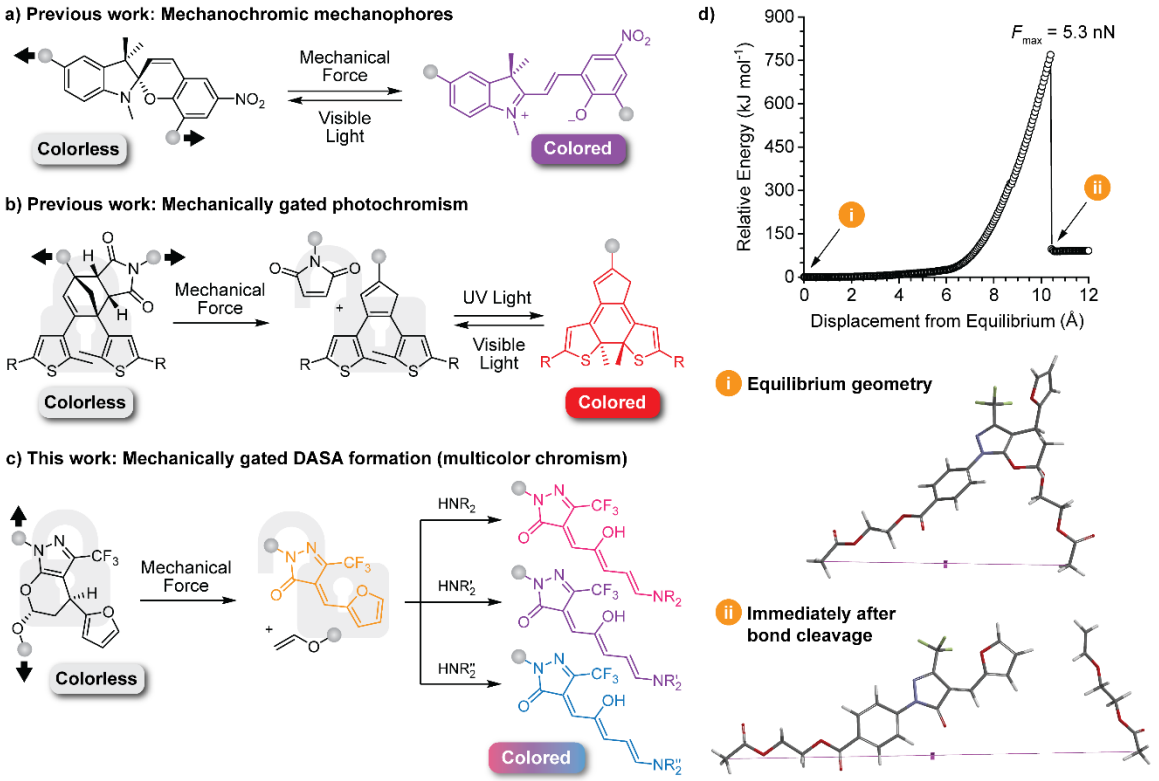

Figure 3.1 Evolution in the design of mechanochromic mechanophores and a platform enabling mechanically gated DASA formation. (a) The reaction of a prototypical spiropyran mechanophore under mechanical force generates a colored merocyanine dye. (b) Mechanical force unmasks a diarylethene photoswitch via a retro-[4+2] cycloaddition reaction, gating the photoisomerization reaction that produces the colored ring-closed form. (c) Mechanically triggered retro-[4+2] cycloaddition reaction reveals an activated furan that reacts with a secondary amine to form a DASA photoswitch. (d) Density functional theory (DFT) calculations using the constrained geometries simulate external force (CoGEF) method predict the desired retro-[4+2] cycloaddition reaction upon mechanical elongation of a hetero-Diels–Alder adduct similar to the model in part (c) with a rupture force (F_{max}) of 5.3 nN. Calculations were performed at the B3LYP/6-31G* level of theory.

independently, which is a general limitation of this class of compounds. In an alternative approach to achieving mechanochromic functionality, our group developed the concept of mechanochemically gated photoswitching.[14,15] This strategy overcomes disadvantages of reversibility and a lack of mechanochemical specificity encountered with typical mechanochromic mechanophores by using mechanical force to unmask a latent photoswitch, which is then converted to a colored species via a photoisomerization reaction (Figure 3.1b). An enticing feature of this general molecular design strategy is that

mechanochemical activation of the mechanophore is decoupled from the ultimate functional response, which provides a high degree of modularity to the system. Nevertheless, while the absorption properties of the dye can be modified by late-stage diversification of the mechanophore, several synthetic manipulations are still required to prepare each distinct polymer.[15] Moreover, the differential mechanochemical activation of mechanophores with intrinsically different reactivity has proved challenging in the solid state.[16,17]

DASAs are a recently established class of highly modular, optically tunable, and robust visible-light photoswitches.[18] Since being introduced by Read de Alaniz and coworkers in 2014, DASAs have been widely developed and used in a variety of applications including sensing,[19–21] drug release,[22] and photoactuatation.[23] Their synthetic accessibility and simple diversification coupled with excellent photophysical properties have driven their rapid adoption.[24] DASAs are derived from simple activated furan precursors that react with secondary amines to produce an intensely colored extended triene donor–acceptor scaffold with extinction coefficients around 100,000 M^{-1} cm^{-1}.[18] Importantly, the color, stability, and photoswitching behavior of DASAs are strongly influenced by the identity of the secondary amine in addition to the electron-withdrawing acceptor group of the activated furan precursor.[25,26]

Similar to the approach employed for mechanically gated photoswitching, we hypothesized that a DASA precursor could be masked as a mechanochemically active hetero-Diels–Alder adduct (Figure 3.1c). In this case, a mechanically promoted retro-[4+2] cycloaddition reaction would reveal the activated furan, which could then be easily differentiated to generate a wide variety of highly colored and functionally diverse DASAs

simply by treatment with different secondary amines. Here, we describe a mechanophore platform based on a masked DASA precursor that enables a mechanochemical multicolor chromogenic response. Mechanochemical activation is achieved in solution using ultrasonication and in solid polymeric materials under tension and compression. After mechanical activation, the addition of various secondary amines produces a chromogenic reaction leading to distinctly colored DASAs, all from a single mechanophore. We demonstrate the power of this mechanochemical platform by establishing the concept of mechanochemical multicolor soft lithography, whereby the iterative application of mechanical force and amine developer is used to print a complex multicolor image in an elastomeric polydimethylsiloxane (PDMS) film.

3.2 Mechanophore Design and Synthesis

We first identified a third-generation DASA photoswitch bearing a CF_3-pyrazolone acceptor, which shifts the thermal equilibrium of the DASA nearly completely to the triene (colored) form.[25] Due to the electron deficiency of the activated furan DASA precursor, we proposed that an inverse electron demand hetero-Diels–Alder reaction between the α,β-unsaturated carbonyl of the pyrazolone and an electron-rich vinyl ether would generate the desired cycloadduct (see Figure 3.1c).[27] The regiochemistry of Diels–Alder mechanophores is paramount in determining their force-sensitivity, with proximal polymer attachment points directing force more efficiently to a single scissile bond in the adduct.[28] Although only bicyclic mechanophores have been investigated, we anticipated that the electronically favored regioisomer would be mechanochemically competent. Indeed, density functional theory (DFT) calculations using the constrained geometries simulate

external force (CoGEF) method[29] predict that mechanical elongation of the hetero-Diels–Alder adduct results in the expected retro-[4+2] cycloaddition reaction to reveal the DASA precursor with an accessible rupture force of 5.3 nN (Figure 3.1d).[30]

Following the successful computational prediction, synthesis of the putative mechanophore was accomplished in a straightforward fashion (Figure 3.2). Activated furan **1** was synthesized on gram scale in two steps from commercially available materials.[23] Next, carbodiimide coupling using *N*-(3-dimethylaminopropyl)-*N*′-ethylcarbodiimide hydrochloride (EDC·HCl) with ethylene glycol produced DASA precursor **2** in 50% yield,

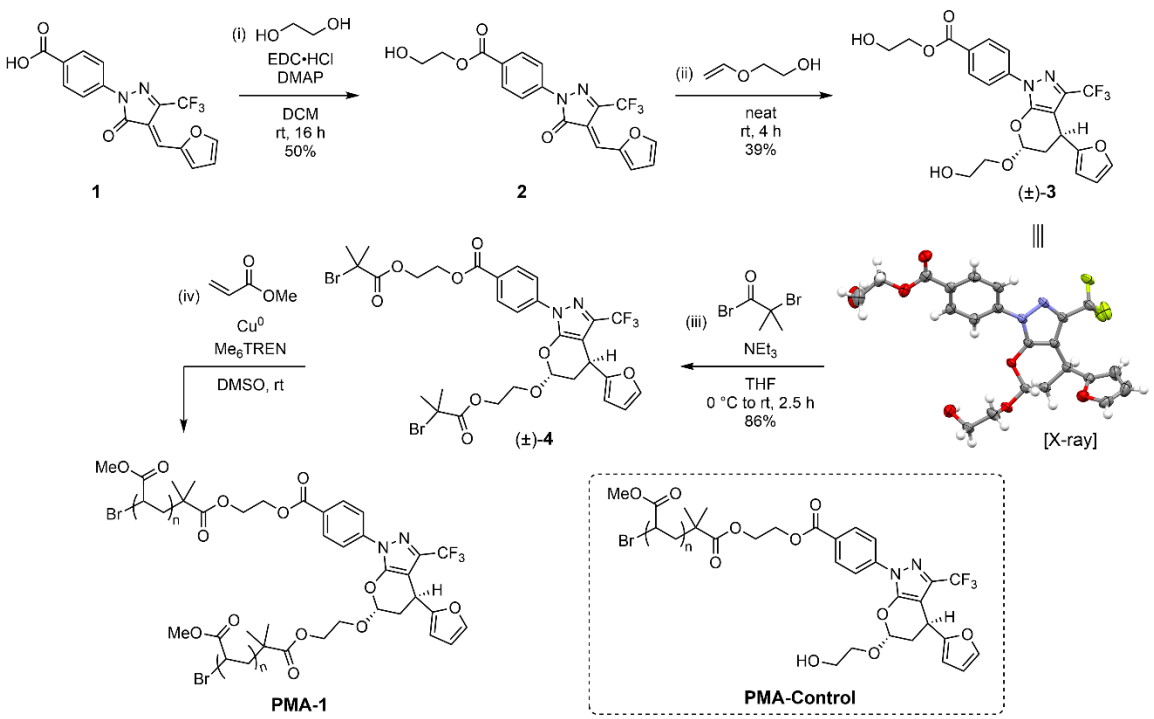

Figure 3.2 Synthesis of linear poly(methyl acrylate) polymers containing the masked DASA precursor at the chain midpoint (PMA-1) and at the chain-end (PMA-Control) for ultrasonication experiments. Conditions: (i) Ethylene glycol (9.6 equiv.), *N*-(3-Dimethylaminopropyl)-*N*′-ethylcarbodiimide hydrochloride (EDC•HCl, 1.2 equiv.), and 4-dimethylaminopyridine (DMAP, 0.07 equiv.) in DCM at room temperature for 16 h to afford 50% yield. (ii) Ethylene glycol vinyl ether (33 equiv.) at room temperature for 4 h to afford 39% yield. (iii) α-Bromoisobutyryl bromide (4.4 equiv.) and triethylamine (3.9 equiv.) in THF at 0 °C to room temperature over 2.5 h to afford 86% yield. (iv) Methyl acrylate (2030 equiv.), copper wire, and tris[2-(dimethylamino)ethyl]amine (Me_6TREN, 3.0 equiv.) in dimethyl sulfoxide at room temperature for 1.5 h. The structure of hetero-Diels–Alder adduct (±)-3 as confirmed by single crystal X-ray diffraction is shown.

followed by an inverse electron demand hetero-Diels–Alder reaction with ethylene glycol vinyl ether to generate cycloadduct (±)-**3** as a racemic mixture in 39% yield. The structure of the hetero-Diels-Alder adduct, which contains two terminal hydroxyl groups for further functionalization to facilitate its incorporation into polymers, was confirmed by single crystal X-ray diffraction (see section 3.7.9 for details). The thermal stability of (±)-**3** was also confirmed by heating the compound in toluene-d_8 at 80 °C for 3 h, which resulted in negligible change to the ^{1}H NMR spectrum (Figure 3.3). When dilute polymer solutions are subjected to ultrasonication, cavitation-induced solvodynamic shear results in the rapid extension of the polymers and mechanical force is maximized near the center of the chain.[4] Following conventional methods,[3] diol (±)-**3** was esterified with α-bromoisobutyryl bromide to afford (±)-**4**, which was used as a bis-initiator in the controlled radical polymerization of methyl acrylate to give mechanophore chain-centered poly(methyl

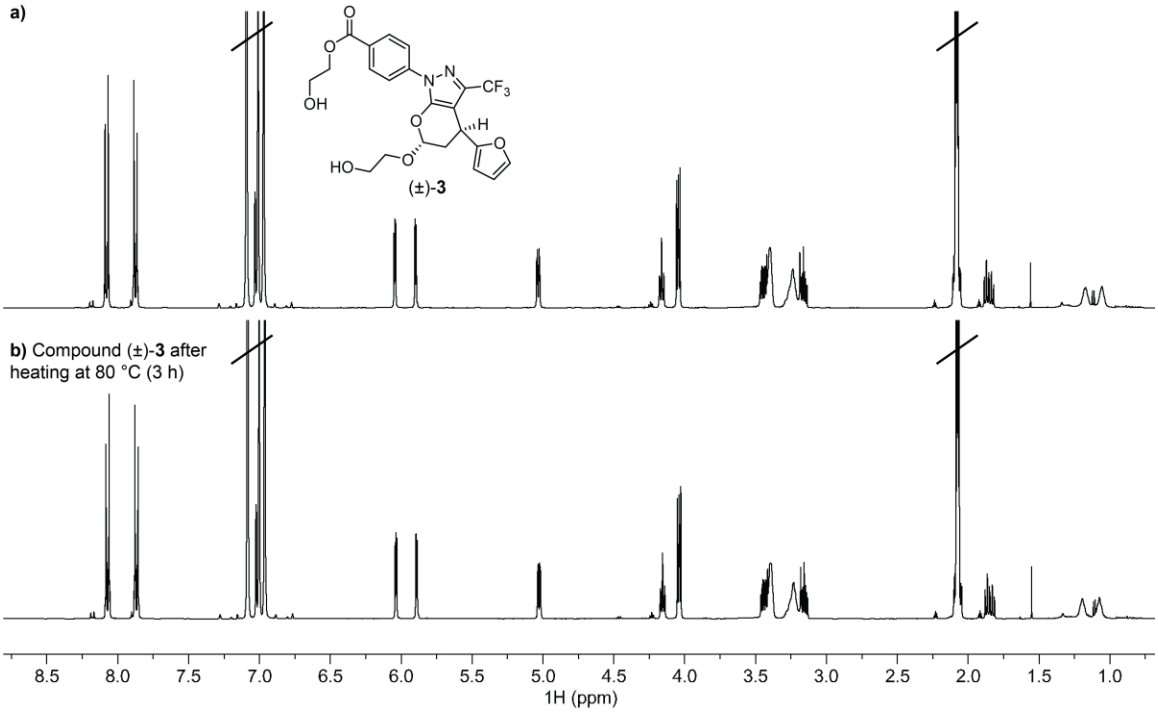

Figure 3.3 ^{1}H NMR spectra (400 MHz, toluene-d_8) of hetero-Diels–Alder adduct (±)-**3** (a) before and (b) after heating at 80 °C for 3 h, illustrating the thermal stability of the adduct.

acrylate) polymer **PMA-1** with M_n = 125 kDa and $Đ$ = 1.15. Separately, a derivative of (±)-**3** containing a single α-bromoisobutyryl ester was used to synthesize control polymer **PMA-Control** incorporating the masked DASA precursor at the chain-end, which is not subjected to mechanical force during ultrasonication.

3.3 Mechanical Activation and Chromogenic Reactivity in Solution

The reactivity of the masked DASA precursor in **PMA-1** was initially evaluated by subjecting a dilute polymer solution (5 mg/mL in THF, 30 mM butylated hydroxytoluene) to 60 min of pulsed ultrasonication (6–9 °C, 1 s on/2 s off, 13.6 W cm^{-2}) followed by treatment with various secondary amines (Figure 3.4a). First, aliquots were removed during sonication at regular intervals for analysis by gel permeation chromatography (GPC) and UV–visible (UV-vis) spectroscopy to characterize the mechanochemical transformation of the hetero-Diels–Alder adduct (Figure 3.6 and Figure 3.5, see section 3.7.3 for details). Ultrasound-induced mechanical activation of **PMA-1** results in the appearance of a new absorption peak at λ_{max} = 378 nm that matches the absorption spectrum of small molecule reference compound **Ref-1**, which was independently prepared to model the expected activated furan product (Figure 3.4b and Figure 3.4c). Approximately 39% mechanophore activation was achieved under these conditions (see section 3.7.5 for details). Additionally, ^{1}H NMR spectra acquired after ultrasonication of **PMA-1** demonstrate the appearance of resonances corresponding to the retro-Diels–Alder products (Figure 3.7). By direct contrast, no reaction was observed by UV-vis or NMR spectroscopy upon ultrasonication of **PMA-Control** under the same conditions (Figure 3.6 and Figure 3.8, respectively), confirming that the reaction of the masked DASA precursor is mechanochemical in nature.

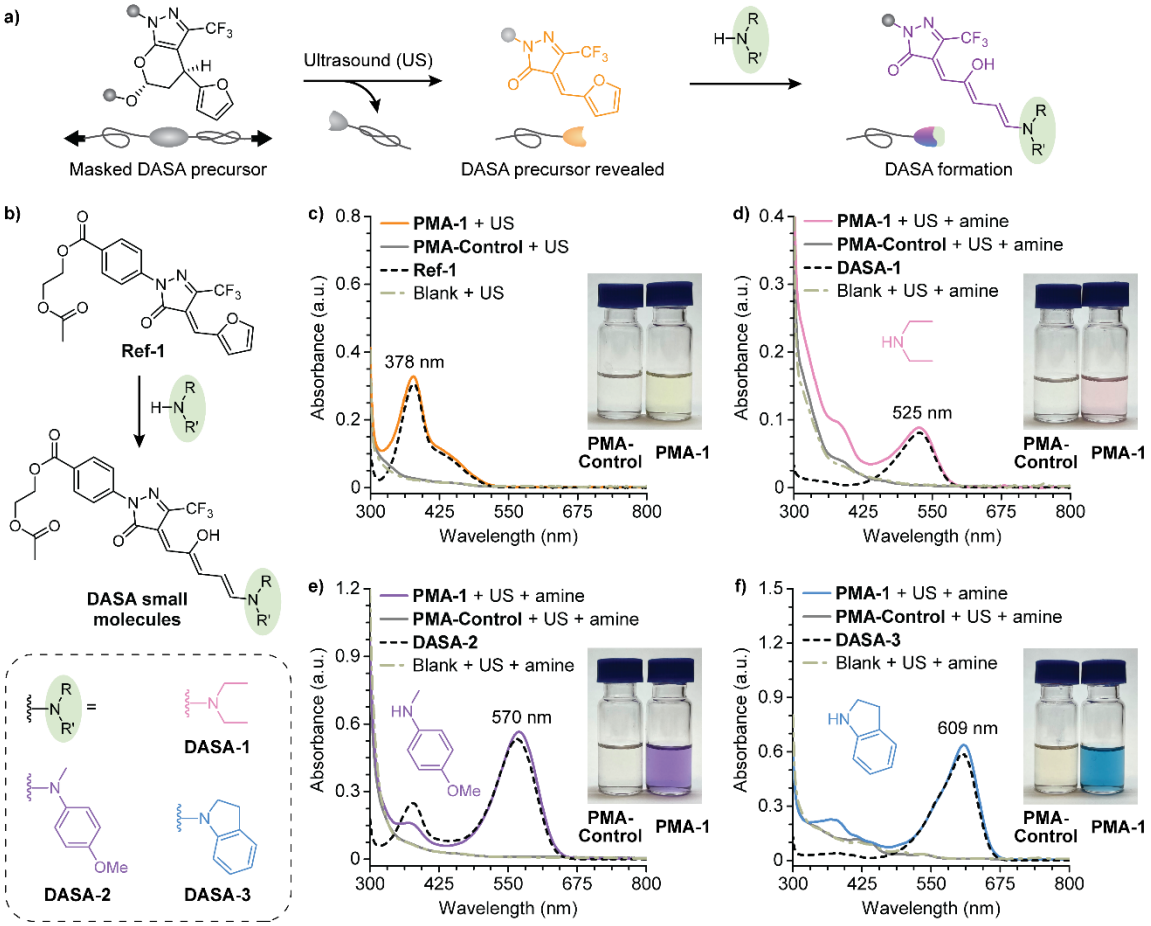

Figure 3.4 Characterization of mechanically gated DASA formation via solution-phase ultrasonication. (a) Scheme illustrating mechanophore activation upon ultrasonication (US) of a chain-centered polymer. Mechanical force induces the retro-[4+2] cycloaddition reaction producing the activated furan, which is converted to a highly colored DASA upon treatment with a secondary amine. (b) Structures of **Ref-1** and small molecule DASA compounds derived from **Ref-1** used as analytical references. (c) UV–vis absorption spectra of **PMA-1**, **PMA-Control**, or a blank solution after 60 min of ultrasonication compared with the absorption spectrum of **Ref-1**. (d-f) Sonicated samples from (c) after being concentrated and redissolved in DCM/HFIP prior to addition of the indicated amine. Spectra of **PMA-1** after ultrasound-induced mechanical activation and amine addition match the spectra of the small molecule compounds, while similar treatment of **PMA-Control** does not lead to DASA formation. Photographs in (c-f) show the corresponding solutions of **PMA-Control** and **PMA-1** after ultrasonication and addition of each amine. The absorption spectra of the small molecule models are scaled arbitrarily for comparison.

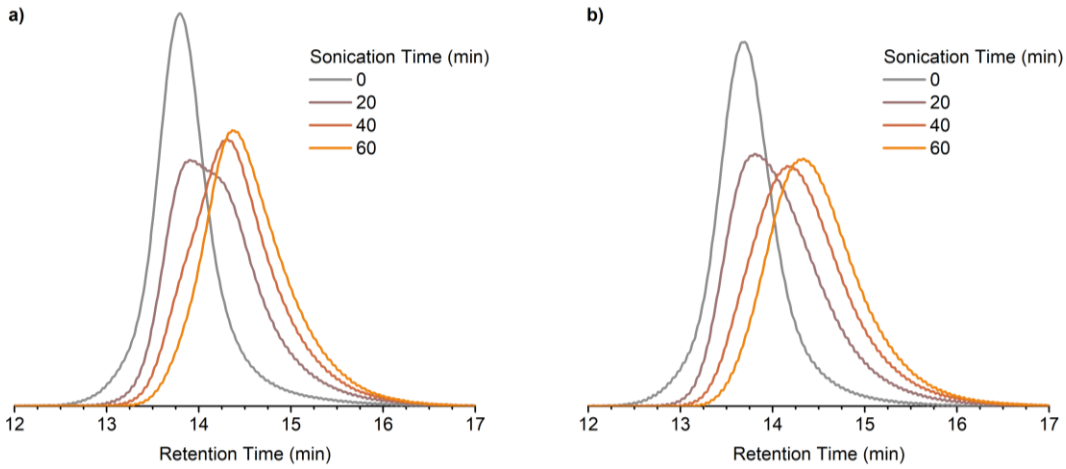

Figure 3.5 Gel permeation chromatograms (refractive index response) illustrating the time-dependent evolution of molecular weight upon ultrasonication (5 mg/mL in THF, 30 mM BHT) of (a) **PMA-1** and (b) **PMA-Control**. Curves are normalized by peak area.

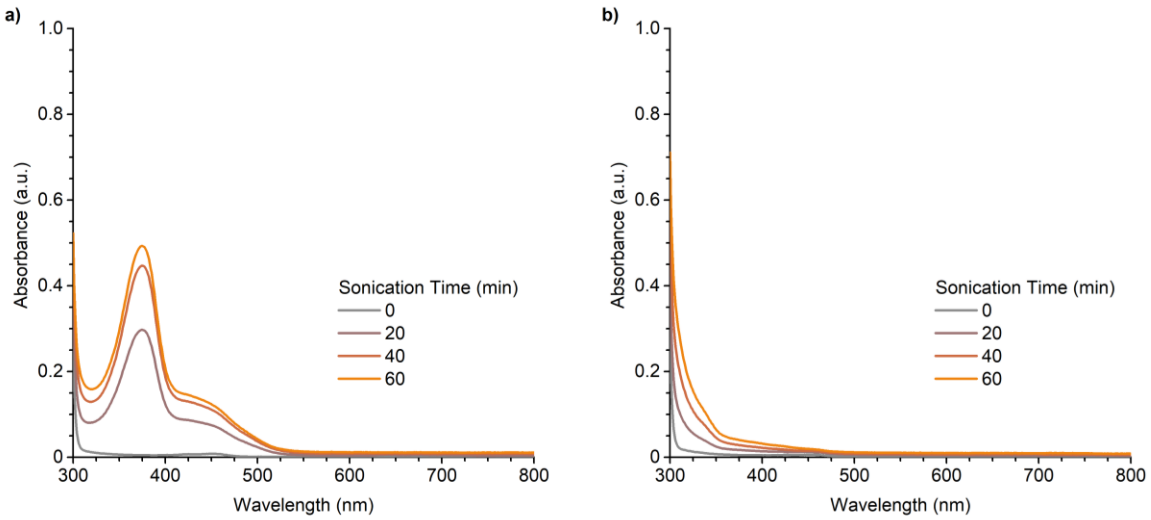

Figure 3.6 Characterization of ultrasound-induced mechanochemical activation of **PMA-1** and **PMA-Control** by UV–vis spectroscopy in THF (5 mg/mL, 30 mM BHT). (a) Ultrasonication of mechanophore chain-centered polymer **PMA-1** generates a new absorption signal with a peak at 375 nm that increases with sonication and matches that of small molecule DASA precursor **Ref-1**. (b) No new absorption peaks are observed upon ultrasonication of mechanophore chain-end control polymer **PMA-Control**.

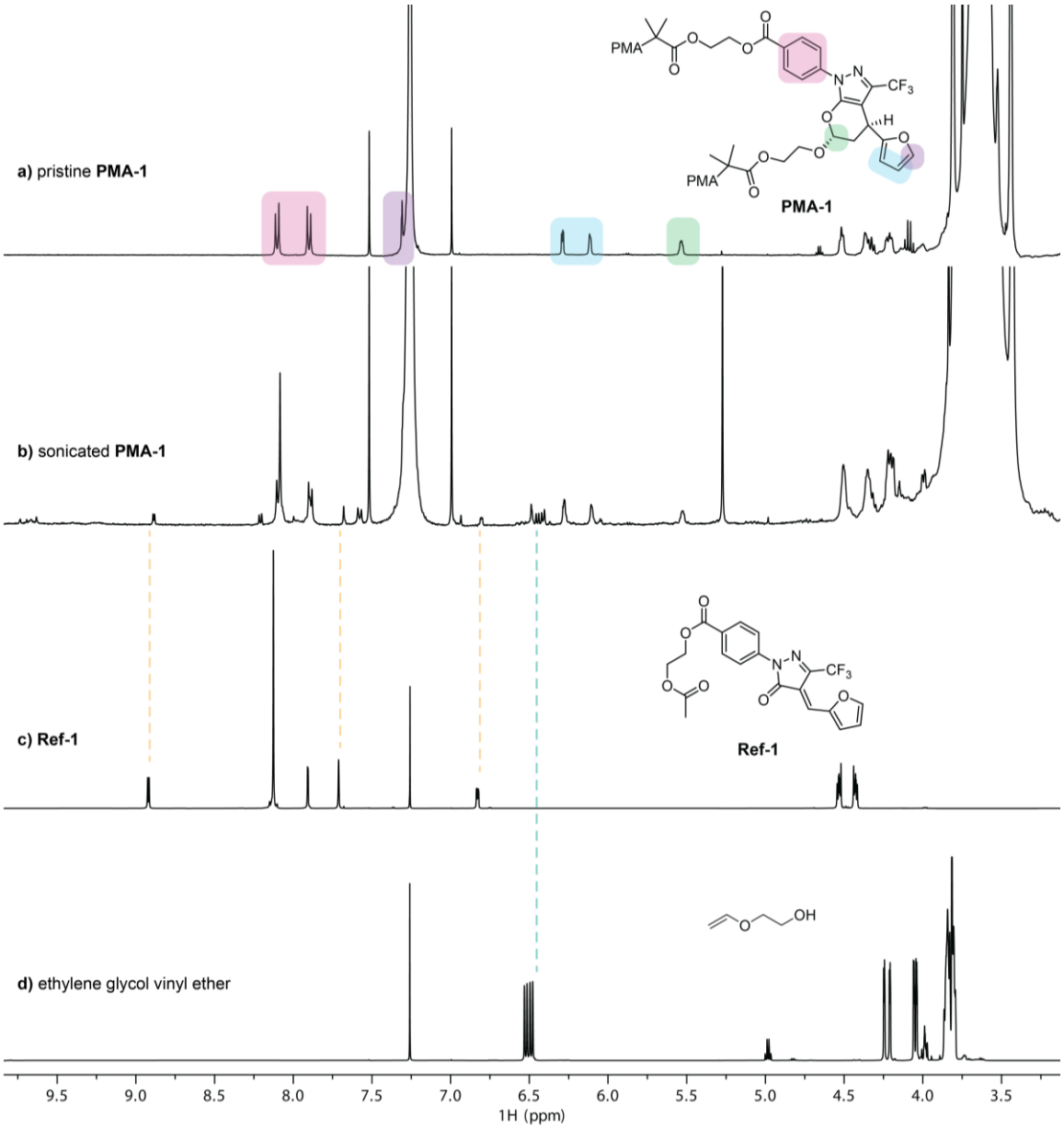

Figure 3.7 ^{1}H NMR spectra (400 MHz, $CDCl_3$) of mechanophore chain-centered **PMA-1** (a) before and (b) after 1 h of ultrasonication, compared to (c) reference small molecule **Ref-1** and (d) ethylene glycol vinyl ether. New peaks consistent with the expected retro-[4+2] cycloaddition reaction to form the activated furan precursor and vinyl ether dienophile appear after mechanochemical activation of **PMA-1**.

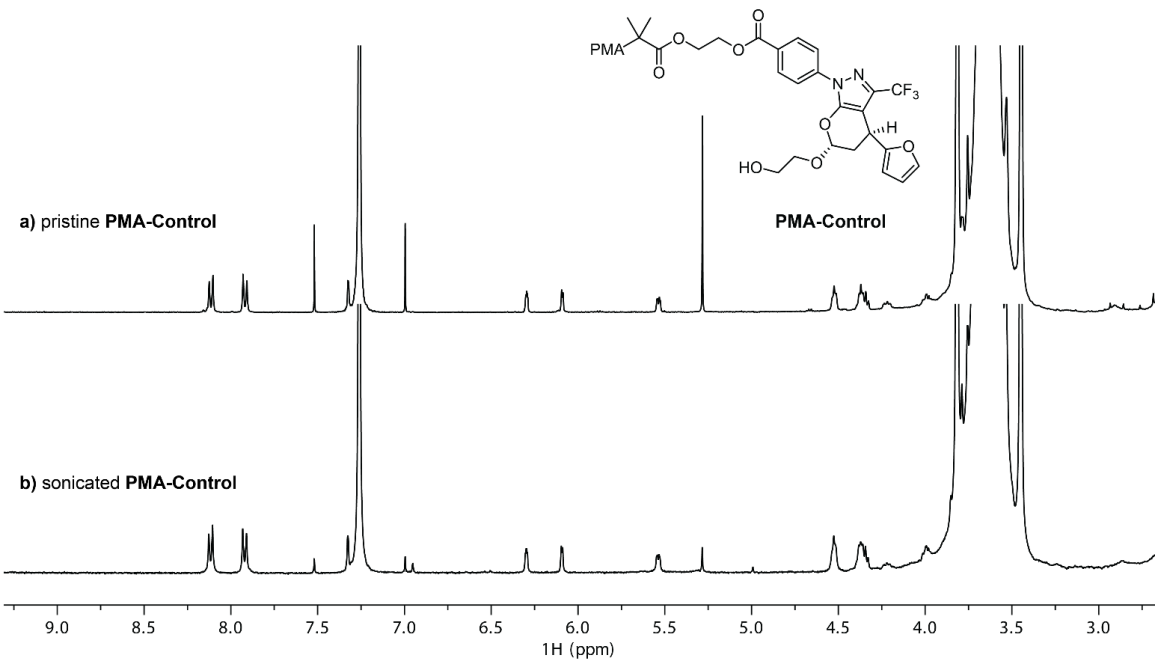

Figure 3.8 ^{1}H NMR spectra (400 MHz, $CDCl_3$) of chain-end functional control polymer **PMA-Control** (a) before, and (b) after 60 min of ultrasonication. No change is observed after ultrasonication, confirming that mechanical force is necessary for mechanophore activation and that non-mechanochemical side reactions are minimal. Small peaks in the spectrum at 7.0 and 5.0 ppm after ultrasonication correspond to residual BHT.

We next investigated DASA formation and the accompanying chromogenic response upon treatment of the mechanochemically generated DASA precursor with different secondary amines as illustrated schematically in Figure 3.4a. Small molecule DASA model compounds **DASA-1**, **DASA-2**, and **DASA-3** were prepared by reaction of **Ref-1** with diethylamine, 4-methoxy-*N*-methylaniline, or indoline, respectively, for spectral comparison as before (Figure 3.4b). The sonicated solution of **PMA-1** was concentrated and then redissolved in a 4:1 (v/v) mixture of dichloromethane (DCM) and 1,1,1,3,3,3-hexafluoro-2-propanol (HFIP), which promotes DASA formation and stabilizes the triene (colored) form.[31] The addition of the same secondary amines as above to the mechanically activated polymer solutions results in the generation of new absorption peaks that match the UV–vis absorption spectra of the corresponding DASA model compounds (Figure 3.4d–f). Notably, the colors of the DASA

products derived from the same activated mechanophore vary widely from pink (λ_{max} = 525 nm) to purple (λ_{max} = 570 nm) to blue (λ_{max} = 609 nm) depending on the identity of the secondary amine used in the DASA-forming step. The absorption spectra recorded after the same treatment of **PMA-Control** are indistinguishable from the blanks in all cases, confirming that DASA formation proceeds only after mechanochemical activation of the masked DASA precursor.

3.4 Mechanically Gated DASA Formation in Polymeric Materials

After confirming the mechanochemical and chromogenic reactivity of the hetero-Diels–Alder mechanophore in solution, we sought to demonstrate mechanophore activation and DASA formation in bulk polymeric materials. Crosslinker (±)-**5a** and monofunctional control molecule (±)-**5b** equipped with two or one terminal vinyl group(s), respectively, were covalently incorporated into elastomeric PDMS materials (2.5 wt% loading) via platinum-catalyzed hydrosilylation (Figure 3.9a and b, see section 3.7.4 for details).[7] The films were optically clear and colorless. Application of tensile force to a strip of **PDMS-1** containing the mechanophore as a crosslinker produced no discernable change in color; however, immersion of the mechanically activated material in a solution of 4-methoxy-*N*-methylaniline (7.3 mM in 9:1 DCM/HFIP) generated a blue-green color selectively in the gauge region of the film (Figure 3.9c). The imperceptible coloration after initial stretching is likely due to the low concentration of the activated mechanophore in conjunction with the relatively low absorptivity of the activated furan DASA precursor (Figure 3.10). The blue-green coloration of the activated material is reversibly photobleached by irradiation with intense white light, with the colored triene form rapidly regenerating within seconds upon

removal of the light source, emphasizing the photoswitching properties of the DASA product (Figure 3.9c and Figure 3.11).[32] Analogous experiments performed using indoline and diethylamine produced similar results (Figure 3.12 and Figure 3.13). Notably, HFIP was

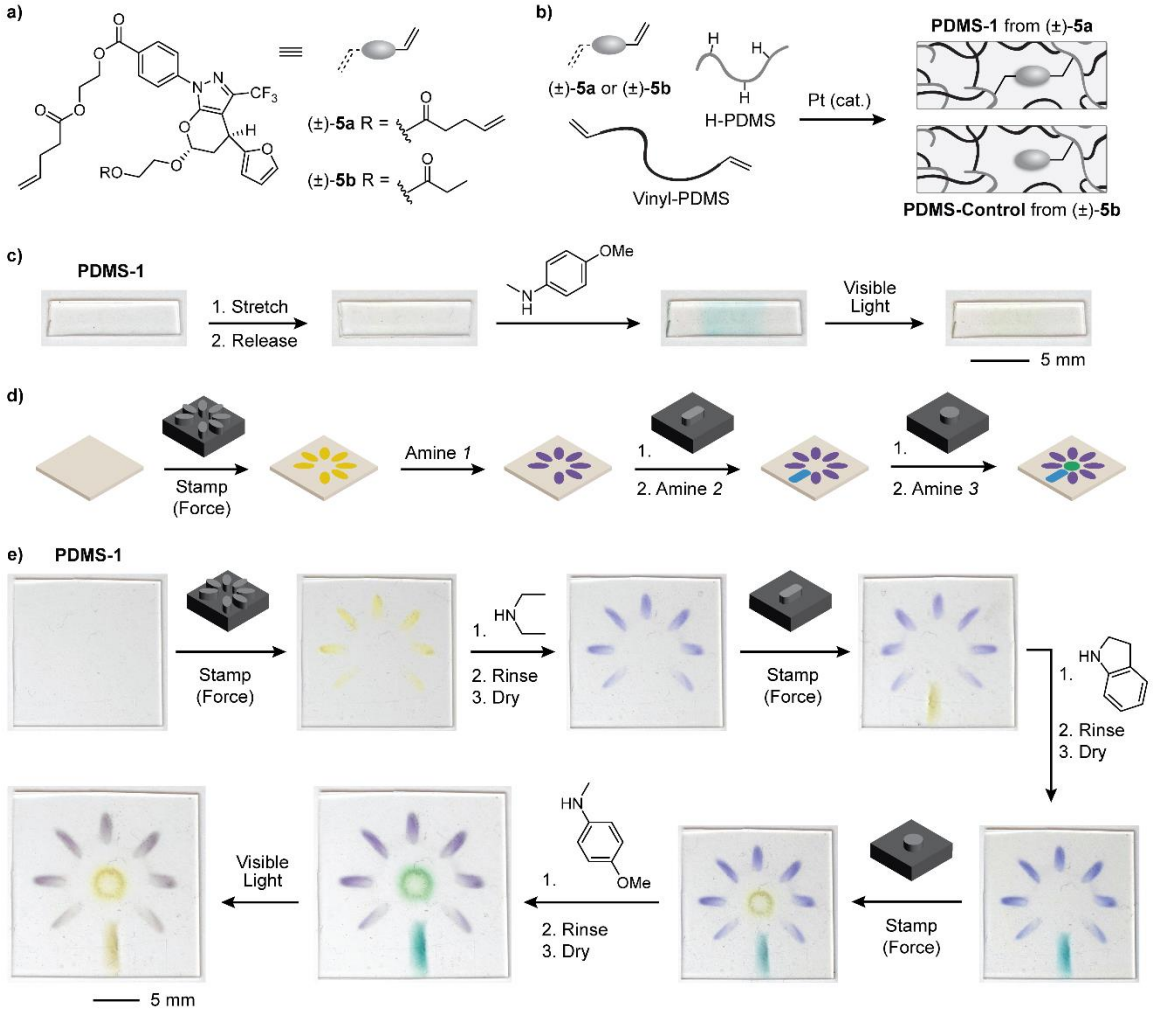

Figure 3.9 Solid-state mechanophore activation in elastomeric PDMS materials and demonstration of mechanochemical multicolor lithography. (a) Structures of bis-functional mechanophore crosslinker (±)-**5a** and mono-functional control molecule (±)-**5b**. (b) Scheme illustrating the covalent incorporation of (±)-**5a** and (±)-**5b** into PDMS (2.5 wt%) via hydrosilylation to produce mechanochemically active **PDMS-1** and control material **PDMS-Control**. cat., catalyst. (c) Tension applied to a strip of **PDMS-1** followed by the addition of 4-methoxy-*N*-methylaniline generates a DASA photoswitch leading to blue−green coloration in the gauge region of the material. Subsequent irradiation with visible light for 30 s results in photoisomerization to the colorless ring-closed form. (d) Schematic representation of the mechanochemical multicolor soft lithography process (STAMMP) with iterative localized compression followed by pattern development via DASA formation using a secondary amine. (e) The STAMMP process applied to **PDMS-1** achieves a complex multicolor image of a flower, which is partially photobleached upon irradiation with visible light.

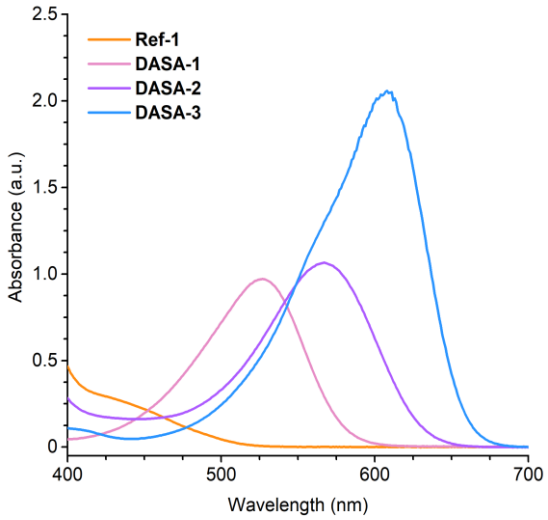

Figure 3.10 Absorption spectra of small molecule reference samples (~26 μM in 4:1 DCM/HFIP with 30 mM BHT). These conditions were chosen to be comparable to those in the ultrasonication experiments.

Figure 3.11 Photographs of a film of mechanochemically active **PDMS-1** containing 2.5 wt% of mechanophore crosslinker (±)-**5a** after manual tensile activation and subsequent immersion for 90 s in a solution of 4-methoxy-*N*-methylaniline (7 mM in 9:1 DCM/HFIP). The blue–green colored DASA is generated in the gauge region of the sample. Subsequent exposure to visible light irradiation for 30 s induces photoswitching to the colorless closed form of the DASA. Cessation of irradiation leads to rapid regeneration of the colored form under ambient conditions.

Figure 3.12 Photographs of a film of mechanochemically active **PDMS-1** containing 2.5 wt% of mechanophore crosslinker (±)-**5a** after manual tensile activation and subsequent immersion for 90 s in a solution of indoline (0.5 vol% in 9:1 DCM/HFIP). The blue–green colored DASA is generated in the gauge region of the sample. Exposure to visible light irradiation for 30 s induces photoswitching to the colorless closed form of the DASA. Cessation of irradiation results in the rapid regeneration of the colored triene form under ambient conditions.

necessary to promote rapid DASA formation with the aryl amines (Figure 3.14), while application of diethylamine in the gas phase was competent for DASA formation (Figure 3.15). No change in color was produced in **PDMS-Control** upon stretching and subsequent exposure to the amine, confirming that mechanical force must be transferred across the mechanophore to induce the retro-Diels–Alder reaction and reveal the requisite precursor for DASA formation (Figure 3.16).

Figure 3.13 Photographs of a film of mechanochemically active **PDMS-1** containing 2.5 wt% of mechanophore crosslinker (±)-**5a** after manual compression and subsequent immersion for 90 s in a solution of diethylamine (0.5 vol% in DCM). The purple colored DASA is generated in the compressed region of the sample. Exposure to visible light irradiation for 30 s induces photoswitching to the colorless closed form of the DASA. Cessation of irradiation results in the regeneration of the colored triene form after several minutes under ambient conditions.

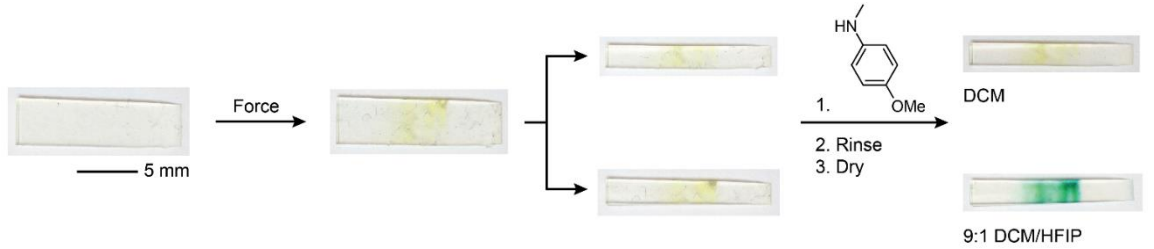

Figure 3.14 Photographs of a film of mechanochemically active **PDMS-1** containing 2.5 wt% of mechanophore crosslinker (±)-**5a** after manual compression. The original sample was cut into two portions after compression and each film was immersed in a solution of 4-methoxy-*N*-methylaniline for 90 s with either DCM or 9:1 DCM/HFIP as the solvent. The sample immersed in the DCM solution (*top*) shows no change in color, indicating no DASA formation. The sample immersed in the 4:1 DCM/HFIP solution shows the generation of a green color in the region of compression, demonstrating the ability of HFIP to promote rapid DASA formation as previously reported by Read de Alaniz and coworkers.[2]

Figure 3.15 Photographs of a film of mechanochemically active **PDMS-1** containing 2.5 wt% of mechanophore crosslinker (±)-**5a** after localized compression via stamping and subsequent exposure to diethylamine vapor for 7 min. The purple-colored DASA is generated in the force-activated region of the sample.

Figure 3.16 Photographs of control film **PDMS-Control** containing 2.5 wt% of monofunctional mechanophore (±)-**5b** after manual tensile activation and subsequent immersion for 90 s in a solution of 4-methoxy-*N*-methylaniline (7 mM in 9:1 DCM/HFIP). No change in color is observed, indicating that force must be applied across the mechanophore to achieve activation and DASA formation.

3.5 Mechanochemical Multicolor Soft Lithography

The unique mechanically gated chromogenic reactivity of the mechanophore presents exciting opportunities for patterning soft materials. We envisioned an iterative process in which the localized application of compressive force using a stamp would reveal the DASA precursor with spatiotemporal precision and the pattern could be "developed" by subsequent treatment with an appropriate amine to generate the colored DASA photoswitch in the regions of mechanical activation. This process, which we refer to as Spatiotemporally Templated Activation for Mechanochemical Multicolor Printing, or STAMMP, is illustrated schematically in Figure 3.9d for the production of a tricolor flower image using three different stamps and three different amines. To reproduce this sequence in the laboratory, a hydraulic press and 3D-printed stamps were used to print the composite image of a flower into a 4 cm^2 film of **PDMS-1** (Figure 3.9e, see section 3.7.6 for additional details). First, a stamp embossed with a flower petal pattern was applied to the PDMS film, generating the yellow-colored DASA precursor in the regions of compression. Next, the film was immersed in a solution of diethylamine (0.5 vol% in DCM) for 90 s, converting the activated furan to the DASA and transforming the color of the petal pattern from yellow to purple. After rinsing the film repeatedly with DCM to remove excess amine and then drying *in vacuo*, the sequence was repeated using separate stamps to form the flower stem and the center of the flower, which were developed using indoline (blue) and 4-methoxy-*N*-methylaniline (green), respectively, in 4:1 DCM/HFIP. Model experiments suggest that DASA formation is efficient under these conditions with complete conversion of the mechanochemically revealed activated furan (Figure 3.17). We also note that the color of DASAs is strongly dependent on the environment (Figure 3.18 and Figure 3.19).[33] The flower image is partially

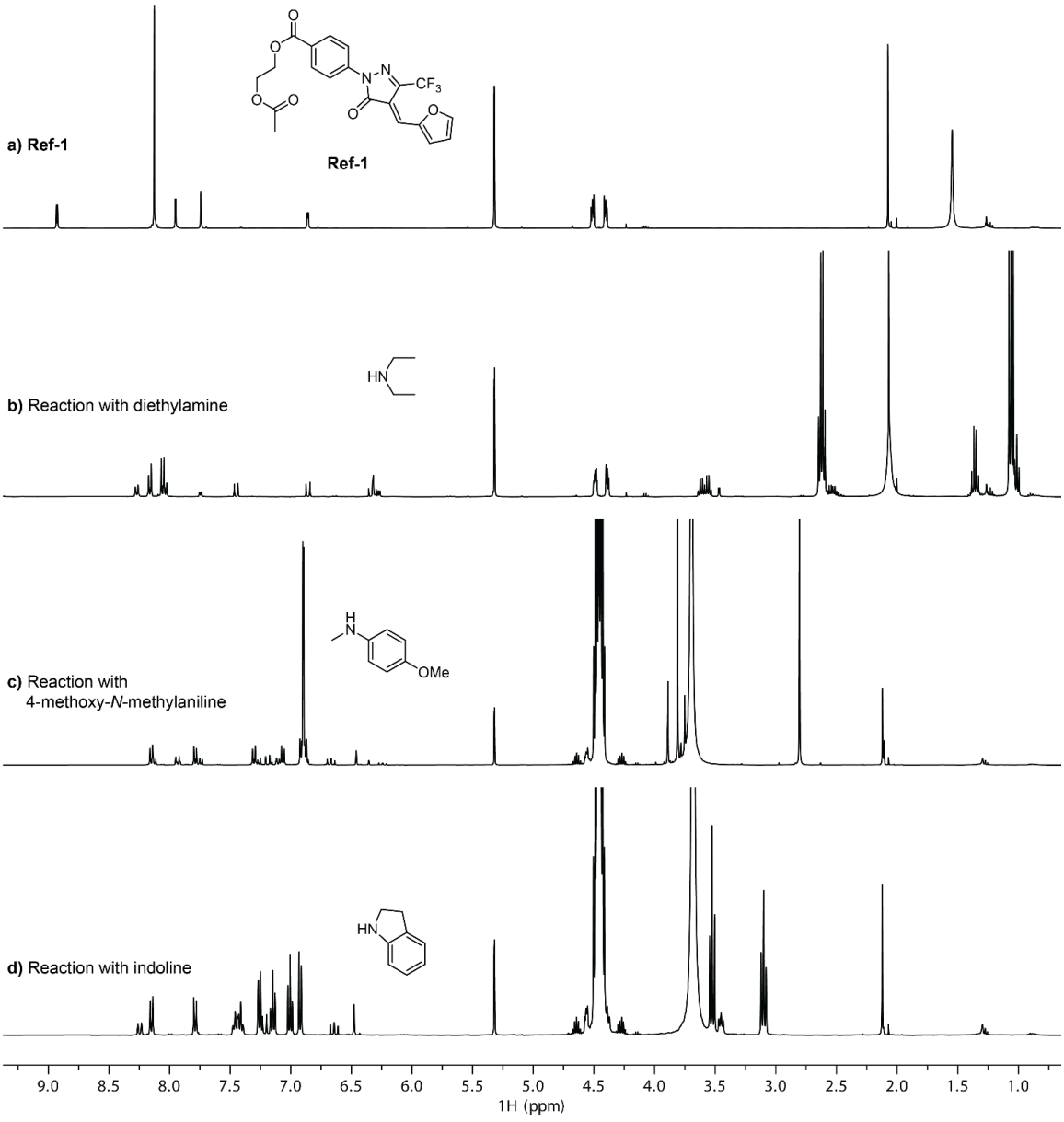

Figure 3.17 ^{1}H NMR spectra (400 MHz) characterizing the reaction of DASA precursor **Ref-1** (10 mM) with different secondary amines (5 equiv) after 5 min of reaction time. (a) **Ref-1** in CD_2Cl_2 as reference. (b) Reaction with diethylamine in CD_2Cl_2. (c) Reaction with 4-methoxy-*N*-methylaniline in 4:1 CD_2Cl_2/HFIP. (d) Reaction with indoline in 4:1 CD_2Cl_2/HFIP. Complete conversion of **Ref-1** is observed after 5 min for each reaction. The solvent conditions and amine concentrations were chosen to mirror the STAMMP demonstrations, although the concentration of activated furan in those experiments is likely lower than that used here.

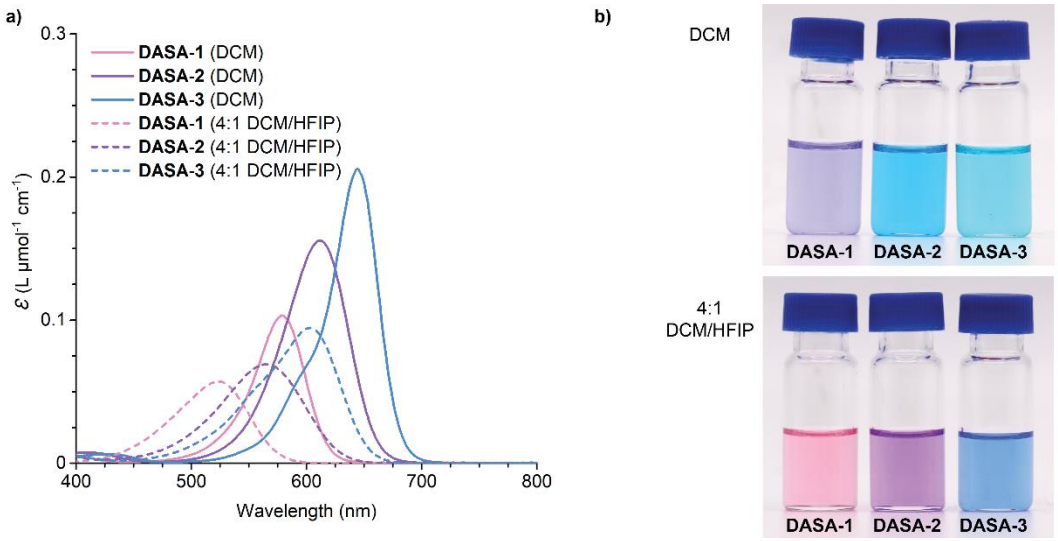

Figure 3.18 Characterization of the changes in absorption for small molecule DASA dyes in different solvent environments. (a) Absorption spectra and (b) photographs of small molecule DASA dyes in DCM and in 4:1 DCM/HFIP. Concentrations: 10 μM in DCM; 8 μM in DCM/HFIP.

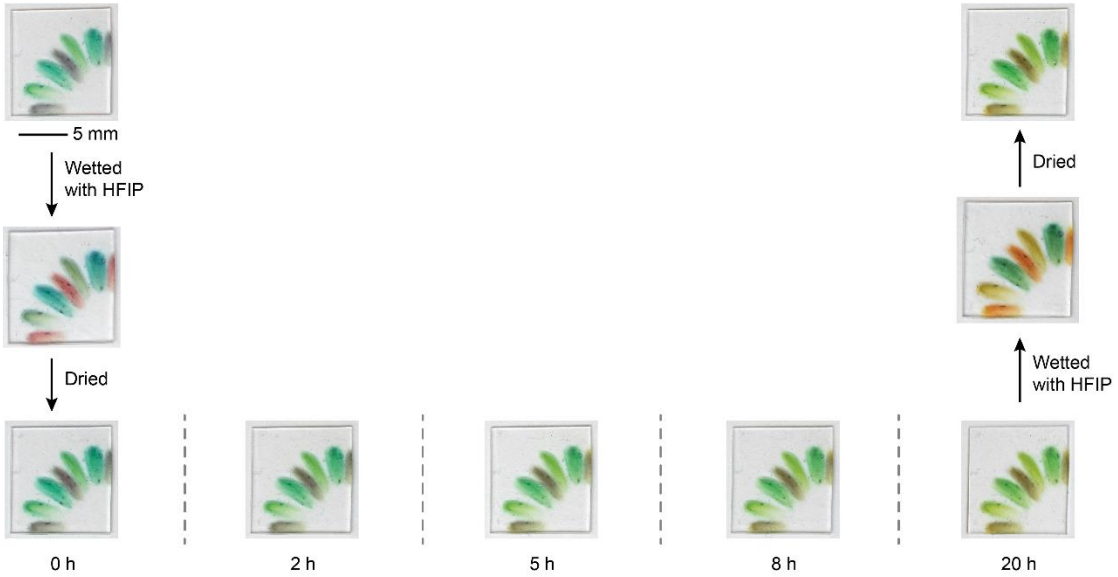

Figure 3.19 Demonstration of the solvatochromic properties of the mechanically printed DASA dyes in a film of **PDMS-1** and their stability in PDMS under ambient conditions on the benchtop. Addition of 4:1 DCM/HFIP causes the color of the DASA dyes to change, consistent with their expected solvatochromic behavior. This color change is reversible upon drying. Some discoloration is observed upon storage of the patterned film under ambient room light, temperature, and atmosphere. Immersion of the film in 4:1 DCM/HFIP after 20 h on the benchtop still leads to a reversible color change, indicating a significant population of DASAs is still present.

photobleached upon irradiation with visible light, demonstrating that the patterned films retain the anticipated photoswitching capabilities of the DASAs. In comparison to the samples activated in tension, incomplete photoisomerization in this case likely reflects the relatively high local concentration of DASAs, which affects the photoisomerization kinetics.[34] An additional print illustrates the use of an alternative order of amine treatment and highlights the different reversion kinetics for each component of the pattern following photoswitching (Figure 3.20 and Figure 3.21). As expected, the identical STAMMP procedure applied to a film of **PDMS-Control** did not produce an image (Figure 3.22). This demonstration illustrates the concept of mechanochemical multicolor soft lithography in which mechanical activation through localized compression reveals a DASA precursor that can be differentiated to generate a diverse range of DASA photoswitches in the same material simply by treatment with different amines. Compared to other soft lithography approaches that are primarily limited to surface functionalization,[35] the STAMMP method achieves three-dimensional pattern formation in the bulk.[6] Finally, we contrast the STAMMP process

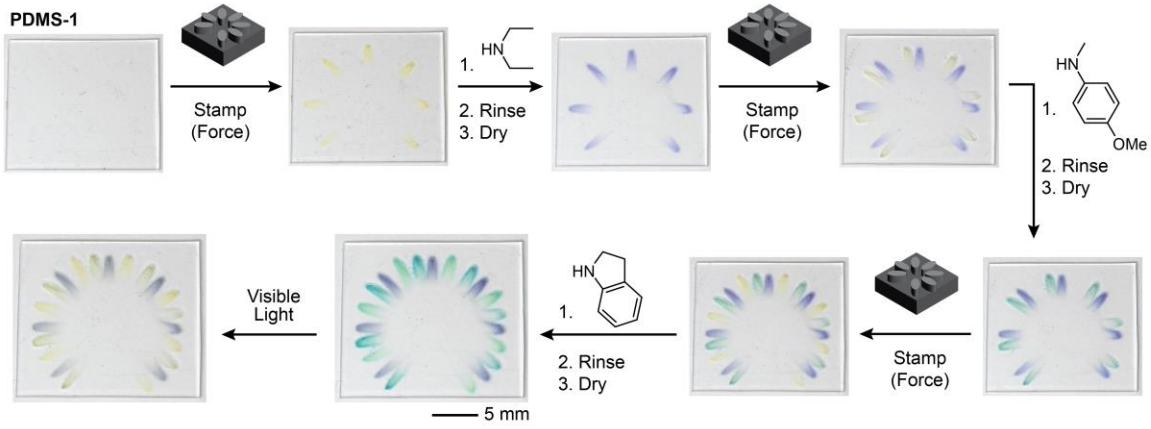

Figure 3.20 Demonstration of the STAMMP process and photoswitching of the final image. Photographs of a 2 × 2 cm film of mechanochemically active **PDMS-1** containing 2.5 wt% of mechanophore crosslinker (±)-**5a** after the sequential application of localized compression and treatment with various amines. Irradiation of the final pattern with visible light for 30 s causes partial photoswitching of the mechanically patterned DASA dyes.

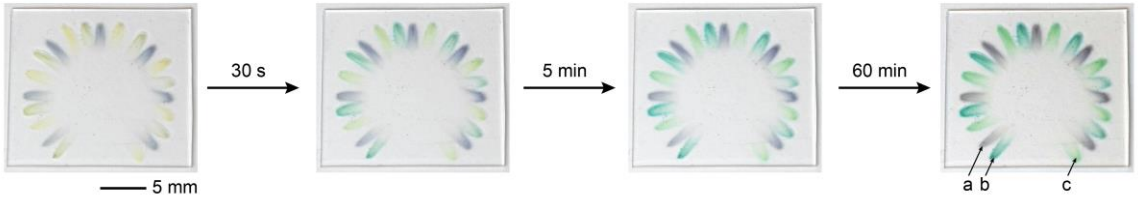

Figure 3.21 Thermal equilibration of the partially photobleached pattern shown in Fig. S16 illustrating differential reversion kinetics for each mechanically patterned DASA dye. The purple-colored DASA dye generated using diethylamine (labeled a) does not fully convert to the colorless form under irradiation. The DASA generated from 4-methoxy-*N*-methylaniline (labeled b) exhibits significant reversion to the colored triene form after only 30 s, while the DASA generated from indoline (labeled c) reverts to the colored triene isomer more slowly.

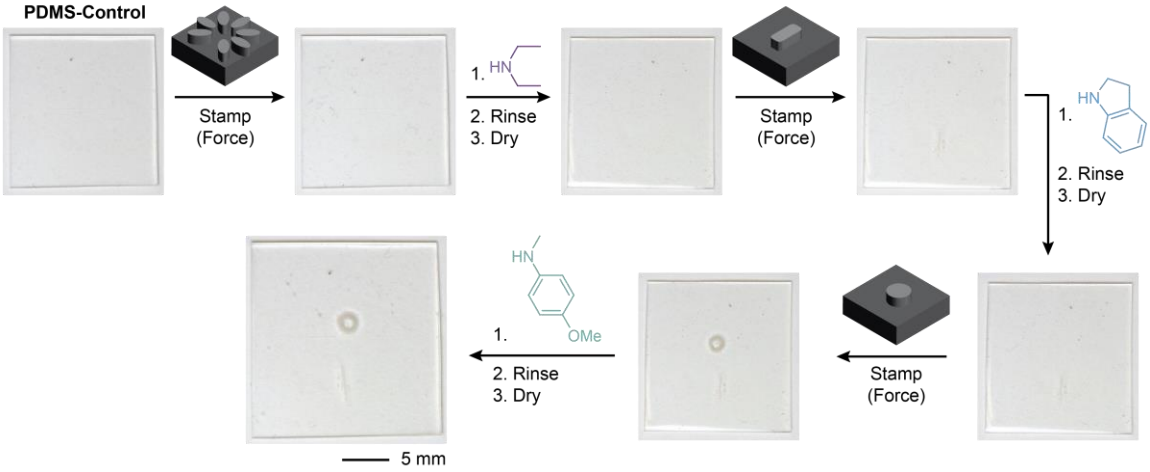

Figure 3.22 Photographs of a 2 x 2 cm film of control polymer **PDMS-Control** containing 2.5 wt% of monofunctional mechanophore (±)-**5b** after sequential application of localized compression and treatment with various amines. No change in color is observed indicating that mechanical force is necessary to achieve image reproduction. Some irreversible deformation of the PDMS material is apparent after the second and third stamping procedures.

with a recent report by Mei *et al*. that leverages force-accelerated amine conjugation to functionalize silicon surfaces following the more conventional lithographic approach.[36]

3.6 Conclusions

We have designed a mechanophore based on a masked DASA precursor that enables a mechanically gated multicolor chromogenic response in polymeric materials. Mechanical force supplied to the mechanophore via solution-phase ultrasonication or

tension/compression in solid materials promotes a retro-Diels–Alder reaction to reveal an activated furan species. Subsequent reaction with a secondary amine produces an intensely colored DASA photoswitch. Critically, the chromogenic response is highly dependent upon the identity of the secondary amine, and thus a variety of DASAs with diverse photophysical and photochemical properties can be generated from a single mechanophore. We leverage the unique reactivity of this system to introduce the concept of mechanochemical multicolor soft lithography whereby a complex multicolor composite image is printed into a mechanophore-crosslinked elastomer through an iterative sequence of localized compression and amine development. This mechanochemical platform affords control and modularity over dye formation using mechanical force and shows great promise for a diverse range of patterning, encryption, and sensing applications. Combined with the unique photoswitching properties of DASAs, we anticipate that this chemistry will empower the creation of new materials with complex stimuli-responsive functionality.

3.7 Experimental Section

3.7.1 General Experimental Details

Reagents from commercial sources were used without further purification unless otherwise noted. Methyl acrylate was passed through a short plug of basic alumina to remove inhibitor immediately prior to use. Dry THF and DCM were obtained from a Pure Process Technology solvent purification system. All reactions were performed under a N_2 atmosphere unless specified otherwise. Column chromatography was performed on a Biotage Isolera system using SiliCycle SiliaSep HP flash cartridges.

NMR spectra were recorded using a 400 MHz Bruker Avance III HD with Prodigy Cryoprobe or a 400 MHz Bruker Avance Neo. All ^{1}H NMR spectra are reported in δ units, parts per million (ppm), and were measured relative to the signals for residual chloroform (7.26 ppm) or toluene (2.09 ppm) in deuterated solvent. All ^{13}C NMR spectra were measured in deuterated solvents and are reported in ppm relative to the signals for chloroform (77.16 ppm). Multiplicity and qualifier abbreviations are as follows: s = singlet, d = doublet, t = triplet, q = quartet, m = multiplet.

High resolution mass spectra (HRMS) were obtained from a JEOL JMS-T2000GC AccuTOF™ GC-Alpha spectrometer equipped with a field desorption (FD) ionization source.

Analytical gel permeation chromatography (GPC) was performed using an Agilent 1260 series pump equipped with two Agilent PLgel MIXED-B columns (7.5 x 300 mm), an Agilent 1200 series diode array detector, a Wyatt 18-angle DAWN HELEOS light scattering detector, and an Optilab rEX differential refractive index detector. The mobile phase was THF at a flow rate of 1 mL/min. Molecular weights and molecular weight distributions were calculated by light scattering using a dn/dc value of 0.062 mL/g (25 °C) for poly(methyl acrylate).

UV–vis absorption spectra were recorded on a Thermo Scientific Evolution 220 spectrometer.

Ultrasound experiments were performed inside a sound abating enclosure using a Vibra Cell 505 liquid processor equipped with a 0.5-inch diameter solid probe (part #630-0217), sonochemical adapter (part #830-00014), and a Suslick reaction vessel made by the Caltech glass shop (analogous to vessel #830-00014 from Sonics and Materials).

Elastomer compression experiments were performed using a Carver hydraulic press (model #3912) applying a force of ≤ 0.5 ton. Photographs were captured using a Canon Rebel SL3 with a 100 mm macro lens and corrected for exposure in Adobe Photoshop. Visible light irradiation was performed using the flashlight of an iPhone 8 or a Pro Tango U2 LED flashlight (1100 lumen).

Compound **1** was synthesized following the procedure reported in the literature.[23]

Chart 3.1 Structures of initiators (±)-**4** and (±)-**S1**, and compounds (±)-**5a** and (±)-**5b** for incorporation into poly(methyl acrylate) and polydimethylsiloxane polymers, respectively.

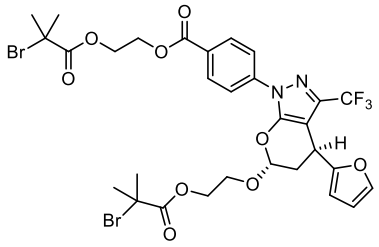

(±)-**4**

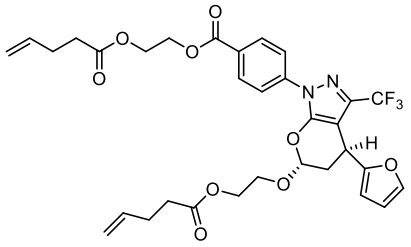

(±)-**5a**

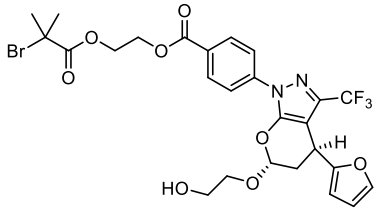

(±)-**S1**

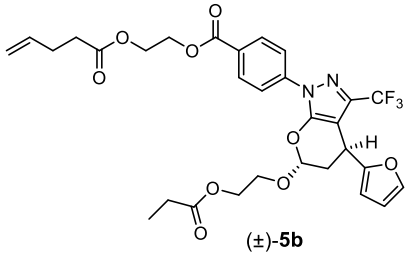

(±)-**5b**

Chart 3.2 Structures of chain-centered polymer **PMA-1** and chain-end control polymer **PMA-Control**.

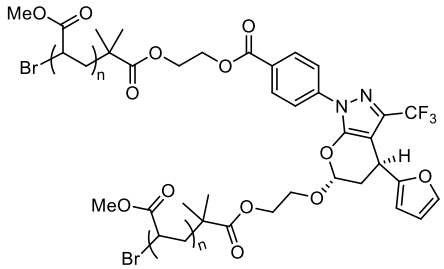

PMA-1

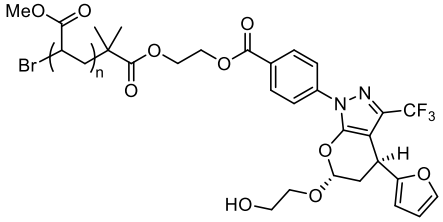

PMA-Control

3.7.2 Synthesis and Characterization of Initiators and Polymers

Scheme 3.1 Synthesis of Hetero-Diels–Alder Mechanophore Diol (±)-**3**

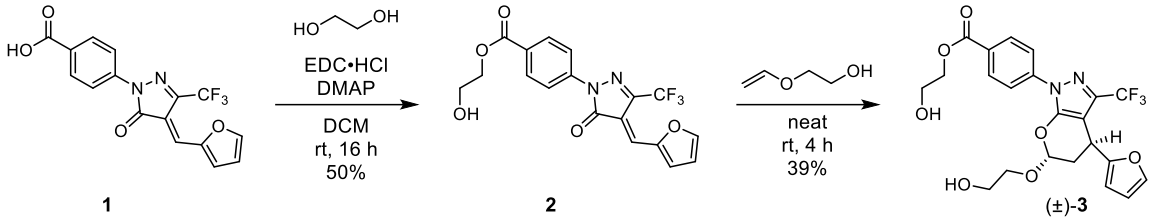

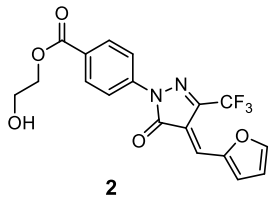

2-hydroxyethyl 4-(4-(furan-2-ylmethylene)-5-oxo-3-(trifluoromethyl)-4,5-dihydro-1H-pyrazol-1-yl)benzoate (2). A round bottom flask equipped with a stir bar was charged with **1** (523 mg, 1.49 mmol) and DCM (20 mL). Ethylene glycol (0.8 mL, 14.3 mmol) was added, and the reaction was cooled to 0 °C in an ice/water bath followed by the addition of EDC•HCl (345 g, 1.80 mmol) and 4-dimethylaminopyridine (12.9 mg, 0.106 mmol). The reaction was capped under an atmosphere of air and allowed to warm to room temperature slowly. After stirring for 21 h, the crude reaction mixture was eluted through a plug of silica gel with EtOAc to provide the title compound as an orange solid (294 mg, 50%).

TLC (EtOAc): R_f = 0.78

^{1}H NMR (400 MHz, $CDCl_3$) δ: 8.92 (d, J = 3.9 Hz, 1H), 8.25 – 8.06 (m, 4H), 7.91 (dd, J = 1.7, 0.6 Hz, 1H), 7.76 – 7.67 (m, 1H), 6.83 (ddd, J = 3.9, 1.7, 0.8 Hz, 1H), 4.57 – 4.40 (m, 2H), 4.06 – 3.89 (m, 2H).

$^{13}C\{^{1}H\}$ NMR (101 MHz, $CDCl_3$) δ: 166.5, 161.7, 151.3, 150.9, 141.8, 141.1 (q, J_{CF} = 37.4 Hz), 132.2, 131.0, 128.7, 126.9, 119.8 (q, J_{CF} = 287.9 Hz), 118.6, 116.0, 115.4, 66.9, 61.7.

HRMS (FD, *m/z*): calcd for $[C_{18}H_{13}N_2O_5F_3]^+$ $(M)^+$, 394.0771; found 394.0767.

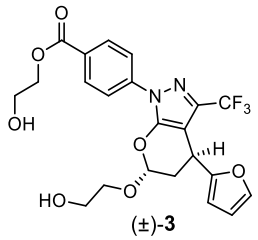

(±)-**3**

2-hydroxyethyl 4-((4S,6R)-4-(furan-2-yl)-6-(2-hydroxyethoxy)-3-(trifluoromethyl)-5,6-dihydropyrano[2,3-c]pyrazol-1(4H)-yl)benzoate ((±)-**3).** A round bottom flask equipped with a stir bar was charged with **2** (247 mg, 0.512 mmol) and ethylene glycol vinyl ether (1.5 mL, 16.9 mmol). The reaction was capped under an atmosphere of air and stirred at room temperature. After 2.5 h, the reaction was diluted with 150 mL of $CHCl_3$ and stirred for an additional 2 h. The reaction was concentrated under reduced pressure and the products were separated by silica gel chromatography (0–40% EtOAc/DCM with 2% MeOH) to provide the title compound as a foamy white solid (117 mg, 39% yield). The structure of (±)-**3** was confirmed by single crystal X-ray diffraction.

TLC (5% MeOH/DCM): R_f = 0.25

^{1}H NMR (400 MHz, $CDCl_3$) δ: 8.17 (d, *J* = 8.1 Hz, 2H), 7.94 (d, *J* = 8.0 Hz, 2H), 7.35 (s, 1H), 6.32 (d, *J* = 2.9 Hz, 1H), 6.12 (d, *J* = 2.9 Hz, 1H), 5.60 – 5.51 (m, 1H), 4.50 (t, *J* = 4.0 Hz, 2H), 4.37 (t, *J* = 6.2 Hz, 1H), 4.00 (dt, *J* = 8.0, 4.5 Hz, 3H), 3.82 (d, *J* = 8.2 Hz, 3H), 2.52 – 2.24 (m, 2H).

$^{13}C\{^{1}H\}$ NMR (101 MHz, $CDCl_3$) δ: 166.2, 154.2, 149.6, 142.1, 141.5, 139.9 (q, J_{CF} = 38.3 Hz), 131.0, 128.2, 120.9 (q, J_{CF} = 270.7 Hz), 120.4, 110.4, 107.1, 102.6, 97.4, 71.5, 66.9, 61.5, 61.2, 33.2, 27.3.

HRMS (FD, *m/z*): calcd for $[C_{22}H_{21}N_2O_7F_3]^+$ $(M)^+$, 482.1295; found 482.1306.

Scheme 3.2 Synthesis of Mechanophore Chain-Centered and Chain-End Control Polymers

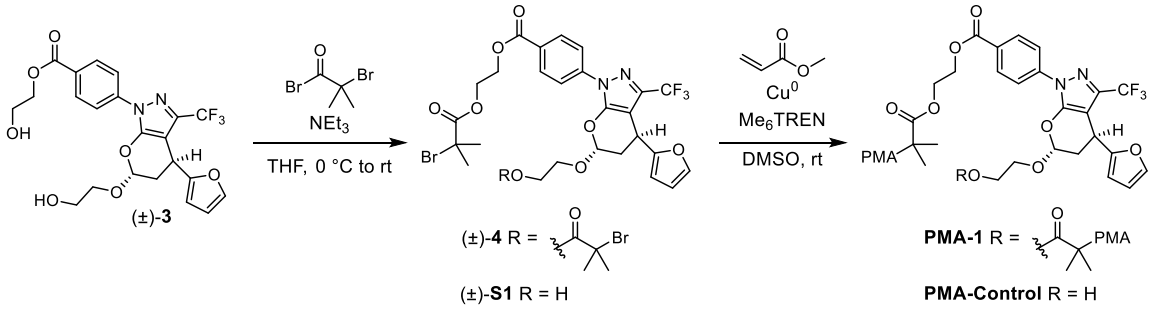

General Procedure A for the Esterification of Alcohols. A flame-dried two-neck flask was charged with the appropriate diol followed by dry THF, triethylamine, and 4-diaminopyridine (if applicable). The solution was cooled to 0 °C in an ice/water bath followed by addition of either α-bromoisobutyryl bromide, 4-pentenoic anhydride, or propionic anhydride. The reaction was left in the ice/water bath to warm to room temperature slowly and stirred for the indicated amount of time. The reaction mixture was then diluted with EtOAc and washed with saturated NH_4Cl, saturated $NaHCO_3$, and brine, dried over Na_2SO_4, filtered, and concentrated under reduced pressure.

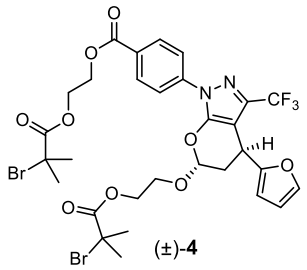

(±)-**4**

2-((2-bromo-2-methylpropanoyl)oxy)ethyl 4-((4S,6R)-6-(2-((2-bromo-2-methylpropanoyl)oxy)ethoxy)-4-(furan-2-yl)-3-(trifluoromethyl)-5,6-dihydropyrano[2,3-c]pyrazol-1(4H)-yl)benzoate ((±)-4). Synthesized according to general procedure A with (±)-**3** (26.9 mg, 0.0558 mmol), THF (2 mL), triethylamine (30 μL, 0.215 mmol), and α-bromoisobutyryl bromide (30 μL, 0.243 mmol). The reaction was stirred for 2.5 h and following workup, purified by eluting the crude material through a plug of basic alumina with DCM. The title compound was obtained as a clear oil (37.6 mg, 86%).

TLC (50% EtOAc/hexanes): R_f = 0.87

^{1}H NMR (400 MHz, $CDCl_3$) δ: 8.22 – 8.07 (m, 2H), 7.96 – 7.88 (m, 2H), 7.33 (dd, *J* = 1.8, 0.8 Hz, 1H), 6.32 (dd, *J* = 3.2, 1.9 Hz, 1H), 6.18 – 6.08 (m, 1H), 5.57 (dd, *J* = 5.1, 2.3 Hz, 1H), 4.69 – 4.48 (m, 4H), 4.44 – 4.28 (m, 3H), 4.09 (ddd, *J* = 11.5, 5.6, 3.1 Hz, 1H), 3.94 (ddd, *J* = 11.5, 6.7, 3.3 Hz, 1H), 2.43 – 2.25 (m, 2H), 1.94 (s, 6H), 1.86 (s, 3H), 1.85 (s, 3H).

^{13}C{^{1}H} NMR (101 MHz, $CDCl_3$) δ: 171.7, 171.6, 165.6, 154.0, 149.3, 142.1, 141.6, 139.9 (q, J_{CF} = 38.4 Hz), 131.1, 128.1, 120.9 (q, J_{CF} = 271.7 Hz), 120.6, 110.4, 107.2, 102.1, 97.8, 67.3, 64.3, 63.6, 62.6, 55.5, 55.4, 33.3, 30.8, 30.7, 27.2.

HRMS (FD, *m/z*): calcd for $[C_{30}H_{31}N_2O_9F_3Br_2]^+$ $(M)^+$, 778.0343; found 778.0334.

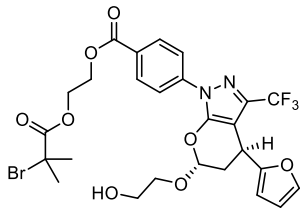

(±)-**S1**

2-((2-bromo-2-methylpropanoyl)oxy)ethyl 4-((4S,6R)-4-(furan-2-yl)-6-(2-hydroxyethoxy)-3-(trifluoromethyl)-5,6-dihydropyrano[2,3-c]pyrazol-1(4H)-yl)benzoate ((±)-S1). Synthesized according to general procedure A with (±)-**3** (62.8 mg, 0.130 mmol), THF (6 mL), triethylamine (20 μL, 0.143 mmol), and α-bromoisobutyryl bromide (16.3 μL, 0.131 mmol). The reaction was stirred for 17 h. Following workup, the crude material was purified by silica gel chromatography (30–80% EtOAc/hexanes) to provide the title compound as a clear oil (9.3 mg, 11%).

TLC (50% EtOAc/hexanes): R_f = 0.46

^{1}H NMR (400 MHz, $CDCl_3$) δ: 8.19 – 8.11 (m, 2H), 7.98 – 7.89 (m, 2H), 7.35 (dd, *J* = 1.9, 0.8 Hz, 1H), 6.32 (dd, *J* = 3.2, 1.9 Hz, 1H), 6.14 – 6.10 (m, 1H), 5.54 (dd, *J* = 6.0, 2.2 Hz, 1H), 4.63 – 4.51 (m, 4H), 4.36 (t, *J* = 6.2 Hz, 1H), 4.06 – 3.97 (m, 1H), 3.86 – 3.76 (m, 3H), 2.46 – 2.27 (m, 2H), 1.94 (s, 6H).

^{13}C{^{1}H} NMR (101 MHz, $CDCl_3$) δ: 171.7, 165.6, 154.2, 149.5, 142.1, 141.6, 140.0 (q, J_{CF} = 38.4 Hz), 131.1, 128.1, 121.0 (q, J_{CF} = 271.7 Hz), 120.5, 110.5, 107.2, 102.6, 97.5, 71.6, 63.6, 62.6, 61.7, 55.5, 33.3, 30.8, 27.4.

HRMS (FD, *m/z*): calcd for $[C_{26}H_{26}N_2O_8F_3Br]^+$ $(M)^+$, 630.0819; found 630.0841.

General Procedure B for the Synthesis of Poly(Methyl Acrylate) (PMA) Polymer Containing a Chain-Centered Mechanophore. PMA polymers were synthesized by controlled radical polymerization following the procedure by Nguyen *et al*.[37] A 25 mL Schlenk flask equipped with a stir bar was charged with initiator (±)-**4** (12.8 mg, 0.0164 mmol), DMSO (3 mL), methyl acrylate (3 mL), and freshly cut copper wire (2.0 cm length, 20 gauge). The flask was sealed, the solution was deoxygenated with three freeze-pump-thaw cycles, and then allowed to warm to rt and backfilled with nitrogen. Me_6TREN (13 μL, 0.0486 mmol) was added via microsyringe. After stirring at rt for 1.5 h, the flask was opened to air and the solution was diluted with DCM. The polymer solution was precipitated into cold methanol (3x) and the isolated material was dried under vacuum to yield 1.77 g of **PMA-1** (62%). M_n = 125 kDa, $Đ$ = 1.15.

Synthesis of PMA-Control. Chain-end control polymer **PMA-Control** was synthesized using general procedure B with initiator (±)-**S1** (9.3 mg, 0.0147 mmol), DMSO (3 mL), methyl acrylate (3 mL), and Me_6TREN (10 μL, 0.0374 mmol). Polymerization for 100 min provided the title polymer (1.59 g, 55%). M_n = 154 kDa, $Đ$ = 1.07.

Scheme 3.3 Synthesis of Mechanophore Crosslinker (±)-**5a** and Monofunctional Control (±)-**5b**

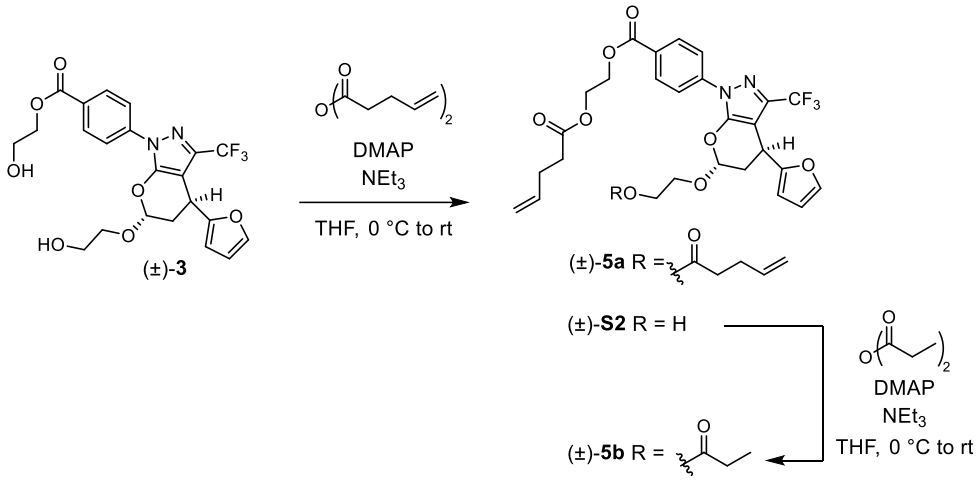

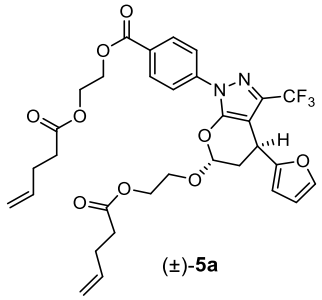

2-(pent-4-enoyloxy)ethyl 4-((4S,6R)-4-(furan-2-yl)-6-(2-(pent-4-enoyloxy)ethoxy)-3-(trifluoromethyl)-5,6-dihydropyrano[2,3-c]pyrazol-1(4H)-yl)benzoate ((±)-**5a).** Synthesized according to general procedure A with (±)-**3** (41.4 mg, 0.0858 mmol), THF (2 mL), triethylamine (40 μL, 0.287 mmol), 4-dimethylaminopyridine (2.4 mg, 0.0196 mmol), and 4-pentenoic anhydride (50 μL, 0.274 mmol). The reaction was stirred for 17 h. After workup, the crude material was purified by silica gel chromatography (10–40% EtOAc/hexanes) to provide the title compound as a clear oil (47.9 mg, 86%).

TLC (50% EtOAc/hexanes): R_f = 0.77

^{1}H NMR (400 MHz, $CDCl_3$) δ: 8.20 – 8.08 (m, 2H), 7.99 – 7.87 (m, 2H), 7.34 (dd, *J* = 1.9, 0.9 Hz, 1H), 6.32 (dd, *J* = 3.2, 1.9 Hz, 1H), 6.16 – 6.09 (m, 1H), 5.88 – 5.70 (m, 2H), 5.53 (dd, *J* = 5.5, 2.3 Hz, 1H), 5.10 – 4.93 (m, 4H), 4.58 – 4.42 (m, 4H), 4.35 (t, *J* = 6.5 Hz, 1H), 4.31 (ddd, *J* = 12.2, 5.9, 3.3 Hz, 1H), 4.21 (ddd, *J* = 12.2, 6.7, 3.2 Hz, 1H), 4.06 (ddd, *J* = 11.3, 5.9, 3.2 Hz, 1H), 3.88 (ddd, *J* = 11.4, 6.7, 3.2 Hz, 1H), 2.50 – 2.43 (m, 2H), 2.43 – 2.26 (m, 8H).

^{13}C{^{1}H} NMR (101 MHz, $CDCl_3$) δ: 173.0, 172.9, 165.6, 154.1, 149.4, 142.1, 141.6, 139.9 (q, J_{CF} = 38.4 Hz), 136.6, 136.5, 131.0, 128.2, 120.9 (q, J_{CF} = 27.7 Hz), 120.5, 115.8, 115.7, 110.4, 107.2, 102.1, 97.7, 67.7, 63.1, 62.8, 62.1, 33.5, 33.3, 33.2, 28.9, 28.8, 27.3.

HRMS (FD, *m/z*): calcd for $[C_{32}H_{33}N_2O_9F_3]^+$ $(M)^+$, 646.2133; found 646.2124.

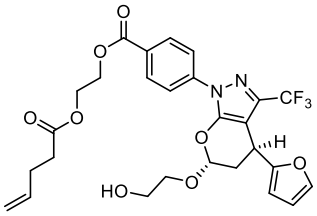

(±)-**S2**

2-(pent-4-enoyloxy)ethyl 4-((4S,6R)-4-(furan-2-yl)-6-(2-hydroxyethoxy)-3-(trifluoromethyl)-5,6-dihydropyrano[2,3-c]pyrazol-1(4H)-yl)benzoate ((±**)-S2).** Synthesized according to general procedure A with (±)-**3** (45.1 mg, 0.0935 mmol), THF (3 mL), triethylamine (40 µL, 0.287 mmol), 4-dimethylaminopyridine (2.5 mg, 0.0205 mmol), and 4-pentenoic anhydride (30 µL, 0.164 mmol). The reaction was stirred for 14 h. After workup, the crude material was purified by silica gel chromatography (30–100% EtOAc/hexanes) to provide the title compound as a clear oil (13.0 mg, 17%).

TLC (50% EtOAC/hexanes): R_f = 0.37

^{1}H NMR (400 MHz, $CDCl_3$) δ: 8.20 – 8.10 (m, 2H), 7.97 – 7.90 (m, 2H), 7.35 (dd, *J* = 1.9, 0.9 Hz, 1H), 6.32 (dd, *J* = 3.3, 1.9 Hz, 1H), 6.15 – 6.08 (m, 1H), 5.89 – 5.74 (m, 1H), 5.54 (dd, *J* = 6.0, 2.3 Hz, 1H), 5.11 – 4.93 (m, 2H), 4.57 – 4.51 (m, 2H), 4.47 – 4.43 (m, 2H), 4.36 (t, *J* = 6.2 Hz, 1H), 4.07 – 3.96 (m, 1H), 3.88 – 3.74 (m, 3H), 2.51 – 2.28 (m, 6H).

^{13}C{^{1}H} NMR (101 MHz, $CDCl_3$) δ: 173.0, 165.7, 154.2, 149.5, 141.6, 140.0 (q, J_{CF} = 38.4 Hz), 136.6, 131.1, 128.2, 121.0 (q, J_{CF} = 271.7 Hz), 120.5, 115.9, 110.4, 107.2, 102.6, 97.5, 71.5, 63.1, 62.2, 61.7, 33.5, 33.3, 28.9, 27.4.

HRMS (FD, *m/z*): calcd for $[C_{27}H_{27}N_2O_8F_3]^+$ $(M)^+$, 564.1714; found 564.1732.

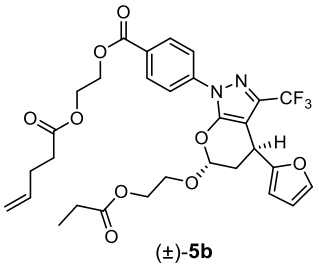

(±)-**5b**

2-(pent-4-enoyloxy)ethyl 4-((4S,6R)-4-(furan-2-yl)-6-(2-(propionyloxy)ethoxy)-3-(trifluoromethyl)-5,6-dihydropyrano[2,3-c]pyrazol-1(4H)-yl)benzoate ((±**)-5b).** Synthesized according to general procedure A with (±)-**S2** (35.2 mg, 0.0624 mmol), THF (6 mL), triethylamine (20 µL, 0.143 mmol), 4-dimethylaminopyridine (1.5 mg, 0.0123 mmol), and propionic anhydride (16 µL, 0.124 mmol). The reaction was stirred for 3 h. After workup, the crude reaction mixture was purified by silica gel chromatography (10–30% EtOAc/hexanes) to provide the title compound as a colorless oil (32.7 mg, 84%).

TLC (25% EtOAC/hexanes): R_f = 0.32

^{1}H NMR (400 MHz, $CDCl_3$) δ: 8.18 – 8.10 (m, 2H), 7.99 – 7.89 (m, 2H), 7.34 (dd, J = 1.8, 0.9 Hz, 1H), 6.32 (dd, J = 3.2, 1.8 Hz, 1H), 6.16 – 6.10 (m, 1H), 5.89 – 5.74 (m, 1H), 5.54 (dd, J = 5.5, 2.3 Hz, 1H), 5.09 – 4.95 (m, 2H), 4.58 – 4.49 (m, 2H), 4.49 – 4.41 (m, 2H), 4.39 – 4.34 (m, 1H), 4.30 (ddd, J = 12.2, 6.0, 3.3 Hz, 1H), 4.21 (ddd, J = 12.2, 6.7, 3.2 Hz, 1H), 4.06 (ddd, J = 11.3, 6.0, 3.2 Hz, 1H), 3.89 (ddd, J = 11.3, 6.7, 3.3 Hz, 1H), 2.51 – 2.43 (m, 2H), 2.43 – 2.30 (m, 4H), 2.26 (q, J = 7.5 Hz, 2H), 1.08 (t, J = 7.6 Hz, 3H).

^{13}C{^{1}H} NMR (101 MHz, $CDCl_3$) δ: 174.4, 173.0, 165.7, 154.2, 149.4, 142.1, 141.6, 140.0 (q, J_{CF} = 38.1 Hz), 136.6, 131.1, 128.2, 121.0 (q, J_{CF} = 269.8 Hz), 120.5, 115.8, 110.4, 107.2, 102.2, 97.7, 67.7, 63.1, 62.7, 62.2, 33.5, 33.2, 28.9, 27.5, 27.3, 9.1.

HRMS (FD, *m/z*): calcd for $[C_{30}H_{31}N_2O_9F_3]^+$ $(M)^+$, 620.1976; found 620.1966.

Scheme 3.4 Synthesis of Reference Small Molecules

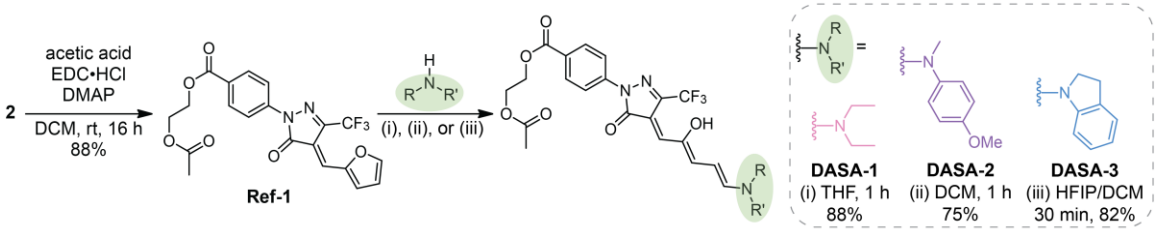

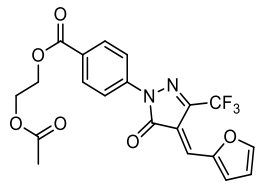

2-acetoxyethyl 4-(4-(furan-2-ylmethylene)-5-oxo-3-(trifluoromethyl)-4,5-dihydro-1H-pyrazol-1-yl)benzoate (Ref-1). A round bottom flask was charged with **2** (41.3 mg, 0.105 mmol), glacial acetic acid (8 µL, 0.140 mmol), EDC•HCl (23.6 mg, 0.123 mmol), 4-

dimethylaminopyridine (1.0 mg, 0.0082 mmol), and dry DCM (4 mL). The reaction was stirred at room temperature for 16.5 h, then diluted with DCM and washed with 1 M HCl (3×), and then brine. The organic fraction was dried over Na_2SO_4, filtered, and concentrated under reduced pressure. The crude product was eluted through a plug of silica gel with 50:50 EtOAc/hexanes to provide the title compound as an orange solid (40.1 mg, 88%).

TLC (50% EtOAC/hexanes): R_f = 0.73

^{1}H NMR (400 MHz, $CDCl_3$) δ: 8.92 (d, J = 3.8 Hz, 1H), 8.13 (s, 4H), 7.91 (dd, J = 1.6, 0.6 Hz, 1H), 7.71 (s, 1H), 6.83 (ddd, J = 3.9, 1.7, 0.8 Hz, 1H), 4.57 – 4.49 (m, 2H), 4.46 – 4.39 (m, 2H), 2.11 (s, 3H).

^{13}C{^{1}H} NMR (101 MHz, $CDCl_3$) δ: 171.1, 165.9, 161.6, 151.3, 150.8, 141.8, 141.0 (q, J_{CF} = 38.4 Hz) 132.1, 130.9, 128.6, 126.8, 119.8 (q, J_{CF} = 272.7 Hz) 118.6, 116.0, 115.4, 62.9, 62.3, 21.0.

HRMS (FD, *m/z*): calcd for $[C_{20}H_{15}N_2O_6F_3]^+$ $(M)^+$, 436.0877; found 436.0883.

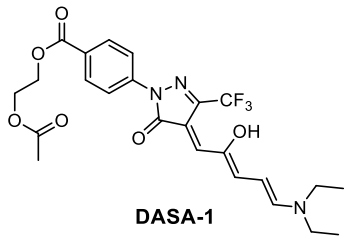

DASA-1

2-acetoxyethyl 4-((E)-4-((2Z,4E)-5-(diethylamino)-2-hydroxypenta-2,4-dien-1-ylidene)-5-oxo-3-(trifluoromethyl)-4,5-dihydro-1H-pyrazol-1-yl)benzoate (DASA-1). A round bottom flask was charged with **Ref-1** (50.3 mg, 0.115 mmol), diethylamine (12.5 μL, 0.121 mmol), and THF (0.4 mL). The reaction was capped under an atmosphere of air and stirred at room temperature. After 1 h, the reaction mixture was concentrated under reduced

pressure and eluted through a short plug of silica gel first with 50% EtOAc/hexanes (10 mL), followed by acetone (7 mL). The acetone fraction was collected and concentrated under reduced pressure to provide the title compound as a dark purple solid (54.4 mg, 93%). Spectral characterization is consistent with similar DASA photoswitches reported by Read de Alaniz.[25] Due to limited solubility, ^{13}C NMR peaks are not tabulated; however, the obtained spectra are included at the end of the SI.

^{1}H NMR (400 MHz, $CDCl_3$) δ: 12.94 (s, 1H), 8.20 – 8.11 (m, 2H), 8.12 – 8.01 (m, 2H), 7.34 (d, *J* = 12.1 Hz, 1H), 6.76 (d, *J* = 12.6 Hz, 1H), 6.34 (s, 1H), 6.24 (t, *J* = 12.3 Hz, 1H), 4.58 – 4.47 (m, 2H), 4.47 – 4.36 (m, 3H), 3.56 (q, *J* = 7.6 Hz, 2H), 3.50 (q, *J* = 7.3 Hz, 2H), 2.10 (s, 3H), 1.34 (t, *J* = 7.3 Hz, 3H), 1.33 (t, *J* = 7.3 Hz, 3H).

HRMS (FD, *m/z*): calcd for $[C_{24}H_{26}N_3O_6F_3]^+$ $(M)^+$, 509.1768; found 509.1778.

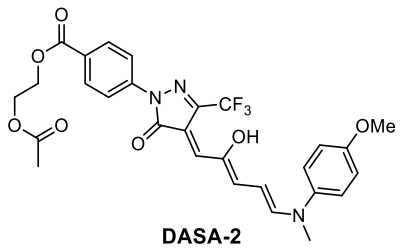

DASA-2

2-acetoxyethyl 4-((E)-4-((2Z,4E)-2-hydroxy-5-((4-methoxyphenyl)(methyl)amino)penta-2,4-dien-1-ylidene)-5-oxo-3-(trifluoromethyl)-4,5-dihydro-1H-pyrazol-1-yl)benzoate (DASA-2). A round bottom flask was charged with **Ref-1** (32.9 mg, 0.0754 mmol), 4-methoxy-*N*-methylaniline (11.9 mg, 0.0867 mmol), and DCM (1 mL). The reaction was capped under an atmosphere of air and stirred at room temperature. After 1 h, Et_2O (3 mL) was added to precipitate the product, which was collected by filtration to provide the title compound as a dark blue solid (32.6 mg, 75%).

Spectral characterization is consistent with similar DASA photoswitches reported by Read de Alaniz.[38] Due to limited solubility, ^{13}C NMR peaks are not tabulated; however, the obtained spectra are included at the end of the SI.

^{1}H NMR (400 MHz, $CDCl_3$) δ: 12.90 (s, 1H), 8.17 – 8.05 (m, 4H), 7.57 – 7.49 (m, 1H), 7.16 (d, *J* = 8.5 Hz, 2H), 6.96 (d, *J* = 8.5 Hz, 2H), 6.75 (d, *J* = 12.2 Hz, 1H), 6.55 (s, 1H), 6.36 (t, *J* = 12.3 Hz, 1H), 4.55 – 4.48 (m, 2H), 4.45 – 4.38 (m, 2H), 3.85 (s, 3H), 3.57 (s, 3H), 2.10 (s, 3H).

HRMS (FD, *m/z*): calcd for $[C_{28}H_{26}N_3O_7F_3]^+$ $(M)^+$, 573.1717; found 573.1719.

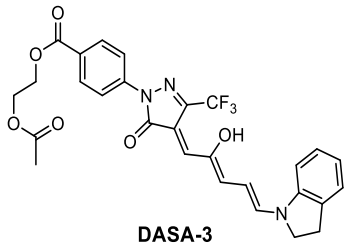

DASA-3

2-acetoxyethyl 4-((E)-4-((2Z,4E)-2-hydroxy-5-(indolin-1-yl)penta-2,4-dien-1-ylidene)-5-oxo-3-(trifluoromethyl)-4,5-dihydro-1H-pyrazol-1-yl)benzoate (DASA-3). A round bottom flask was charged with **Ref-1** (28.1 mg, 0.0644 mmol), indoline (8 μL, 0.0678 mmol), HFIP (0.16 mL) and DCM (0.64 mL). The reaction was capped under an atmosphere of air and stirred at room temperature. After 30 min, Et_2O (8 mL) was added to precipitate the product, which was collected by filtration to provide the title compound as a black solid (29.2 mg, 82%). Spectral characterization is consistent with similar DASA photoswitches reported by Read de Alaniz.[25] Due to limited solubility, ^{13}C NMR peaks are not tabulated; however, the obtained spectra are included at the end of the SI.

^{1}H NMR (400 MHz, $CDCl_3$) δ: 8.20 – 8.04 (m, 4H), 7.78 (d, *J* = 12.4 Hz, 1H), 7.45 (s, 1H), 7.29 (d, *J* = 8.0 Hz, 1H), 7.14 (t, *J* = 7.5 Hz, 1H), 7.08 (d, *J* = 8.1 Hz, 1H), 6.77 (d, *J* = 12.3 Hz, 1H), 6.56 (s, 1H), 6.34 (t, *J* = 12.3 Hz, 1H), 4.56 – 4.49 (m, 2H), 4.46 – 4.39 (m, 2H), 4.20 (t, *J* = 8.0 Hz, 2H), 3.34 (t, *J* = 7.9 Hz, 2H), 2.11 (s, 3H).

HRMS (FD, *m/z*): calcd for $[C_{28}H_{24}N_3O_6F_3]^+$ $(M)^+$, 555.1612; found 555.1620.

3.7.3 Description of Ultrasonication Experiments

General Procedure for Ultrasonication Experiments. An oven-dried sonication vessel was fitted with rubber septa, placed onto the sonication probe, and allowed to cool under a stream of dry argon. The probe tip was situated 1 cm above the bottom of the sonication vessel. The vessel was charged with a solution of the polymer in anhydrous THF (5.0 mg/mL, 20 mL, 30 mM BHT) and submerged in an ice bath. The solution was sparged continuously with argon beginning 10 min prior to sonication and for the duration of the sonication experiment. Pulsed ultrasound (1 s on/2 s off, 30% amplitude, 20 kHz, 13.6 W/cm^2) was then applied to the system. Aliquots (1.0 mL) were removed at specified time points (sonication "on" time) and filtered through a 0.45 μm PTFE syringe filter prior to analysis by GPC and UV-vis absorption spectroscopy. In order to remove BHT for analysis by NMR spectroscopy, the sonicated solution was concentrated, the polymer was redissolved in DCM and then precipitated into stirring hexanes (4×), and the isolated material was dried under vacuum. Ultrasonic intensity was calibrated using the method described by Berkowski et al.[4]

DASA Formation from PMA-1 via Ultrasound-Induced Mechanochemical Activation. For the experiments shown in Figure 3.4, solutions were subjected to ultrasonication for 60 min as described above. Aliquots of the sonicated solution were concentrated under reduced pressure and the residual polymer was redissolved in an equal volume of DCM to provide a 5 mg/mL solution of polymer (40 μM). For DASA formation using diethylamine, 0.8 mL of the DCM solution was combined with 0.2 mL of HFIP and ~4 μL (40 μmol) of diethylamine to provide a final solution containing ~32 μM polymer (~12 μM activated furan, see section 3.7.5 below) and 40 mM diethylamine (3,300 equiv). For DASA formation using 4-methoxy-*N*-methylaniline and indoline, 0.8 mL of the DCM solution was combined with 0.2 mL of HFIP and 0.05 mL of a 6.4 mM amine solution (in DCM) to provide a final solution containing ~30 μM polymer (~12 μM activated furan, see section 3.7.5 below) and ~300 μM amine (25 equiv). Reactions were allowed to proceed for approximately 10 min prior to analysis by UV-vis spectroscopy.

Table 3.1 Determined M_n (kDa) and absorbance (λ_{max} = 375 nm) values upon ultrasonication of **PMA-1** and **PMA-Control** in THF.

	PMA-1		**PMA-Control**	
Sonication Time (min)	$M_{n,t}$ **(kDa)**	**Abs at 375 nm (a.u.)**	$M_{n,t}$ **(kDa)**	**Abs at 375 nm (a.u.)**
0	125	0.00509	154	0.00534
20	79.3	0.297	86.6	0.0172
40	61.7	0.447	64.3	0.0284
60	55.6	0.493	53.5	0.0403
70	52.4	0.487	--	--
80	48.6	0.463	46.0	0.0571

3.7.4 Preparation of Polydimethylsiloxane (PDMS) Materials

PDMS materials covalently incorporating the hetero-Diels–Alder adducts (2.5 wt %) were prepared following previously reported procedures using the two-part Sylgard® 184 elastomer kit (Dow Corning).[7,39]

Procedure for preparation of PDMS-1 films. A 20 mL scintillation vial was charged with (±)-**5a** (53.0 mg) and 0.2 mL xylene. Sylgard® 184 prepolymer base (2.01 g) was added and the contents were thoroughly mixed in a vortex mixer to form a homogeneous, colorless dispersion. Sylgard® 184 curing agent (0.206 g) was added and the contents were mixed thoroughly using a vortex mixer. The mixture was pipetted onto a clean 5 cm x 5 cm delrin plate, which was placed inside a vacuum chamber and evacuated under high vacuum (~30 mTorr) for 3 h. The delrin plate was then transferred to an oven and the film was cured at 80 °C for 3 h. After curing, the plate was removed from the oven and the PDMS film was peeled off and cut into squares and strips with a razor blade.

Procedure for preparation of PDMS-Control films. A 20 mL scintillation vial was charged with (±)-**5b** (23.0 mg) and 0.1 mL xylene. Sylgard® 184 prepolymer base (1.00 g) was added and the contents were thoroughly mixed in a vortex mixer to form a homogeneous, colorless dispersion. Sylgard® 184 curing agent (0.101 g) was added and the contents were mixed thoroughly using a vortex mixer. The mixture was pipetted onto a clean 2.5 cm x 5 cm delrin plate, which was placed inside a vacuum chamber and evacuated under high vacuum (~30 mTorr) for 3 h. The delrin plate was then transferred

to an oven and the film was cured at 80 °C for 3 h. After curing, the plate was removed from the oven and the PDMS film was peeled off and cut into squares and strips with a razor blade.

3.7.5 Determination of Mechanophore Activation and DASA Formation Efficiency with Ultrasonication

Characterization of Activation Efficiency for the Hetero-Diels–Alder Mechanophore. Samples of **Ref-1** in THF at various concentrations were prepared and UV-vis spectra were acquired to construct the calibration curve shown in Figure 3.23. The concentration of activated furan species produced upon ultrasonication of **PMA-1** was determined from UV-vis absorption measurements using this calibration curve. The absorbance at 375 nm corresponding to the λ_{max} of the activated furan reached a maximum after 60 min of ultrasonication, indicating the generation of activated furan species with a concentration of

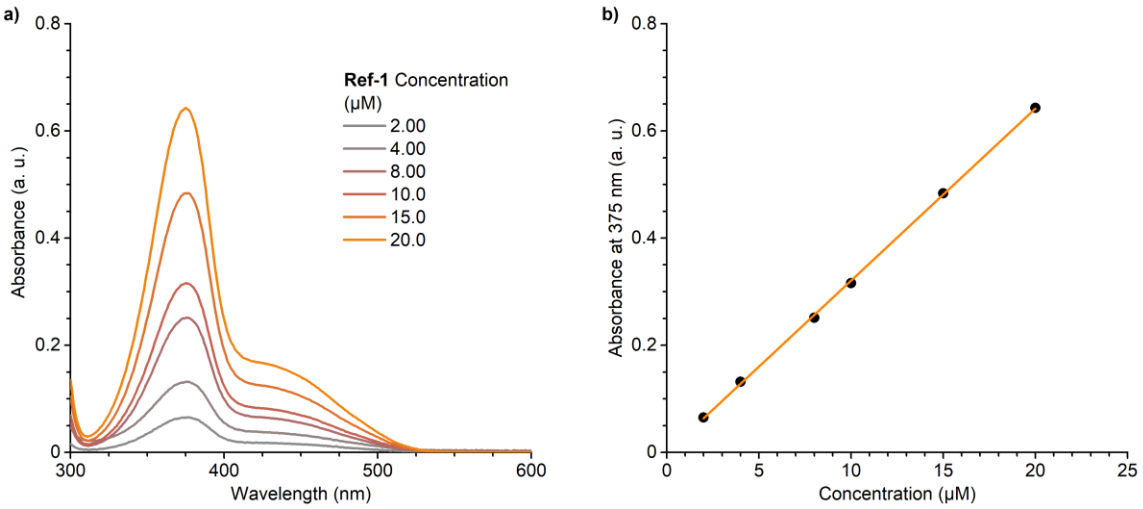

Figure 3.23 Construction of a calibration curve to determine the extinction coefficient for small molecule DASA precursor **Ref-1**. (a) UV-vis absorption spectra, and (b) absorbance at 375 nm for solutions of **Ref-1** in THF as a function of concentration. A linear regression of the data in (b) gives the extinction coefficient ε = 32,100 L mol^{-1} cm^{-1}.

~15.4 μM (Figure 3.24). Dividing this value by the concentration of initial mechanophore (40 μM, 5 mg/mL polymer), provides a mechanophore activation efficiency of 39%. We note that at extended sonication times, some degradation of the activated furan is observed as evidenced by a decrease in the absorbance at 375 nm (see Figure 3.24). Thus, the mechanophore activation efficiency measured here is likely underestimated.

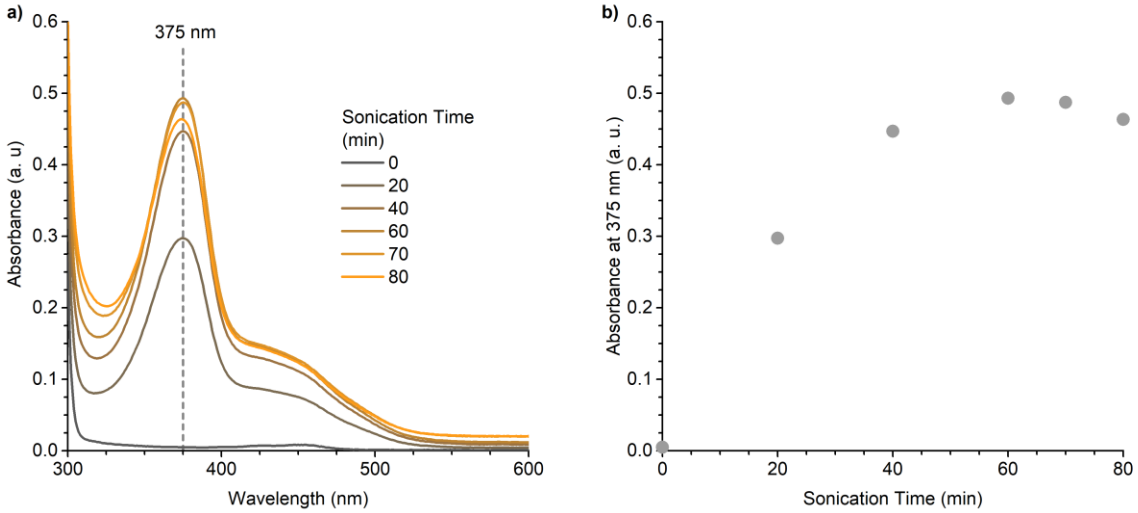

Figure 3.24 Extended ultrasonication of **PMA-1** (5 mg/mL in THF with 30 mM BHT) leads to some degradation of the activated furan product as evidenced by attenuation of the absorbance at 375 nm after 60 min of sonication. (a) UV-vis spectra acquired during ultrasonication. (b) Absorbance at 375 nm plotted as a function of sonication time.

Characterization of DASA Formation Efficiency Under Dilute Ultrasonication Conditions. Samples of small molecules **DASA-1**, **DASA-2**, and **DASA-3** in 4:1 DCM/HFIP at various concentrations in the general range achieved during the sonication experiments were prepared and UV-vis spectra were acquired to construct the calibration curves shown in Figure 3.25. The extinction coefficients calculated from these curves are estimates due to the equilibrium that exists between the open, colored triene and closed colorless isomers of the DASAs. Nevertheless, the ratio of open and closed isomers is expected to be the same as that for the samples produced in the ultrasonication experiments.

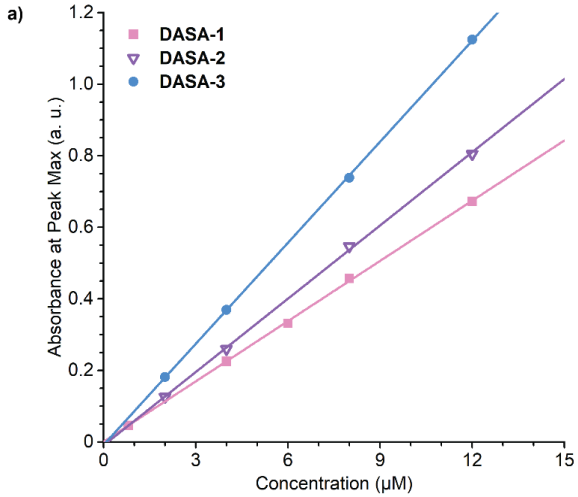

b)

	ε (L mol^{-1} cm^{-1})
DASA-1	56,100
DASA-2	68,300
DASA-3	94,100

Figure 3.25 Calibration curves constructed for the experimental determination of the concentration of DASAs generated from ultrasound-induced mechanical activation of **PMA-1** and subsequent amine addition. (a) Absorbance at the respective peak maxima for solutions of **DASA-1**, **DASA-2**, and **DASA-3** in 4:1 DCM/HFIP as a function of concentration. Linear regressions for each data set provide the extinction coefficients tabulated in (b). The extinction coefficients measured here only reflect the concentration of the open, colored triene isomer present at equilibrium under these conditions, which may not be 100%. However, the linearity of the curves indicates the equilibrium composition comprising the open, colored triene isomer and the closed colorless isomer remains constant across this concentration range for each DASA compound. No difference was observed for **DASA-1** in the presence of 36 mM $HNEt_2$.

Thus, the calculated extinction coefficients should report on the concentration of DASAs in the sonicated samples. The concentration of mechanically generated activated furan as calculated above for each solution was approximately 12 μM, representing the theoretical maximum concentration of each DASA. The experimentally measured absorbance values at the λ_{max} associated with each DASA product formed after treatment of the sonicated polymer solution was then converted to DASA concentration using the extinction coefficients determined under similar conditions (Figure 3.25), and these values were divided by the theoretical maximum concentration to estimate the yield of each DASA (**Table 3.2**). Under these dilute conditions, yields were determined to be 13%, 69%, and 57% for reaction of the mechanically generated activated furan with diethylamine, 4-methoxy-*N*-methylaniline, and indoline, respectively. We note that the lower DASA formation efficiencies determined here

are likely due to the low concentration. The large excess of diethylamine in that particular case may also result in degradation, although no difference in the calibration curve was observed upon the addition of 36 mM diethylamine. We contrast these results with those illustrated above in Figure 3.17, which demonstrate the quantitative conversion of the activated furan in more concentrated solutions using 5 equiv of amine.

Table 3.2 Determination of DASA concentrations in dilute conditions after 60 min ultrasonication of **PMA-1** and treatment with various amines in 4:1 DCM/HFIP (concentration of activated furan ~12 μM).

	Diethylamine (DASA-1)	**4-methoxy-*N*-methylaniline (DASA-2)**	**Indoline (DASA-3)**
λ_{max}	525 nm	570 nm	609 nm
Abs	0.0885	0.565	0.637
ε **(L mol^{-1} cm^{-1})**	56,100	68,300	94,100
[DASA]	1.6 μM	8.3 μM	6.8 μM
DASA Yield	13%	69%	57%

3.7.6 Details of the STAMMP Procedure Applied to PDMS Films

Procedure for Patterning Using Localized Compressive Force. STAMMP experiments were conducted using 2 x 2 cm squares, or smaller strips, of **PDMS-1** and **PDMS-Control**. The stamps used to apply localized compression were 3D printed from poly(lactic acid) (PLA) with embossed regions in the shape of the desired patterns. A minimum amount of force was applied to visually activate the material without causing irreversible deformation or tearing of the PDMS. After compression, the films were immersed in a solution of the appropriate amine for 90 s: 0.5 vol% $HNEt_2$ in DCM; 0.5 vol% indoline in DCM/HFIP; or 7 mM 4-methoxy-*N*-methylaniline in DCM/HFIP. HFIP was not used with diethylamine due

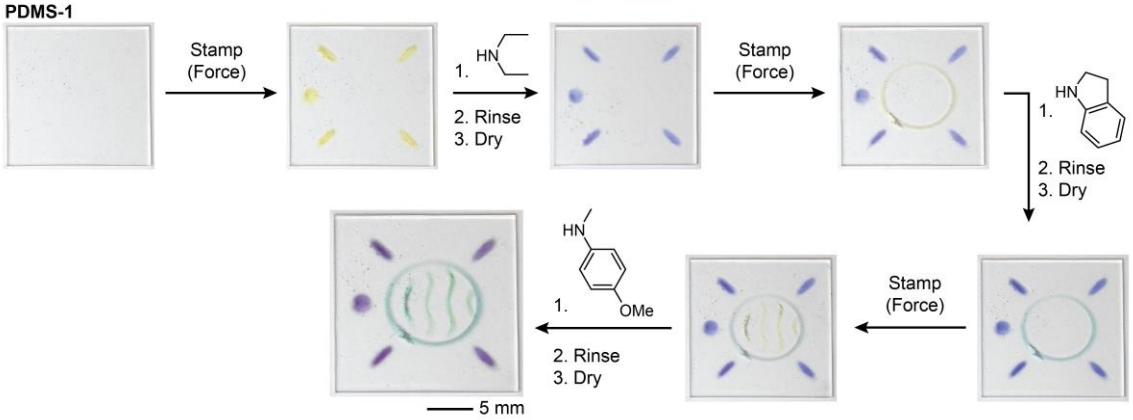

Figure 3.26 Demonstration of the STAMMP process with a turtle patterns. Photographs of a film of mechanochemically active **PDMS-1** containing 2.5 wt% of mechanophore crosslinker (±)-**5a** after an iterative process of localized compression followed by pattern development via DASA formation using diethylamine, indoline, and 4-methoxy-*N*-methylaniline.

to fuming that was observed at these higher concentrations (cf. ultrasonication experiments). For the mixtures of DCM/HFIP, solvent ratios of 4:1 and 9:1 (v/v) were used for various experiments, with no noticeable difference in performance. After reaction with the amine, the films were washed by immersing in DCM to remove residual amine and HFIP, replacing the solvent with fresh DCM several times over the course of at least 10 min. The films were then dried under high vacuum for 30 min to remove excess DCM before the next stamping step. All steps were conducted under ambient room light and atmosphere on the benchtop (stamping) or in a fume hood (washing/drying). An image of a turtle was prepared using the STAMMP process, as illustrated in Figure 3.26.

STAMMP Procedure with Regions of Overlapping Patterns. To investigate whether the DASAs produced in the STAMMP process were stable to further application of compressive force, the STAMMP process was applied to a film with overlapping patterns (Figure 3.27). A first set of DASAs was produced via compression using the flower petal stamp and a

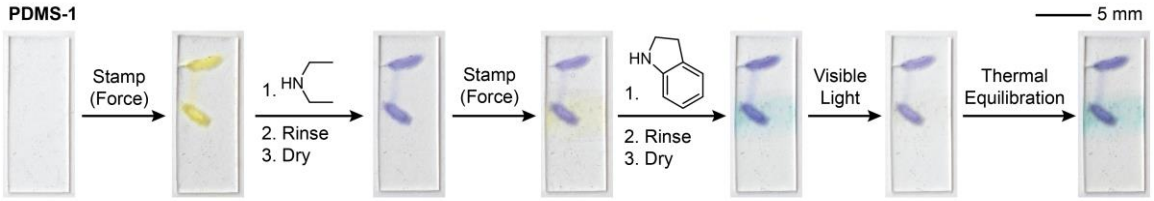

Figure 3.27 Demonstration of the STAMMP process with overlapping patterns. Photographs of a film of mechanochemically active **PDMS-1** containing 2.5 wt% of mechanophore crosslinker (±)-**5a** after an iterative process of localized compression followed by pattern development via DASA formation using diethylamine and indoline.

hydraulic press, followed by treatment of the film with diethylamine and then the standard washing/drying procedure as detailed above. Subsequently, a second DASA feature was produced with multiple manual compression cycles using the flower stem stamp, followed by treatment with indoline, ensuring partial overlap between the two DASAs. Note that the second DASA pattern was intentionally made fainter so as to not completely obscure the first DASA and to permit efficient photobleaching. No difference in color was observed between the portion of the first pattern that experienced further compressive force compared to the region of the pattern that was not exposed to additional compression in the second printing step. This is most clearly visible upon photoirradiation of the film with white light, which primarily causes photobleaching of the DASAs derived from indoline produced in the second printing step.

3.7.7 DASA Stability in the Presence of Different Amines: Influence on the Order of DASA Formation

To investigate the influence of the order of amine addition to the mechanically revealed activated furan, samples of DASA small molecules **DASA-1**, **DASA-2**, and **DASA-3** were dissolved in CD_2Cl_2 or 4:1 CD_2Cl_2/HFIP at a concentration of 5 mM, the amine of interest

was added (5 equiv), and then ^{1}H NMR spectra were acquired at various intervals starting 5 min after amine addition to determine stability of the DASA. Similar to the conditions used in the STAMMP demonstrations, experiments with $HNEt_2$ were conducted in CD_2Cl_2, while all others were conducted in 4:1 CD_2Cl_2/HFIP.

DASA-1 is stable in the presence of 4-methoxy-*N*-methylanline and indoline for at least 20 min (Figure 3.28 and Figure 3.29). **DASA-2** displays limited stability in the presence of indoline, with partial degradation observed after 20 min (Figure 3.30). However, we note that amine treatment is significantly more transient in the STAMMP process, which would preclude much of this undesired degradation. **DASA-3** is stable for more than 20 min in the presence of 4-methoxy-*N*-methylaniline (Figure 3.31). On the other hand, addition of $HNEt_2$ to solutions of **DASA-2** and **DASA-3** leads to complete conversion of the substrate, generating products with spectra consistent with the closed isomers of the DASAs (Figure 3.32 and Figure 3.33). Upon drying the mixture with **DASA-3** and redissolving in a solution of 4:1 CD_2Cl_2/HFIP, the open triene form was recovered, albeit with some degradation (Figure 3.34). The different reactivity of the dialkyl amine is likely due to its increased basicity, which has been observed in similar systems.[40] Based on these results, DASA formation using diethylamine was selected as the first step in all of the STAMMP demonstrations.

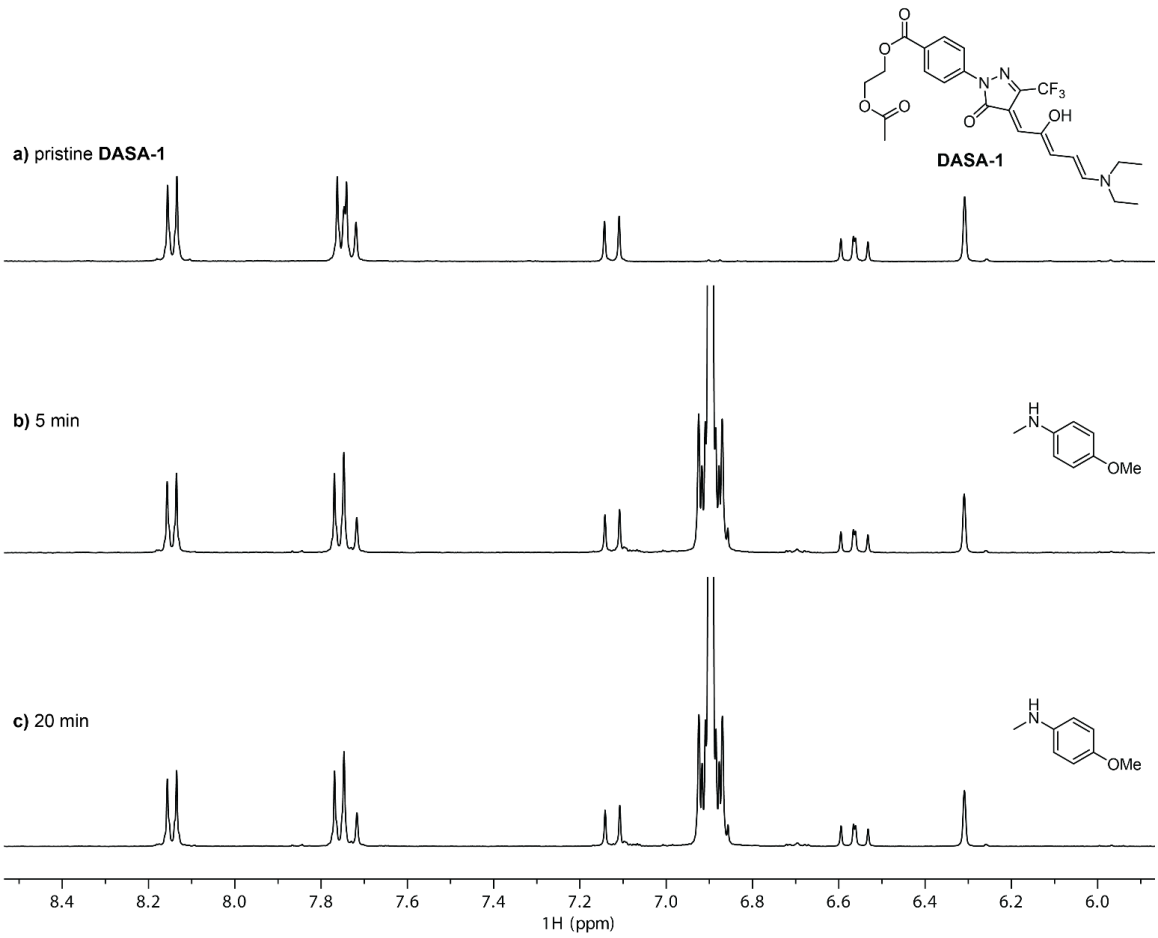

Figure 3.28 ^{1}H NMR spectra (400 MHz, 4:1 CD_2Cl_2/HFIP) illustrating the stability of **DASA-1** in the presence of 4-methoxy-*N*-methylaniline (5 equiv). Spectra of (a) pristine **DASA-1** in CD_2Cl_2, and **DASA-1** in the presence of 4-methoxy-*N*-methylaniline after (b) 5 min and (c) 20 min. The solvent conditions were chosen to mirror those in the STAMMP demonstrations.

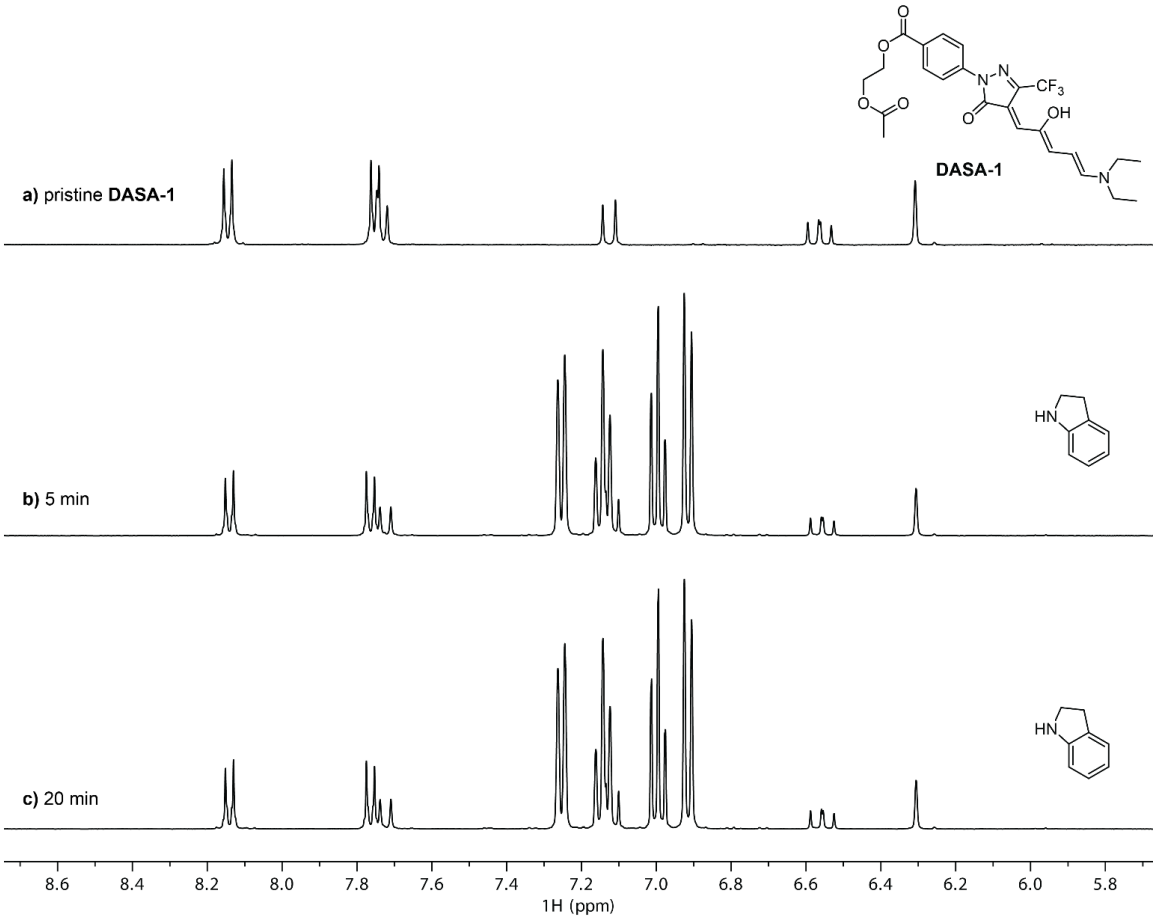

Figure 3.29 ^{1}H NMR spectra (400 MHz, 4:1 CD_2Cl_2/HFIP) illustrating the stability of **DASA-1** in the presence of indoline (5 equiv). Spectra of (a) pristine **DASA-2** in CD_2Cl_2, and **DASA-2** in the presence of indoline after (b) 5 min and (c) 20 min. The solvent conditions were chosen to mirror those in the STAMMP demonstrations.

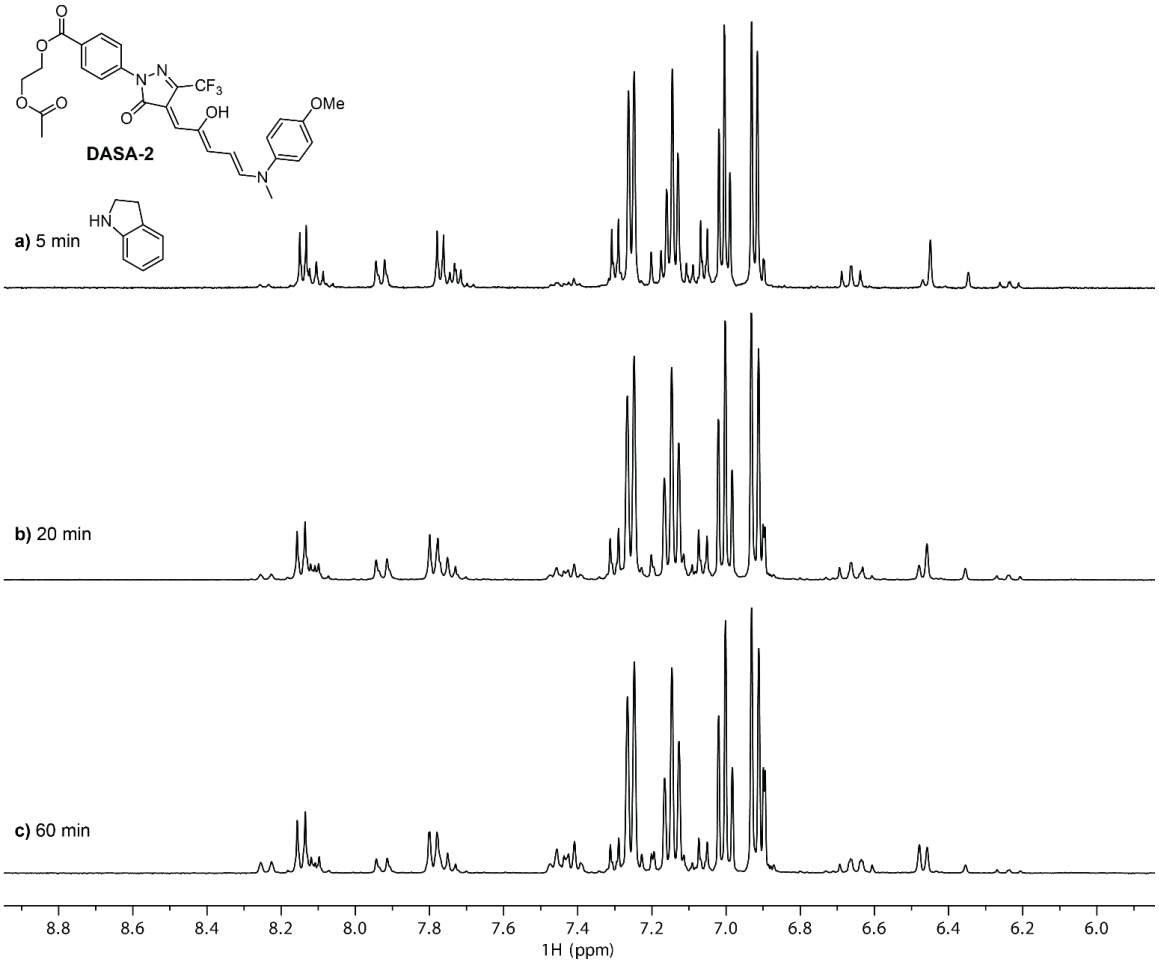

Figure 3.30 ^{1}H NMR spectra (400 MHz, 4:1 CD_2Cl_2/HFIP) illustrating the partial stability of **DASA-2** in the presence of indoline (5 equiv). **DASA-2** is relatively stable upon short exposure to indoline, but small peaks are observed to grow in over a period of 60 min indicating reactivity. The solvent conditions were chosen to mirror those in the STAMMP demonstrations.

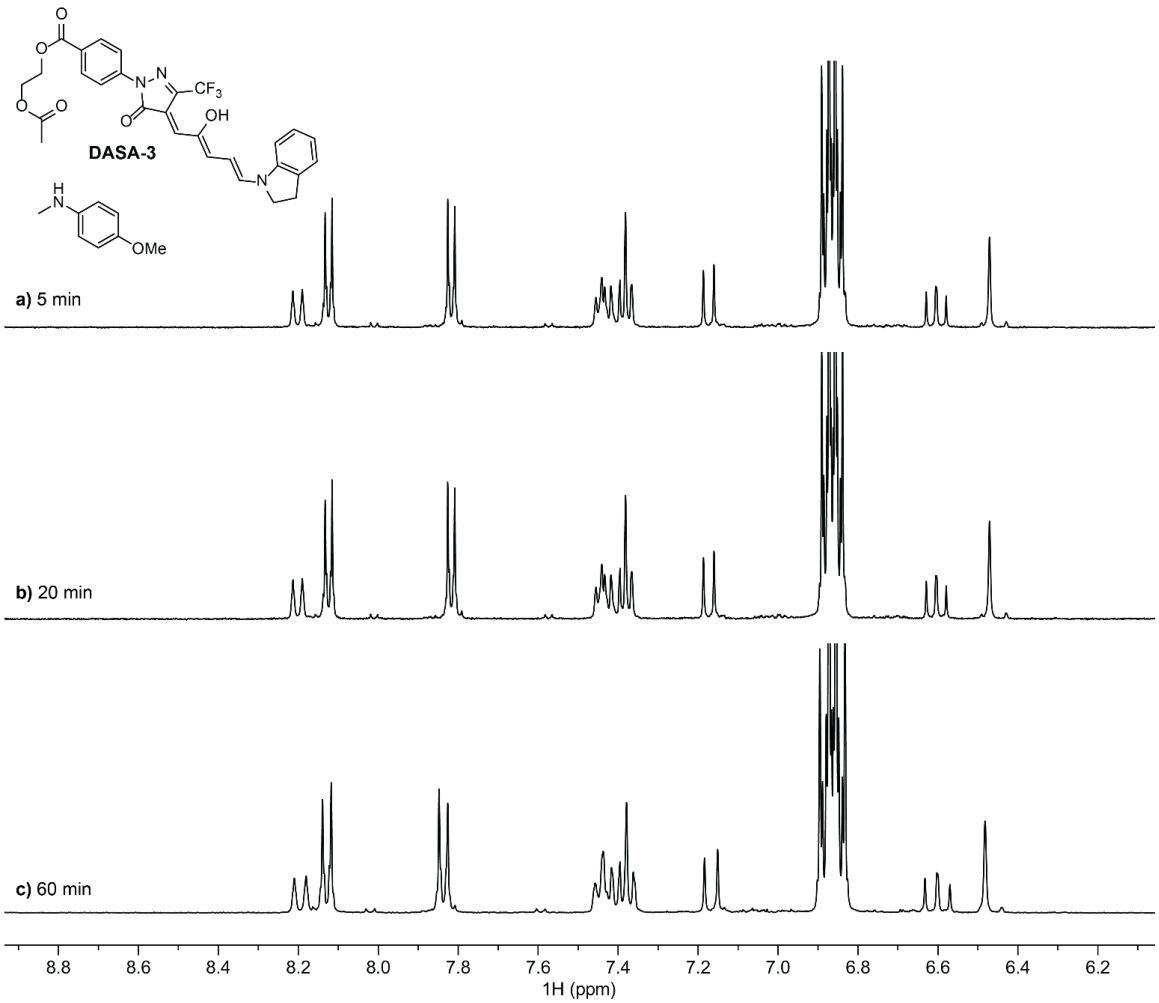

Figure 3.31 ^{1}H NMR spectra (400 MHz, 4:1 CD_2Cl_2/HFIP) illustrating the stability of **DASA-3** in the presence of 4-methoxy-*N*-methylaniline (5 equiv). No spectral changes are observed up to 60 min after amine addition. The solvent conditions were chosen to mirror those in the STAMMP demonstrations.

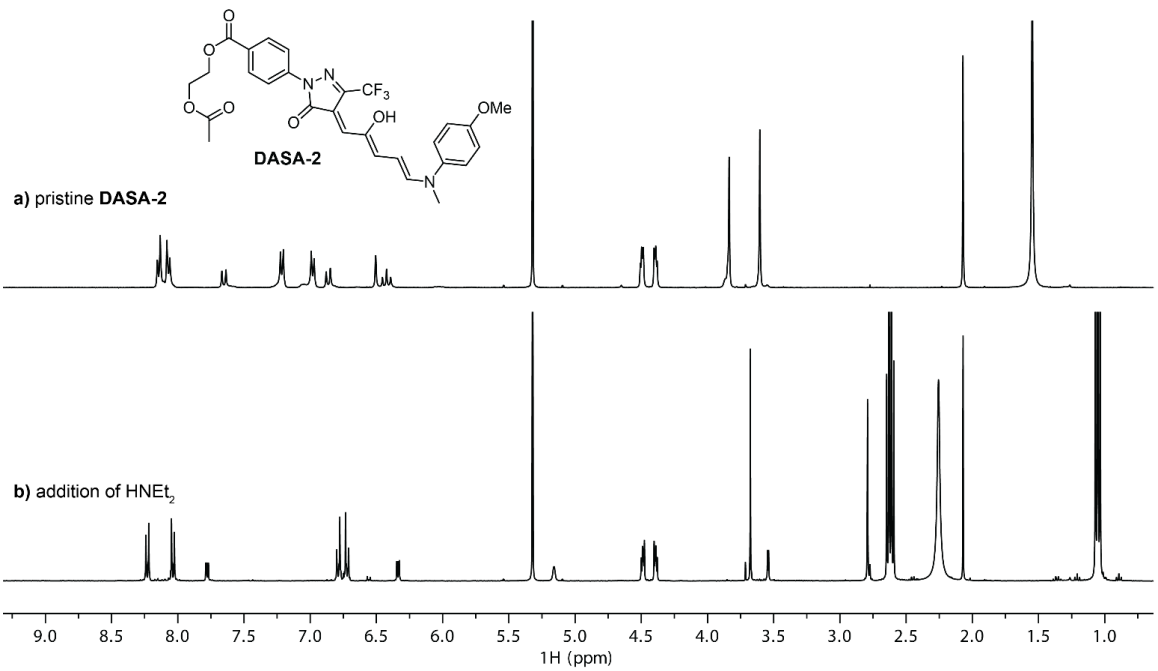

Figure 3.32 ^{1}H NMR spectra (400 MHz, CD_2Cl_2) illustrating the reactivity of **DASA-2** in the presence of $HNEt_2$ (5 equiv). (a) Spectrum and structure of **DASA-2** in CD_2Cl_2, and (b) the spectrum recorded 5 min after the addition of $HNEt_2$. The spectrum in (b) is consistent with the structure of the closed colorless isomer. The solvent conditions were chosen to mirror those in the STAMMP demonstrations.

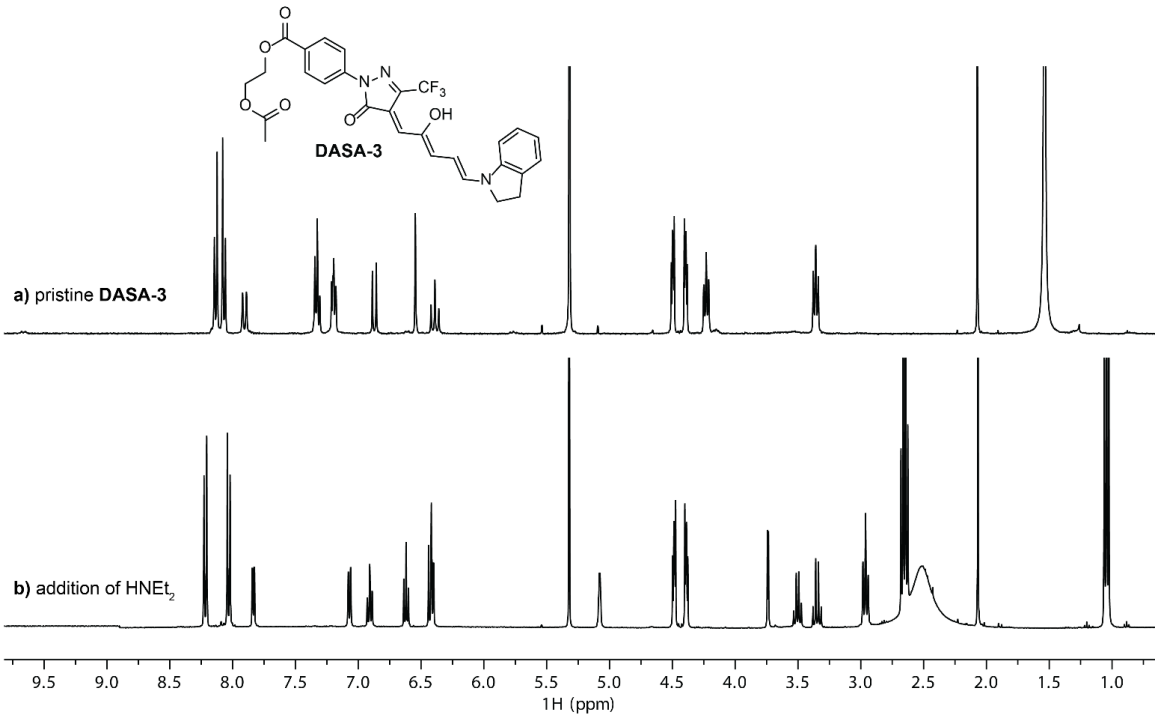

Figure 3.33 ^{1}H NMR spectra (400 MHz, CD_2Cl_2) illustrating the reactivity of **DASA-3** in the presence of $HNEt_2$ (5 equiv). (a) Spectrum and structure of **DASA-3** in CD_2Cl_2, and (b) the spectrum recorded 5 min after the addition of $HNEt_2$. The spectrum in (b) is consistent with the structure of the closed colorless isomer. The solvent conditions were chosen to mirror those in the STAMMP demonstrations.

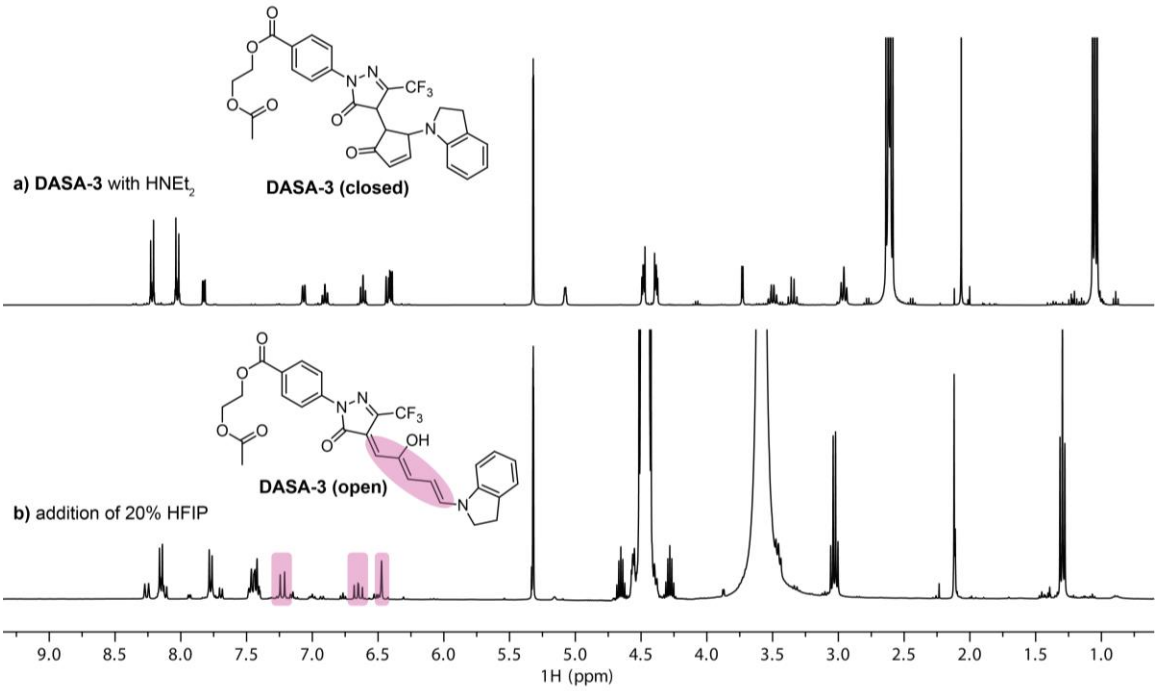

Figure 3.34 ^{1}H NMR spectra (400 MHz, CD_2Cl_2) illustrating the reversion of the closed isomer of **DASA-3** to the open, colored triene form upon exposure to HFIP. (a) Spectrum and structure of the closed isomer of **DASA-3** in CD_2Cl_2 produced via treatment of **DASA-3** with 5 equiv of diethylamine. (b) Spectrum of the same solution after being concentrated and redissolved in 4:1 CD_2Cl_2/HFIP suggesting regeneration of the ring-opened isomer, as indicated by the highlighted peaks characteristic of the triene bridge.

3.7.8 DFT Calculations (CoGEF)

CoGEF calculations were performed using Spartan '18 Parallel Suite according to previously reported methods.[29,30] A truncated model of the mechanophore with terminal acetoxy groups was used. Ground state energies were calculated using DFT at the B3LYP/6-31G* level of theory. Starting from the equilibrium geometry of the unconstrained molecule (energy = 0 kJ/mol), the distance between the terminal methyl groups of the structure was increased by 0.05 Å increments and the energy was minimized at each step. The maximum force associated with the mechanochemical retro-[4+2] reaction was calculated from the slope of the curve immediately prior to bond cleavage. XYZ coordinates for the computed structures corresponding to the equilibrium (force-free) geometry, the structures immediately prior to bond cleavage, and the structure after bond cleavage are provided in Appendix B.

3.7.9 Single Crystal X-ray Diffraction

Crystals for X-ray diffraction were grown by slow diffusion of pentane into a solution of compound (±)-**3** in diethyl ether. Low-temperature diffraction data (ϕ-and ω-scans) were collected on a Bruker AXS D8 VENTURE KAPPA diffractometer coupled to a PHOTON II CPAD detector Cu K_α radiation (λ = 1.54178 Å) from an IμS micro-source for the structure of compound (±)-**3** (V21285). The structure was solved by direct methods using SHELXS[41] and refined against F^2 on all data by full-matrix least squares with SHELXL-2017[42] using established refinement techniques.[43] All non-hydrogen atoms were refined anisotropically. Unless otherwise noted, all hydrogen atoms were included into the model at geometrically calculated positions and refined using a riding model. The isotropic displacement parameters of all hydrogen atoms were fixed to 1.2 times the U value of the atoms they are linked to (1.5

times for methyl groups). All disordered atoms were refined with the help of similarity restraints on the 1,2- and 1,3-distances and displacement parameters as well as enhanced rigid bond restraints for anisotropic displacement parameters.

Compound (±)-**3** (V21285) crystallizes in the triclinic space group *P*-1 with two molecules in the asymmetric unit. The ester group on one of the molecules was disordered over two positions, likely caused by motion in the long chain, resulting in a B-level alert. Additional disordered components were attempted but did not result in a better model. The elongated ellipsoids are a result of this motion. The hydrogen atoms on the terminal hydroxide could not be freely refined and were refined using a riding model.

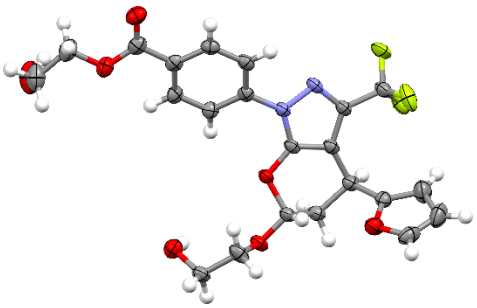

Identification code	V21285	
Empirical formula	C44 H42 F6 N4 O14	
Formula weight	964.81	
Temperature	100(2) K	
Wavelength	1.54178 Å	
Crystal system	Triclinic	
Space group	P-1	
Unit cell dimensions	a = 11.1428(14) Å	a= 98.053(5)°.

	b = 13.7818(18) Å b= 91.979(7)°.
	c = 14.4837(18) Å g = 102.092(9)°.
Volume	2148.7(5) $Å^3$
Z	2
Density (calculated)	1.491 Mg/m^3
Absorption coefficient	1.109 mm^{-1}
F(000)	1000
Crystal size	0.200 x 0.150 x 0.150 mm^3
Theta range for data collection	3.088 to 74.574°.
Index ranges	-13<=h<=13, -17<=k<=17, -13<=l<=17
Reflections collected	27256
Independent reflections	8656 [R(int) = 0.0349]
Completeness to theta = 67.679°	99.8 %
Absorption correction	Semi-empirical from equivalents
Max. and min. transmission	0.7538 and 0.6168
Refinement method	Full-matrix least-squares on F^2
Data / restraints / parameters	8656 / 260 / 675
Goodness-of-fit on F^2	1.047
Final R indices [I>2sigma(I)]	R1 = 0.0585, wR2 = 0.1681
R indices (all data)	R1 = 0.0669, wR2 = 0.1773
Extinction coefficient	n/a
Largest diff. peak and hole	0.560 and -0.394 $e.Å^{-3}$

3.8 References

(1) Caruso, M. M.; Davis, D. A.; Shen, Q.; Odom, S. A.; Sottos, N. R.; White, S. R.; Moore, J. S. Mechanically-Induced Chemical Changes in Polymeric Materials. *Chem. Rev.* **2009**, *109*, 5755–5798.

(2) Beyer, M. K.; Clausen-Schaumann, H. Mechanochemistry: The Mechanical Activation of Covalent Bonds. *Chem. Rev.* **2005**, *105*, 2921–2948.

(3) Li, J.; Nagamani, C.; Moore, J. S. Polymer Mechanochemistry: From Destructive to Productive. *Acc. Chem. Res.* **2015**, *48*, 2181–2190.

(4) Berkowski, K. L.; Potisek, S. L.; Hickenboth, C. R.; Moore, J. S. Ultrasound-Induced Site-Specific Cleavage of Azo-Functionalized Poly(ethylene glycol). *Macromolecules* **2005**, *38*, 8975–8978.

(5) Kim, G.; Lau, V. M.; Halmes, A. J.; Oelze, M. L.; Moore, J. S.; Li, K. C. High-intensity focused ultrasound-induced mechanochemical transduction in synthetic elastomers. *Proc. Natl. Acad. Sci.* **2019**, *116*, 10214–10222.

(6) Davis, D. A.; Hamilton, A.; Yang, J.; Cremar, L. D.; Van Gough, D.; Potisek, S. L.; Ong, M. T.; Braun, P. V.; Martínez, T. J.; White, S. R.; Moore, J. S.; Sottos, N. R. Force-induced activation of covalent bonds in mechanoresponsive polymeric materials. *Nature* **2009**, *459*, 68–72.

(7) Gossweiler, G. R.; Hewage, G. B.; Soriano, G.; Wang, Q.; Welshofer, G. W.; Zhao, X.; Craig, S. L. Mechanochemical Activation of Covalent Bonds in Polymers with Full and Repeatable Macroscopic Shape Recovery. *ACS Macro Lett.* **2014**, *3*, 216–219.

(8) Kingsbury, C. M.; May, P. A.; Davis, D. A.; White, S. R.; Moore, J. S.; Sottos, N. R. Shear activation of mechanophore-crosslinked polymers. *J. Mater. Chem.* **2011**, *21*, 8381–8388.

(9) Versaw, B. A.; Zeng, T.; Hu, X.; Robb, M. J. Harnessing the Power of Force: Development of Mechanophores for Molecular Release. *J. Am. Chem. Soc.* **2021**, *143*, 21461–21473.

(10) Chen, Z.; Mercer, J. A. M.; Zhu, X.; Romaniuk, J. A. H.; Pfattner, R.; Cegelski, L.; Martinez, T. J.; Burns, N. Z.; Xia, Y. Mechanochemical unzipping of insulating polyladderene to semiconducting polyacetylene. *Science* **2017**, *357*, 475–479.

(11) Ramirez, A. L. B.; Kean, Z. S.; Orlicki, J. A.; Champhekar, M.; Elsakr, S. M.; Krause, W. E.; Craig, S. L. Mechanochemical strengthening of a synthetic polymer in response to typically destructive shear forces. *Nat. Chem.* **2013**, *5*, 757–761.

(12) Ghanem, M. A.; Basu, A.; Behrou, R.; Boechler, N.; Boydston, A. J.; Craig, S. L.; Lin, Y.; Lynde, B. E.; Nelson, A.; Shen, H.; Storti, D. W. The role of polymer mechanochemistry in responsive materials and additive manufacturing. *Nat. Rev. Mater.* **2020**, *6*, 84–98.

(13) Chen, Y.; Mellot, G.; Luijk, D. van; Creton, C.; Sijbesma, R. P. Mechanochemical tools for polymer materials. *Chem. Soc. Rev.* **2021**, *50*, 4100–4140.

(14) Hu, X.; McFadden, M. E.; Barber, R. W.; Robb, M. J. Mechanochemical Regulation of a Photochemical Reaction. *J. Am. Chem. Soc.* **2018**, *140*, 14073–14077.

(15) Barber, R. W.; Robb, M. J. A modular approach to mechanically gated photoswitching with color-tunable molecular force probes. *Chem. Sci.* **2021**, *12*, 11703–11709.

(16) Kim, T. A.; Robb, M. J.; Moore, J. S.; White, S. R.; Sottos, N. R. Mechanical Reactivity of Two Different Spiropyran Mechanophores in Polydimethylsiloxane. *Macromolecules* **2018**, *51*, 9177–9183.

(17) Lin, Y.; Barbee, M. H.; Chang, C.-C.; Craig, S. L. Regiochemical Effects on Mechanophore Activation in Bulk Materials. *J. Am. Chem. Soc.* **2018**, *140*, 15969–15975.

(18) Helmy, S.; Leibfarth, F. A.; Oh, S.; Poelma, J. E.; Hawker, C. J.; Read de Alaniz, J. Photoswitching Using Visible Light: A New Class of Organic Photochromic Molecules. *J. Am. Chem. Soc.* **2014**, *136*, 8169–8172.

(19) Balamurugan, A.; Lee, H. A Visible Light Responsive On–Off Polymeric Photoswitch for the Colorimetric Detection of Nerve Agent Mimics in Solution and in the Vapor Phase. *Macromolecules* **2016**, *49*, 2568–2574.

(20) Diaz, Y. J.; Page, Z. A.; Knight, A. S.; Treat, N. J.; Hemmer, J. R.; Hawker, C. J.; Read de Alaniz, J. A Versatile and Highly Selective Colorimetric Sensor for the Detection of Amines. *Eur. J. Chem.* **2017**, *23*, 3562–3566.

(21) Chen, Q.; Diaz, Y. J.; Hawker, M. C.; Martinez, M. R.; Page, Z. A.; Xiao-An Zhang, S.; Hawker, C. J.; Read de Alaniz, J. Stable Activated Furan and Donor–Acceptor Stenhouse Adduct Polymer Conjugates as Chemical and Thermal Sensors. *Macromolecules* **2019**, *52*, 4370–4375.

(22) Poelma, S. O.; Oh, S. S.; Helmy, S.; Knight, A. S.; Burnett, G. L.; Soh, H. T.; Hawker, C. J.; Alaniz, J. R. de. Controlled drug release to cancer cells from modular one-photon visible light-responsive micellar system. *Chem. Commun.* **2016**, *52*, 10525–10528.

(23) Lee, J.; Sroda, M. M.; Kwon, Y.; El-Arid, S.; Seshadri, S.; Gockowski, L. F.; Hawkes, E. W.; Valentine, M. T.; Read de Alaniz, J. Tunable Photothermal Actuation Enabled by Photoswitching of Donor–Acceptor Stenhouse Adducts. *ACS Appl. Mater. Interfaces* **2020**, *12*, 54075–54082.

(24) Helmy, S.; Oh, S.; Leibfarth, F. A.; Hawker, C. J.; Read de Alaniz, J. Design and Synthesis of Donor–Acceptor Stenhouse Adducts: A Visible Light Photoswitch Derived from Furfural. *J. Org. Chem.* **2014**, *79*, 11316–11329.

(25) Hemmer, J. R.; Page, Z. A.; Clark, K. D.; Stricker, F.; Dolinski, N. D.; Hawker, C. J.; Read de Alaniz, J. Controlling Dark Equilibria and Enhancing Donor–Acceptor Stenhouse Adduct Photoswitching Properties through Carbon Acid Design. *J. Am. Chem. Soc.* **2018**, *140*, 10425–10429.

(26) Lerch, M. M.; Szymański, W.; Feringa, B. L. The (photo)chemistry of Stenhouse photoswitches: guiding principles and system design. *Chem. Soc. Rev.* **2018**, *47*, 1910–1937.

(27) Pałasz, A.; Pałasz, T. Knoevenagel condensation of cyclic ketones with benzoylacetonitrile and N,N′-dimethylbarbituric acid. Application of sterically hindered condensation products in the synthesis of spiro and dispiropyrans by hetero-Diels–Alder reactions. *Tetrahedron* **2011**, *67*, 1422–1431.

(28) Stevenson, R.; De Bo, G. Controlling Reactivity by Geometry in Retro-Diels–Alder Reactions under Tension. *J. Am. Chem. Soc.* **2017**, *139*, 16768–16771.

(29) Beyer, M. K. The mechanical strength of a covalent bond calculated by density functional theory. *J. Chem. Phys.* **2000**, *112*, 7307–7312.

(30) Klein, I. M.; Husic, C. C.; Kovács, D. P.; Choquette, N. J.; Robb, M. J. Validation of the CoGEF Method as a Predictive Tool for Polymer Mechanochemistry. *J. Am. Chem. Soc.* **2020**, *142*, 16364–16381.

(31) Clerc, M.; Stricker, F.; Ulrich, S.; Sroda, M.; Bruns, N.; Boesel, L. F.; Alaniz, J. R. de. Promoting the Furan Ring-Opening Reaction to Access New Donor–Acceptor Stenhouse Adducts with Hexafluoroisopropanol. *Angew. Chem. Int. Ed.* **2021**, *60*, 10219–10227.

(32) Clerc, M.; Tekin, C.; Ulrich, S.; Freire, R. V. M.; Salentinig, S.; Bruns, N.; Boesel, L. F. Donor–Acceptor Stenhouse Adduct-Polydimethylsiloxane-Conjugates for Enhanced Photoswitching in Bulk Polymers. *Macromol. Rapid Commun.* **2022**, *43*, 2200120.

(33) Sroda, M. M.; Stricker, F.; Peterson, J. A.; Bernal, A.; Read de Alaniz, J. Donor–Acceptor Stenhouse Adducts: Exploring the Effects of Ionic Character. *Chem. Eur. J.* **2021**, *27*, 4183–4190.

(34) Lui, B. F.; Tierce, N. T.; Tong, F.; Sroda, M. M.; Lu, H.; Alaniz, J. R. de; Bardeen, C. J. Unusual concentration dependence of the photoisomerization reaction in donor–acceptor Stenhouse adducts. *Photochem. Photobiol. Sci.* **2019**, *18*, 1587–1595.

(35) Xia, Y.; Whitesides, G. M. Soft Lithography. *Angew. Chem. Int. Ed.* **1998**, *37*, 550–575.

(36) Mei, Y.; Huang, W.; Di, W.; Wang, X.; Zhu, Z.; Zhou, Y.; Huo, F.; Wang, W.; Cao, Y. Mechanochemical Lithography. *J. Am. Chem. Soc.* **2022**, *144*, 9949–9958.

(37) Nguyen, N. H.; Rosen, B. M.; Lligadas, G.; Percec, V. Surface-Dependent Kinetics of Cu(0)-Wire-Catalyzed Single-Electron Transfer Living Radical Polymerization of Methyl Acrylate in DMSO at 25 °C. *Macromolecules* **2009**, *42*, 2379–2386.

(38) Hemmer, J. R.; Poelma, S. O.; Treat, N.; Page, Z. A.; Dolinski, N. D.; Diaz, Y. J.; Tomlinson, W.; Clark, K. D.; Hooper, J. P.; Hawker, C.; Read de Alaniz, J. Tunable Visible and Near Infrared Photoswitches. *J. Am. Chem. Soc.* **2016**, *138*, 13960–13966.

(39) Robb, M. J.; Kim, T. A.; Halmes, A. J.; White, S. R.; Sottos, N. R.; Moore, J. S. Regioisomer-Specific Mechanochromism of Naphthopyran in Polymeric Materials. *J. Am. Chem. Soc.* **2016**, *138*, 12328–12331.

(40) Chen, T.-Y.; Cai, Y.-D.; Jiang, S.-Q.; Cai, W.; Tong, M.-L.; Bao, X. Light- and Chemical-Stimuli-Induced Isomerization of Donor−Acceptor Stenhouse Adducts. *ChemPhotoChem* **2021**, *5*, 559–564.

(41) Sheldrick, G. M. Phase annealing in SHELX-90: direct methods for larger structures. *Acta Cryst. A* **1990**, *46*, 467–473.

(42) Sheldrick, G. M. SHELXT – Integrated space-group and crystal-structure determination. *Acta Cryst. A* **2015**, *71*, 3–8.

(43) Müller, P. Practical suggestions for better crystal structures. *Crystallography Reviews* **2009**, *15*, 57–83.

Appendix B

Spectra Relevant to Chapter 3:

Mechanically gated formation of donor–acceptor Stenhouse adducts enabling mechanochemical multicolor soft lithography

XYZ Coordinates for Salient Geometries

Equilibrium Geometry

C	0.911220	2.814881	-1.244839
C	1.684014	1.962912	-0.446286
C	1.436105	0.595814	-0.415509
C	0.387848	0.070662	-1.183594
C	-0.389948	0.911516	-1.991425
C	-0.124207	2.274361	-2.021166
C	1.232101	4.266044	-1.226863
O	0.428568	4.985848	-2.050171
C	0.678724	6.400774	-2.075982
C	-0.307817	6.983132	-3.072778
O	2.109449	4.772257	-0.555427
O	-0.061365	8.399906	-3.084941
N	0.100318	-1.317657	-1.174585
C	0.395180	-2.274353	-0.238751
C	-0.117609	-3.479139	-0.661297
C	-0.737118	-3.148246	-1.891071
N	-0.606341	-1.867914	-2.207410
C	-1.452860	-4.077420	-2.821899
F	-2.275865	-4.897727	-2.122691
F	-0.590435	-4.868893	-3.497612
F	-2.195003	-3.418280	-3.724852
O	1.049353	-2.006137	0.911898
C	0.882784	-3.065840	1.904067
C	1.062109	-4.443128	1.274690
C	0.012890	-4.734918	0.164971
C	0.390889	-5.952291	-0.621408
C	-0.203293	-7.163884	-0.811424
C	0.667361	-7.918344	-1.665842
C	1.726924	-7.109017	-1.931883
O	1.579934	-5.907813	-1.300711
O	-0.381265	-2.998741	2.479121
C	-0.631454	-1.857551	3.309132
C	-0.652859	-2.304952	4.764216
O	-0.941562	-1.131503	5.543771
C	-0.866480	9.129970	-3.898610
C	-0.515015	10.596505	-3.821057
O	-1.738555	8.642454	-4.580712
C	-0.997122	-1.318676	6.888175
C	-1.300961	-0.021082	7.597511
O	-0.818194	-2.393138	7.414463
H	2.489377	2.389311	0.142325
H	2.050129	-0.056586	0.191287

H	-1.185293	0.481841	-2.587479
H	-0.725933	2.926328	-2.643934
H	1.713120	6.591172	-2.376654
H	0.533589	6.823724	-1.077219
H	-0.157225	6.567117	-4.073763
H	-1.342372	6.786390	-2.776217
H	1.675442	-2.835674	2.624863
H	2.066995	-4.489310	0.842966
H	0.998555	-5.198321	2.063348
H	-0.950070	-4.955685	0.641653
H	-1.155661	-7.475681	-0.405535
H	0.514069	-8.922704	-2.035144
H	2.624038	-7.220323	-2.521546
H	-1.602834	-1.444669	3.021287
H	0.123486	-1.080828	3.147695
H	-1.420481	-3.066942	4.929938
H	0.309845	-2.727367	5.070972
H	-0.645362	10.959265	-2.795990
H	-1.159090	11.159920	-4.496797
H	0.535167	10.748074	-4.090205
H	-1.384512	-0.204428	8.669089
H	-2.232227	0.410202	7.216703
H	-0.503194	0.704780	7.407139

Geometry Two Steps Prior to Bond Cleavage

C	0.164710	4.153488	-1.892949
C	1.135905	3.643552	-0.986330
C	0.967494	2.483780	-0.176775
C	-0.217697	1.725747	-0.193269
C	-1.223378	2.257304	-1.040598
C	-1.042828	3.410813	-1.856466
C	0.643932	5.480168	-2.751379
O	-0.065438	6.081451	-3.814220
C	0.623838	7.333149	-4.461545
C	-0.154525	8.023981	-5.714301
O	1.710266	5.942362	-2.412052
O	0.553142	9.267695	-6.326256
N	-0.337449	0.219721	0.269937
C	-0.299447	-0.898527	1.313428
C	-0.269087	-2.065056	0.573039
C	-0.356845	-1.702041	-0.787502
N	-0.401635	-0.401834	-0.942954
C	-0.463328	-2.554445	-2.018668
F	-1.461917	-3.462335	-1.895775
F	0.672106	-3.246142	-2.265223

F	-0.722502	-1.815670	-3.108920
O	-0.368054	-0.958255	2.712113
C	0.170716	-2.290027	3.498987
C	0.856043	-3.148768	2.472202
C	-0.080020	-3.403536	1.263069
C	0.474371	-4.502659	0.412651
C	-0.054156	-5.653462	-0.090470
C	1.006666	-6.322775	-0.784529
C	2.104506	-5.532925	-0.646338
O	1.803156	-4.422633	0.086537
O	-0.795760	-3.113836	4.255479
C	-0.232918	-3.906166	5.443989
C	-1.139174	-5.176030	5.938863
O	-0.578656	-5.984891	7.140889
C	-0.089559	9.898897	-7.431798
C	0.493116	11.277688	-8.274833
O	-1.134430	9.463385	-7.848259
C	-1.339588	-7.116127	7.569735
C	-0.943100	-8.157630	8.878337
O	-2.356403	-7.406436	6.991198
H	2.093291	4.149663	-0.925139
H	1.814398	2.165736	0.424871
H	-2.163913	1.725081	-1.133496
H	-1.880457	3.695424	-2.488147
H	1.610603	6.995878	-4.777269
H	0.742174	8.054029	-3.652884
H	-0.267612	7.304001	-6.525209
H	-1.144875	8.357078	-5.402790
H	0.825269	-1.781077	4.205509
H	1.775343	-2.671576	2.120141
H	1.129920	-4.098388	2.941739
H	-1.040545	-3.759853	1.657854
H	-1.081811	-5.975765	0.004117
H	0.950498	-7.259778	-1.320101
H	3.126102	-5.603570	-0.988129
H	-0.121930	-3.201591	6.272733
H	0.754191	-4.286472	5.165775
H	-2.126790	-4.823862	6.237250
H	-1.253511	-5.880449	5.114671
H	-0.319022	11.998141	-8.186604
H	0.599618	10.929898	-9.301646
H	1.430375	11.666783	-7.876872
H	-0.818068	-9.132938	8.408987
H	-1.835714	-8.135442	9.502369
H	-0.049604	-7.851928	9.423227

Geometry Immediately Prior to Bond Cleavage

C	0.164346	4.171131	-1.899352
C	1.129480	3.674429	-0.978940
C	0.965002	2.511885	-0.172363
C	-0.209285	1.737698	-0.204066
C	-1.209347	2.253950	-1.068379
C	-1.033109	3.411394	-1.880171
C	0.639382	5.502350	-2.755279
O	-0.063573	6.096239	-3.827176
C	0.618900	7.356664	-4.467505
C	-0.147739	8.034832	-5.736086
O	1.697829	5.974127	-2.405435
O	0.551958	9.288486	-6.339425
N	-0.313275	0.230663	0.263248
C	-0.294246	-0.889359	1.313475
C	-0.259412	-2.055520	0.571654
C	-0.326719	-1.693707	-0.790554
N	-0.364868	-0.393824	-0.947951
C	-0.430432	-2.546106	-2.022121
F	-1.426860	-3.456889	-1.897354
F	0.706144	-3.236088	-2.271369
F	-0.693098	-1.807331	-3.112699
O	-0.372453	-0.947963	2.707793
C	0.169020	-2.310179	3.515147
C	0.854956	-3.148784	2.475455
C	-0.085967	-3.393789	1.265475
C	0.451141	-4.506680	0.422187
C	-0.092071	-5.664634	-0.048123
C	0.953367	-6.356135	-0.744220
C	2.057394	-5.569922	-0.639805
O	1.775341	-4.442814	0.075011
O	-0.790829	-3.136760	4.262037
C	-0.234210	-3.919149	5.463334
C	-1.126369	-5.206050	5.940168
O	-0.573700	-6.005091	7.152528
C	-0.083729	9.910571	-7.454293
C	0.487708	11.301684	-8.286624
O	-1.115058	9.458737	-7.886993
C	-1.322970	-7.149860	7.569019
C	-0.932863	-8.182899	8.887696
O	-2.324865	-7.456713	6.973334
H	2.079661	4.192277	-0.904668
H	1.807893	2.202550	0.439019
H	-2.139875	1.706906	-1.179429
H	-1.864913	3.684968	-2.524459

H	1.616411	7.033300	-4.763530
H	0.710047	8.082504	-3.659681
H	-0.237062	7.313396	-6.548582
H	-1.147208	8.355307	-5.440919
H	0.812667	-1.785115	4.219210
H	1.769804	-2.660260	2.127167
H	1.134743	-4.103465	2.932214
H	-1.050179	-3.738582	1.662188
H	-1.119527	-5.979460	0.071388
H	0.882655	-7.304976	-1.257802
H	3.072172	-5.654607	-0.997295
H	-0.156254	-3.213128	6.294316
H	0.765868	-4.275354	5.201082
H	-2.123844	-4.867420	6.220788
H	-1.216672	-5.912441	5.114383
H	-0.338518	12.007233	-8.207301
H	0.611976	10.959230	-9.313241
H	1.412963	11.706137	-7.875826
H	-0.800384	-9.161150	8.426879
H	-1.830497	-8.158253	9.503938
H	-0.046847	-7.868190	9.438882

Geometry After Bond Cleavage

C	-0.065709	4.647031	-2.406291
C	-0.205857	4.138020	-1.108745
C	-0.292403	2.770775	-0.878530
C	-0.245551	1.889201	-1.969382
C	-0.106692	2.384654	-3.274330
C	-0.012752	3.753954	-3.485787
C	0.001436	6.120970	-2.580435
O	0.212187	6.482177	-3.874149
C	0.241786	7.894798	-4.125455
C	0.585726	8.053821	-5.596241
O	-0.116601	6.929966	-1.681795
O	0.680786	9.471042	-5.828589
N	-0.325736	0.489429	-1.768134
C	-0.727360	-0.220452	-0.623778
C	-0.644789	-1.649000	-1.039045
C	-0.205733	-1.580265	-2.419429
N	-0.030285	-0.351416	-2.814875
C	0.067822	-2.681730	-3.406511
F	-1.035360	-3.431768	-3.627238
F	1.034717	-3.508711	-2.951086
F	0.466593	-2.194475	-4.590234
O	-1.060004	0.242712	0.457310

C	0.401097	-3.463934	4.798879
C	0.782200	-2.986372	3.612144
C	-0.948009	-2.590353	-0.097115
C	-0.947125	-4.005842	-0.073105
C	-1.142420	-4.866888	0.995152
C	-1.016691	-6.184008	0.489125
C	-0.754269	-6.046274	-0.849230
O	-0.710874	-4.746863	-1.203363
O	0.762714	-4.699585	5.252991
C	-0.085076	-5.262769	6.248287
C	0.708494	-6.352893	6.949614
O	-0.146673	-6.862213	7.989222
C	1.015047	9.836805	-7.090758
C	1.027849	11.339318	-7.240220
O	1.239173	9.045678	-7.979132
C	0.390230	-7.842117	8.761971
C	-0.581344	-8.289199	9.829044
O	1.504690	-8.278192	8.590731
H	-0.228993	4.831537	-0.275715
H	-0.398055	2.385556	0.126234
H	-0.072450	1.692908	-4.106551
H	0.107896	4.135232	-4.494059
H	0.990296	8.375921	-3.490985
H	-0.732029	8.334353	-3.886733
H	1.537360	7.570803	-5.839020
H	-0.187340	7.624440	-6.240618
H	-0.197526	-2.876479	5.498677
H	0.525698	-1.971623	3.328597
H	1.393585	-3.572430	2.934412
H	-1.229060	-2.146892	0.858471
H	-1.315173	-4.568529	2.018283
H	-1.118775	-7.109723	1.036560
H	-0.588549	-6.752737	-1.649603
H	-0.991300	-5.682118	5.789202
H	-0.395962	-4.498832	6.976979
H	0.986408	-7.158212	6.263774
H	1.627514	-5.943073	7.377952
H	0.056378	11.666760	-7.626636
H	1.789978	11.621920	-7.968659
H	1.203016	11.837038	-6.285049
H	-0.099522	-9.035723	10.460376
H	-1.476591	-8.716157	9.363804
H	-0.902038	-7.438977	10.438822

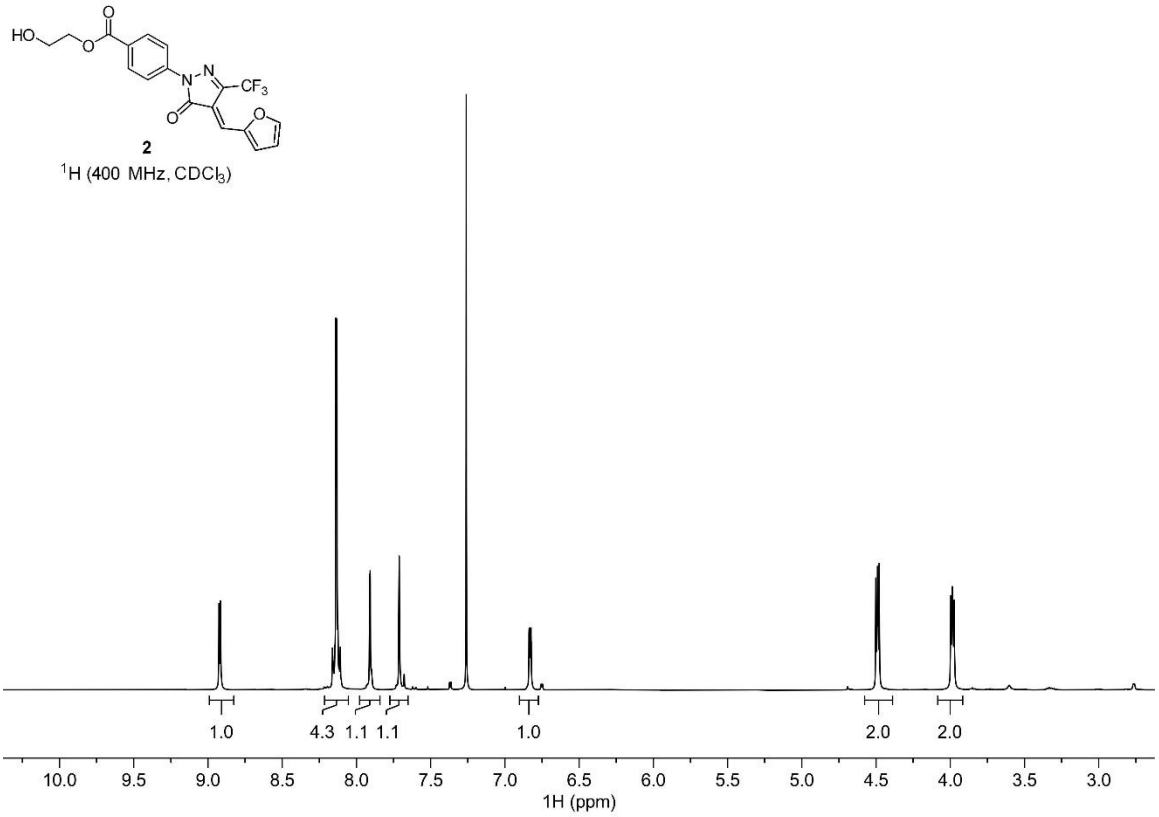
HO
O
O
N
N
CF3
O
O
2
1H (400 MHz, CDCl3)
1.0
4.3
1.1
1.1
1.0
2.0
2.0
10.0
9.5
9.0
8.5
8.0
7.5
7.0
6.5
6.0
5.5
5.0
4.5
4.0
3.5
3.0
1H (ppm)

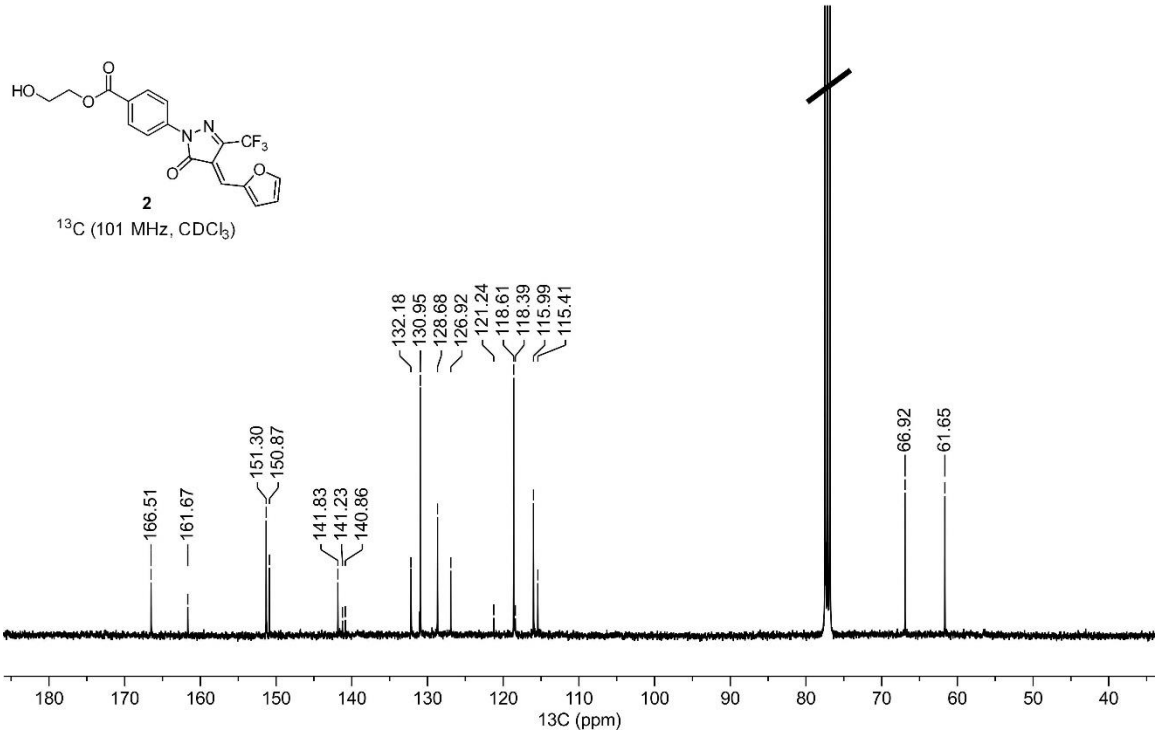
HO
O
O
N
N
CF3
O
O
2
13C (101 MHz, CDCl3)
166.51
161.67
151.30
150.87
141.83
141.23
140.86
132.18
130.95
128.68
126.92
121.24
118.61
118.39
115.99
115.41
66.92
61.65
180
170
160
150
140
130
120
110
100
90
80
70
60
50
40
13C (ppm)

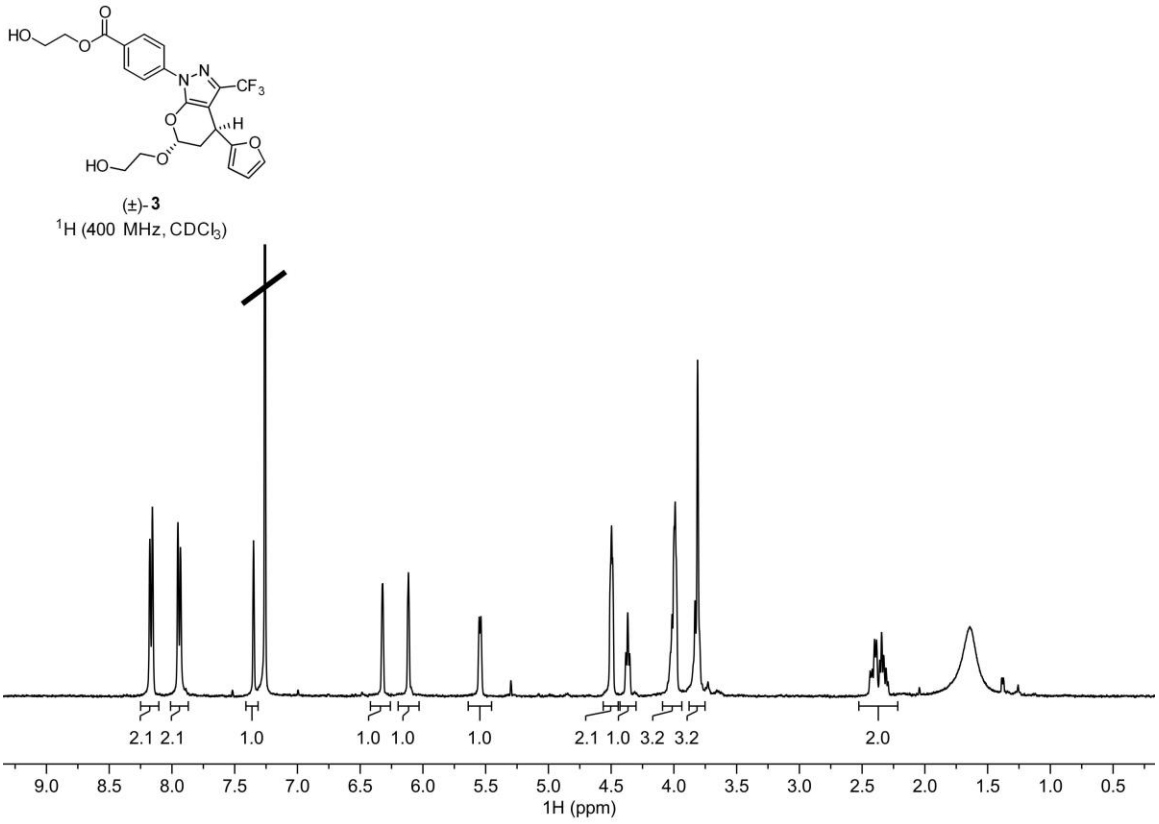
(±)-3
1H (400 MHz, CDCl3)
2.1 2.1 1.0 1.0 1.0 1.0 2.1 1.0 3.2 3.2 2.0
1H (ppm)

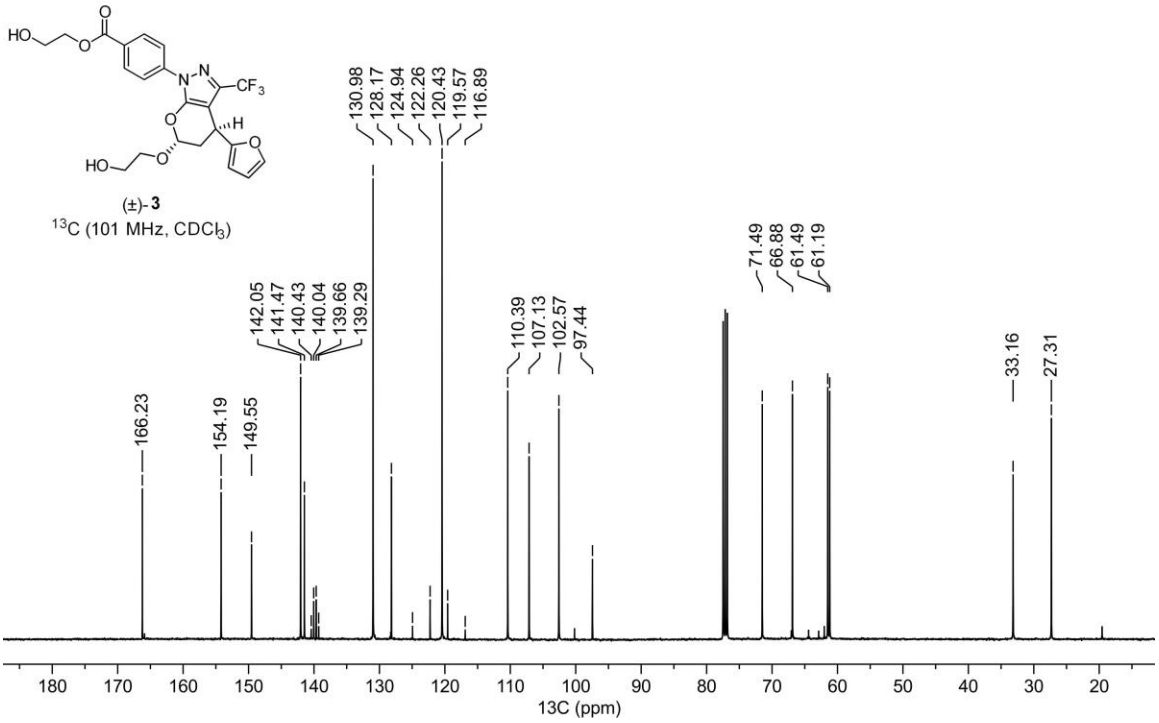
(±)-3
13C (101 MHz, CDCl3)
166.23
154.19
149.55
142.05
141.47
140.43
140.04
139.66
139.29
130.98
128.17
124.94
122.26
120.43
119.57
116.89
110.39
107.13
102.57
97.44
71.49
66.88
61.49
61.19
33.16
27.31
13C (ppm)

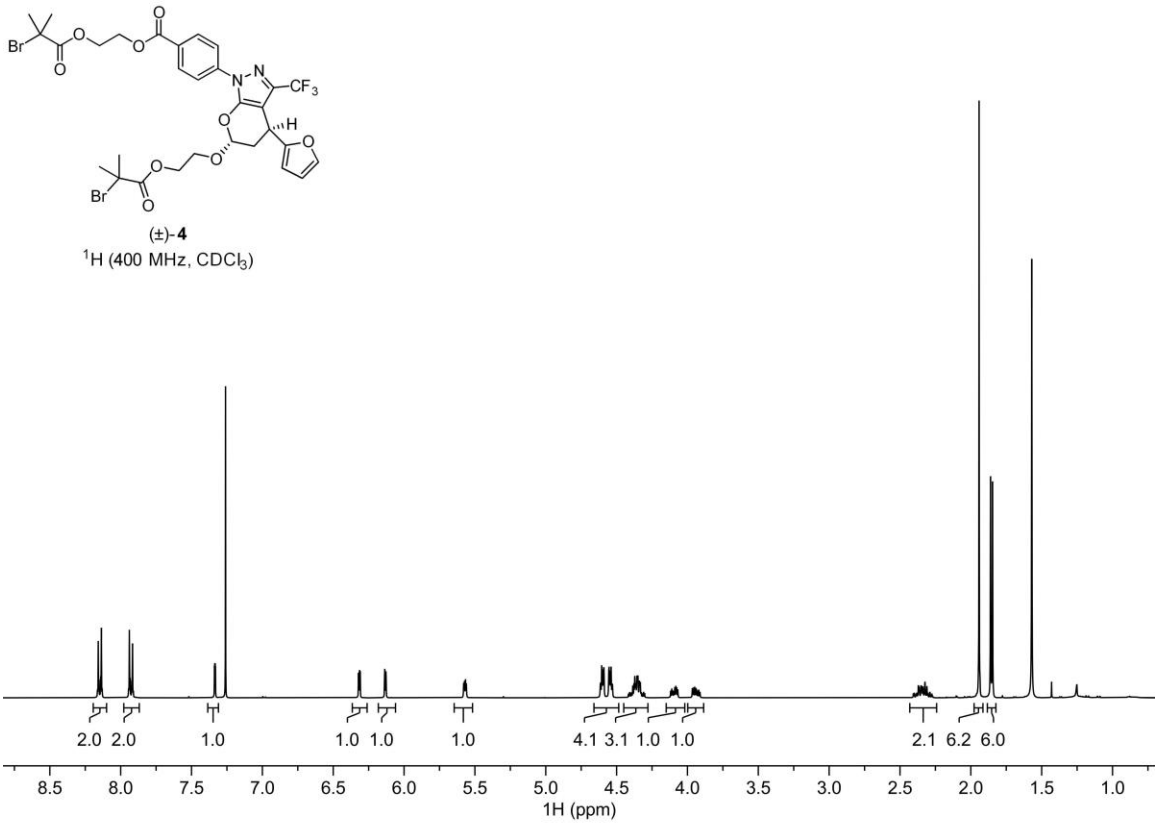
(±)-4
1H (400 MHz, CDCl3)
2.0 2.0 1.0 1.0 1.0 1.0 4.1 3.1 1.0 1.0 2.1 6.2 6.0
1H (ppm)

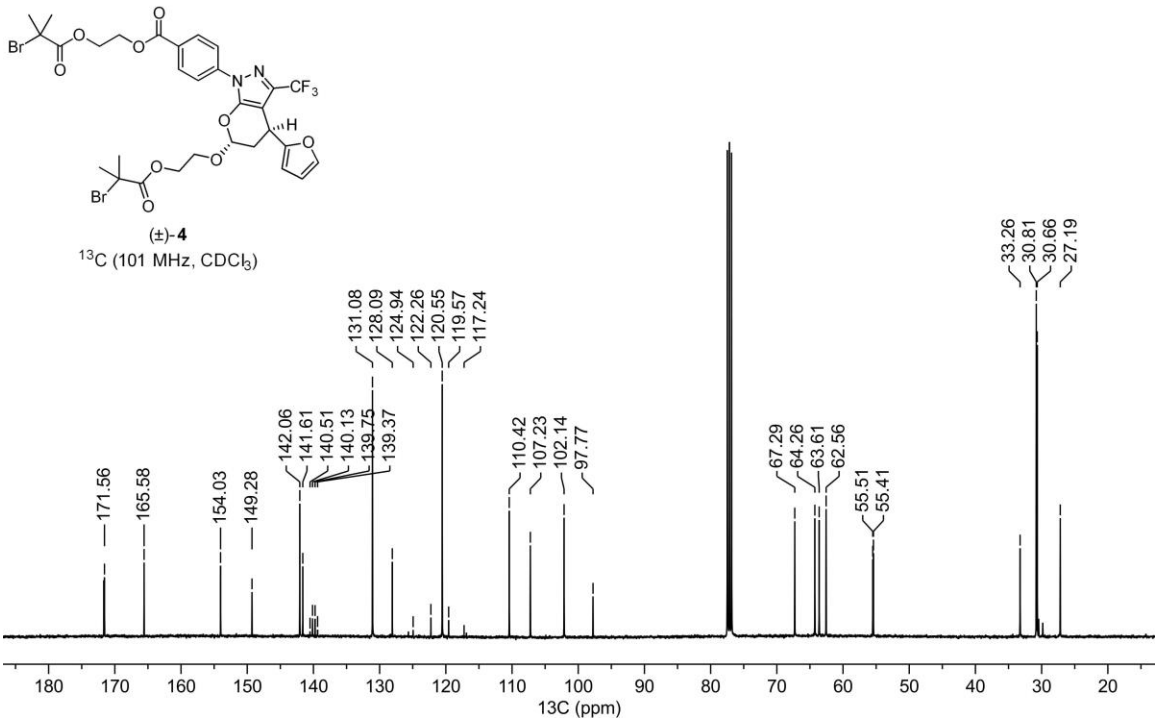
(±)-4
13C (101 MHz, CDCl3)
171.56
165.58
154.03
149.28
142.06
141.61
140.51
140.13
139.75
139.37
131.08
128.09
124.94
122.26
120.55
119.57
117.24
110.42
107.23
102.14
97.77
67.29
64.26
63.61
62.56
55.51
55.41
33.26
30.81
30.66
27.19
13C (ppm)

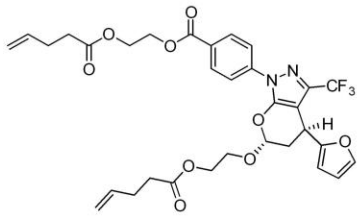

(±)-**5a**

^{1}H (400 MHz, $CDCl_3$)

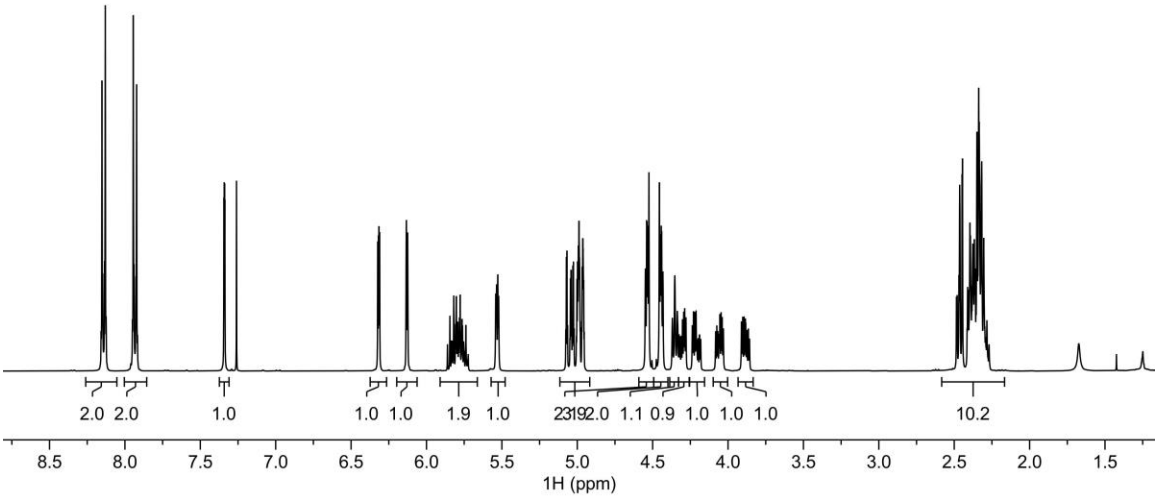

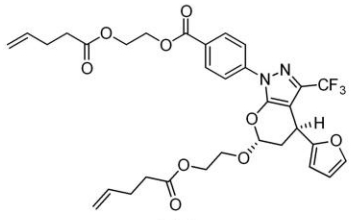

(±)-**5a**

^{13}C (101 MHz, $CDCl_3$)

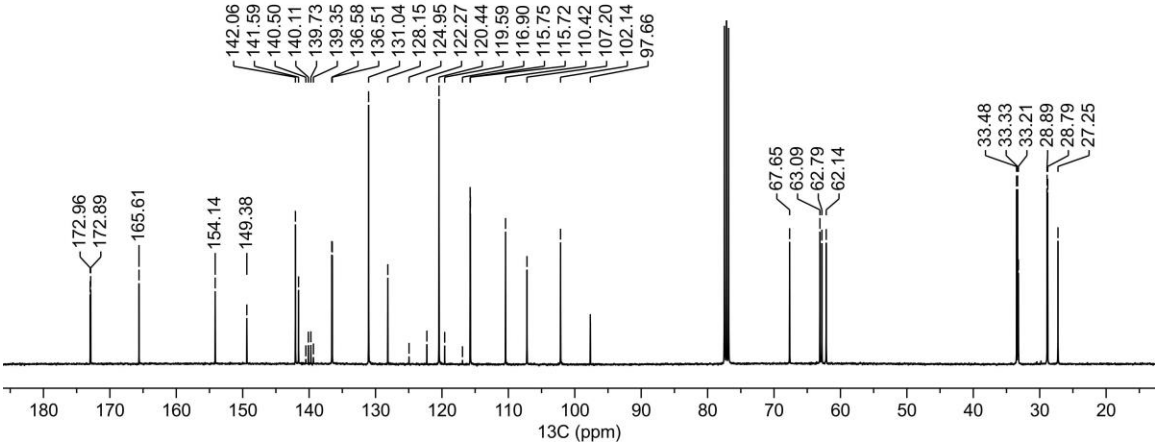

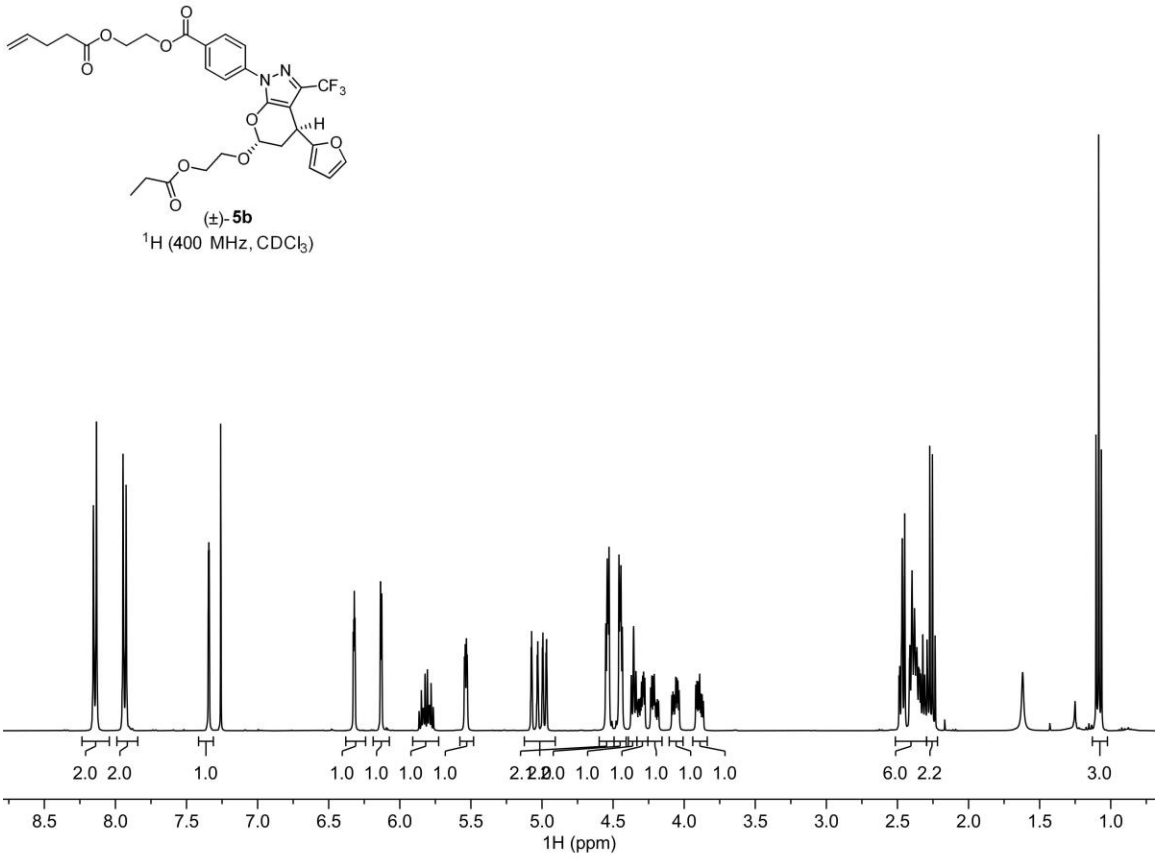
(±)-5b
1H (400 MHz, CDCl3)
2.0 2.0 1.0 1.0 1.0 1.0 2.2 2.0 1.0 1.0 1.0 1.0 1.0 6.0 2.2 3.0
8.5 8.0 7.5 7.0 6.5 6.0 5.5 5.0 4.5 4.0 3.5 3.0 2.5 2.0 1.5 1.0
1H (ppm)

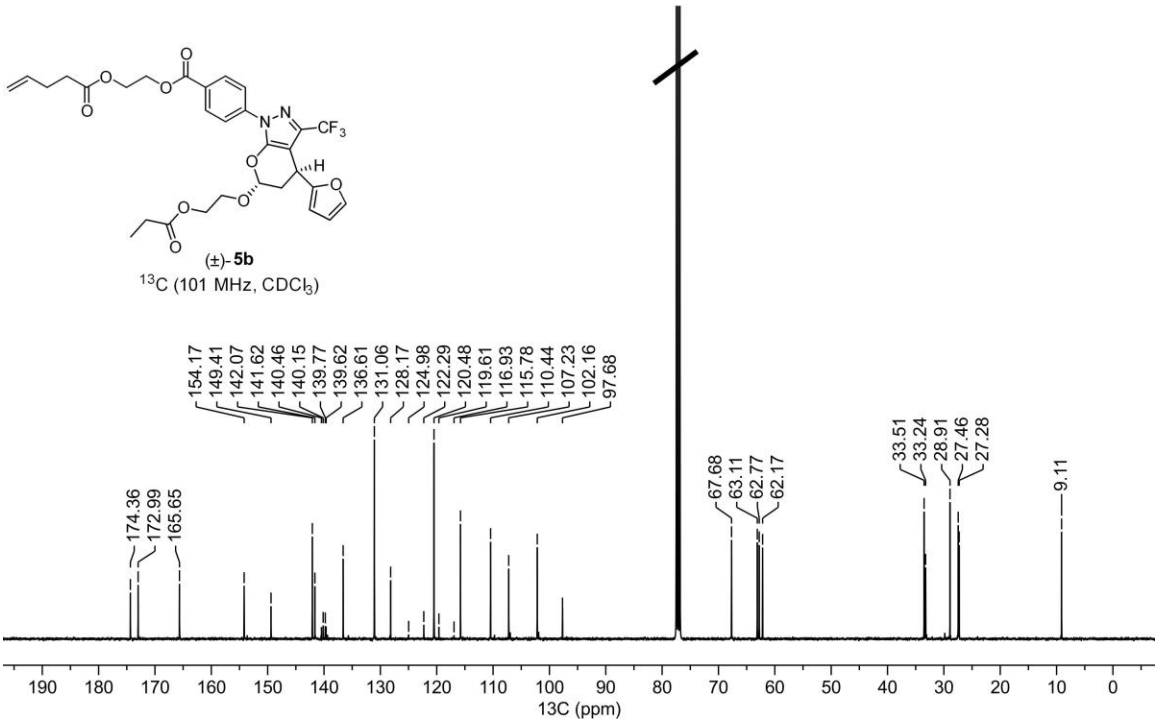
(±)-5b
13C (101 MHz, CDCl3)
154.17
149.41
142.07
141.62
140.46
140.15
139.77
139.62
136.61
131.06
128.17
124.98
122.29
120.48
119.61
116.93
115.78
110.44
107.23
102.16
97.68
174.36
172.99
165.65
67.68
63.11
62.77
62.17
33.51
33.24
28.91
27.46
27.28
9.11
190 180 170 160 150 140 130 120 110 100 90 80 70 60 50 40 30 20 10 0
13C (ppm)

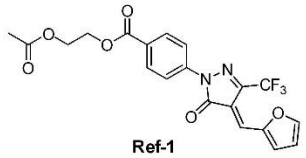

Ref-1

^{1}H (400 MHz, $CDCl_3$)

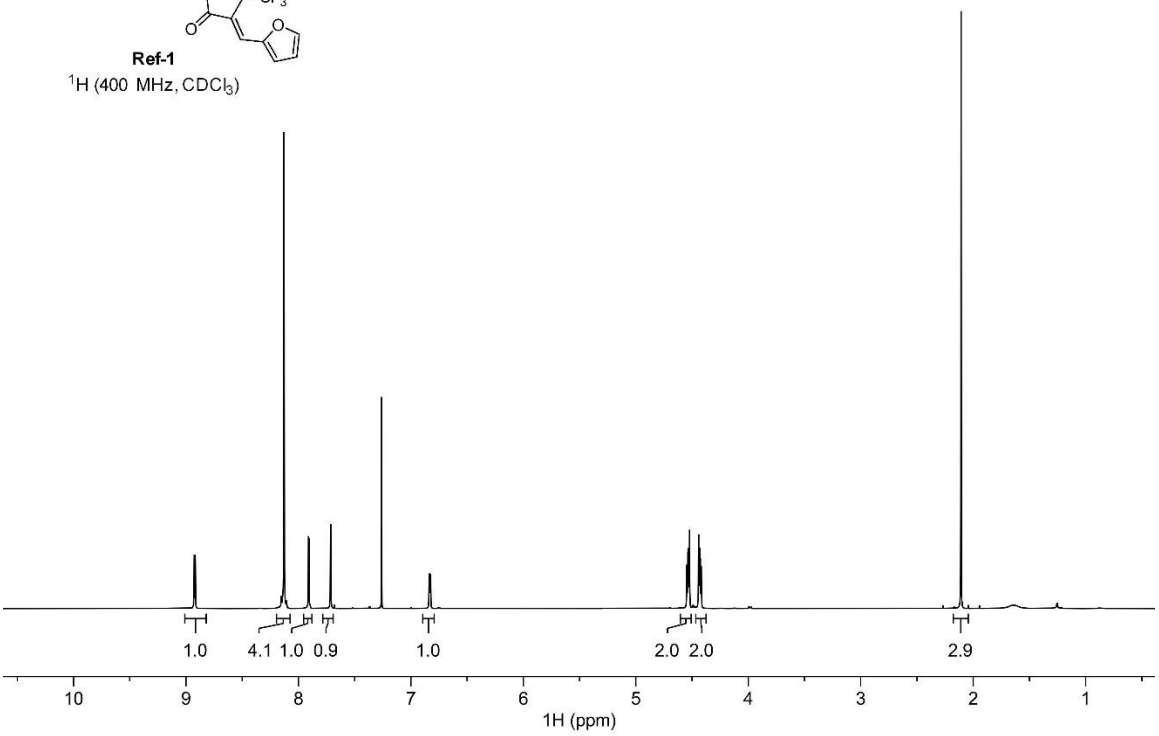

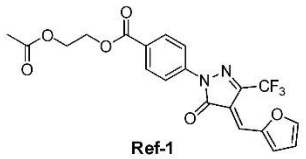

Ref-1

^{13}C (101 MHz, $CDCl_3$)

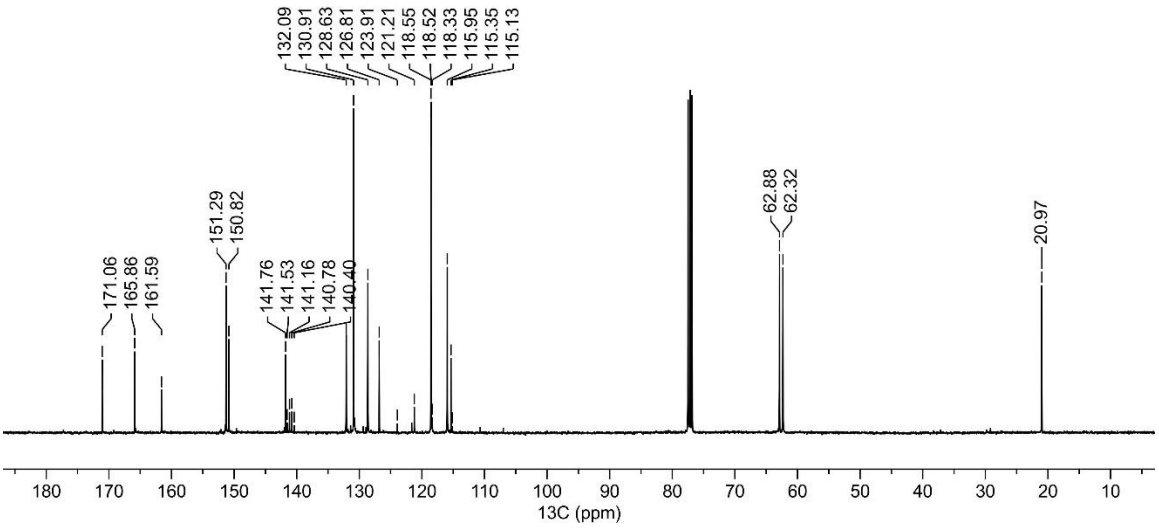

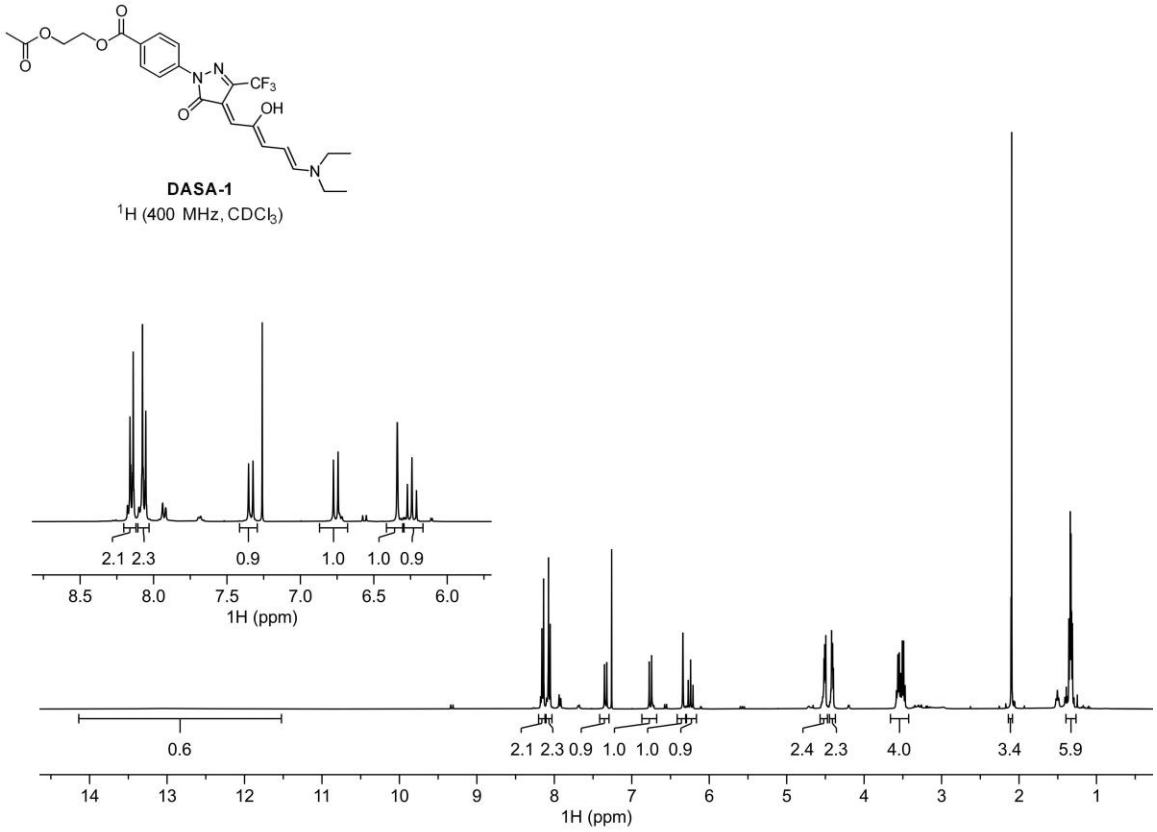
DASA-1
1H (400 MHz, CDCl3)
2.1 2.3
0.9
1.0
1.0 0.9
8.5
8.0
7.5
7.0
6.5
6.0
1H (ppm)
0.6
2.1 2.3 0.9 1.0 1.0 0.9
2.4 2.3
4.0
3.4
5.9
14
13
12
11
10
9
8
7
6
5
4
3
2
1
1H (ppm)

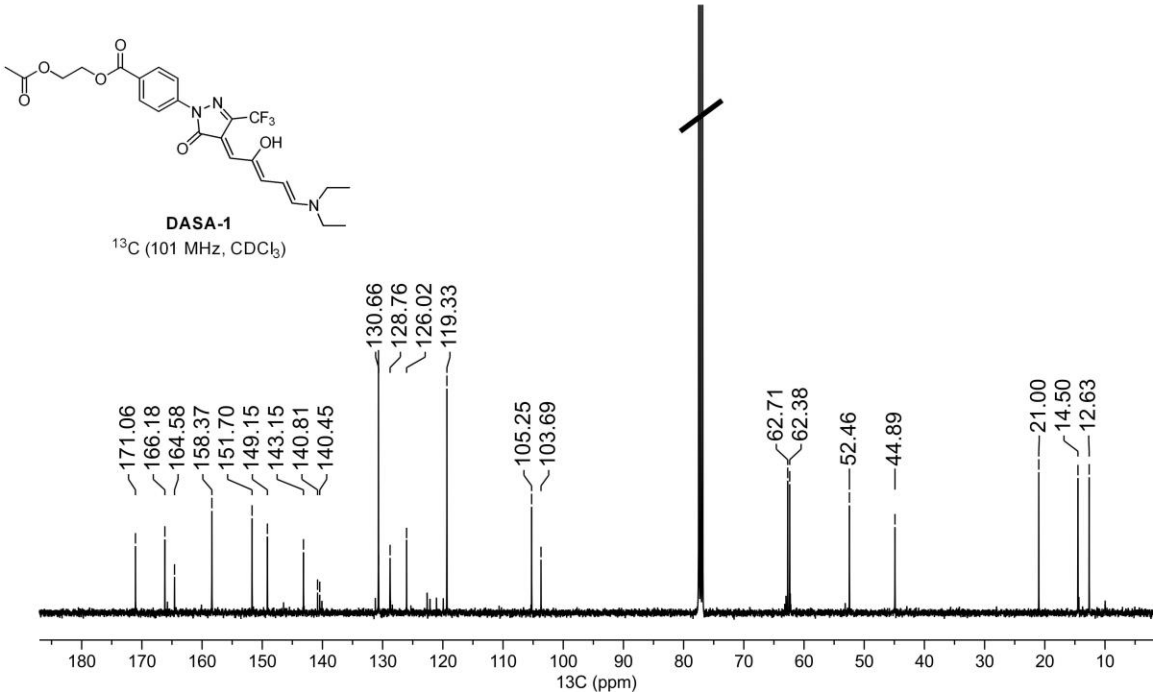
DASA-1
13C (101 MHz, CDCl3)
171.06
166.18
164.58
158.37
151.70
149.15
143.15
140.81
140.45
130.66
128.76
126.02
119.33
105.25
103.69
62.71
62.38
52.46
44.89
21.00
14.50
12.63
180
170
160
150
140
130
120
110
100
90
80
70
60
50
40
30
20
10
13C (ppm)

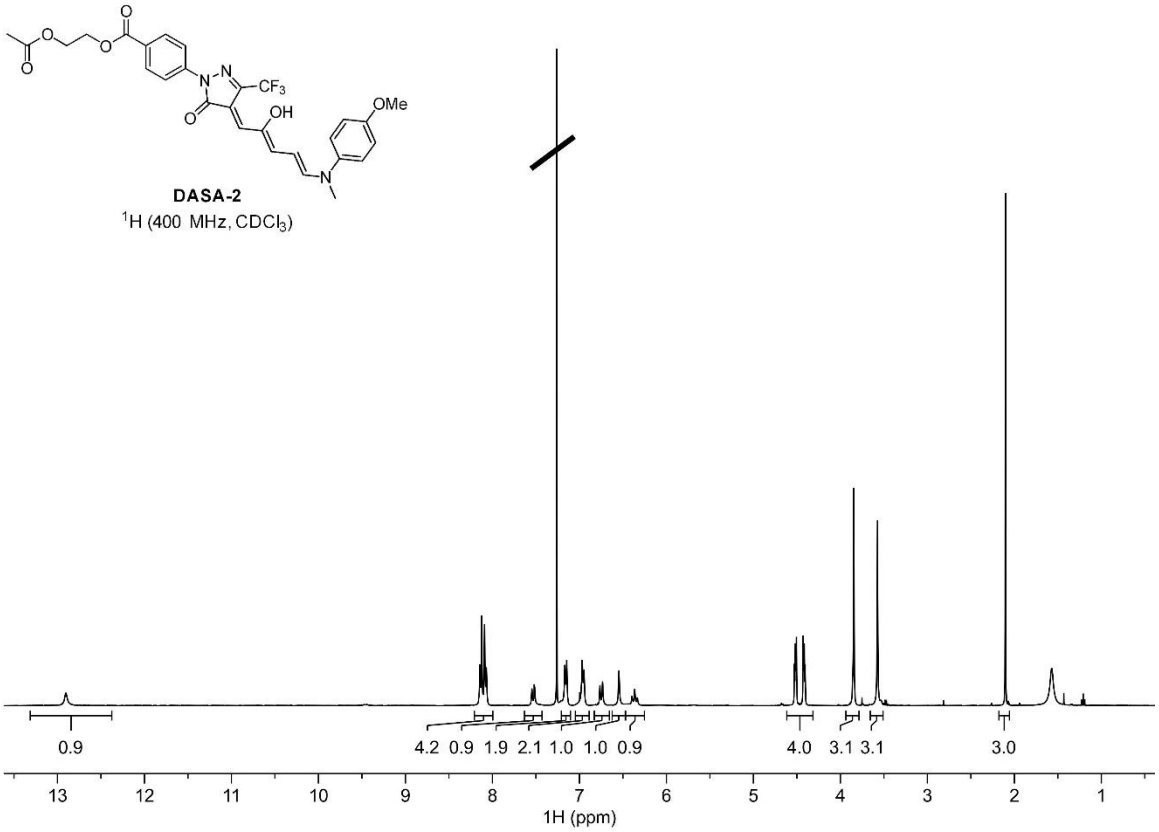
DASA-2
1H (400 MHz, CDCl3)
0.9
4.2 0.9 1.9 2.1 1.0 1.0 0.9
4.0 3.1 3.1
3.0
1H (ppm)

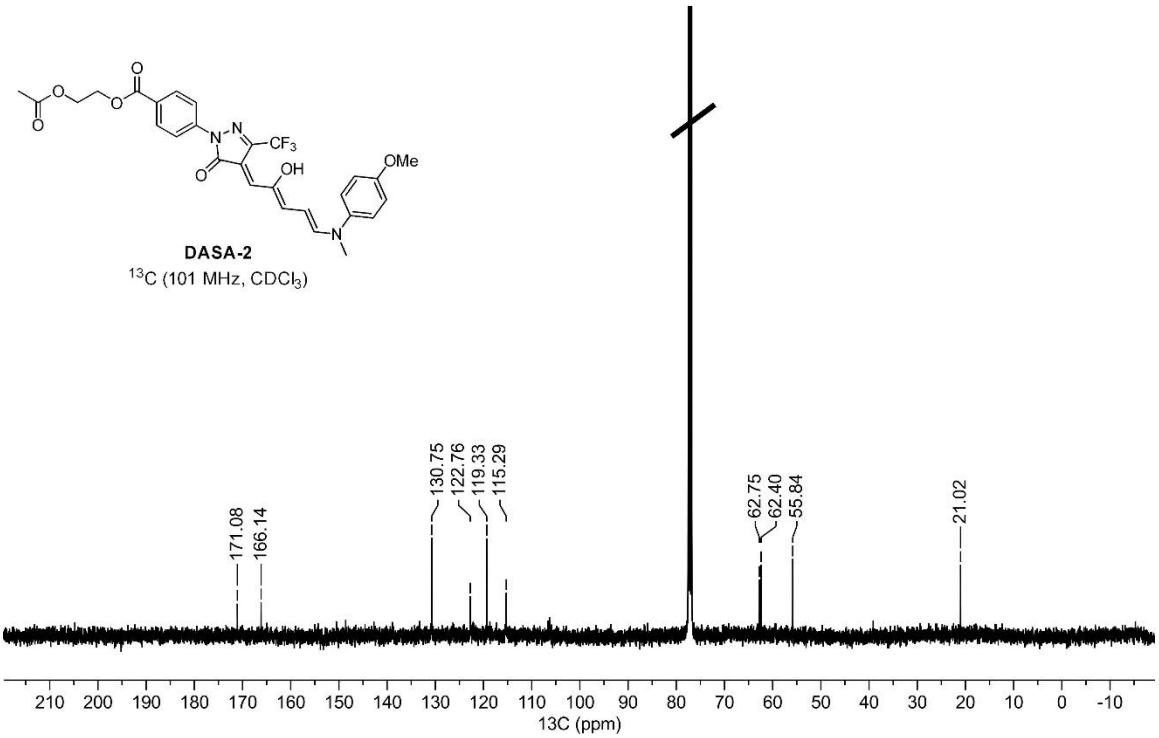
DASA-2
13C (101 MHz, CDCl3)
171.08
166.14
130.75
122.76
119.33
115.29
62.75
62.40
55.84
21.02
13C (ppm)

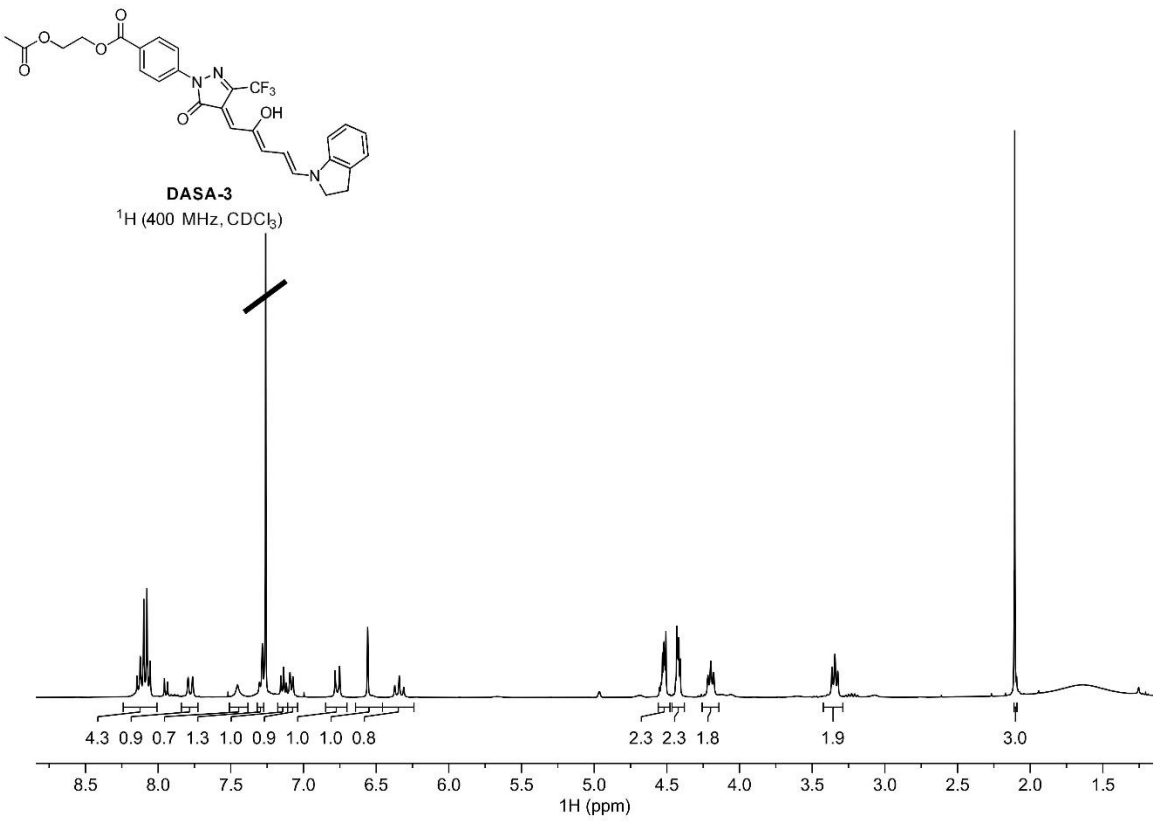
DASA-3
1H (400 MHz, CDCl3)
4.3 0.9 0.7 1.3 1.0 0.9 1.0 1.0 0.8
2.3 2.3 1.8
1.9
3.0
1H (ppm)

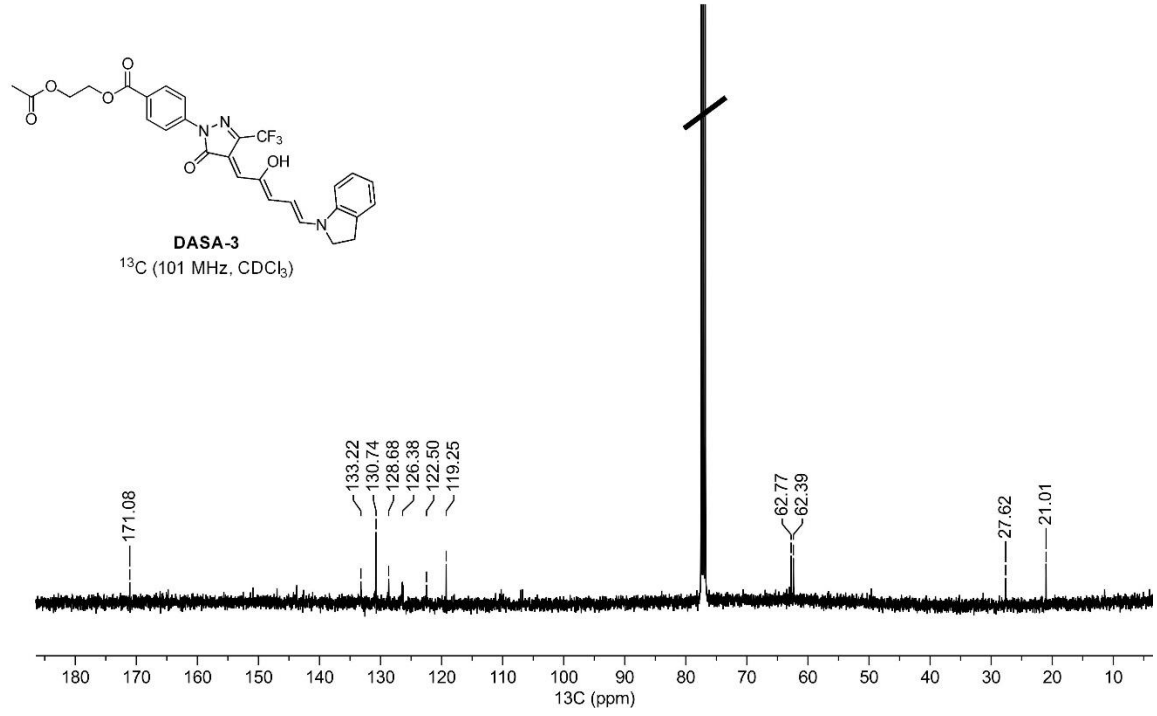
DASA-3
13C (101 MHz, CDCl3)
171.08
133.22
130.74
128.68
126.38
122.50
119.25
62.77
62.39
27.62
21.01
13C (ppm)

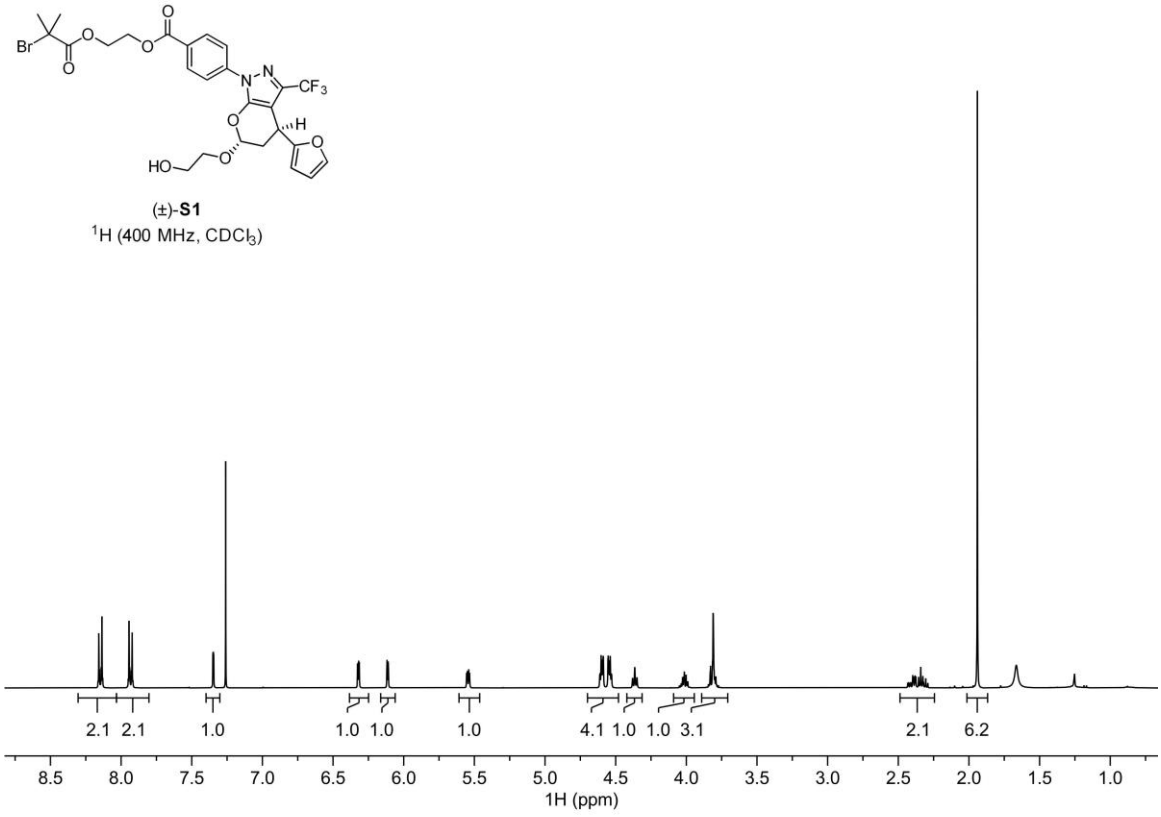
(±)-S1
1H (400 MHz, CDCl3)
2.1 2.1 1.0 1.0 1.0 1.0 4.1 1.0 1.0 3.1 2.1 6.2
1H (ppm)

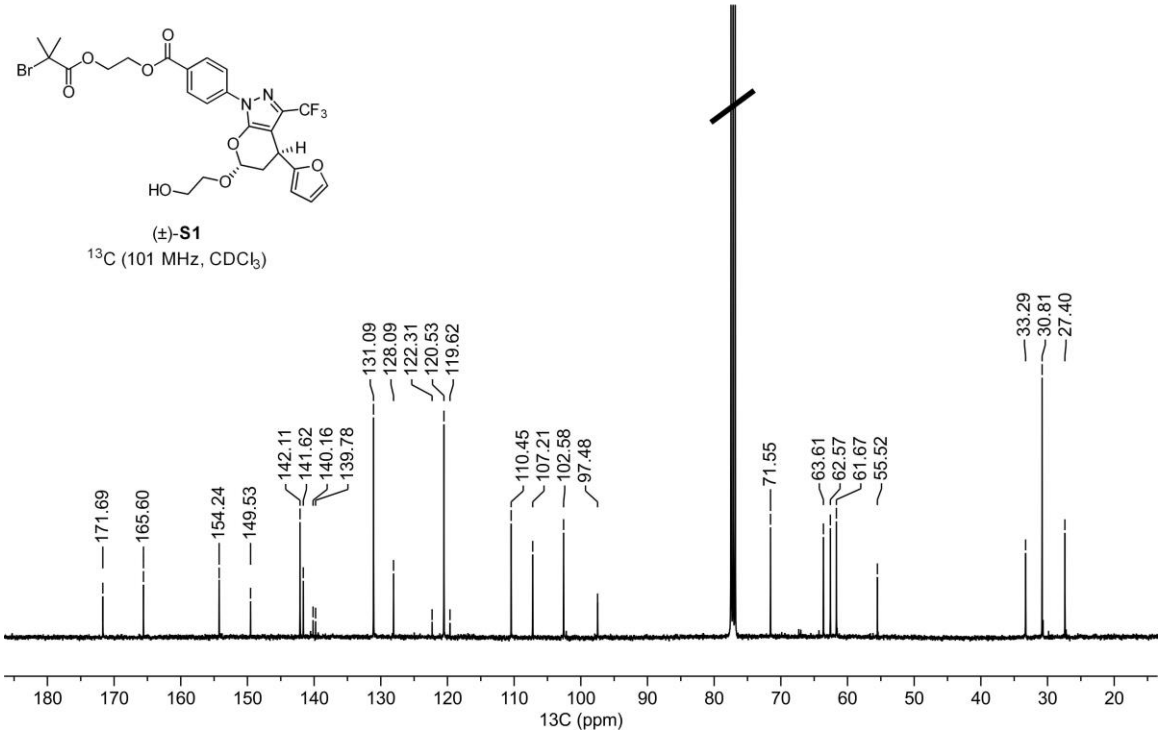
(±)-S1
13C (101 MHz, CDCl3)
171.69
165.60
154.24
149.53
142.11
141.62
140.16
139.78
131.09
128.09
122.31
120.53
119.62
110.45
107.21
102.58
97.48
71.55
63.61
62.57
61.67
55.52
33.29
30.81
27.40
13C (ppm)

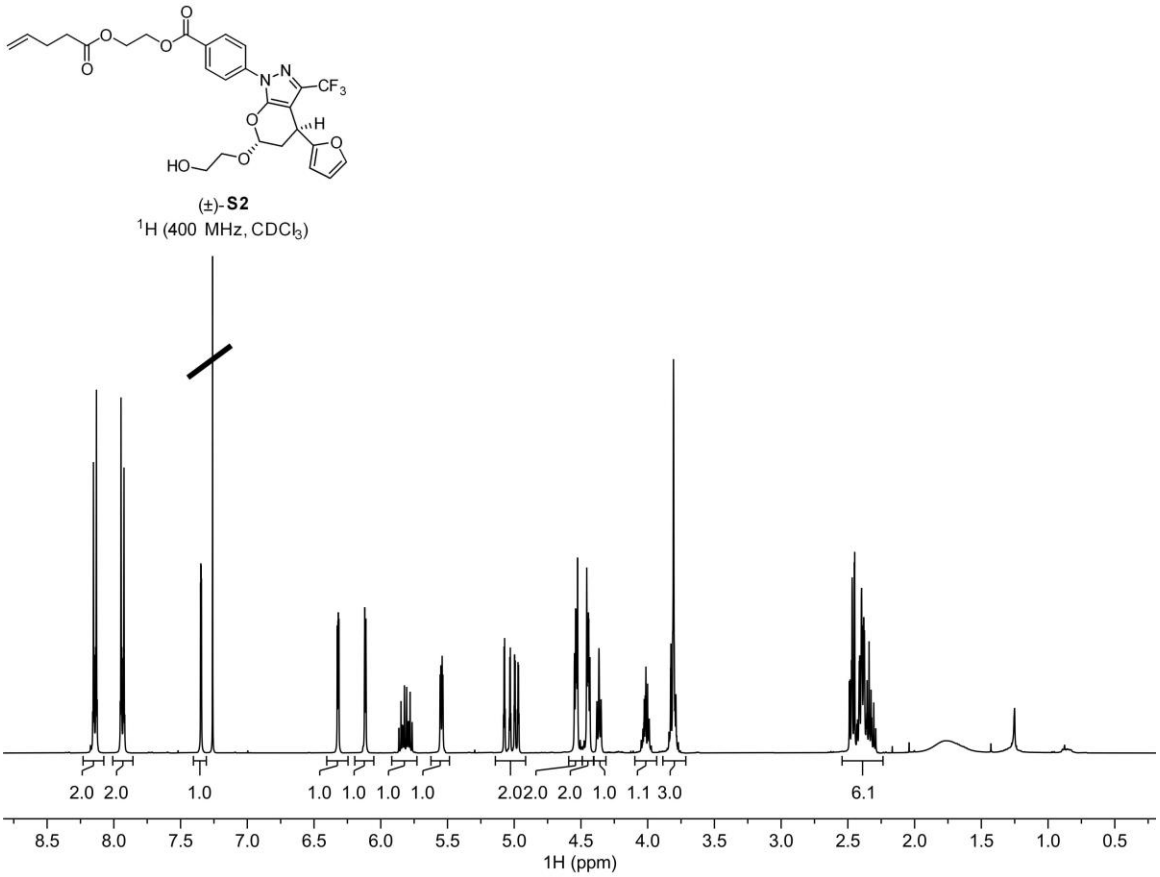
(±)-S2
1H (400 MHz, CDCl3)
2.0 2.0 1.0 1.0 1.0 1.0 1.0 2.02.0 2.0 1.0 1.1 3.0 6.1
1H (ppm)

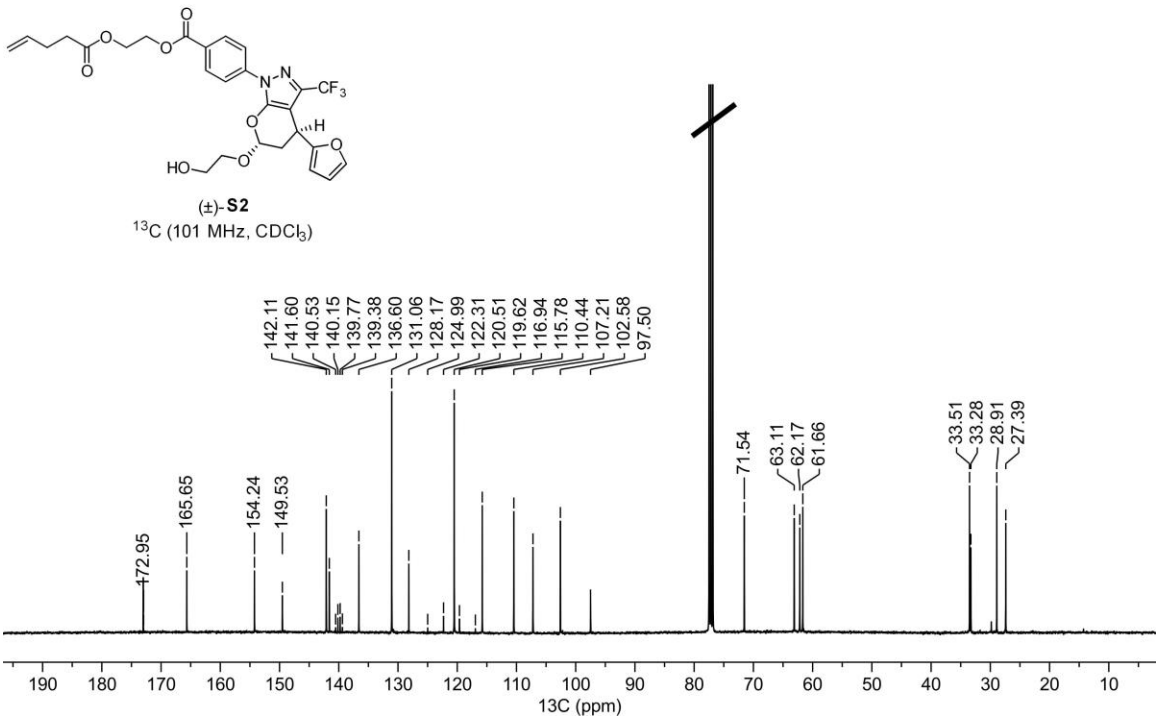
(±)-S2
13C (101 MHz, CDCl3)
142.11
141.60
140.53
140.15
139.77
139.38
136.60
131.06
128.17
124.99
122.31
120.51
119.62
116.94
115.78
110.44
107.21
102.58
97.50
172.95
165.65
154.24
149.53
71.54
63.11
62.17
61.66
33.51
33.28
28.91
27.39
13C (ppm)